THE
PHYSICAL REVIEW

A journal of experimental and theoretical physics established by E. L. Nichols in 1893

SECOND SERIES, VOL. 72, No. 11 DECEMBER 1, 1947

On the Separation of Isotopes in Quantity by Electromagnetic Means

LLOYD P. SMITH, W. E. PARKINS,* AND A. T. FORRESTER†
Department of Physics, Cornell University, Ithaca, New York
(Received February 18, 1942)**

The limitations imposed by space charges on the separation of ions in the usual magnetic mass spectrograph and the possibility of trapping electrons in the ion beam are described. It is found that high voltages and intense magnetic fields are required for moderate ion currents unless these are neutralized. Calculations are given on velocity modulated or interrupted ion beams and the performance of a modulated separator is described. The theory of a radial magnetic separator is given in some detail and an experimental arrangement of such a separator proved more successful than the separator employing modulation. Some ion sources and suggested improvements are described.

INTRODUCTION

AMONG the various methods which have been used to separate small quantities of isotopes, those making use of the action of a suitable combination of static or time dependent electric and magnetic fields on ions have always been attractive. This is largely due to the fact that such methods can be used to cleanly separate almost any element as long as only very small quantities are desired.

The extension of these methods to a point where large amounts of material could be separated and still retain the advantages mentioned above has been beset with two main difficulties. The first being the production of the large ion currents necessary for the transport of a large quantity of material. So much progress has been made in ion sources, that at the present time there is no limitation set by inability to produce large numbers of ions. Consequently we shall not discuss the general construction of ion sources but confine the discussion to the particular ion sources used in the separators to be described later. The source might again in the future set a limit on the quantity of material that can be

FIG. 1. Ion beams in the Dempster type mass spectrograph showing space charge divergence.

* Now located at University of Southern California, Los Angeles, California.
† Now located at RCA Laboratories, Princeton, New Jersey.
** This paper was received for publication on the date indicated but was voluntarily withheld from publication until the end of the war.

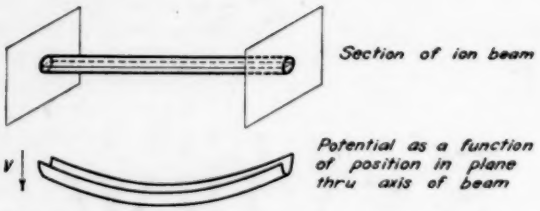

FIG. 2a. Potential distribution over a section through the axis of a beam.

separated because of velocity and space distributions of the ions, but this seems unlikely.

The second and major problem is to retain sufficient resolution in spite of the enormous space charge connected with large ion current. It may be said that as far as electromagnetic methods are concerned, their successful use for large scale separations lies in the development of a method which eliminates the large space charge forces or prevents these large forces from interfering with the applied electromagnetic forces effecting the separation.

The account to follow represents the authors' analyses and experimental investigations of promising methods conducted for the past several years which have led to a successful radial magnetic separator.

ORDINARY MAGNETIC MASS SPECTROGRAPH AND THE SPACE CHARGE PROBLEM

When a conventional mass spectrograph such as the Dempster type is considered for the purpose of separating large quantities of isotopes, one encounters a very serious limitation on the rate at which isotopes can be separated because of large space charge forces unless the space charge can be reduced in some way. An estimate of this limitation can be arrived at as follows. Consider a beam of ions of the type that would exist in a Dempster 180-degree focusing mass spectrograph, the envelope of ion paths of both isotopes being shown in Fig. 1. The beam will be assumed very long in a direction at right angles to the plane of the figure. If the change in curvature of the outermost ion path is small compared to the change in position along the center of the beam, a simple application of Gauss' theorem gives the outward force on the ions traversing the outermost paths due to space charge. This is

$$F=2\pi Ie/v, \tag{1}$$

where I is the total current in the beam per unit length perpendicular to the plane of the figure and v is the mean velocity of the ions. It is at once evident that the force on the outermost ions is independent of the thickness of the beam. Consequently the outermost ions will be subject to a constant outward force all along the beam and the trajectories of the particles on the boundary of the beam are therefore circles of radii r_1 and r_2 defined by

$$Mv^2/r_{1,2}=Hev\pm 2\pi Ie/v. \tag{2}$$

This yields for the thickness of the beam at the 180° position

$$\Delta s\equiv 2(r_2-r_1)=(8\pi e/M)(Ia^2/v^3), \tag{3}$$

where a is the unperturbed radius.

Since even without space charge the beams composed of two different isotopes focus at points very close together at B we may assume that the two beams almost coincide over the whole distance and that the outermost ions in both beams are subject to the same space charge forces. Thus both beams will have about the same thickness Δs in the neighborhood of B.

The total separation of the focal points for the two beams of isotopes at B neglecting space charge is

$$\Delta x=\frac{|M_2-M_1|}{M_1}a. \tag{4}$$

The maximum rate of deposition of cleanly separated isotopes will occur when the beam current is chosen so that the divergence Δs of each beam is equal to the separation Δx. If the spread becomes greater than the separation, i.e., $\Delta s>\Delta x$, then the area at B per unit depth of beam covered by either of the pure isotopes is Δx, and the rate of deposition of pure isotopes per unit depth of beam is proportional to $(\Delta x/\Delta s)I$. But according to Eq. (3) Δs is also proportional to I, so that nothing is gained for a current greater than that necessary to make $\Delta s=\Delta x$. From expressions (3) and (4) this gives

$$I=\frac{M_1}{8\pi e}\frac{v^3}{a}\frac{|M_2-M_1|}{M_1}.$$

Using the expression $M_1v^2/a=Hev/c$ which determines the radius of the central ion path and

the expression $v^2=2eV/M_1$, we have

$$I=\frac{1}{4\pi}\frac{|M_2-M_1|}{M_1}\frac{e}{M_1c}VH.$$

This is the limiting current. The mass $\mathfrak{M}$ deposited per unit time will be

$$\mathfrak{M}=\frac{\eta}{4\pi}\frac{|M_2-M_1|}{M_1}\frac{VH}{c}\text{ grams/sec.},$$

where η is the abundance ratio of the isotope in question. When V is in volts and H is in gausses the number of milligrams per hour that can be separated is

$$\mathfrak{M}(\text{milligrams/hr})=3.19\times10^{-8}\times\eta\frac{|A_2-A_1|}{A_1}V\text{ (volts)}\cdot H\text{ (gausses)}, \quad (5)$$

where A_1 and A_2 are the mass numbers of the isotopes. In terms of practical units and mass numbers the limiting current is

$$I(\text{ma/cm})=0.855\times10^{-6}\eta\frac{|A_2-A_1|}{A_1^2}V\cdot H. \quad (6)$$

It at once becomes evident from the above expressions that the space charge imposes a drastic limitation on the rate of separation even for very high voltages and fields. For example the rate of separation of calcium 44 from Ca 40 (a very favorable case) where $\eta=1/20$, is only about 0.12 milligrams per hour per centimeter even when $V=50{,}000$ volts and $H=15{,}000$ gausses. The total ion current in such a beam would be 1.6 ma per cm. Aside from the considerable problems attached to the use of such high voltage, it must be concluded that this method is not feasible unless the space charge can be at least in part neutralized.

In using such high voltages care would have to be exercised in designing the accelerating electrode system to prevent under or over focusing of the beam as it enters the separation region. There is also some question as to whether such high energy ions could be successfully collected at the collecting electrodes because of heating and sputtering.

Electronic Space Charge Neutralization of Beams

At first sight it would appear that effective neutralization of the large space charge in intense ion beams would be hard to realize because of the great mobility of the electrons compared to that of the ions. However an ion beam wherein the ions are not being accelerated by externally applied electric fields has the ability to trap low energy electrons so that they are confined to move along the axis of the beam. This is due to the fact that in an unneutralized ion beam the electric field is directed away from the axis of the beam and consequently the force on an electron is always toward the center of the beam. The ion beam forms a space charge trough, so to speak, and low energy electrons once in the beam cannot get far away from the axis. They can however move along the axis of the beam but even near the ends of the beam the electrode potentials can be arranged so as to prevent low energy electrons once in the beam from getting out. The potential distribution in an ion beam is shown in Fig. 2a. If electrons can be successfully trapped then a large number can accumulate and effectively reduce the space charge.

When a magnetic field is present as in the Dempster type mass spectrograph, the electrons can be even more effective and migrate throughout the beam even though a strong magnetic field is present. Since there is a force on the electron toward the center of the beam, an electron initially at rest in the beam will execute very small cycloid-like paths as shown in Fig. 2b. If at any time it should lose kinetic energy by suffering a collision, it will move nearer the center of the beam. If near the end of the beam there is a small retarding force the electron will move across the beam to the other side and return as shown. In this way electrons can eventually migrate to any part of the beam.

The mean velocity of the electron along the beam would be of the order $v_e=(E/H)c$, where E is the electric field at right angles to the beam In an unneutralized beam E could be of the order

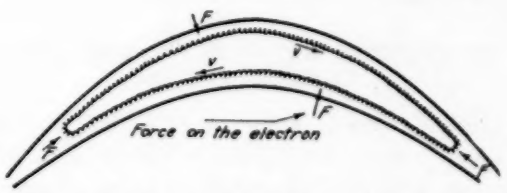

FIG. 2b. Possible electron path through the ion beam in an ordinary mass spectrograph indicating the trapping of slow electrons.

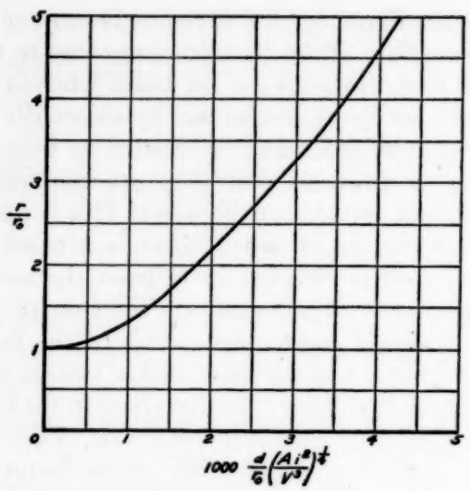

FIG. 3. Natural divergence of a beam of circular cross section in which only radial forces are assumed. r_0 is the original radius; r the final radius; d, distance traveled; i, total current; V, initial voltage; and A, the atomic weight of the particles. Practical units used throughout.

of a thousand volts per cm and the migration would take place quite rapidly. However, if we suppose the ion density is not high, or the beam has been partially neutralized already, and take E to be even 10 volts per cm, then in a field of 2000 gausses,

$$v_e \approx 5\times 10^5 \text{ cm/sec.}$$

An ion of mass number 200 would have a velocity of the order

$$v_i \approx 10^5\ V \text{ (volts)},$$

where V is the energy of the ions in electron volts. This might be of the order 3600 volts for instance. Then

$$v_i \approx 6\times 10^6 \text{ cm/sec.}$$

which is some 10 times the migration velocity of the electrons. Consequently these electrons could be very effective in neutralizing space charge. Such electrons might be introduced into the beam by ionization of gas atoms, or by appropriately placed electron emitters.

MODULATION METHODS AND THE SPACE CHARGE PROBLEM

Methods which make use of a time variation of electric fields for effecting isotope separation are also severely influenced by space charge. In these methods usually an attempt is made either to velocity modulate a uniform beam of ions or to interrupt the beam periodically and then make use of a drift space to obtain separation. In such cases the space charge gives rise to two difficulties. One is the rapid space charge divergence of the beam and the other has to do with the shielding effect of ions surrounding the modulating electrodes.

The divergence of a beam in the form of a sheet of infinite width is given essentially by an expression already used. If d is the distance along the beam measured from a point where the ions were traveling in parallel paths, then the divergence is given by

$$\frac{z}{z_0}=1+2.04\times 10^6 \frac{d^2 I}{z_0}\frac{A}{V^3}, \tag{7}$$

where z_0 is the original thickness of the beam, I is the current per unit length in the infinite direction in amperes, V the voltage of the beam, and A is the atomic weight of the ion.

When the beam has cylindrical cross section the expression is a more complicated function of the distance d along the beam. This expression has been derived by several authors[1] and may be written in the form

$$d=1.75\times 10^{-3}\, r_0\left(\frac{V^3}{AI^2}\right)^{\frac{1}{2}} \int_0^{\log r/r_0} \exp\,[y^2]dy, \tag{8}$$

where I is the beam current, V energy of ions in electron volts, r_0 the initial radius, r the radius at distance d, and A is the atomic weight of the ion. For convenience a plot of this function is given in Fig. 3. As an example of the order of magnitude of the divergence to be expected in useful beams, it is readily found from Fig. 3 that a 10-ma, 10,000-volt beam of ions of mass 40 will diverge from an initial radius of 1 cm to a radius of 3 cm in a distance of 5.6 cm.

If parallelism of ion paths is important, it is evident that unless high initial voltages are used practical currents for separation are impossible. If high voltages are used one encounters most of the problems previously discussed in connection with high voltage beams. A further complication is introduced in the modulation of high voltage beams because this requires that the frequency and amplitude of the

[1] See for instance: L. P. Smith and P. L. Hartman, J. App. Phys. 11, 220 (1940).

modulation field must be made high. In any practical arrangement this turns out to be a source of difficulty and especially so if any modulation voltage other than a sinusoidal one is desired. Another difficulty with modulation schemes is the necessity for sharp potential gradients in certain regions. This may be difficult in a region of high space charge, even when grids are used.

The use of a magnetic field in the direction of the beam to prevent divergence is not very effective as is shown below. Calculations can be made for the maximum radius attained by a particle on the outside of a beam of circular cross section. Such a particle moves periodically between a maximum and minimum radius as it progresses in the axial direction. Except for this axial motion, conditions are not unlike those in a magnetron. Hull[2] has shown that, for a charged particle moving in a homogeneous magnetic field and a symmetrical radial electric field F (function of r only, the magnetic field being in the z direction), where initial conditions at $r=r_0$ are taken to be

$$\mu_0=(dr/dt)_0, \quad v_0=r_0(d\theta/dt)_0, \quad w_0=(dz/dt)_0, \tag{9}$$

the radial velocity squared may be written

$$\left(\frac{dr}{dt}\right)^2=\frac{2eV}{m}-H^2\left(\frac{e}{2m}\right)^2r^2\left(1-\frac{r_0^2}{r^2}\right)^2 -H\frac{e}{m}r_0v_0\left(1-\frac{r_0^2}{r^2}\right)+v_0^2\left(1-\frac{r_0^2}{r^2}\right)+u_0^2, \tag{10}$$

where

$$V_r=\int_{r_0}^{r}Fdr. \tag{11}$$

Putting $dr/dt=0$, Hull obtained an implicit expression for the maximum radius r_m which the particle can reach, i.e.,

$$V_{r_m}=H^2\frac{e}{8m}r_m^2\left(1-\frac{r_0^2}{r_m^2}\right)^2 +\left(\frac{Hr_0v_0}{2}-\frac{v_0^2}{2e/m}\right)\left(1-\frac{r_0^2}{r_m^2}\right)-\frac{u_0^2}{2e/m}. \tag{12}$$

In order to find the maximum radius reached by the beam confined by an axial magnetic field, we shall determine that of an ion starting on the edge of the beam at r_0. For this maximum radius the ion can be assumed to remain on the outside of the beam as it diverges outward. From Gauss' theorem the effective radial electric field expressed in terms of the beam current I, is

$$F=\frac{2Ic^2}{rw_0}.$$

Making use of the expression (11) we find

$$V_{r_m}=\frac{2Ic^2}{w_0}\log\frac{r_m}{r_0}. \tag{13}$$

Substituting (13) in Eq. (12) and letting $v_0=0$, the maximum radius can be determined from the equation

$$\frac{2Ic^2}{w_0}\log\frac{r_m}{r_0}=\frac{H^2er_0^2}{8m}\left(\frac{r_m^2}{r_0^2}-2+\frac{r_0^2}{r_m^2}\right)-\frac{m}{2e}u_0^2. \tag{14}$$

On setting $\rho=\log(r_m/r_0)$, this equation becomes

$$\frac{2Ic^2}{w_0}\rho=\frac{H^2er_0^2}{2m}\sinh^2\rho-\frac{m}{2e}u_0^2. \tag{15}$$

Changing (15) from e.m.u. to practical units gives

$$2.72\times10^{10}\frac{A^{\frac{1}{2}}I}{(V_z)^{\frac{1}{2}}H^2r_0^2}\rho+2.09\times10^4\frac{AV_R}{H^2r_0^2}=\sinh^2\rho. \tag{16}$$

A is the atomic weight of the singly charged ions,

$$V_z=\left|\frac{mw_0^2}{2e}\right|, \quad \text{and} \quad V_R=\left|\frac{mu_0^2}{2e}\right|.$$

Solutions for r_m are most easily obtained by first finding a graphical solution for ρ. To illustrate the magnitude of the maximum radius for certain conditions, consider a particle with only z velocity on the edge of a 1-cm diameter, 10-ma, 10,000-volt beam of mass 40 ions. If the magnetic field is 5000 gauss, this radius is 18.6 cm. It is also important to know how rapidly the beam

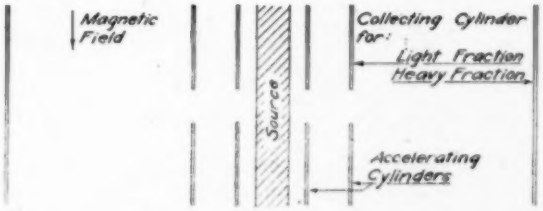

FIG. 4. Schematic diagram for radial magnetic separator.

[2] A. W. Hull, Phys. Rev. 18, 31 (1921).

diverges. To do this would require a determination of the time required for a particle to reach the maximum radius. For our purposes this may be avoided in the following manner. It may be said that until the ion has reached a distance of about one-half the maximum radius the magnetic force in the r direction is small compared to the electric force. It is plausible to assume therefore that until the ion has reached a radius of about $\frac{1}{2}r_m$, the divergence would be fairly close to that produced by the space charge alone as given in Fig. 3. Consequently the magnetic field cannot be regarded as an effective preventive for space charge divergence of an ion beam.

An axial magnetic field would only prove useful if slow electrons were allowed to be present in the beam. These electrons could be confined to any cross-section beam and furnish the necessary negative space charge to prevent divergence of the ions. This principle has been used by Finkelstein[3] in an intense ion source.

Possible Use of Divergence

In view of the space charge troubles in the operation of modulation devices, an interesting modification suggests itself. This would involve making use of space charge divergence in the actual separation. The natural divergence of a group of charged particles will carry the lighter particles to greater radial distances than it does heavy particles in the same time. Collectors arranged in the proper positions could collect only particles of one mass. An alternative method of operation would be to apply certain potentials to a set of collectors and make use of the fact that the lighter particles of successive bunches also acquire greater energies as the bunch diverges. As far as is known, no separation devices have been designed on these principles, but it presents an interesting possibility. The chief difficulty with such a method would be in producing periodic bunches of space charge before the divergence took place.

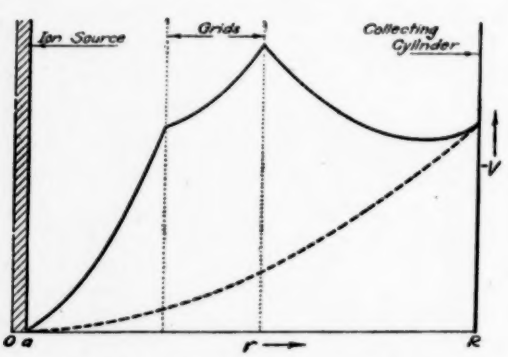

FIG. 5. Potential distribution showing critical condition at the collecting cylinder.

THE RADIAL MAGNETIC SEPARATOR AND THE SPACE CHARGE PROBLEM

Attempts to devise an instrument whose resolution would be independent of space charge, at least to the first order led to the radial magnetic separator. As shown in Fig. 4, the ions are produced at the center of the apparatus and are accelerated radially by one or more cylindrical grids or slits. Under the action of an axial magnetic field the particles describe orbits which depend on their masses in such a manner as to permit the collection of the heaviest ions on a cylindrical electrode, of diameter large compared to the source, while the remaining light fraction is turned back towards the center and can be collected by electrodes of suitable geometry.

The advantageous feature of this method lies in the fact that the potential required to turn back a particle after it has traveled out to some radius depends only on the radius and, as can be seen from Eq. (12), not at all on the variation in potential over the region through which it has traveled. Therefore, except insofar as the space charge produces fields in the axial direction, it has no effect, until the raising of the potential due to space charge is sufficient to stop some heavy ions before they reach the outer cylinder. It is to be emphasized that although this provides a limitation on the current, as calculated below, it does not alter the fact that only the heaviest ions can reach the outer cylinder and that the remaining fraction, enriched in light ions, can be collected as it moves back towards the center.

If the length of the apparatus is not large compared with its diameter, then space charge forces will produce fields in the axial direction. Since this interferes with the resolution only insofar as it produces a spread in radial velocities, its effect is secondary.

[3] A. T. Finkelstein, Rev. Sci. Inst. 11, 94 (1940).

A feature not to be overlooked in this apparatus is that a single ion source can be used to feed an extended apparatus.

An estimate of the current limitation imposed by space charge may be arrived at by the following analysis. For a given set of conditions (positions of the electrodes, their potentials with respect to the ion source, and the strength of the magnetic field) the current to the outer cylinder has a limiting value determined by the condition that the magnitude of the potential at all points between the collecting cylinder and the source must be greater than that of the potential given by Eq. (12), i.e.,

$$V_0=-\frac{1}{8c^2}\frac{e}{M}H^2r^2\left(1-\frac{a^2}{r^2}\right)^2.$$

H is in gauss and all other quantities in e.s.c.g.s. units. Here a is the distance from the center at which the charged particles start. It is assumed that all the particles start at the same distance from the center with zero velocity. V_0 is the potential taken with respect to their starting position. Since we are interested only in distances for which

$$a/r\ll 1,$$

we may use

$$V_0=-\frac{1}{8c^2}\frac{e}{M}H^2r^2. \tag{17}$$

The nature of the problem is made clear by reference to Fig. 5, which shows a source of small diameter surrounded by grids to supply sufficient potential to remove ions and send them to the outer cylinder. The problem of removing sufficient ions from the source out to the 1st grid, in the case of an arc type source, which is a practical necessity if large ion currents are desired, is automatically taken care of. The space charge in the arc must increase sufficiently to force most of the ions formed radially outwards. We shall be concerned only with the region between the outermost grid and the collecting cylinder, where we wish to find what the distribution is for the critical conditions. From this we can find what is the minimum potential which must be placed on a grid at a fixed distance from the center to obtain a given current to the outer cylinder.

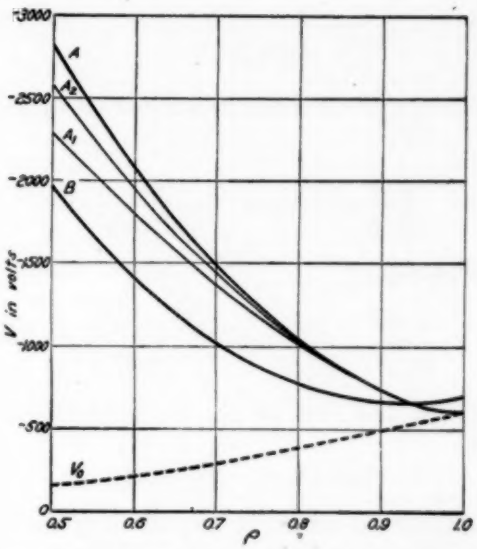

FIG. 6. Potential distributions for critical conditions as a function of the fractional distance from the center to the collecting cylinder for Li^7 ions for: 3.63 ma per cm; 1350 gauss; 14 cm radius. A shows the distribution when the ions reach the outer cylinder with zero radial velocity; B when the potential is adjusted to just stop the Li^6 ions. Both were obtained numerically. A_1 is the approximation obtained to A by taking the first term and A_2 by taking all of the computed terms of the series. The effect of Li^6 ions on the potential has been neglected.

If the ions strike the cylinder with zero radial velocity, i.e.,

$$V(R)=V_0(R), \tag{18}$$

then the limiting current condition is

$$V'(R)=V_0'(R). \tag{19}$$

If symmetry eliminates the z and φ coordinates from Poisson's equation, we have

$$\frac{1}{r}\frac{d}{dr}r\frac{dV}{dr}=-4\pi\rho. \tag{20}$$

Since

$$I=2\pi r\rho v_r$$

is the radial current per unit length, we obtain

$$\frac{d}{dr}r\frac{dV}{dr}=-\frac{2I}{v_r}.$$

The radial motion is governed by the Brillouin potential[4] P, i.e.,

$$M\frac{d^2r}{dt^2}=-e(\partial P/\partial r),$$

[4] Leon Brillouin, Phys. Rev. 60, 385 (1941).

where

$$P = V - V_0.$$

In terms of this variable our differential equation is

$$\frac{d}{dr}r\frac{d}{dr}(P+V_0) = \frac{-2I}{(-2eP/M)^{\frac{1}{2}}},$$

which becomes

$$\frac{d}{dr}r\frac{dP}{dr} - \frac{1}{2c^2}\frac{e}{M}H^2r = -I\left(\frac{2M}{eP}\right)^{\frac{1}{2}}. \tag{21}$$

From (18) and (19) we get the boundary conditions

$$P(R)=0; \qquad P'(R)=0. \tag{22}$$

The differential equation can be simplified by the use of the dimensionless variables

$$\rho = r/R, \quad \Phi = \alpha P, \quad \alpha = \left(\frac{e/M}{2I^2R^2}\right)^{\frac{1}{2}}.$$

Equation (21) becomes

$$(-\Phi)^{\frac{1}{2}}\left\{\frac{d}{d\rho}\rho\frac{d\Phi}{d\rho} - K\rho\right\} = -1, \tag{23}$$

where

$$K = \left(\frac{(e/m)^2R^2}{4I}\right)^{\frac{1}{2}}\frac{H^2}{c^2}.$$

The boundary conditions for Φ are

$$\Phi(\rho)=0; \qquad \Phi'(\rho)=0 \qquad \text{at } \rho=1. \tag{24}$$

If we write (23) in the form

$$(-\Phi)^{\frac{1}{2}}\{\rho\Phi'' + \Phi' - K\rho\} = -1,$$

it becomes apparent that $\Phi'' \to \infty$ as $\rho \to 1$. Therefore as $\rho \to 1$, the solution of this equation approaches the solution of

$$\Phi_0''(-\Phi_0)^{\frac{1}{2}} = -1; \quad \Phi_0(1)=0; \quad \Phi_0'(1)=0.$$

This is readily seen to be satisfied by

$$\Phi_0 = -(9/4)^{2/3}(1-\rho)^{4/3}. \tag{25}$$

Φ_0 is close to the exact solution of (23) where

$$\rho \approx 1$$

and

$$|\Phi_0' - K| \ll \Phi_0''.$$

For a given value of K the approximate solution can be used as a starting point for a numerical solution of (23), and from Φ, the potential

$$V = P + V_0 = \frac{\Phi}{\alpha} + V_0$$

can easily be found. This is a tedious process and each numerical integration is valid for only one choice of K.

In order to find a series solution substitute

$$u^2 = -2^{\frac{1}{2}}\Phi = -2^{\frac{1}{2}}\alpha P$$

and obtain the differential equation

$$u\frac{d}{d\rho}\rho u\frac{du}{d\rho} = 1 - K'\rho u, \tag{26}$$

where

$$K' = K/2^{\frac{1}{2}}.$$

From Φ_0 we get the solution to this differential equation valid for ρ close to one,

$$u_0 = (9/2)^{\frac{1}{2}}(1-\rho)^{\frac{1}{2}}. \tag{27}$$

This suggests a solution of the form

$$u = \sum_{k=2}^{\infty} c_k(1-\rho)^{k/3}. \tag{28}$$

In Eq. (26) let

$$x = (1-\rho)^{\frac{1}{2}} \tag{29}$$

and try a solution of the form

$$u = c_2x^2 + c_3x^3 + c_4x^4 + \cdots. \tag{30}$$

Values of several of the constants are:

$$\begin{aligned}
c_2 &= (9/2)^{\frac{1}{2}},\\
c_3 &= 0,\\
c_4 &= -\frac{K}{20}(9)^{\frac{1}{2}},\\
c_5 &= \frac{4}{15}\left(\frac{9}{2}\right)^{\frac{1}{2}},\\
c_6 &= -\frac{27}{14}\frac{K^2}{100}\frac{1}{2^{\frac{1}{2}}},\\
c_7 &= -\frac{28}{405}(9)^{\frac{1}{2}}K,\\
c_8 &= \left(\frac{9}{2}\right)^{\frac{1}{2}}\left\{\frac{67}{405} - \frac{827}{1008}\frac{K^3}{1000}\right\}.
\end{aligned} \tag{31}$$

The series converges slowly and is therefore not very satisfactory. For a specific case, chosen

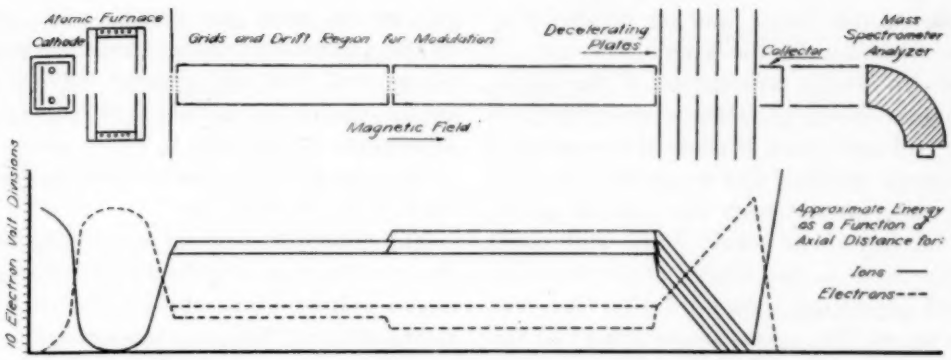

FIG. 7. Schematic diagram of isotope separator making use of velocity modulation. Approximate applied potentials may be obtained from the energy diagram.

because it can be compared with available experimental data, the value has been obtained and plotted in Fig. 6. There the potential obtained from u_0 (curve A_1) and that obtained using all of the terms of the series for which the coefficients have been calculated (curve A_2) are compared with the exact solution (curve A) obtained numerically.

The requirement that particles strike the outer cylinder with zero radial velocity is too stringent, for in practice they would be collected with some radial velocity. Let us suppose that the potential on the outer cylinder is adjusted to the correct value to just stop the lighter isotope, in the case for which the calculations have been made, the Li^6 ions.

$$V(R)=\frac{-1}{8c^2}\frac{e}{M_6}H^2r^2, \tag{32}$$

where M_6 represents the mass of the Li^6 ions. Take for the other boundary condition, as before,

$$V'(R)=V_0'(R),$$

although in this case this condition is too severe.

For this case it might be expected that an ordinary power series could be used, but the solution so obtained converges so slowly as to be altogether impractical. The result of numerical integration can be seen in curve B in Fig. 6.

For the range of ρ covered in Fig. 6, A_1 is a sufficiently good approximation to the exact solution, so that we may use the analytic expression for A_1 to find the manner in which the potential varies with I, e/M, H, and R. It is also reasonable to suppose that curve B varies in approximately the same manner as curve A.

The expression for A, is, from Eq. (25)

$$V=V_0+\Phi_0/\alpha$$
$$=-\left\{\frac{1}{8c^2}\frac{e}{M}H^2r^2+\frac{81}{8}\frac{I^2R^4}{e/M}(1-\rho)^{4/3}\right\}.$$

Except for ρ close to 1, V_0 may be neglected in comparison with Φ_0/α. We then obtain the proportionality equation

$$V\sim I^4R^4M^4 \tag{33}$$

for a fixed value of ρ. It will be noticed that to this order of approximation V is independent of the magnetic field.

EXPERIMENTS ON A MODULATION SEPARATOR

After consideration of the advantages and disadvantages of the various separation methods mentioned in the foregoing analysis two schemes appeared sufficiently promising to be investigated experimentally. The first of these is a velocity modulation method making use of electron space charge neutralization.

The apparatus is schematically shown in Fig. 7. All of it except for the mass spectrograph analyzer is located inside a series of coaxial coils which provides a magnetic field of a few hundred gausses. The ion source is modeled after that described by Finkelstein.[3] The system is designed so that the electrons which produce the ions also furnish the space charge neutralization. They are accelerated from the cathode, pass

through the atomic beam, and on through the system to the ion collector where they are repelled and sent back; whereafter, if they have not lost too much energy, they are available for producing still more ions. If these electrons have lost any energy on their trip to the ion collector and back, they cannot reach the cathode again, but will be forced to travel back and forth through the system furnishing negative space charge and producing ions until they are lost out of the beam. The approximate energy of the electrons as a function of distance is shown in Fig. 7 also. Because of low electronic mass each trip through the modulation region takes place so quickly that only in rare cases will the electron's energy be modified by its passage through this region. The magnetic field serves to hold the electrons in a fairly well defined beam. The potential trough formed by the electrons in turn serves to keep the ions from diverging.

Ions are produced by electron collision in the atomic jet and are sent through the modulation region, but for the ions the energy with which they emerge depends on their mass. The frequency and amplitude of the modulation voltage as well as the initial ion energy and drift region lengths are adjusted to allow only one mass ion to emerge with increased energy. Next the ions pass through a set of electrodes having progressively higher potentials. This slows the ions and finally causes all of them to stop except those which have received the increased energy in the modulation region, these being only ions of the desired isotope. The ions stopped before the last

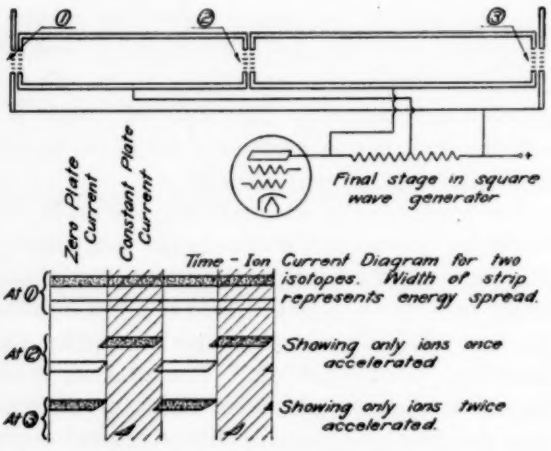

FIG. 8. Modulator and its principle of operation.

grid for the most part diverge and are collected on the nearby electrodes, some may return down the system, but this number will be small. To aid in the adjustment for obtaining the best separation conditions, a mass spectrograph is used to analyze the ions passing through a small opening in the collector.

The potential arrangement requires the arc drop (cathode to atomic jet) be greater than the initial voltage given the ions as they pass into the modulator. This requires low voltages as long as the ion beam can be held together. With low ion energies modulation with a sinusoidal voltage cannot be very effective, but at the same time other wave forms are not difficult to obtain for low amplitudes. A square wave is most desirable here, making possible the pure separation of almost half of the ions of the desired type leaving the source. Such a square wave is used, produced by a generator of the type described by Parkins and Smith.[5] Because of slight ion energy spread due to the source, completely pure separation of the desired isotope cannot be obtained here in less than three modulations. Three pairs of grids are used, the connections made to the load resistor in the square wave generator as indicated in Fig. 8. This figure also diagrammatically shows the principle of giving increased energy to ions of only one isotope.

The cathode is a dispenser type and a modification of that described by Hull.[6] One loop of molybdenum stocking containing the BaO-Al_2O_3 eutectic serving as the heater and dispenser is centered in front of a flat molybdenum emitting surface. The hole in the front of the cathode shield determines the beam diameter and was made $\frac{1}{4}$ in. smaller than the molybdenum stocking loop so that no bombardment of the stocking could take place.

The furnace is a double-walled cylindrical unit made from molybdenum sheet. A tungsten coil with insulating refractory beads is placed between the walls and serves to vaporize the material to be separated. Calcium was used in the experiments and was simply put in the metallic state on the floor of the furnace.

Grids are of $\frac{1}{16}$-in. wide tantalum ribbon, all

[5] W. E. Parkins and Lloyd P. Smith, Phys. Rev. 57, 108 (1940).
[6] A. W. Hull, Phys. Rev. 56, 86 (1939).

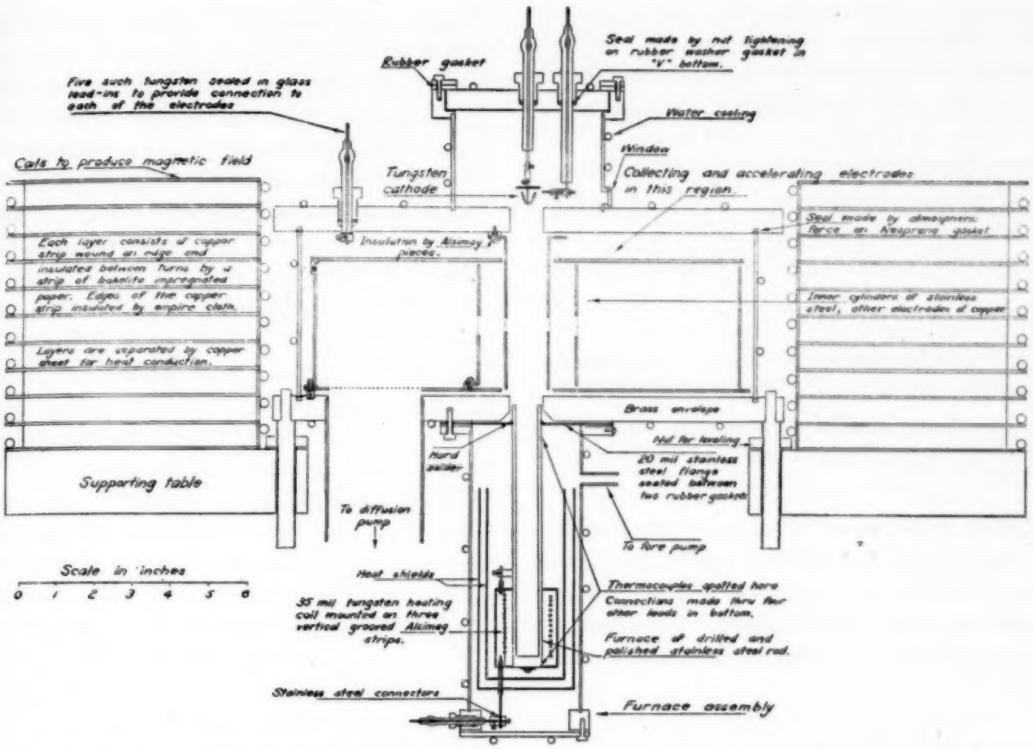
Seal made by nut tightening on rubber washer gasket in "V" bottom.
Rubber gasket
Five such tungsten sealed in glass lead-ins to provide connection to each of the electrodes
Water cooling
Window
Coils to produce magnetic field
Tungsten cathode
Collecting and accelerating electrodes in this region.
Each layer consists of copper strip wound on edge and insulated between turns by a strip of bakelite impregnated paper. Edges of the copper strip insulated by empire cloth.
Insulation by Alsimag pieces.
Seal made by atmospheric force on Neoprene gasket
Layers are separated by copper sheet for heat conduction.
Inner cylinders of stainless steel, other electrodes of copper
Brass envelope
Nut for leveling
Hard solder
20 mil stainless steel flange seated between two rubber gaskets
Supporting table
To diffusion pump
To fore pump
Scale in inches
0 1 2 3 4 5 6
Heat shields
Thermocouples spotted here
Connections made thru four other leads in bottom.
35 mil tungsten heating coil mounted on three vertical grooved Alsimag strips.
Furnace of drilled and polished stainless steel rod.
Stainless steel connectors
Furnace assembly

FIG. 9. Apparatus used in the investigation of the radial magnetic separator showing typical electrode arrangement.

lined up in winding and presenting only their narrow edges to the beam. The drift region shields are of ½-in. diameter stainless steel tubing adjustable in length. The plate electrodes are of 20-mil non-magnetic stainless steel.

The entire unit, only 18 in. long, is mounted on three glass rods fixed in a brass base plate. Tungsten sealed in glass leads are brought in through the base plate making use of rubber gaskets as shown in Fig. 9. To save space one glass tube carries eight of the low current leads. The base plate with all electrodes is assembled and then placed inside the system, the seal being made at the base plate rim with a rubber gasket. The mass spectrograph analyzer is a permanent part of the system.

In the operation of this modulation device it was not difficult to produce an arc and obtain large ion currents at the input end of the modulator. However, only extremely small ion currents were ever measured at the collector. The difficulty with the scheme lies in obtaining effective electron neutralization of the ion beam, and this is the feature upon which the attainment of large transport in low energy ion beams depends. Reasons for ineffective electron neutralization are:

1. Too many variations in electron energy are present.
2. The arc drop is so difficult to adjust that an independently controlled initial electron energy is impossible.
3. At the points where the electrons are turned back too many of them are lost. This takes place near the collector because the increased negative space charge causes the attainment of larger radii as predicted by Eq. (15). Near the cathode loss of electrons takes place by scattering due to the fact the electron collision cross section is so high for low energy electrons.

EXPERIMENTS ON THE RADIAL MAGNETIC SEPARATOR

From Eq. (12) it can be seen that a pure separation of two isotopes can be made in the radial magnetic separator only if the contributing ions are formed at positions having a limited variation in radii and potentials. For a pure separation the voltage spread allowable in the source is equal to the difference in critical voltages for the ions of the two isotopes if all particles are

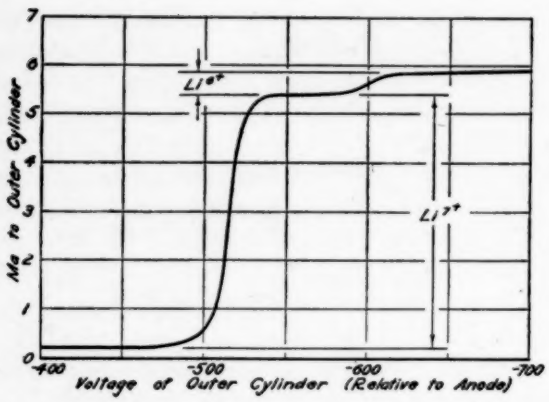

FIG. 10. Current-voltage characteristic of the outer cylinder of the radial separator obtained with the electrode arrangement in Fig. 6.

assumed to start from the same initial radius with zero energy. Energies of ions upon formation may always be neglected. Should all ions be formed in a region of constant potential, the allowable spread in starting radii may be found from:

$$\frac{r_m^2+2r_{01}^2+(r_{01}^2/r_m^2)}{r_m^2+2r_{02}^2+(r_{02}^2/r_m^2)}=\frac{M_1}{M_2},$$

where M_1 and M_2 are the masses of the two types of ions, r_{01} and r_{02} are their initial radii, and r_m is the radius of the outer cylinder. This equation was obtained by equating critical voltages. Choosing an r_0 for ions of one mass, for instance r_{01}, the two solutions for r_{02} will define the range of allowable initial radii of ions of the other mass for complete separation. If a source is used in which the initial radius and potential both vary, the calculation of conditions for complete separation will have to include both effects.

There are other factors which may cause mixing of the isotopes. These may be listed:

1. Excessive deviations of the applied electric field from a purely radial field,
2. Non-uniformities in the magnetic field,
3. Asymmetry in space charge fields,
4. Space charge potential variation in the z direction in the separation region,
5. Space charge oscillations which succeed in varying the energies of the particles.

The first factor may always be overcome by improving the electrode geometry and choice of potentials, using grids if necessary. The second presents even less of a problem; a sufficiently homogeneous magnetic field is easy to obtain. The last three factors concern space charge effects and all have been found to be present. It is difficult to estimate the extent to which these effects will influence the resolution.

For the experimental investigation of the radial magnetic separator lithium was used. The vertical magnetic field made possible an ion source of definite radius by providing a means for confining an electron beam. A cathode was placed on the axis of the system facing a furnace from which lithium was vaporized. With the furnace as the anode a low voltage arc could be struck, from which considerable ion current could be drawn off in the radial direction.

Dispenser and oxide coated cathodes were tried, but not found superior to the simpler tungsten type. Because of the chemical activity of molten lithium and the necessity for the use of non-magnetic materials throughout, the furnace was made of stainless steel. Means of heating the furnace in air were not very successful, but enclosing the furnace in a separate vacuum chamber and heating by a tungsten coil proved to be satisfactory. To conserve lithium and prevent excessive scattering, a collimated atomic beam was obtained and the material removed in collimation returned to the reservoir. This was accomplished by use of a long vertical furnace heated at the bottom. The temperature at the top of the furnace was not far above the melting point of lithium so that much of the vapor impinging on the walls was condensed and returned by gravitational flow. The furnace could not be narrowed at any point or the molten lithium would cling and close the opening. Also, it was found the inside walls had to be smooth to assure satisfactory refluxing action. A platinum coating applied to the inside of the furnace was helpful in this respect.

To obtain samples of the lithium isotopes the collecting surfaces in the separation chamber must be sufficiently cool to condense the material. The early experiments were done with the first cylinder (numbered from the inside) water cooled to prevent heat from the arc and collected current from raising the electrode temperatures excessively. This, however, did not allow the flexibility of potentials necessary in these first measurements. All electrodes (three cylinders and

two end plates) were then insulated from one another and from the metal envelope so that potentials could be controlled and currents measured individually. The first two cylinders were used in a variety of forms, experimenting with grids, slit sizes, and cylinder radii. A typical arrangement for the entire system is shown in Fig. 9.

To determine the success of the separation and optimum operating conditions, current to either the second or third cylinder was plotted against voltage on the third cylinder arc and magnetic field conditions remaining constant. When this voltage is too positive, ions will not arrive at the third cylinder, but return for the most part to the second. As the third cylinder becomes sufficiently negative, ions of the heavy isotope arrive, increasing the current there and decreasing it at the second cylinder; at a still more negative voltage, ions of the light isotope cause a similar variation in currents to these cylinders. As a result the current to either cylinder as a function of the voltages applied to the third cylinder has plateaus to be identified with the ions of each isotope present. The fact that the magnitude of the differences in current between plateaus are proportional to the relative abundance of the isotopes in question constitutes a check on their identity. In Fig. 10 a current-voltage characteristic taken for the third cylinder is reproduced.

Not only do these characteristics furnish a measure of the quality of the separation, but they are useful in forming a better understanding of the action of the separator. Characteristics for the other electrodes are helpful in this connection. To save the tedious point by point plotting, an oscilloscope may be used to trace the curves. For this scheme a 60-cycle voltage is connected in series with the d.c. voltage applied to the third cylinder, and is also connected across the horizontal plates of the oscilloscope. A resistance carrying the current to the electrode in question is connected across the vertical plates. During long runs while separation is in progress such an oscilloscope would be invaluable in checking operating conditions, the a.c. need only interrupt the separation process for a few seconds.

One of the greatest difficulties proved to be suppression of oscillations which were spontaneously generated and found on all electrodes. Various connections of capacitances and inductances were never uniformly successful in reducing their intensity. It was finally found they arose in the arc region and could be removed only by proper control of the space charge conditions there. Stopping all oscillations also removed peculiar space charge potential distribution in the arc region which was shown to be present by measurement of current to the various electrodes. This proper control was brought about by keeping the arc current fairly small (below ½ ampere) and putting a negative voltage (usually 500 or 600) on the first cylinder. This potential caused considerable current to be drawn from the arc, more the larger the arc current. Making the first cylinder sufficiently negative would, of course, finally extinguish the arc. At the same time the accelerating voltage on the first cylinder was desirable because it increased the current passing into the separation region. Actual ion currents removed from the arc to the first cylinder and separation regions were often as great as one third of the arc current. The fact that these measured currents were ion currents was assured by the effect of the first

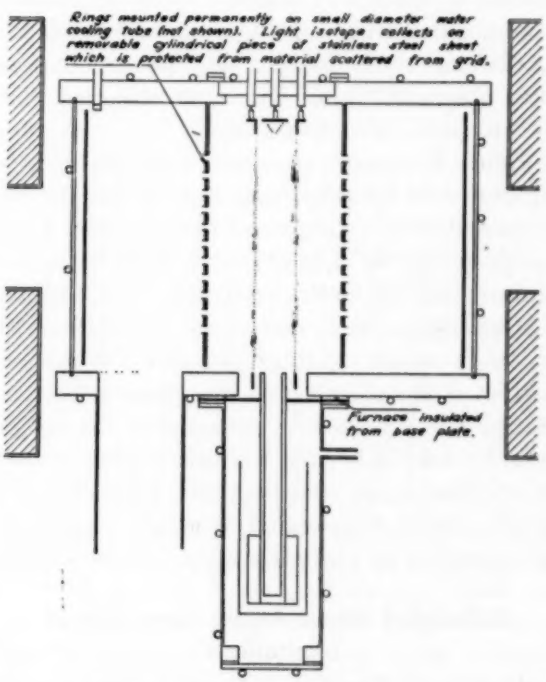
Rings mounted permanently on small diameter water cooling tube (not shown). Light isotope collects on removable cylindrical piece of stainless steel sheet which is protected from material scattered from grid.
Furnace insulated from base plate.

FIG. 11. Modification of the apparatus recommended for the quantity collection of pure Li^6.

cylinder potential on the saturation current to the third cylinder. For a second check it was noted that the ratio of current to the first cylinder to the current through the first slit was always approximately equal to the ratio of the effective length of the first cylinder to the length of the slit.

Through a $\frac{3}{8}$-in. slit in the first cylinder, 8-ma saturation currents to the third cylinder were shown to be separated by a characteristic not unlike that in Fig. 10. Larger currents could be brought into the separation region but not without altering the arc sufficiently to bring about the undesirable space charge conditions, and with them apparent incomplete separation of the isotopes. Through a $3\frac{1}{4}$-in. slit (only grids used for the first and second cylinders) 30 ma were shown by the third cylinder characteristic to be well separated. In this latter case currents to the end plates were large. Both measurements quoted were made with the end plates and second cylinder at the same potential as the third cylinder.

Experiments were also made with a source consisting of a nickel cylinder coated with spodumene and mounted concentric with the system axis at the slit. When the cylinder was heated, as much as 1 ma was obtained through a $\frac{3}{8}$-in. slit, giving good separation. From the spodumene some sodium and potassium ions were observed. Other ions were observed with the arc source also, in particular Li_2^+.

Figure 11 shows a proposed apparatus for the separation of Li^6. Provision is made for the use of current from an extended region of arc. Bombardment of the first grid will be sufficient to prevent lithium from condensing and clogging the openings, and at the second cylinder, which is cooled, the use of grids is avoided. The top and bottom of the system take the place of the end plates. These are at the potential of the second cylinder, and it is expected this whole unit will be operated at the third cylinder potential. The third cylinder is insulated to make possible the measurement of current-voltage characteristics.

Calculated *versus* Actual Space Charge Limitations

The results of the space charge calculations made in the previous sections and shown in Fig. 6 correspond to actual ion currents of lithium for which clean cut separation of Li^6 and Li^7 was achieved. According to the calculations the potential at a point half-way between the ion source and outer collecting cylinder should be of the order of 2000 volts below the source potential in order that a current of 3.63 ma per cm be collected at the outer cylinder. However such currents were actually measured when the potential there was less than 600 volts below the source potential. While it is true that the actual apparatus is limited in length, the influence of the end plates on the potential at the center cannot be appreciable since the distance between end plates is comparable to the distance between the source and the outer cylinder. Also since there was very little ion current to the end plate compared to that to the outer cylinder it must be concluded that the positive space charge in the separation region is not as great as it would have to be if only the positive ions making up the current to the outer wall were present there. Consequently it must be concluded that the space charge is neutralized in some manner. This could take place by means of trapped electrons as discussed in the second section.

The fact that partial space charge neutralization takes place even when no effort was made to accomplish it indicates that neutralization could be made very much more effective by introducing electrons by any of a number of special ways.

It must then be concluded that there is at present no indication that space charge is limiting the current that can be collected by this method.

Extension of Apparatus

In order to collect large amounts of material and extend the separation to large masses, the modifications necessary are clearly indicated. Extremely large ion sources can be built and the apparatus extended indefinitely in the axial direction repeating the unit shown in Fig. 11. For heavier masses the diameter of the apparatus must be enlarged several fold and higher voltages and fields must be used. On the basis of the work reported here, the radial separator appears to have unusual promise as a large scale large mass separator.

Angular Distribution of Neutrons from Targets Bombarded by 190-Mev Deuterons[1,2]

A. C. HELMHOLZ, EDWIN M. MCMILLAN, AND DUANE C. SEWELL
Radiation Laboratory, Department of Physics, University of California, Berkeley, California

(Received August 1, 1947)

It is found that 190-Mev deuterons striking a thin target produce a beam of neutrons concentrated about the forward direction of the deuterons. The angular distribution of intensity in this beam has been studied, using as target materials Be, Al, Cu, Mo, Sn, Ta, Pb, and U. The shape of the distributions is represented approximately by the function $(1+a\theta^2)^{-1}$, and the measured widths in radians between points of half-intensity can be given approximately as $0.155+0.00060Z$, where Z is the atomic number of the target material. It is pointed out that these data fit within a few percent a simple theory of neutron production, according to which the proton is "stripped" from the deuteron by striking a target nucleus, leaving the neutron free.

I. INTRODUCTION

WHEN the 184-inch synchro-cyclotron of the Radiation Laboratory at the University of California was first put into operation,[3] one of the earliest observations made was a rough survey of the angular distribution of the neutrons emitted from an internal target. This was done with a portable ionization chamber; it was found that the neutrons came out as a rather sharp beam, whose axis was along the direction of the incident deuterons. More accurate measurements seemed worth while, and a track was set up so that the chamber could be set at known positions across the beam, while the ratios of the readings to those of a fixed monitor chamber were obtained. In this way it was found that the beam had a half-width (width between points of half-maximum intensity) of about $\frac{1}{8}$ radian.

For the more detailed measurements reported here, another method was used. Small samples of materials capable of being activated by fast neutrons were placed in an array across the beam, and their activities measured by a Geiger counter after bombardment. This method has the following advantages: (1) all samples get exactly the same exposure time, obviating the need of a monitor and the consequent added chance of error; (2) since the samples could be placed immediately in contact with the $1\frac{3}{4}$-in. thick steel wall of the cyclotron vacuum chamber, any effect of scattering by this wall is minimized; and (3) by suitable choice of samples with high activation thresholds, neutrons degraded below a certain energy by inelastic scattering from surrounding matter are not detected.

II. EXPERIMENTAL ARRANGEMENT

Figure 1 is a plan view of the cyclotron, showing the location of the internal target on the end of the probe, the final orbit of the deuterons, and the direction of the neutron beam. The targets placed on the end of the probe were all of the same shape, being in the form of truncated wedges with a width at the edge of $\frac{1}{16}$ in. The target materials used were Be, Al, Cu, Mo, Sn, Ta, Pb, and U. The samples to be activated were fastened to the surface of the vacuum tank, along horizontal and vertical lines intersecting at the center of the neutron beam. All of the data given in this paper were taken using as detectors disks of pure graphite, $1\frac{11}{16}$ in. in diameter and $\frac{1}{8}$ in. thick. The only activity observed was the 20.5 minute C^{11} formed by the reaction $C^{12}(n,2n)C^{11}$, with a threshold at 20 Mev. Some other runs were made with copper samples, using the reaction $Cu^{63}(n,2n)Cu^{62}$ (threshold about 10 Mev); these agreed well with the carbon results. However, copper is a less satisfactory material than carbon because the presence of decay periods other than the desired 10-minute period complicates the decay correction.

[1] Reported at the Stanford meeting of the American Physical Society, July 11–12, 1947.
[2] Observations of a similar kind at lower deuteron energy have been made by R. B. Roberts and P. H. Abelson, Phys. Rev. **72**, 76 (1947).
[3] W. M. Brobeck, E. O. Lawrence, *et al.*, Phys. Rev. **71**, 449 (1947).

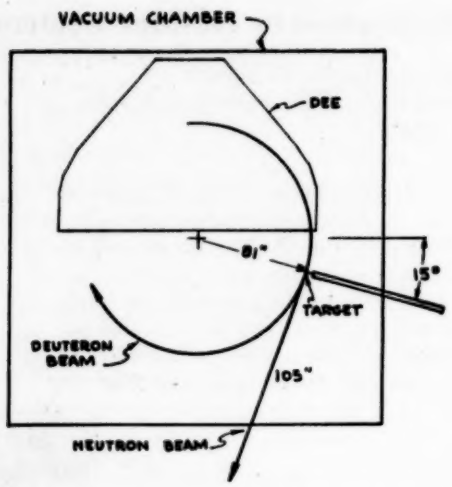

FIG. 1. Experimental arrangement, showing the path of the deuterons inside the cyclotron, the position of the internal target, and the direction of the neutron beam. The carbon samples were placed on the outer surface of the vacuum-chamber wall; the 105-in. dimension is the distance from the target to the sample in the center of the beam.

III. FIRST SERIES OF MEASUREMENTS

In this series, carbon samples were placed on 2-in. or 3-in. centers covering a horizontal range of ± 56 in. or a vertical range of ± 20 in. from the center of the neutron beam. Greater vertical heights come into the shadow of the magnet poles. The samples were exposed for a time sufficient to give an initial activity on the center sample of about 5000 to 10,000 counts per minute; the exposure times required were of the order of 5 to 15 minutes, depending on the deuteron current, the maximum current being estimated at about $\frac{1}{2}$ microampere. The activities were then measured with a Geiger counter, taking at least 1000 counts for each reading. All of the measurements were corrected for decay and for lack of counting resolution at the higher rates. In the case of the horizontal distributions, it was also necessary to correct for the variation of distance with angle.

Vertical distributions were taken with targets of Be, Cu, Sn, Pb, and U. These curves are very similar to one another in shape, but have slightly different widths. The curve with a Cu target is shown by the circles and solid line in Fig. 2; the curves with Be and U targets are given in the following paper by Dr. Serber. The shape of these curves can be represented with considerable accuracy by the empirical relation: intensity $\sim(1+a\theta^2)^{-1}$, where θ is the distance from the center in radians, and a is a constant characteristic of the target material.

Horizontal distributions were taken with targets of Be, Cu, Sn, and U. The central portions of these are nearly identical to the corresponding vertical distributions. The outer portions on the left side correspond to extensions of the vertical curves to greater angles; on the right side (away from the center of the cyclotron) they deviate appreciably from the vertical curves. For the case of a copper target, the outer parts of the horizontal distribution are shown as dashed lines in Fig. 2. The extra intensity on the right is certainly caused by deuterons striking the dee, which was confirmed by the fact that the dee acquired an appreciable induced activity on an area near the target. Because of this distortion of the horizontal curves, only the vertical curves were used in the half-width measurements. The empirical equation given above, when extended to $\theta=-0.4$, falls below the dashed line by about a factor of two. The shape of the extreme wings of the curve is not to be taken too seriously because of the probable presence of a weak background arising from nuclear processes in the target other than that responsible for the sharp neutron beam. No attempt was made to evaluate this background or to correct for it, since it can have only a small effect on the shape of the main part of the beam.

IV. SECOND SERIES OF MEASUREMENTS

Since the results of the first series showed that the distributions all have the same form, but have apparently significant variations in width, a second series of measurements aimed particularly at determining the half-widths was made. Only vertical distributions were measured, and for each exposure only nine samples were used, in groups of three with $1\frac{11}{16}$-in. spacing between centers bracketing the peak of the curve and the two half-intensity points. With the smaller number of samples it was possible to get three or four readings on each one, and to plot for each a decay curve, minimizing the possibility of error in the activity determinations. All the target elements used in the first series were

repeated in this way, and, in addition, Al, Mo, and Ta were used. Also, in order to obtain some idea of the precision of the measurements from internal consistency, several independent runs were made for each of the target materials; these were done in random order among the various targets. All of the half-width measurements are given in Table I. These values are plotted against atomic number in Fig. 3. The mean of the total spreads of values for the different targets is ±3 percent, which can be taken as a rough measure of the degree of precision of the measurements. The theoretical values are also given in Fig. 3.

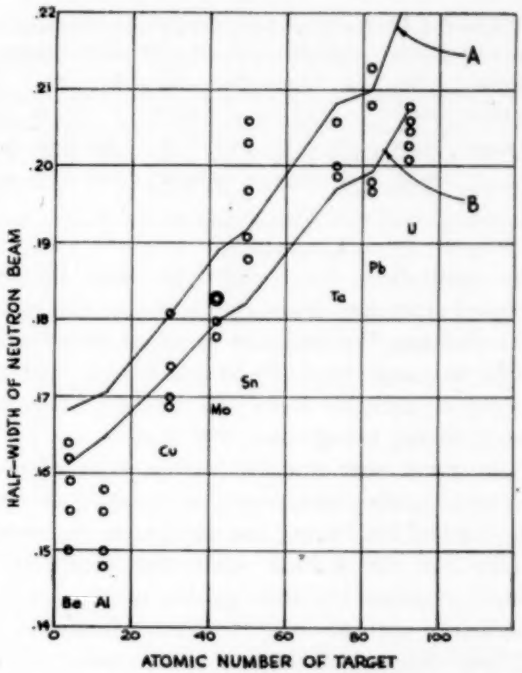

FIG. 3. All measurements of neutron beam half-width (width between points of half-maximum intensity) plotted against atomic number of target. The ordinate scale is in radians; note that its origin is below the bottom of the plot. The broken lines *A* and *B* connect the theoretical half-widths computed for the various targets in the "opaque nucleus" and "transparent nucleus" approximations, respectively. These lines are irregular because the corrections for energy loss and scattering depend on the density of the material.

V. PROPERTIES OF DEUTERON BEAM

In order to interpret these results, it is necessary to know certain things about the deuterons striking the target, particularly their energy and their spatial and angular distribution. The discussion of these matters is closely tied in with the more general problem of understanding the operation of the synchro-cyclotron, and some of the material used in the following discussion comes from observations made by members of the cyclotron group for the latter purpose.

First, some conclusion must be made about the *energy* of the deuterons. The nominal energy given by the radius (81 in.) and magnetic field (14,250 oersteds) is 195 Mev. However, the possibility must not be ignored that the radius of curvature of the orbit may differ from the geometrical radius at the probe; this can be caused by a displacement of the magnetic center of the field from the geometrical center of the tank, or by radial oscillations of the deuterons in their orbit. The first effect mentioned is easily checked. From measurements of the azimuthal and radial variations of the field, it is possible to compute the displacement of the magnetic center; at the 81-in. radius, this was found to be about $\frac{3}{4}$ in, in a direction nearly perpendicular to the probe radius. This displacement was verified by measurements of the current to the probe when two defining vanes were put in from the left and bottom of Fig. 1; it makes a negligible change in the energy. The other effect is harder to measure, and a detailed discussion would go beyond the limits of the subject of this paper. The observations made show that radial oscillations certainly exist, and that their amplitudes probably range from about zero to about two inches. Since the oscillating ions always strike the target near the peak of

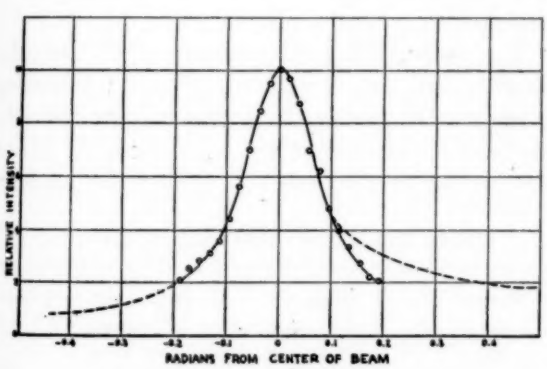

FIG. 2. Distribution curves for neutrons from a copper target. Circles and solid line: Vertical distribution. Dashed lines: Outer parts of horizontal distribution. Central part of horizontal distribution coincides with vertical distribution. The horizontal curve on the right contains some neutrons caused by deuterons striking the dee.

TABLE I. Half-widths of neutron beams in radians.

Target	Be	Al	Cu	Mo	Sn	Ta	Pb	U
1st series	0.162	—	0.174	—	0.203	—	0.213	0.205
2d series	0.159	0.155	0.181	0.178	0.206	0.200	0.208	0.201
	0.164	0.158	0.170	0.183	0.197	0.199	0.197	0.208
	0.155	0.148	0.169	0.183	0.191	0.206	0.198	0.203
	0.150	0.150		0.180	0.188			0.206

the oscillation, the amplitude must be subtracted from the probe radius to get the radius of curvature. We therefore estimate the effective radii to range from 79 in. to 81 in., and the deuteron energies from 185 to 195 Mev, the mean energy being about 190 Mev.

We must next consider the question of what happens to the deuterons while passing through the target. Dr. Serber has computed the energy losses and the R.M.S. scattering angles for a single passage through $\frac{1}{16}$ in. of the various materials, with the results noted in Table II.

Since the vertical angle of the deuteron orbit is limited to about 0.01 radian by the dee aperture, it is apparent that for targets from Cu to U most of the deuterons passing through the target once will strike the dee before making a second passage through the target, and the contribution from those that do go through again with reduced energy will not be important. In the cases of Be and Al, it would take several passages for the R.M.S. scattering angle to reach 0.01 radian, and therefore, there must be an appreciable number of deuterons going through the target several times. However, the energy loss in these cases is small, and the multiple passages through the target do not make a serious error in the mean energy. A small correction for the energy losses in a single passage has been applied to all the computed half-widths.

Next, we can examine sources of angular spread other than the intrinsic width of the neutron beam. One such source is the multiple scattering in the target, as given in Table II. This becomes appreciable in the heavier targets, and is included in the calculated results of the accompanying theoretical paper. Other sources of spread are the spatial and angular spread of the incident deuterons. The easiest to determine is the *spatial distribution* of the deuteron beam striking the target. This is found by making a radio-autograph of the target after bombardment. The activity is concentrated in a thin band not over $\frac{1}{8}$ in. wide along the edge, with a vertical distribution in the form of a peaked curve having a half-width of $\frac{1}{8}$ in., corresponding to an angle of 0.01 radian at the sample position. The *vertical angular spread* of the deuterons is limited by the dee aperture to ± 0.01 radian, and is actually less than that, since the vertical oscillations of the orbits are observed to be considerably smaller than the available aperture; the half-width is certainly not greater than 0.01 radian. These spreads are random, and therefore must be combined with the intrinsic widths according to the rules for random errors—that is, the total spread is of the order of the square root of the sum of the squares of the separate spreads and the intrinsic width. Thus the resultant errors are of the order of 1 percent and can be neglected.

VI. DISCUSSION

The fact that measurements with detectors having different thresholds, or with an ionization chamber, lead to consistent results, can be interpreted in two ways. Either most of the neutrons in the beam have energies above the highest threshold, or else if there is present a considerable fraction of lower energy neutrons, these are also distributed in a beam of about the same width. The theoretical interpretation of the mechanism of neutron production favors the former possibility. This is also consistent with measurements of the transition effects observed when paraffin is placed in front of an ionization chamber.

The theoretical interpretation of the angular distributions is given in detail in a following paper by Dr. Serber. It is shown there that the probable chief mechanism is a process in which the proton of the deuteron strikes the nucleus,

TABLE II. Effect of target on deuteron beam.

Material	Energy loss	R.M.S. scattering angle
Be	1.9 Mev	0.0025 radian
Al	2.6	0.0060
Cu	7.0	0.017
Mo	7.0	0.021
Sn	5.0	0.019
Ta	10.3	0.035
Pb	6.5	0.030
U	11.8	0.043

leaving the neutron free. The neutron velocity at this instant is compounded of the deuteron velocity and the relative motion of the neutron with respect to the center of mass of the deuteron. The transverse component of the relative motion gives the angular spread, and the longitudinal component should give a spread of energy with a half-width of about 30 to 40 Mev about the mean neutron energy, which should be about 95 Mev. It is easy to see from this picture that the magnitude of the angular spread should be of the order of the ratio of the relative internal momentum to the total momentum, or the square root of the ratio of the deuteron-binding energy to its kinetic energy. Thus the spread should be about $(2.18/190)^{\frac{1}{2}}$ or 0.11 radian, which is indeed of the correct order. There is also to be expected an additional spread caused by the deflection of the deuterons in the Coulomb fields of the nuclei responsible for their dissociation, and this additional spread should increase with atomic number. The observed shapes of the curves obtained in the first series of measurements agree with the computed shapes, as illustrated in the following paper. The theoretical half-widths as a function of atomic number are indicated by the solid lines in Fig. 3, which are computed using the two limiting forms of the theory, the "opaque nucleus" approximation *A* being probably better for the heavier elements, and the "transparent nucleus" approximation *B* for the lighter elements. It will be seen that either curve fits the experimental data with reasonable accuracy; in only two cases, Al and Sn, are the means of the experimental points more than 3 percent from the nearest theoretical curve, and these deviations we believe are probably not significant. Nothing has been said so far about the relative neutron yields from the different targets. These ratios were hard to determine, since no means were available for measuring the deuteron currents passing through the thin targets, and only very crude estimates were made; the theory indicates that there should be no great variation of yield with atomic number, and the experimental estimates are not inconsistent with this.

To conclude, we can say that a simple theory involving no arbitrary parameters fits the observed distribution curves with regard to shape, absolute width, and variation of width with atomic number within a few percent, and, therefore, that the presumption is strong that the theory is a correct interpretation of the mechanism of neutron production responsible for the beam.

ACKNOWLEDGMENTS

The authors wish to express their appreciation to Professor E. O. Lawrence for his interest and encouragement in this work, to Dr. R. L. Thornton and the cyclotron operating crew for their help in making the exposures, and to Miss Alice Dodson for her aid in computing the data.

This paper is based on work performed under Contract No. W-7405 Eng-48 with the Atomic Energy Commission, in connection with the Radiation Laboratory, University of California.

The Production of High Energy Neutrons by Stripping*

R. SERBER
Radiation Laboratory, Department of Physics, University of California, Berkeley, California

(Received August 28, 1947)

When a target is bombarded with high energy deuterons, a narrow beam of high energy neutrons is produced by a process in which the proton in the deuteron strikes the edge of the nucleus and is stripped off, while the neutron misses and continues on its way. The cross section for this stripping process is $\sigma=\frac{1}{2}\pi RR_d$, where R is the nuclear radius and R_d is the deuteron radius, or $\sigma=5A^{\frac{1}{3}}\times10^{-26}$ cm². The yield of neutrons from a ½-in. Be target (in which the energy loss for 190-Mev deuterons is 20 Mev) is nearly 2 percent. The neutrons come out with an energy spread around $\frac{1}{2}E_d$ having a half-width $\Delta E_{\frac{1}{2}}=1.5(E_d\epsilon_d)^{\frac{1}{4}}$. Here E_d is the kinetic energy of the deuteron, ϵ_d its binding energy. For light nuclei the half-width of the neutron angular distribution is $\Delta\theta_{\frac{1}{2}}=1.6(\epsilon_d/E_d)^{\frac{1}{2}}$. The half-width increases somewhat with atomic number, primarily because of the deflection of the deuteron by the Coulomb field as it approaches the nucleus, and, to a lesser extent, because of multiple scattering in the target. The increase in half-width from Be to U is about 25 percent. The calculated half-widths and angular distributions agree well with the measurements of Helmholz, McMillan, and Sewell.

An equal number of high energy protons are produced by stripping processes in which it is the neutron that hits the nucleus.

I. INTRODUCTION

THERE are several processes by which high energy neutrons may be produced when a target is bombarded by high energy deuterons. A deuteron passing at some distance from an atomic nucleus, say two or three times the nuclear radius, may be disintegrated by the Coulomb field of the nucleus.[1] Or, when the deuteron grazes the edge of the nucleus, the proton may strike it and be stripped off, while the neutron misses and continues with almost the velocity of the incident deuteron. And, finally, a high energy neutron can be produced by a direct collision between one of the particles of the deuteron and a nuclear particle.

It is the second process, the stripping process, which will be discussed in this paper. Its characteristics depend primarily on the fact that the deuteron is a very loosely-bound system, the proton and neutron actually spending most of their time outside the range of their mutual forces. For deuterons of kinetic energy considerably larger than the deuteron binding energy, the collision time of the proton with a nuclear particle will be small compared to the period of the relative motion of neutron and proton within the deuteron, and the momentum transferred to the proton will be large compared to the momentum of the relative motion. The proton is thus effectively stripped off instantaneously; there is no reaction on the neutron, which continues its flight with the momentum it had at the instant of collision. This momentum is the sum of the momentum attributable to the motion of the center of mass of the deuteron, plus that attributable to the motion of the neutron within the deuteron. The former is $p_0=(ME_d)^{\frac{1}{2}}$, where M is the proton mass and E_d is the kinetic energy of the deuteron, while the latter is of the order $p_1=(M\epsilon_d)^{\frac{1}{2}}$, with $\epsilon_d=2.18$ Mev the binding energy of the deuteron. The neutron will therefore emerge within an angle to the direction of the deuteron beam of about $\theta\sim(p_1/p_0)=(\epsilon_d/E_d)^{\frac{1}{2}}\sim6°$ for $E_d=190$ Mev. The energy of the neutrons will mostly be in a band given by

$$E=(p_0\pm p_1)^2/2M\sim\tfrac{1}{2}E_d[1\pm2(\epsilon_d/E_d)^{\frac{1}{2}}]\sim\tfrac{1}{2}E_d\pm20 \text{ Mev}.$$

The most striking feature of the stripping effect is thus the production of a very narrow cone of neutrons with energy about half that of the deuterons. This prediction has been confirmed on the 184-in. cyclotron in a series of experiments carried out by Helmholz, McMillan, and Sewell; these are reported in the preceding paper.

It is just the narrowness of the cone which distinguishes the stripped neutrons from those produced by direct nuclear encounters, although

* Originally reported at the July 1947 meeting of the American Physical Society.

[1] J. R. Oppenheimer, Phys. Rev. **47**, 845 (1935); S. M. Dancoff, Phys. Rev. **72**, 163 (1947).

the total number of neutrons from the two processes are expected to be about the same. For the latter, the formula for the characteristic angle would have, in place of ϵ_d, an energy ϵ_n of the order of the kinetic energy of particles in the nucleus, $\epsilon_n \sim 20$ Mev. The cone would be over three times as wide, and, since the intensity in the forward direction is proportional to the inverse square of the cone width, only a 10 percent contribution might be expected from these neutrons. Furthermore, it can be shown that in consequence of the fact that the struck particle is bound in the nucleus, collisions with small momentum transfers are discouraged, and the forward intensity is smaller even than the above estimate would indicate. The other process which produces high energy neutrons, the disintegration by the electric field, has a cross section which is proportional to Z^2, and small compared to the stripping cross section except for the heaviest nuclei. Even for U, according to estimates by Dancoff,[2] the cross section for the electric field disintegration is only one-quarter the stripping cross section.

II. THE STRIPPING CROSS SECTION

If the incident deuterons have high energy, the neutron passes the nucleus so quickly that its displacement perpendicular to the line of motion of the deuteron during the time of passage is negligible. In a typical impact, the proton will fail to clear the edge of the nucleus by a distance of the order of the "deuteron radius", $R_d = \frac{1}{2}\hbar/(M\epsilon_d)^{\frac{1}{2}} = 2.1 \times 10^{-13}$ cm, while the neutron will miss by a like distance. The proton will strike the nucleus a distance $l = (2RR_d)^{\frac{1}{2}}$ in front of a plane through the center of the nucleus. Here R is the nuclear radius, which we suppose appreciably larger than R_d. The neutron traverses this distance in a time l/v, where v is the deuteron velocity. The neutron (or proton) will have a velocity normal to the direction of the deuteron motion of the order $(\epsilon_d/M)^{\frac{1}{2}}$, so its displacement in this direction is $(\epsilon_d/M)^{\frac{1}{2}}l/v$. This displacement is unimportant provided it is small compared to R_d, i.e., $(\epsilon_d/M)^{\frac{1}{2}}l/v < R_d$, a relation which may be rewritten, remembering that $E_d = Mv^2$,

$$E_d > 2(R/R_d)\epsilon_d. \tag{1}$$

[2] S. M. Dancoff, private communication.

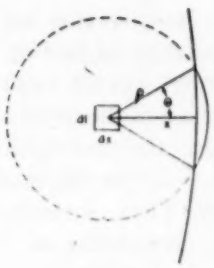

FIG. 1.

The limiting energy given by (1) is, even for the heaviest nuclei, $E_d > 20$ Mev.

The above argument shows that only the (projected) positions of neutron and proton in a plane perpendicular to the deuteron motion need be considered in calculating the cross section: we have only to ask for the probability that at the instant of collision the proton will be within a circle in this plane of radius equal to the nuclear radius, while the neutron will be outside it. Consider a collision in which the separation between proton and neutron (projected in the plane) is ρ. The cross section for the proton hitting a distance x inside the nucleus, within an interval dx, and within an interval dl along the circumference of the nucleus, is just $dxdl$. In the interest of simplicity, we suppose the nuclear radius, R, large compared to the deuteron radius, R_d, so that the curvature of the edge of the nucleus within a distance R_d can be neglected, and the edge considered straight. The probability that the neutron will miss the nucleus is just the fraction of the circumference of a circle of radius ρ which lies outside the nucleus (see Fig. 1); its value is θ/π. The total cross section for proton hitting and neutron missing is thus

$$\sigma(\rho) = \int\int (\theta/\pi) dx dl.$$

The integration over dl gives just the circumference of the nucleus, $2\pi R$. Since $x = \rho\cos\theta$, we have $dx = -\rho\sin\theta d\theta$, and the integral over dx becomes

$$(\rho/\pi)\int_0^{\pi/2} \theta\sin\theta d\theta = \rho/\pi,$$

so

$$\sigma(\rho) = 2R\rho. \tag{2}$$

Equation (2) gives the cross section when proton and neutron are separated a distance ρ;

to get the total cross section we must multiply (2) by the probability of finding such a separation, and integrate over all values of ρ. If $\psi_d(r)$ is the wave function of the deuteron in its ground state, $|\psi_d(r)|^2 d\mathbf{r}$ is the probability of finding an $n-p$ separation r in the three-dimensional volume element $d\mathbf{r}$. Thus, introducing cylindrical coordinates, the probability of a separation ρ is

$$2\pi\rho d\rho \int_{-\infty}^{\infty} |\psi_d(r)|^2 dz,$$

and the total stripping cross section is

$$\sigma = 4\pi R \int_{-\infty}^{\infty} dz \int_0^{\infty} |\psi_d(r)|^2 \rho^2 d\rho. \tag{3}$$

We can change the variable of integration from z to r by using the relation $r^2=\rho^2+z^2$, which gives $dz=rdr/(r^2-\rho^2)^{\frac{1}{2}}$, and transforms (3) into

$$\sigma = 8\pi R \int_0^{\infty} |\psi_d(r)|^2 r dr \int_0^{r} (\rho^2 d\rho)/(r^2-\rho^2)^{\frac{1}{2}}.$$

The integration over ρ gives $(\pi/4)r^2$, so finally

$$\sigma = 2\pi^2 R \int_0^{\infty} |\psi_d(r)|^2 r^3 dr$$

$$= (\pi/2) R \int r |\psi_d(r)|^2 d\mathbf{r}, \tag{4}$$

remembering that $d\mathbf{r}=4\pi r^2 dr$. The integral in (4) has a simple interpretation: it gives just $\frac{1}{2}$ the average separation of neutron and proton in the deuteron. Calling this separation R_d, we have for the stripping cross section

$$\sigma = (\pi/2) R R_d. \tag{5}$$

If we take

$$\psi_d = (\alpha/2\pi)^{\frac{1}{2}} e^{-\alpha r}/r, \quad \alpha = (M\epsilon_d)^{\frac{1}{2}}/\hbar, \tag{6}$$

we find $R_d = 1/(2\alpha) = 2.1\times10^{-13}$ cm, the result previously quoted.

In actuality, the deuteron wave function has the form (6) only outside the range of $n-p$ forces. If the finite range of the forces were taken into account, a somewhat larger value of R_d would be obtained. However, in considering the stripping effect we are only interested in the narrow neutron beam which comes off nearly in the forward direction, and these neutrons are produced in collisions in which the neutron and proton are outside the range of their forces at the instant of collision. Collisions which occur with neutron and proton within the range of the forces will give rise to a wide angular distribution, similar to that resulting from direct nuclear encounters, and may be lumped with the latter effect. Thus, within the limits of unambiguity inherent in the separation of the effects, it is proper to ignore the finite range of the forces.

The derivation of (5) has been carried out as if the nucleus were completely opaque to the neutron and proton. In fact, there will be a finite mean-free path, of the order of 4×10^{-13} cm, for a particle to make a collision in traversing nuclear matter. So in some cases, even though the neutron does not miss the nucleus, it may pass through the edge without being disturbed. However, this effect is balanced out by the approximately equal number of cases in which the proton passes through the edge without a collision.

If we take $R=1.5A^{\frac{1}{3}}\times10^{-13}$ cm, (5) becomes

$$\sigma = 5A^{\frac{2}{3}}\times10^{-26}\ \text{cm}^2. \tag{7}$$

The stripping cross section ranges from 0.1 barn

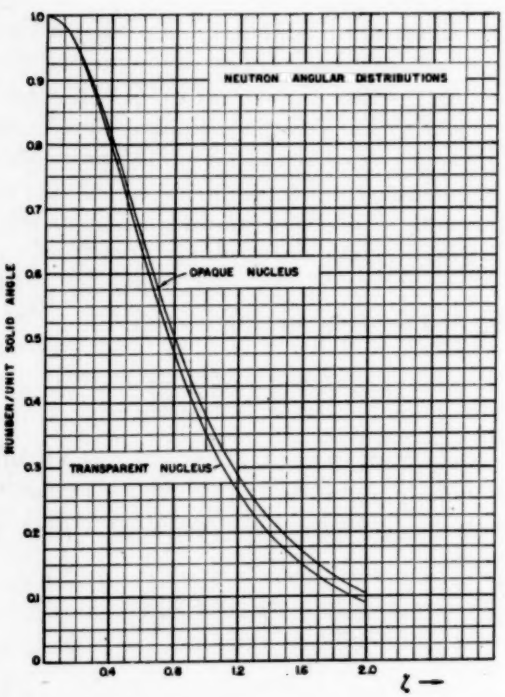

FIG. 2. Neutron angular distributions for transparent and opaque nuclei. Relative number of neutrons per unit solid angle plotted against $\zeta=\theta/\theta_0$.

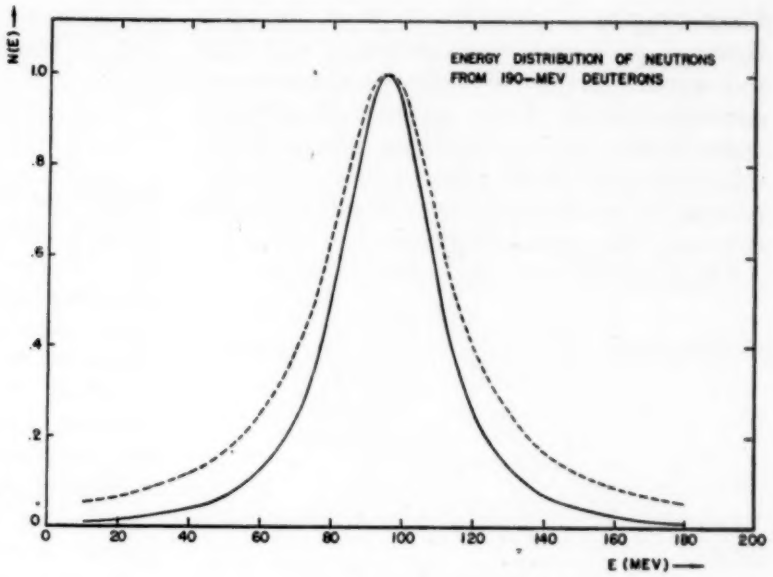

FIG. 3. Energy distribution of neutrons from 190-Mev deuterons. Solid curve, opaque nucleus; dotted curve, transparent nucleus.

for Be to 0.3 barn for U. The yield of neutrons in one passage of the deuteron beam through a $\frac{1}{16}$-in. target, such as is often used in the 184-in. cyclotron, is 1/500 for Be, 1/400 for U.

There is, of course, an equal yield of high energy protons from collisions in which it is the neutron that strikes the nucleus, and the proton which misses.

III. ANGLE AND ENERGY DISTRIBUTIONS

We shall first calculate the angular distribution with the assumption that the nucleus is completely transparent to neutrons. The reason, in addition to the simplicity of this case, is that the model of a transparent nucleus is one limiting case, of which the model of a completely opaque nucleus is the other. Since, as we shall see, the angular distributions to be expected of these two limits turn out to be very little different, we gain by the comparison a considerable confidence in the reliability of the results. Alternatively, we can describe the transparent case as that to be expected in the limit of a very small nucleus, $R \ll R_d$. In our treatment of the opaque case we consider $R \gg R_d$. Treatment of the opposite limit therefore provides some insight into the error likely to be caused by applying the opaque model to light nuclei, where R is not very large compared to R_d, and effects of curvature of the edge of the nucleus and transparency might be expected to show.

The simplicity of the transparent nucleus case lies in the fact that the distribution of neutron momenta due to its motion in the deuteron is just that characteristic of the ground state of the deuteron, without any modification resulting from adding a condition that the neutron has to miss the nucleus.

The probability, $P(\mathbf{p})$, that the neutron in the deuteron has a momentum $\mathbf{p}$ in the interval $d\mathbf{p}$ is

$$P(\mathbf{p}) = |\psi(\mathbf{p})|^2,$$

$$\psi(\mathbf{p}) = (1/\hbar^{\frac{1}{2}}) \int \psi_d \exp[-(i/\hbar)\mathbf{p}\cdot\mathbf{r}]d\mathbf{r}. \quad (8)$$

Using (6), we find

$$\begin{aligned} \psi(\mathbf{p}) &= (1/\pi)[(M\epsilon_d)^{\frac{1}{2}}/(M\epsilon_d + p^2)], \\ P(\mathbf{p}) &= (1/\pi^2)[(M\epsilon_d)^{\frac{1}{2}}/(M\epsilon_d + p^2)^2]. \end{aligned} \quad (9)$$

To get the total momentum of the emergent neutron, we have to add to $\mathbf{p}$ the momentum in the z direction

$$p_0 = (ME_d)^{\frac{1}{2}}[1 + (E_d/8Mc^2)]$$

caused by the motion of the center of mass of the deuteron. The second term in the bracket is a small relativistic correction term.

If we denote by $p_\perp$ the magnitude of the component of $\mathbf{p}$ perpendicular to z, the angle of emergence of the deuteron is

$$\theta = (p_\perp/p_0). \quad (10)$$

More strictly, we should write $\theta=p_\perp/(p_0+p_z)$. However, p_z is small compared to p_0, and since p_z is equally likely to be positive or negative, the correction terms in the angular distribution linear in p_z/p_0 drop out, and we are left with a correction only of the order $(p_z/p_0)^2\sim\epsilon_d/E_d\sim 1$ percent. It can readily be verified explicitly that this correction term is negligible.

The probability of a given value of $p_\perp$ is

$$P(p_\perp)2\pi p_\perp dp_\perp=\int_{-\infty}^{\infty}\frac{(M\epsilon_d)^{\frac{1}{2}}dp_z}{\pi^2(M\epsilon_d+p_\perp^2+p_z^2)^2}\cdot 2\pi p_\perp dp_\perp$$

$$=\frac{(M\epsilon_d)^{\frac{1}{2}}}{2\pi(M\epsilon_d+p_\perp^2)^{\frac{1}{2}}}\cdot 2\pi p_\perp dp_\perp.$$

Expressing this in terms of θ by means of (10), we find

$$P(\theta)d\Omega=(1/2\pi)[\theta_0/(\theta_0^2+\theta^2)^{\frac{1}{2}}]d\Omega, \quad (11)$$

where

$$\theta_0=(\epsilon_d/E_d)^{\frac{1}{2}}[1-(E_d/8Mc^2)], \quad (12)$$

and $d\Omega=2\pi\theta d\theta$ is the element of solid angle. Or, if angles are measured in terms of θ_0, $\zeta=\theta/\theta_0$,

$$P(\zeta)d\Omega_\zeta=(1/2\pi)[1/(1+\zeta^2)^{\frac{1}{2}}]d\Omega_\zeta, \quad (13)$$

with $\Omega_\zeta=2\pi\zeta d\zeta$.

A graph of $2\pi P(\zeta)$ is given in Fig. 2. $P(\zeta)$ falls to half its maximum value at $\zeta=0.7664$. Thus the half-width of the angular distribution (full width at half-maximum) is $\zeta_{\frac{1}{2}}=2\times 0.7664=1.533$, or $\theta_{\frac{1}{2}}=1.533\theta_0$.

The energy of the emergent neutron is

$$E=(1/2M)[(p_0+p_z)^2+p_\perp^2]$$
$$=(1/2M)[p_0^2+2p_0p_z+p^2].$$

Since, for the main part of the distribution, $p_0\gg p$, we may neglect the last term and write

$$E=\tfrac{1}{2}E_d+(E_d/M)^{\frac{1}{2}}p_z. \quad (14)$$

It will be noted that, while the angular distribution depends on $p_\perp$, the energy distribution depends on p_z.

From (9) we find for the probability of a given p_z

$$P(p_z)dp_z=(2/\pi)(M\epsilon_d)^{\frac{1}{2}}\int_0^\infty\frac{p_\perp dp_\perp}{(M\epsilon_d+p_z^2+p_\perp^2)^2}dp_z$$

$$=\frac{(M\epsilon_d)^{\frac{1}{2}}}{\pi(M\epsilon_d+p_z^2)}dp_z.$$

Changing variables from p_z to E by means of (14), we find for the energy distribution

$$P(E)dE=\frac{(\epsilon_dE_d)^{\frac{1}{2}}}{\pi[(E-\frac{1}{2}E_d)^2+\epsilon_dE_d]}dE. \quad (15)$$

This gives an energy distribution centered around $E=\frac{1}{2}E_d$, with a half-width $\Delta E_{\frac{1}{2}}=2(\epsilon_dE_d)^{\frac{1}{2}}=41$ Mev for $E_d=190$ Mev. A plot of Eq. (15) is given by the dotted curve in Fig. 3.

The extreme tails of this distribution are, of course, not to be believed, in particular the part for which $E>E_d$, which violates energy conservation. Here it is no longer true that $p_0\gg p$, and, concomitantly, our assumption that the collision of the proton with the nucleus can be regarded as sudden, with no reaction on the neutron, is evidently no longer valid.

We now turn to the calculation of the angular distribution for an opaque nucleus. Referring to Fig. 1, we introduce the coordinates z in the direction of the deuteron, x perpendicular to the edge of the nucleus, and y parallel to the edge of the nucleus. In doing the calculation analogous to (8) we now have to impose the condition that the neutron misses and the proton hits the nucleus, i.e., we are to take $\psi_d=0$ unless $x_n>0$ and $x_p<0$. The y and z integrations in (8) are unaltered; after performing them we are left with a wave function which can be written

$$\psi(p_y,p_z,x_n,x_p)=h^{-\frac{1}{2}}\int_{-\infty}^{\infty}\psi(p_x',p_y,p_z)$$
$$\times\exp[(i/\hbar)p_x'(x_n-x_p)]dp_x', \quad (16)$$

with $\psi(p_x,p_y,p_z)$ given by (9). We next express the wave function in terms of the momentum variables p_x for the neutron, p_{xp} for the proton:

$$\psi(p_y,p_z,p_x,p_{xp})$$
$$=h^{-1}\int_0^\infty dx_n\int_{-\infty}^0 dx_p\psi(p_y,p_z,x_n,x_p)$$
$$\times\exp[-(i/\hbar)(p_xx_n+p_{xp}x_p)]$$
$$=-\hbar^{\frac{1}{2}}(2\pi)^{-\frac{1}{2}}\int_{-\infty}^{\infty}\frac{\psi(p_x'p_yp_z)}{(p_x'-p_x)(p_x'+p_{xp})}dp_x'.$$

The poles in the denominator are to be avoided by deforming the contour of integration into the

upper half-plane. Since $\psi(p_x', p_y, p_z)$ has one pole in the upper half-plane, this integral can be evaluated in terms of the residue at the pole. We find

$$\psi(p_y, p_z, p_x, p_{xp}) = \frac{\hbar^{\frac{1}{2}}(M\epsilon_d)^{\frac{1}{4}}}{(2\pi)^{\frac{1}{2}}P(p_x - iP)(p_{xp} + iP)},$$

where

$$P = (M\epsilon_d + p_y^2 + p_z^2)^{\frac{1}{2}}.$$

The probability of a given neutron momentum is

$$\begin{aligned} P_1(\mathbf{p}) &= \int_{-\infty}^{\infty} |\psi(p_y, p_z, p_x, p_{xp})|^2 dp_{xp} \\ &= \frac{\hbar(M\epsilon_d)^{\frac{1}{2}}}{8\pi^3 P^2(p_x^2 + P^2)} \int_{-\infty}^{\infty} \frac{dp_{xp}}{(p_{xp}^2 + P^2)} \\ &= \frac{\hbar}{8\pi^2} \frac{(M\epsilon_d)^{\frac{1}{2}}}{P^3(p_x^2 + P^2)}. \end{aligned} \tag{17}$$

Equation (17) gives the differential cross section per unit length of the circumference of the nucleus. We have now to integrate around the circumference, in analogy with the integral over dl in the derivation of the total cross section. We must remember that the x and y axes rotate as we go around the nucleus. If ϕ is the azimuthal angle around the circumference, we can write $p_x = p_\perp \cos\phi$, $p_y = p_\perp \sin\phi$, $dl = R d\phi$, and the differential cross section is

$$d\sigma = \frac{\hbar(M\epsilon_d)^{\frac{1}{2}}R}{8\pi^2(M\epsilon_d + p^2)} \times \int_0^{2\pi} \frac{d\phi}{(M\epsilon_d + p_z^2 + p_\perp^2 \sin^2\phi)^{\frac{1}{2}}} d\mathbf{p}. \tag{18}$$

To get the angular distribution, we integrate (18) over p_z,

$$d\sigma = [\hbar(M\epsilon_d)^{\frac{1}{2}}R/8\pi^2] \int_0^{2\pi} d\phi \int_{-\infty}^{\infty} \frac{dp_z}{(M\epsilon_d + p_\perp^2 + p_z^2)(M\epsilon_d + p_z^2 + p_\perp^2 \sin^2\phi)^{\frac{1}{2}}} \cdot 2\pi p_\perp dp_\perp. \tag{19}$$

To carry out the integrations,[3] we change variable from p_z to a new variable ψ, defined by

$$\tan\psi = p_z/(M\epsilon_d + p_\perp^2 \sin^2\phi)^{\frac{1}{2}}.$$

The double integral in (19) becomes

$$\begin{aligned} &2\int_0^{\pi/2} \cos^2\psi d\psi \int_0^{2\pi} \frac{d\phi}{(M\epsilon_d + p_\perp^2 \sin^2\phi)(M\epsilon_d + p_\perp^2 \cos^2\psi + p_\perp^2 \sin^2\psi \sin^2\phi)} \\ &= \frac{2}{(M\epsilon_d + p_\perp^2)} \int_0^{\pi/2} \cos\psi d\psi \int_0^{2\pi} \left[\frac{1}{M\epsilon_d + p_\perp^2 \sin^2\phi} - \frac{\sin^2\psi}{M\epsilon_d + p_\perp^2 \cos^2\psi + p_\perp^2 \sin^2\psi \sin^2\phi} \right] d\phi \\ &= \frac{4\pi}{(M\epsilon_d + p_\perp^2)^{\frac{1}{2}}} \int_0^{\pi/2} \left[\frac{1}{(M\epsilon_d)^{\frac{1}{2}}} - \frac{\sin^2\psi}{(M\epsilon_d + p_\perp^2 \cos^2\psi)^{\frac{1}{2}}} \right] \cos\psi d\psi \\ &= \frac{4\pi}{M^2\epsilon_d^2} \frac{1}{(1+\zeta^2)^{\frac{1}{2}}} \{1 - (1/2\zeta^3)[(1+\zeta^2)\tan^{-1}\zeta - \zeta]\}, \end{aligned}$$

where ζ is the same variable used in (13), $\zeta = p_\perp/(M\epsilon_d)^{\frac{1}{2}} = \theta/\theta_0$. Putting this in (19) gives

$$d\sigma = [RR_d/\pi(1+\zeta^2)^{\frac{1}{2}}] \times \{1 - (1/2\zeta^3)[(1+\zeta^2)\tan^{-1}\zeta - \zeta]\} d\Omega_\zeta. \tag{20}$$

It can readily be verified that integration over $d\Omega_\zeta$ again gives (5) for the total cross section.

Comparing (20) and (13), we see that the angular distribution for the opaque nucleus differs from that for the transparent nucleus by the factor in the curly bracket. The angular distribution given by (20) is also plotted in Fig. 2, and we see the two distributions are not very different. The half-width given by (20) is $\theta_{\frac{1}{2}} = 1.601\theta_0$, only 4 percent wider than that given by (13). The distribution (20) has a higher tail at large angles than (13), an effect that can be

[3] I am indebted to Dr. Joseph Weinberg for this integration.

interpreted as caused by the additional diffraction of the neutrons around the edge of the nucleus.

The calculation of the energy distribution of the neutrons parallels the derivation of (15). We first integrate (18) over $p_\perp$; this integral is elementary, and gives

$$\int_0^\infty \frac{p_\perp dp_\perp}{(M\epsilon_d+p_z^2+p_\perp^2)(M\epsilon_d+p_z^2+p_\perp^2\sin^2\phi)^{\frac{1}{2}}} = \frac{1}{2(M\epsilon_d+p_z^2)^{\frac{1}{2}}\cos^2\phi}\left\{\frac{1}{\cos\phi}\ln\left(\frac{1+\cos\phi}{1-\cos\phi}\right)-2\right\}.$$

The integration over ϕ gives just a numerical factor, which is equal to π^2. Finally, changing variables from p_z to E by means of (14), (18) becomes

$$d\sigma = \tfrac{1}{4}\pi R R_d \frac{E_d\epsilon_d}{[(E-\frac{1}{2}E_d)^2+E_d\epsilon_d]^{\frac{1}{2}}}dE. \quad (21)$$

The energy distribution (21) has a half-width $\Delta E_{\frac{1}{2}}=1.533(E_d\epsilon_d)^{\frac{1}{2}}$, i.e., $\Delta E_{\frac{1}{2}}=31$ Mev for $E_d=190$ Mev. A plot of the energy distribution for this deuteron energy is given by the solid curve in Fig. 3. It will be remarked that some neutrons are to be expected with an energy considerably larger than $\frac{1}{2}E_d$: 3 percent of the area of the curve lies between 150 Mev and 190 Mev.

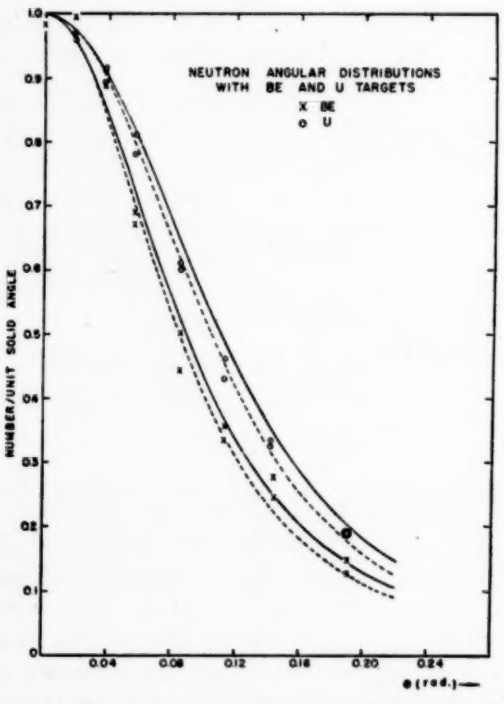

FIG. 4. Measured and calculated angular distributions for Be and U targets. Experimental points from measurements by Helmholz, McMillan, and Sewell. Curves for opaque nucleus (solid line) and transparent nucleus (dotted line) are included for comparison.

Comparison of (15) and (21) shows that the energy distribution, unlike the angular distribution, is appreciably different in the transparent and opaque cases, the latter giving a narrower distribution.

IV. EFFECT OF THE COULOMB FIELD ON THE ANGULAR DISTRIBUTION

The observed half-widths of the neutron distribution are found to increase slowly with atomic number. This effect can be understood as being caused by the nuclear Coulomb field, which deflects the deuteron slightly before the stripping process takes place. There are two sources of deflection. The first is an intrinsic one: the bending of the deuteron's orbit in the field of the nucleus at whose surface the deuteron is stripped. The second is due to the finite thickness of the target; multiple scattering produces a fanning out of the deuteron beam as it traverses the target. The angle of deflection attributable to the first cause is[4]

$$\theta_c = E_b/2E_d,$$

where $E_b=Ze^2/R$ is the barrier height. For 190-Mev deuterons bombarding U, $\theta_c=0.037$. The angle of deflection caused by multiple scattering in passing through the target can be calculated from the usual formula[5]; the results for a number of elements are tabulated in the preceding paper by Helmholz, McMillan, and Sewell. Although both angles are small, they are by no means negligible compared to the width of the neutron distribution.

Since the angular distributions given by (20) and (13) are very little different, we shall simplify our treatment of the Coulomb effects by treating the transparent nucleus case. The results can then be translated to the opaque case by multiplying by the factor by which (20) and (13) differ.

[4] Since $Ze^2/\hbar v=1.5$ for 190-Mev deuterons and a U target, it seems adequate to use a classical description to obtain an estimate of the spreading due to the Coulomb field.

[5] E. J. Williams, Proc. Roy. Soc. **169**, 531 (1939).

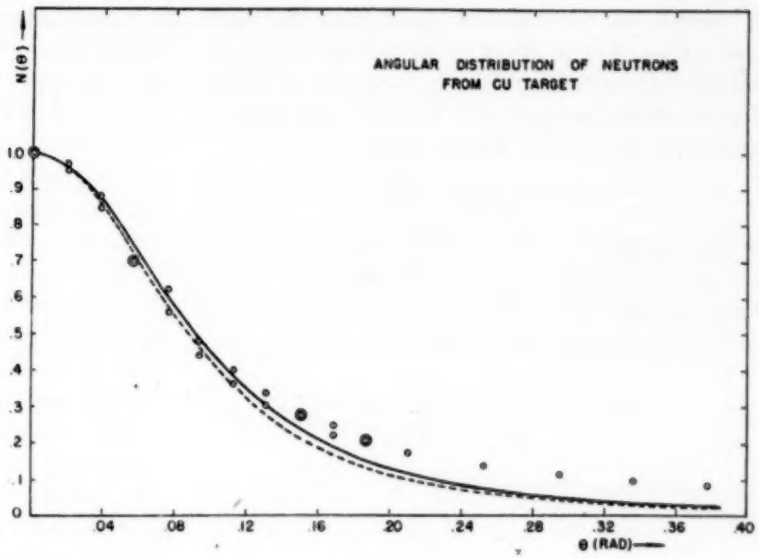

FIG. 5. Measured and calculated angular distributions for a Cu target. Solid curve, opaque nucleus; dotted curve, transparent nucleus. The fact that at large angles the experimental points lie above the curves is presumably due to the production of neutrons, with a wider angular distribution, by processes other than stripping.

We first treat the effect of the deflection by the field of the nucleus which does the stripping. Using the same coordinate system employed in the calculation of the angular distribution from an opaque nucleus, the effect of the bending of the deuteron's orbit is to give the neutron an added momentum $p_0\theta_c$ in the x direction. The distribution function (9) is altered by having p_x replaced by $p_x-p_0\theta_c$. Equation (13) is changed to

$$P(\zeta)d\Omega_\zeta=\int_0^{2\pi}\frac{d\phi}{2\pi[1+\zeta^2\sin^2\theta+(\zeta\cos\theta-\zeta_c)^2]^{\frac{1}{2}}}\zeta d\zeta \tag{22}$$

$$=\int_0^{2\pi}\frac{d\phi}{2\pi[1+\zeta^2+\zeta_c^2-2\zeta\zeta_c\cos\phi]^{\frac{1}{2}}}\zeta d\zeta,$$

where

$$\zeta_c=p_0\theta_c/(M\epsilon_d)^{\frac{1}{2}}=\tfrac{1}{2}E_b/(E_d\epsilon_d)^{\frac{1}{2}}.$$

The integral appearing in (22) is a Legendre function[6] of argument

$$u=\frac{1+\zeta^2+\zeta_c^2}{[(1+\zeta^2+\zeta_c^2)^2-4\zeta^2\zeta_c^2]^{\frac{1}{2}}},$$

$$P(\zeta)d\Omega_\zeta=\frac{u^{\frac{1}{2}}P_{\frac{1}{2}}(u)}{2\pi(1+\zeta^2+\zeta_c^2)^{\frac{1}{2}}}d\Omega_\zeta. \tag{23}$$

The function $P_{\frac{1}{2}}(u)$ is given by the rapidly convergent series

$$P_{\frac{1}{2}}(u)=1+\frac{3}{4}\left(\frac{u-1}{2}\right)-\frac{15}{64}\left(\frac{u-1}{2}\right)^2+\frac{35}{256}\left(\frac{u-1}{2}\right)^3-\cdots.$$

For the purpose of making the further correction for multiple scattering, it is more convenient, and sufficiently accurate, to expand the integrand of (22) in powers of ζ_c. This gives

$$P(\zeta)d\Omega_\zeta=[1/2\pi(1+\zeta^2)^{\frac{1}{2}}]\times\{1+\zeta_c^2f_1(\zeta)+\zeta_c^4f_2(\zeta)\}d\Omega_\zeta, \tag{24}$$

where

$$f_1(\zeta)=3(\tfrac{3}{2}\zeta^2-1)/2(1+\zeta^2)^2,$$

$$f_2(\zeta)=15[1-5\zeta^2+(15/8)\zeta^4]/8(1+\zeta^2)^4.$$

Since (22) is symmetrical in ζ and ζ_c, a better approximation for $\zeta<\zeta_c$ can be obtained simply by interchanging ζ and ζ_c in (24).

The effect of multiple scattering is to give the deuteron beam, after traversing a thickness t of the target, a Gaussian spread of directions with a mean-square angle of scattering proportional to t. The angles θ_s quoted by Helmholz, McMillan, and Sewell are the root mean-square angles after traversing the full target thickness, T. At thickness t, the mean square angle of the Gaussian distribution is thus θ_s^2t/T, or expressed

[6] See, for example, E. T. Whittaker and G. N. Watson, *A Course of Modern Analysis* (Cambridge University Press, Teddington, England, 1920), p. 314.

in terms of the spread in ζ, $\zeta_s^2 t/T$, with $\zeta_s=\theta_s(E_d/\epsilon_d)^{\frac{1}{2}}$. The effect of spreading the distribution (24) by this additional Gaussian distribution is given by applying to (24) the integral operator $G=\exp\{(\zeta_s^2 t/4T)\Delta\}$, where

$$\Delta=(\partial/\zeta\partial\zeta)(\zeta\partial/\partial\zeta)$$

is the Laplacian operator. Since the width of the Gaussian distribution is small compared to the width of the distribution (24), the exponential can be expanded, and the operator written

$$G=\left\{1+\frac{\zeta_s^2 t}{4T}\Delta+\frac{\zeta_s^4 t^2}{32T^2}\Delta^2\right\}.$$

Averaging over the thickness of the target, we get

$$G=\left\{1+\frac{1}{8}\zeta_s^2\Delta+\frac{1}{96}\zeta_s^4\Delta^2\right\}.$$

Applying this operator to (24), and to the corresponding formula with ζ and ζ_c interchanged, we find

$$\begin{aligned}P(\zeta)d\Omega_\zeta&=\frac{1}{2\pi(1+\zeta^2)^{\frac{1}{2}}}\{1+(\zeta_c^2+\tfrac{1}{2}\zeta_s^2)f_1(\zeta)\\&+(\zeta_c^4+2\zeta_c^2\zeta_s^2+\tfrac{2}{3}\zeta_s^4)f_2(\zeta)\}d\Omega_\zeta,\quad \zeta\geqslant\zeta_c,\\&=\frac{1}{2\pi(1+\zeta_c^2)^{\frac{1}{2}}}\{1+\tfrac{1}{2}\zeta_s^2 f_1(\zeta_c)+\tfrac{2}{3}\zeta_s^4 f_2(\zeta_c)\\&+[f_1(\zeta_c)+2\zeta_s^2 f_2(\zeta_c)]\zeta^2\}d\Omega_\zeta,\quad \zeta<\zeta_c.\end{aligned}\tag{25}$$

Equation (25) gives the neutron angular distribution for the transparent model; the formula for the opaque model is obtained by multiplying (25) by the correction for the opacity of the nucleus, the factor in curly brackets in (20).

The increase in half-width caused by the intrinsic scattering is, in first approximation, proportional to ζ_c^2, i.e., to $E_b^2\sim Z^2/R^2\sim Z^2/A^{\frac{1}{3}}$. The increase caused by multiple scattering is proportional to ζ_s^2, or, for given target thickness, to $Z^2\rho/A$. Because of the factor ρ this is not a smooth function of atomic number. With the $\frac{1}{16}$-in. thick targets used in the experiments, the intrinsic Coulomb effect contributes between 90 percent (in Be) and 60 percent (in U) of the total increase in half-width.

The Coulomb field will widen the proton distribution even more than the neutron distribution, since the proton in leaving the nucleus is bent through twice the angle the deuteron is in approaching it. The intrinsic Coulomb effect here is much larger than the multiple scattering, and the angular distribution can be obtained from (23), with ζ_c replaced by $3\zeta_c$.

An additional, smaller effect of the Coulomb field has been pointed out to me by Professor McMillan. The kinetic energy of the deuteron when it reaches the nucleus has been reduced by the amount E_b. Thus E_d in the foregoing formulae is to be taken not as the bombarding energy (corrected for energy loss in the target), but as this minus E_b. An interesting consequence is that the center of the neutron energy distribution will be shifted to lower energy by an amount $\frac{1}{2}E_b$ (7 Mev in U), while the proton, since it regains the energy E_b in escaping, will have its energy distribution shifted upwards by this amount.

Figures 4 and 5 show the calculated neutron angular distributions for targets of Be, U and Cu, and the distributions measured by Helmholz, McMillan, and Sewell. Figure 3 of their paper shows the measured half-widths for a number of elements, and the calculated half-widths The agreement is seen to be quite satisfactory.

A word remains to be said about the neutrons produced by the Coulomb-field disintegration of the deuteron. As previously mentioned, estimates by Dancoff indicate that about one-quarter as many neutrons would be produced in this way as by stripping. Whether, and to what extent, the experimental data might be taken to show the smallness of such an effect depends on the expected angular distribution of the neutrons. This will be the subject of a forthcoming paper by Professor Dancoff, whom I wish to thank for a number of discussions of the electric-field breakup, as well as of the stripping effect.

I am indebted also to Mr. T. B. Taylor, who carried out most of the computations.

This paper is based on work preformed under Contract No W–7405–Eng–48, with the Atomic Energy Commission, in connection with the Radiation Laboratory, University of California, Berkeley, California.

Disintegration of the Deuteron in Flight

S. M. DANCOFF
Physics Department, University of Illinois, Urbana, Illinois
(Received August 11, 1947)

A calculation is made of the cross section for the disintegration of high velocity deuterons by nuclei in their paths. In this paper attention is centered on those processes in which there is no direct nuclear collision, and where the disintegration is due to electric forces. The cross section for 200-Mev deuterons proves to be of the order $2\times10^{-29}Z^2$ cm^2 where Z is the atomic number of the bombarded element. Large yields may be expected in typical cases. The two ejected particles need not share the energy equally; neutrons of energy 75 Mev to 125 Mev may be expected. They emerge in a fairly well collimated beam whose half-width at half-maximum is about 4°.

Quantitatively this process proves usually to be less important than the disintegration involving a direct nuclear collision in which one of the two particles escapes.

1. INTRODUCTION

THE possibility that projected deuterons of sufficiently high energy will be disintegrated by collision with nuclei in their paths has been pointed out by Oppenheimer.[1] His calculations are supplemented in this paper by methods suitable for the case of very high energy deuterons, such as are produced in the Berkeley 200-Mev synchro-cyclotron. A distinction must be made between direct nuclear collisions, in which one or both of the particles in the deuteron collide with the nuclear matter, and electric collisions, in which only the long-range electric forces play a part. A detailed treatment is given here for the latter process.

2. THEORY

We calculate the probability of the disintegration of the deuteron by the electric forces encountered on its collision with a heavy nucleus of charge Ze. We carry out the calculation in the frame in which the center of gravity of the deuteron is initially at rest. The heavy nucleus is taken to be incident along the x axis with velocity v. The electrostatic potential energy of the deuteron is

$$V=Ze^2/[(r_{p\perp})^2+(r_{pz}-vt)^2]^{\frac{1}{2}} \qquad (1)$$

where r_{pz} and $r_{p\perp}$ are the components of the protons coordinate along the x axis and transverse to it. We write

$$\mathbf{r}_p=\mathbf{R}+\tfrac{1}{2}\boldsymbol{\rho}$$

where $\mathbf{R}$ is the position vector of the deuteron's center of gravity and $\boldsymbol{\rho}$ is the vector from neutron to proton. Transitions are induced from an initial state

$$\psi_0=L^{-\frac{3}{2}}\exp i(\mathbf{k}_0\cdot\mathbf{R})\cdot U_0(\rho)e^{iE_0t/\hbar}$$

to a final state

$$\psi_1=L^{-\frac{3}{2}}\exp i(\mathbf{k}_1\cdot\mathbf{R})\,U_1(\rho)e^{iE_1t/\hbar}.$$

E_0 and E_1 are the total energies of the respective states. For the energies involved here, the Born approximation should give reasonably good results except for the heaviest elements. Accordingly, plane waves are taken for the center of gravity wave functions and they are normalized to unit integral in a cube of side L. The initial propagation vector, k_0, will henceforth be set equal to zero. $U_0(\rho)$ is the ^3S ground state wave function of the deuteron and $U_1(\rho)$ is a state in the continuum which will prove to be a ^3P, as in the usual photoelectric disintegration of the deuteron. U_0 is normalized to unit quadratic integral and U_1 to unit energy.

After the collision has taken place the probability amplitude of ψ_1 has grown (in first order) to a value

$$A_1=(i/\hbar)\int_{-\infty}^{\infty}dt\,V_{01}e^{i\omega t}, \qquad (2)$$

where $\hbar\omega=E_1-E_0$ and V_{01} is the spatial part

[1] J. R. Oppenheimer, Phys. Rev. **47**, 845 (1945).

of the matrix element. This is

$$A=2i(Ze^2/\hbar v)\int\int d\mathbf{R}d\boldsymbol{\varrho}$$
$$\times L^3\exp(i\mathbf{k}\cdot\mathbf{R})U_1^*(\rho)U_0(\rho)$$
$$\times\exp(-i\omega r_{p\perp}/v)K_0(\omega r_{p\perp}/v) \quad (3)$$

where K_0 is the Bessel function of imaginary argument. Now the volume element may as well be written $d\mathbf{r}_p d\boldsymbol{\varrho}$ and, accordingly

$$A_1=(2i/L^3)(Ze^2/\hbar v)I_pI_\rho,$$

with

$$I_p=\int d\mathbf{r}_p\exp[i(\mathbf{k}\cdot\mathbf{r}_p-\omega r_{pz}/v)]K_0(\omega r_{p\perp}/v),$$
$$I_\rho=\int d\rho\exp[-i\tfrac{1}{2}(\mathbf{k}\cdot\boldsymbol{\varrho})]U_1^*(\rho)U_0(\rho). \quad (4)$$

Now for disintegrations of deuterons of energy up to 200 Mev the center of gravity recoil, k, is quite small and the product $(k\rho/2)$ is well under 0.1 for the important range of the variables. Consequently we expand the exponential and keep only the second term $(-i\mathbf{k}\cdot\boldsymbol{\varrho}/2)$. It follows that U_1 must be a ^3P state with $(\cos\theta)$ angular dependence about k as an axis. We have

$$I_\rho=-\tfrac{1}{2}ik(\rho_z)_{01}. \quad (5)$$

The matrix element is that of the dipole moment and is well known from the literature.[2] We obtain

$$I_\rho=-\tfrac{1}{2}ik\hbar(8/3\pi M)^{\frac{1}{2}}(\epsilon_0\epsilon_1^3)^{\frac{1}{2}}/(\epsilon_0+\epsilon_1)^2. \quad (6)$$

M is the proton mass, ϵ_0 the binding energy of the deuteron, and ϵ_1 the disintegration energy in state ψ_1.

To get I_p, we note first that the two-dimensional integral

$$\int d\mathbf{r}_{p\perp}K_0(\omega r_{p\perp}/v)\exp i(\mathbf{k}\cdot\mathbf{r}_{p\perp})$$
$$=2\pi/(k_\perp^2+(\omega/v)^2), \quad (7)$$

$\mathbf{k}_\perp$ and $\mathbf{r}_{p\perp}$ being the transverse components of the respective vectors. Also

$$\int_{-L/2}^{L/2}dr_{px}\exp[ir_{px}(k_x-\omega/v)]$$
$$=2\sin[(k_x-\omega/v)L/2]/(k_x-\omega/v). \quad (8)$$

As we let $L\to\infty$, the integral (8) will result in the restriction $k_x-\omega/v=0$, which means that (7) may be replaced by $(2\pi/k^2)$. Finally

$$I_p=4\pi\sin[(k_x-\omega/v)L/2]/k^2(k_x-\omega/v). \quad (9)$$

Now the probability that a transition has taken place is $|A_1|^2$ and the cross section is

$$\sigma=|A_1|^2L^2,$$
$$\sigma d\epsilon_1 d\mathbf{k}d\Omega_1=(16\cdot 8\pi/3L^4)(Ze^2/\hbar v)^2$$
$$\times(\hbar^2/Mk^2)(\epsilon_0\epsilon_1^3)^{\frac{1}{2}}/(\epsilon_0+\epsilon_1)^4$$
$$\times\{\sin^2[(k_x-\omega/v)L/2]/(k_x-\omega/v)^2\}$$
$$\times(L/2\pi)^3d\mathbf{k}d\epsilon_1\{(3/4\pi)\cos^2\gamma\}d\Omega_1.$$

This gives the differential cross section for transition to a state for which the center of gravity propagation vector is in $d\mathbf{k}$, the disintegration energy is in $d\epsilon_1$, and the proton's direction is in $d\Omega_1$. The factor $(L/2\pi)^3$ is necessary to convert the normalization of the wave functions to unit $\mathbf{k}$. The factor $(3/4\pi)\cos^2\gamma$ takes account of the angular distribution of the ejected protons, γ being the angle between $\mathbf{r}_p$ and $\mathbf{k}$.

We are not interested in the $\mathbf{k}$ distribution so we first integrate over that variable. If θ_k is the polar angle of $\mathbf{k}$ and θ_1 is the polar angle of the proton direction (with the x axis as pole), then

$$\int d\mathbf{k}\{\cos^2\gamma\cdot\sin^2[(k_x-\omega/v)L/2]/k^2(k_x-\omega/v)^2\}$$
$$=\tfrac{1}{2}\pi^2L[\tfrac{1}{2}(3\cos^2\theta_1-1)\cos^2\theta_k$$
$$+\sin^2\theta_1\cdot\ln\cos\theta_k]^1_{(\cos\theta_k)\min}. \quad (11)$$

Here the integral over k has been carried out first and the circumstance that $L\to\infty$ guarantees that contributions to this integral are restricted to the point

$$k=\omega/v\cos\theta_k. \quad (12)$$

Thus, when the integral over $\cos\theta_k$ is performed, the variable has a lower limit corresponding to the largest value that k may take; and this lower limit is indicated in (11).

[2] H. Bethe and R. Peierls, Proc. Roy. Soc. **A148**, 146 (1935).

The fact that k is really bounded may be verified by going back to (7). For large k, the integral comes mainly from small values of $r_{p\perp}$, i.e., from small impact parameters. Now in fact, for impact parameters smaller than a certain distance, R_0, the collision has the character of a direct nuclear collision. It is not our purpose to consider such collisions in this paper. We have therefore to restrict the values of $r_{p\perp}$ included to those equal to or greater than R_0. This can be approximately achieved by setting $k_{\max}=(1/R_0)$; this is certainly the right order of magnitude, and any better specification of $k_{\max}$ is made difficult by the somewhat hazy character of the separation between "nuclear" and "electric" collisions. The sensitiveness of the results to the details of the cut-off will be discussed in a later section. Now $\hbar\omega$ is the energy exchange:

$$\hbar\omega=\epsilon_1+\epsilon_0+\hbar^2k^2/4M. \tag{13}$$

The last term, which is the energy in the center of gravity motion, is very small and may be dropped from (13) as far as the determination of the lower limit is concerned. We have

$$(\cos\theta_k)_{\min}=(\epsilon_0+\epsilon_1)R_0/\hbar v=1/\Gamma, \tag{14}$$

R_0 may be taken as the radius of the nucleus plus the radius of the deuteron. The integral (11) becomes

$$\tfrac{1}{2}\pi^2L[\tfrac{1}{2}(3\cos^2\theta_1-1)(1-\Gamma^{-2})+\sin^2\theta_1\cdot\ln\Gamma] \tag{15}$$

and the differential cross section becomes

$$\sigma d\epsilon_1 d\Omega_1=(2/\pi)(Ze^2/\hbar v)^2(\hbar^2/M)\times[(\epsilon_0\epsilon_1^3)^{\frac{1}{2}}/(\epsilon_0+\epsilon_1)^4]d\epsilon_1 d\Omega_1\cdot[\tfrac{1}{2}(3\cos^2\theta_1-1)(1-\Gamma^{-2})+\sin^2\theta_1\cdot\ln\Gamma]. \tag{16}$$

It is instructive to compare this formula with the corresponding one obtained on calculating this process by the method of virtual quanta. In this picture the field of the passing heavy nucleus is replaced by a superposition of quanta; each travelling parallel to the path of the nucleus, and each capable of producing the photoelectric effect in the deuteron if its frequency is sufficiently high.

The calculation results in the formula:

$$\sigma d\epsilon_1 d\Omega_1=(2/\pi)(Ze^2/\hbar v)^2(\hbar^2/M)\times[(\epsilon_0\epsilon_1^3)^{\frac{1}{2}}/(\epsilon_0+\epsilon_1)^4]d\epsilon_1 d\Omega_1\sin^2\theta_1\cdot\ln\Gamma'. \tag{17}$$

The quantity Γ' is identical with Γ above except for a factor $(1-v^2/c^2)^{\frac{1}{2}}$ which appears in the denominator of the former and which makes a negligible difference in the present connection. Otherwise (17) is just the part of (16) that comes from the second term in the bracket. This is to be understood as follows. For the method of virtual quanta to be valid, the velocity must be sufficiently high so that the electric field is essentially transverse and the Poynting flux longitudinal. Now if the Poynting flux in the field of the passing particle is separated into a longitudinal and a transverse part, it can be shown that the total momentum transfer associated with the longitudinal flux is greater than that of the transverse flux by just a factor $\ln\Gamma'$, providing Γ' is large compared to unity. Thus the first term in the bracket of (16), which will be negligible in the limit of large values of Γ, is to be identified with the effect of longitudinal electric fields (transverse Poynting vector). In the case under consideration the two terms are of the same order of magnitude, the important values of Γ being in the range 2 to 3.

The first term gives no contribution to the total cross section, but only affects the angular distribution. We account for this by remarking that a longitudinal electric field cannot by itself break up the deuteron, since it can supply no net impulse. However, it can change the direction of emergence of the ejected protons. In particular it can cause particles to be ejected in the forward direction. Whereas there are no particles in the forward direction for a transverse electric field alone, in the present case of 200 Mev deuterons, the distribution has almost a maximum in the forward direction.

3. TOTAL CROSS SECTION

Integration of (16) over the angles gives for the distribution in ϵ_1:

$$d\epsilon_1=(16/3)(Ze^2/\hbar v)^2(\hbar^2/M)\times[(\epsilon_0\epsilon_1^3)^{\frac{1}{2}}/(\epsilon_0+\epsilon_1)^4](d\epsilon_1)\ln\Gamma. \tag{18}$$

The integration over ϵ_1 is carried out numerically. A value of R_0 of 1.1×10^{-12} cm is chosen, corresponding to the sum of deuteron and nuclear radii for about atomic weight 100. This implies a maximum disintegration energy, $(\epsilon_1)_{\max}$, of about

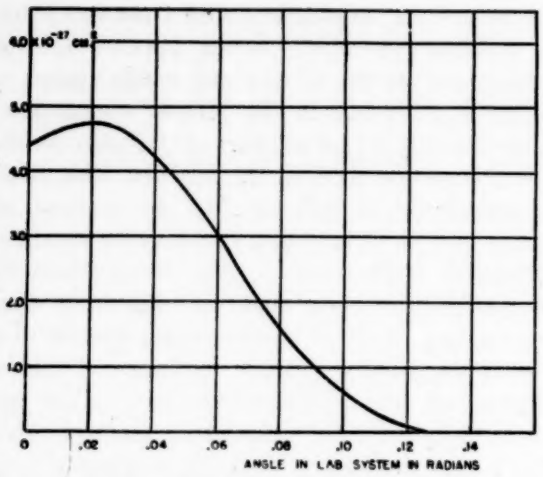

FIG. 1. $N(\theta)$: Angular distribution of emergent neutrons [Number in $d\theta$ is $Z^2N(\theta)d(\cos\theta)$].

5.6 Mev. At this energy, both proton and neutron have very low velocities and the neglect, implied in (1), of all interaction except the instantaneous coulomb interaction, is here justified. The result of the integration for 200 Mev deuterons is

$$\sigma = 2.01\times10^{-29}Z^2 \text{ cm}^2. \tag{19}$$

The same calculation has been carried out for 185-Mev deuterons on U^{238}. For this case the Born approximation is more questionable. It is nevertheless included, since only for large values of Z will the effect discussed here be experimentally prominent. The total cross section becomes

$$\sigma = 1.35\times10^{-29}Z^2 \text{ cm}^2. \tag{19'}$$

The yield is most conveniently expressed by the method of the first reference. For 200-Mev deuterons, $A=100$, the total cross section may also be written

$$\sigma = 0.338Z^2e^4/Mv^2\epsilon_0.$$

This formula gives fairly accurately the variation with energy in the neighborhood of 200 Mev.

If the deuteron traverses material with N atoms/cm³ and loses energy dE by ionization then the yield of the above process in that thickness is

$$\text{Yield in } dE = N\sigma dE/(dE/dx)$$

where

$$dE/dx = (4\pi Ze^4N/mv^2)\ln(2mv^2/I)$$

and m is the electronic mass. I is an average ionization potential of about 80 ev. If we neglect the variation of the logarithm over a small range of velocities, then

$$\text{Yield in } dE = 1.90\times10^{-6}Z\cdot dE/\epsilon_0.$$

Thus the yield per unit energy interval is approximately independent of the energy. If the deuteron loses by ionization an amount ΔE (in Mev), then the yield is

$$\text{Yield } (\Delta E) = 8.72\times10^{-7}Z(\Delta E). \tag{20}$$

The corresponding formula for 185-Mev deuterons, $A=238$ is

$$\text{Yield } (\Delta E) = 5.85\times10^{-7}Z(\Delta E). \tag{20'}$$

4. ANGULAR DISTRIBUTION

We now wish to transform the differential cross section into the laboratory system. We propose to use as independent variables, instead of the ϵ_1, θ_1 of (16), the total kinetic energy and angle of ejection of the proton (or neutron) measured in the laboratory system of coordinates. The Lorentz equations of transformation are

$$\begin{aligned} p\cos\theta &= \gamma^{-1}(p'\cos\theta' - vW/c^2), \\ p\sin\theta &= p'\sin\theta', \\ W &= \gamma^{-1}(-vp'\cos\theta' + W'). \end{aligned} \tag{21}$$

The unprimed system is the laboratory system, the primed system is one moving in the $-x$ direction with the initial velocity v of the deuteron. $\gamma=(1-v^2/c^2)^{-\frac{1}{2}}$. The momenta of the ejected proton in the two systems are p and p'. W and W' are the respective total energies. The polar angles of the momentum vector in the two systems (the $+x$ axis being pole) are θ and θ'.

Since the motions are always non-relativistic in the primed system, we may set

$$W' = Mc^2 + (p')^2/2M.$$

We may also write

$$\mathbf{p}' = \pm\mathbf{p}_1 + \hbar\mathbf{k}/2$$

the first term being the momentum of the proton (or neutron) in the deuteron system, the second being the contribution of the center of gravity momentum. Now

$$p'\cos\theta' = \pm p_1\cos\theta_1 + \tfrac{1}{2}\hbar k\cos\theta_k$$

the angles having been defined in (11). If we

use the relation obtained from (12) and (13),

$$\hbar kv\cos\theta_k=\epsilon_1+\epsilon_0+\hbar^2k^2/4M$$
$$=\epsilon_0+(\hbar^2k^2/4M)+(p_1^2/M). \quad (22)$$

We arrive at the following:

$$W=\gamma^{-1}[Mc^2-\tfrac{1}{2}\epsilon_0$$
$$\pm p_1v\cos\theta_1\mp\hbar(\mathbf{p}_1\cdot\mathbf{k})/2M]. \quad (23)$$

The sum of the energies of proton and neutron in the laboratory system is thus

$$W_p+W_n=(2Mc^2-\epsilon_0)/\gamma \quad (24)$$

which guarantees the covariance of energy in the collision.

Now we can show that the last term in (23) is considerably smaller than any other, and we will neglect it in the following. If we add to the resulting equation the second of (21), the resulting pair is

$$p_1\cos\theta_1=[Mc^2-\gamma W-\tfrac{1}{2}\epsilon_0]/v,$$
$$p_1\sin\theta_1=p\sin\theta. \quad (25)$$

In the second of Eq. (25), the transverse component of $\mathbf{k}$ has been neglected. A numerical study shows that this is valid for the cases under consideration. These may be used to calculate the Jacobian of the transformation from $(\epsilon_1, \cos\theta_1)$ to $(T, \cos\theta)$, T being the kinetic energy of one of the ejected particles: $T=W-Mc^2$. We get

$$d\epsilon_1 d(\cos\theta_1)=dTd(\cos\theta)$$
$$\times\{-4T\cos\theta/v(M\epsilon_1)^{\frac{1}{2}}\}(1+\xi) \quad (26)$$

where $\xi=T_0/2Mc^2$, T_0 being the initial kinetic energy per particle. In obtaining (26) we have for brevity neglected terms of the order $(T-T_0)/Mc^2$ compared to unity, introducing errors of the order of one to two percent.

Since in the present setup the deuteron is incident in the $-x$ direction the angle θ_l that the emergent particle makes with the direction of incidence is the supplement of θ above. If we write $\mu=\cos\theta_l$, then the differential cross section is

$$\sigma dTd\mu=4(Ze^2/\hbar v)^2(\hbar^2/M)$$
$$\times[(\epsilon_0\epsilon_1^3)^{\frac{1}{2}}/(\epsilon_0+\epsilon_1)^4]dTd\mu(4T\mu/v(M\epsilon_1)^{\frac{1}{2}})$$
$$\times(1+\xi)[\tfrac{1}{2}(3\cos^2\theta_1-1)(1-\Gamma^{-2})$$
$$+\sin^2\theta_1\cdot\ln\Gamma] \quad (27)$$

where

$$\epsilon_1=2T(1-\mu^2)(1+\xi)$$
$$+((1+3\xi)/2T_0)(T_0-T-\tfrac{1}{2}\epsilon_0)^2,$$
$$\cos\theta_1=[(T_0-T-\epsilon_0/2)/(2\epsilon_1T_0)^{\frac{1}{2}}](1+\tfrac{3}{2}\xi).$$

Equation (27) has been integrated numerically. Figure 1 shows the angular distribution of all neutrons (or protons) regardless of energy, and Fig. 2 shows the energy distribution integrated over all angle. Both figures are for 185-Mev deuterons on U^{238}.

Graphical integration to get the total cross section from Figs. 1 or 2 yields a value of 1.31×10^{-29} cm^2 which is in reasonable agreement with the value of 1.35×10^{-29} cm^2 found by staying in the deuteron system. The remaining discrepancy is due to the neglect of the center of gravity recoil at several points.

Angle-energy distributions were also derived for the case of 200-Mev deuterons, $A=100$. There are no significantly different features from the case presented in the figures. Again the total cross section checks the value previously obtained.

5. DISCUSSION OF CUT-OFF PROCEDURE

The numerical results obtained here are to some extent sensitive to the details of the cut-off applied to the coulomb potential at the nuclear radius (or to the momentum transferred to the center of gravity of the deuteron. See Eq. (14) and preceding.). The procedure employed above

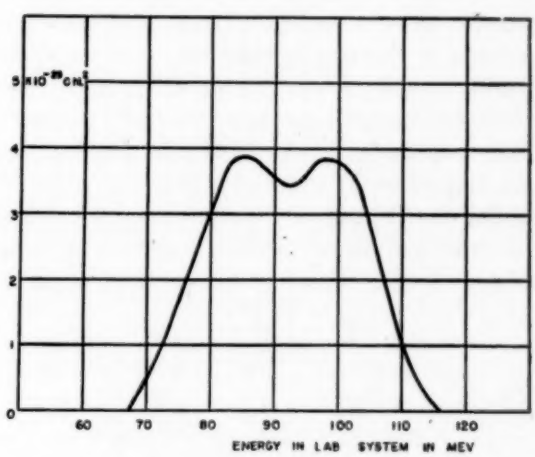

FIG. 2. $N(E)$: Energy distribution of emergent neutrons [Number in dE is $Z^2N(E)d(E/T_0)$, where $T_0=92.5$ Mev].

of cutting off the momentum transfer is equivalent to replacing the singular coulomb potential by one identical with it except for having deleted from it all spatial fourier components with wave number $>(1/R_0)$. In this way it was hoped to calculate only the effect of the acceleration experienced outside R_0 and to omit all effects concerned with the direct nuclear collision. An alternative procedure is to make the cut-off in configuration space, permitting the potential to keep its coulomb shape down to R_0, then flattening it out for smaller separation. The resulting spectrum of fourier components does not end abruptly at $(1/R_0)$ but contains also higher wave numbers whose intensity depends on the precise shape of the fictitious potential. For example, if the potential is taken to be constant inside R_0, the spectrum of components above $(1/R_0)$ is of some importance, due to the kink in the potential at the point R_0. An estimate of the results that would be obtained with this model indicates that the total cross section for 185-Mev deuterons on uranium would be increased from $1.35\times10^{-29}Z^2$ cm^2 to $2.5\times10^{-29}Z^2$ cm^2 the estimate of the latter number being good to about 15 percent. At the same time the angular distribution would be modified since the large angle scattering processes are somewhat more dependent on the high fourier components than are the small angle processes. Thus the half angle would be increased from 4.05°, as on Fig. 1, to 4.4°.

On the other hand, if the fictitious potential is cut off in a smooth way inside R_0, without the introduction of a kink, the results are very little different from those previously calculated on the basis of the momentum cut-off. On physical grounds, such a smooth model seems more reasonable for the purpose of this calculation.

The point is mentioned because a comparison with experiment seems to indicate that the angular distribution of Fig. 1 (when compounded with the curve of Serber for the stripping process) is too narrow to agree with observation. The use of the "flat" cut-off would leave the discrepancy almost as large. Although from a theoretical point of view the question still contains the uncertainty mentioned above, the extent of this uncertainty seems much too small to permit a hope of reconciling the calculations with observation.

6. CONCLUSIONS

Electric disintegration of 200-Mev deuterons occurs with fairly high probability. For example, in a target with $Z=40$, the disintegration cross section is 3.2×10^{-26} cm^2. The products are widely spread in energy, values of 80 Mev up to 120 Mev occurring with prominence. The resultant neutron or proton beam is well collimated, having a half width at half maximum of slightly over 4°.

The electric disintegration is to be compared in importance with the disintegration involving a direct nuclear collision in which one of the particles collides with the nucleus while the other escapes (shearing). Assuming that the deuteron is so energetic as to be undeflected by the coulomb field, and assuming also that the average proton-neutron separation, ρ, is small compared to the nuclear radius, a, the cross section for the shearing process is $(\pi a\rho/4)$. This is considerably larger than that for the electric process, except for very high Z. For uranium, the processes should be of comparable importance (although the formulae used above to estimate the cross sections for the two processes can hardly be quantitatively trustworthy for so large a nuclear charge). A detailed discussion of the shearing process will be given by Serber, to whom thanks are due for critical discussions of the problems treated above.

This work was carried out in part under the auspices of the Manhattan District at the Radiation Laboratory, University of California.

Effect of Nuclear Motion of the Hyperfine Structure of the Ground Term of Hydrogen

G. BREIT AND R. E. MEYEROTT
Yale University, New Haven, Connecticut*

(Received August 19, 1947)

The correction factor for the effect of nuclear motion on the hyperfine structure of hydrogen is discussed. It is found that this factor can be represented by $(1+m/M)^{-3}$ to within terms of order $(m/M)\alpha^2 \log\alpha$, where m, M are, respectively, the masses of the electron and nucleus while α is the fine structure constant. It is assumed that the Coulomb potential is that of a point charge for distances greater than $r_0=e^2/mc^2$ and that for distances smaller than r_0 it is of the order mc^2. This assumption makes it possible to treat the problem by means of existing theories. First-order perturbation theory for the effect of the nuclear magnetic field is employed. The reasons for doing the work are explained in the introduction. The calculations for the part of the proton's magnetic moment following from Dirac's equation are described in Section II. Section III is concerned with the effect of the part of the magnetic moment of the proton which is not accounted for by Dirac's equation and is referred to as the Pauli part. The deuteron is also discussed in Section III.

I. INTRODUCTION

THE recent results[1] on the hyperfine structure of hydrogen make it desirable to make sure of the correction for the nuclear mass motion to the theoretically expected formula for the hyperfine structure splitting. Fermi's result[2] for the energy splitting of s terms of single-electron spectra for a stationary nucleus is proportional to the product of the magnetic moments of the electron and the nucleus and contains besides, as a factor, the square of the non-relativistic Schrödinger function at the stationary nucleus $\psi_S^2(0)$. The latter quantity has the dimensions of the cube of a reciprocal length. Together with the product of the magnetic moments it gives a dimensionally correct combination for the expression of an energy. The quantity $\psi_S^2(0)$ is for hydrogen $1/\pi a_H^3 n^3$, where a_H is the Bohr radius. Its appearance suggests that to within a constant factor it replaces the mean of the reciprocal electron-nucleus distance and that for a nucleus of finite rather than infinite mass the formula for the energy splitting has to be modified by the introduction of the factor

$$(1+m/M)^{-3},$$

which represents the reciprocal of the cube of the ratio of the spatial extension of the wave function for finite and infinite mass. Here m, M stand, respectively, for the masses of the electron and the nucleus. It is in fact well-known that for the non-relativistic quantum-mechanical two-body problem the unnormalized wave function is obtainable from that of the one-body problem of mass m with $M=\infty$ by stretching a graph of the latter in such a way as to increase all interparticle distances in the ratio $1+m/M$, which is the reciprocal of the corresponding ratio of reduced masses.

The above simple arguments make it plausible to assume that the inverse cube of the reduced mass ratio represents the correction factor to Fermi's formula apart from typically relativistic corrections.[3] A partial confirmation of this view has been obtained previously in connection with estimates of the magnetic energy contribution to the binding energy of the deuteron and is referred to below in connection with Eq. (6.1) of the present paper. It was found that the non-relativistic limit for this energy is obtained by employing Fermi's formula with the interpretation of $\psi_S^2(0)$ as the square of the non-relativistic Schrödinger function for the relative motion of proton and neutron. By the non-relativistic limit one means here the asymptotic form in the limit $c=\infty$, where c is the velocity of light.

The arguments given above are not as con-

*Assisted by Contract N6ori-44, Task Order XVI of the Office of Naval Research.

[1] J. E. Nafe, E. B. Nelson, and I. I. Rabi, Phys. Rev. 71, 914 (1947).

[2] E. Fermi, Zeits. f. Physik 60, 320 (1930).

[3] G. Breit, Phys. Rev. 35, 1447 (1930).

vincing, however, as is desirable. The accuracy of the experiments at Columbia is very high, and there is a need for a careful analysis of the effects neglected in the inverse cube of reduced mass-correction factor. The arguments for the employment of this factor have, in fact, a number of defects. In the first place the mean of the inverse cube of the interparticle distance diverges in the non-relativistic limit for s terms. The simple argument based on the similarity transformation which has been given above is, therefore, not correct even though there is no doubt that it has something to do with the true state of things. Secondly, the considerations concerning the magnetic energy of proton and neutron in the deuteron have to do only with the special case of particles of equal masses. Besides, they have been carried out on the assumption that the interaction energy between the proton and neutron is of a non-singular type. Characteristic effects of the inverse-square field of force might have been overlooked. Thirdly, the order of magnitude of what is neglected in the $(1+m/M)^{-3}$ correction factor has not been previously estimated.

The calculations reported on below are reassuring concerning the validity of the simple correction factor. They show that the effects neglected are of the order $(m/M)\alpha^2 \log\alpha$, where α is the fine structure constant. In obtaining this result it was assumed that the nucleus has a finite radius of the order e^2/mc^2, where e is the electronic charge. For distances smaller than this amount the inverse-square law potential was supposed to be inapplicable. The calculations would have failed if the inverse-square law of force were supposed to apply at all distances. Some of the integrals entering the answer would have diverged logarithmically. The starting point for the calculation would also be an uncertain one if the assumption of a finite radius were not made. By making the potential finite rather than infinite at small distances the velocity of the nucleus is kept small, and the discussion by means of a Hamiltonian of known type is possible.

II. EFFECT FOR PROTON OBEYING DIRAC'S EQUATION

A. General Assumptions

The wave equation will be taken to be

$$(p_0+\boldsymbol{\alpha}_e\mathbf{p}_e+\boldsymbol{\alpha}_M\mathbf{p}_M+\beta_e mc+\beta_M Mc-Y/c)\psi=0, \quad (1)$$

where

ψ = 16 component wave function ψ_{ab}; $(a, b) = 1, 2, 3, 4$.

$p_0=-\hbar\partial/ic\partial t+e^2/cr$.

$Y=(e^2/2)[(\boldsymbol{\alpha}_e\boldsymbol{\alpha}_M)/r+(\boldsymbol{\alpha}_e\mathbf{r})(\boldsymbol{\alpha}_M\mathbf{r})/r^3]$.

$\boldsymbol{\alpha}_e=(\alpha_{ex}, \alpha_{ey}, \alpha_{ez})$ = vector having for components direct products of the first three Dirac matrices for the electron index, a, and a unit matrix for the proton index b; the original representation of Dirac is used here so that the parts of α_{ex}, α_{ey} referring to the subscript a have, respectively, elements 1, 1, 1, 1 and $-i, i, -i, i$ on the diagonal perpendicular to the principal diagonal starting at the upper right-hand corner.

$\boldsymbol{\alpha}_M$ = vector having for components the first three Dirac matrices for proton index b; conventions followed for $\boldsymbol{\alpha}_M$ are similar to those for $\boldsymbol{\alpha}_e$, reversing a with b and the words proton and electron.

β_e = matrix diagonal in b and operating on a as Dirac's α_4; the representation is such that the only non-vanishing matrix elements of α_4 are on the principal diagonal and have the values 1, 1, -1, -1 starting at the upper left-hand corner.

β_M = matrix diagonal in a, operating on b as Dirac's α_4; the conventions regarding representation are like those for β_e.

m = electron mass.

M = proton mass.

e = electronic charge—a positive number.

c = velocity of light.

$\mathbf{p}_e=(\hbar/i)(\partial/\partial x_e, \partial/\partial y_e, \partial/\partial z_e)$.

$\mathbf{p}_M=(\hbar/i)(\partial/\partial x_M, \partial/\partial y_M, \partial/\partial z_M)$.

$\mathbf{r}_e=(x_e, y_e, z_e)$ = electron coordinates.

$\mathbf{r}_M=(x_M, y_M, z_M)$ = proton coordinates.

r = distance between nucleus and electron.

It is convenient to list at this stage the meaning of some of the symbols which are introduced later in this paper as well.

α = fine structure constant $e^2/\hbar c$.

ψ_S = non-relativistic Schrödinger function.

$\psi_S(0)$ = value of ψ_S for $r=0$.

$\mu_0=e\hbar/2mc$ = electronic Bohr magneton.

$\mu_{0M}=e\hbar/2Mc$ = nuclear Bohr magneton.

$\mathbf{J}\hbar$ = angular momentum of relative motion.

$\rho=(1-\alpha^2)^{\frac{1}{2}}$.

R.P. stands for the real part of quantity to the right of symbol R.P.

Equation (1) is only approximate. Arguments previously[4] discussed show that it is a good equation to within the order v^2/c^2, where v stands for the velocity of either particle. The velocity of the electron is, of course, large when it is close to the proton and in the corresponding region of configuration space the validity of Eq. (1) may be questioned. It is clear, however, that the error introduced by this effect can be made to be vanishingly small by making M very large, because the effect of high electron velocity is represented in a relativistically consistent and supposedly correct manner by Dirac's equation for an electron subject to the action of an electromagnetic field.

The term in Y represents the combined effect of the magnetic interaction between the particles and the correction to the electrostatic interaction owing to the finiteness of the velocity of light. It will be omitted at first, and its effect will be taken into account later by means of a first-order perturbation calculation. Omitting the term in $-Y/c$, one finds from Eq. (1) that

$$\begin{aligned}(p_0+Mc+\boldsymbol{\alpha}_e\mathbf{p}_e+\beta_e mc)\Phi+(\boldsymbol{\sigma}_M\mathbf{p}_M)\Psi=0,\\(p_0-Mc+\boldsymbol{\alpha}_e\mathbf{p}_e+\beta_e mc)\Psi+(\boldsymbol{\sigma}_M\mathbf{p}_M)\Phi=0,\end{aligned}\tag{1.1}$$

where Ψ and Φ are 8-component wave functions obtained from ψ by restricting the proton index b in ψ_{ab} to the values 3, 4, in the case of Ψ, and to the values 1, 2 in the case of Φ. In the notation employed from Eq. (1.1) on the rows corresponding to $b=1, 2$ are arranged to have the same position and order in Φ as the rows corresponding to $b=3, 4$ have in Ψ. The vectors $\boldsymbol{\sigma}_M$ have for components matrices which are direct products of unit matrices in the electron index a and Pauli matrices in the proton index. The operator $\mathbf{p}_e+\mathbf{p}_M$ represents the total momentum. It commutes with the Hamiltonian which corresponds to Eq. (1) whether one neglects Y or not. It is, therefore, possible to confine the discussion to such ψ that

$$(\mathbf{p}_e+\mathbf{p}_M)\psi=0.\tag{1.2}$$

It follows from the last equation that every ψ_{ab} is a function only of the relative coordinates

$$x=x_e-x_M,\quad y=y_e-y_M,\quad z=z_e-z_M,\tag{1.3}$$

and is independent of the centroid coordinates $(m\mathbf{r}_e+M\mathbf{r}_M)/(m+M)$. Consequently, one has also

$$(\mathbf{p}_e+\mathbf{p}_M)\Psi=0,\quad (\mathbf{p}_e+\mathbf{p}_M)\Phi=0.\tag{1.4}$$

Because of Eq. (1.3), the relative momentum operator,

$$\mathbf{p}=(h/i)(\partial/\partial x,\ \partial/\partial y,\ \partial/\partial z),\tag{1.5}$$

has the property

$$\mathbf{p}\Psi=\mathbf{p}_e\Psi,\quad \mathbf{p}\Phi=\mathbf{p}_e\Phi.\tag{1.6}$$

For states of definite total energy E one has

$$cp_0=E+e^2/r=(M+m)c^2+\epsilon+e^2/r,\tag{1.7}$$

where ϵ is the energy of the system in excess of the sum of the rest mass energies of the two particles. In view of Eq. (1.6), one may replace $\mathbf{p}_e$ in Eq. (1.1) by $\mathbf{p}$, and, similarly, on account of Eq. (1.4) one may replace $\mathbf{p}_M$ in Eq. (1.1) by $-\mathbf{p}$. From now on the subscript e will be dropped in α_e and β_e. The first line in Eq. (1.1) is used next to express Φ in terms of Ψ. Substitution of the result into the second line gives

$$(p_0-Mc+\boldsymbol{\alpha}\mathbf{p}+\beta mc-A/c)\Psi=0,\tag{2}$$

where

$$A=c(\boldsymbol{\sigma}_M\mathbf{p})(p_0+Mc+\boldsymbol{\alpha}\mathbf{p}+\beta mc)^{-1}(\boldsymbol{\sigma}_M\mathbf{p}).\tag{2.1}$$

Denoting by the sign † the conjugate transposed of a matrix one finds also

$$\begin{aligned}\Phi^\dagger\Phi=\Psi^\dagger(\boldsymbol{\sigma}_M\mathbf{p})\\\times(p_0+Mc+\boldsymbol{\alpha}\mathbf{p}+\beta mc)^{-2}(\boldsymbol{\sigma}_M\mathbf{p})\Psi.\end{aligned}\tag{2.2}$$

Since $p_0\Psi\sim Mc\Psi$, one finds that through most of the configuration space

$$\Phi^\dagger\Phi\cong\Psi^\dagger(p^2/4M^2c^2)\Psi\cong\alpha^2(m/2M)\Psi^\dagger\Psi,\tag{2.3}$$

where α is the fine-structure constant. The factor multiplying $\Psi^\dagger\Psi$ in Eq. (2.3) is of the order of 1.5×10^{-8}. The effect of Φ on the normalization integral may be neglected therefore. Calculations with Eq. (2) may be carried on accordingly without reference to Φ. The

[4] G. Breit, Phys. Rev. **34**, 553 (1929); Phys. Rev. **36**, 383 (1930); Phys. Rev. **39**, 616 (1932).

operator A of Eq. (2.1) is expanded by means of

$$(p_0+Mc+\alpha\mathbf{p}+\beta mc)^{-1}$$
$$=(p_0+Mc)^{-1}-(p_0+Mc)^{-1}(\alpha\mathbf{p}+\beta mc)$$
$$\times(p_0+Mc)^{-1}+(p_0+Mc)^{-1}$$
$$\times[(\alpha\mathbf{p}+\beta mc)(p_0+Mc)^{-1}]^2+\cdots. \quad (2.4)$$

In view of the fact that $(\alpha\mathbf{p}+\beta mc)\Psi$ is of the order $mc^2\alpha^2\Psi$, the second term in the above expansion is of the order $m\alpha^2/M$ of the first, and the third term is of the order $m\alpha^2/M$ of the second. The contributions to the energy arising from the first term are of the order of the non-relativistic effect of the nuclear motion, those arising from the second term are still of interest for the hyperfine structure being of the order

$$(e^2/2a_H)(m/M)^2\alpha^2\sim 0.5\times 10^{-5}\ \text{cm}^{-1}.$$

The third term is of the order 10^{-13} cm^{-1} and may be neglected. In view of the fact that the second term in Eq. (2.4) is on the limit of what is of interest it will be taken account of at the end of the calculation, and it will be neglected at first. The consideration of the first and main term in Eq. (2.4) has to be carried out in more detail, however. One has

$$c(\sigma_M\mathbf{p})(p_0+Mc)^{-1}(\sigma_M\mathbf{p})=c(p_0+Mc)^{-1}p^2$$
$$-\hbar^2(e^2/r^3)(p_0+Mc)^{-2}(r\partial/\partial r)+A_1, \quad (2.5)$$

where

$$A_1=(he^2/r^3)(p_0+Mc)^{-2}[\mathbf{r}\times\mathbf{p}]\cdot\sigma_M. \quad (2.6)$$

The term A_1 is the analog of the Thomas term. If the Thomas terms were appreciable, complications would arise. An estimate of the effect of A_1 will be made, therefore, at this stage. The estimate may be carried out in the approximation of neglecting nuclear motion. One finds that in the state in which the proton spin and the electronic angular momentum are parallel, the expectation value of A_1 is

$$\langle A_1\rangle\cong(\pi m/3M)\alpha^2(eh/mc)(eh/Mc)\psi_S^2(0). \quad (2.7)$$

The intermediate steps leading to this formula are straightforward and are omitted. The contribution to the hyperfine-structure separation arising from the operator A_1 is 4 times the value of $\langle A_1\rangle$ given in Eq. (2.7) and is thus

$$(16\pi m/3M)\alpha^2\mu_0\mu_{0M}\psi_S^2(0).$$

This is $m\alpha^2/2M\cong 1.5\times 10^{-8}$ times the hyperfine structure splitting

$$(32\pi/3)\mu_0\mu_{0M}\psi_S^2(0),$$

which is expected according to Fermi's formula. The effect of A_1 is seen to be negligible, and it will be omitted below.

By means of Eqs. (2), (2.1), (2.5), and with the omission of A_1 as well as of the second term in Eq. (2.4), one obtains

$$[p_0-Mc+\alpha\mathbf{p}+\beta mc-(p_0+Mc)^{-1}p^2$$
$$+\hbar^2(e^2/cr^2)(p_0+Mc)^{-2}\partial/\partial r]\Psi=0. \quad (3)$$

A special solution is found by arranging for Ψ to be the direct product of the function for index b, which corresponds to $\binom{1}{0}$ upward orientation of the proton spin and of a column matrix in the index a having elements depending on angles in the same way as for Dirac's equation in a central field for upward orientation of the electronic angular momentum. The non-vanishing components of Ψ are then

$$\Psi_{1,1}=izf/r, \quad \Psi_{2,1}=i(x+iy)f/r, \quad \Psi_{3,1}=g.$$

Substitution into Eq. (3) shows that it suffices to satisfy the radial equations

$$(p_0-Mc-mc)g$$
$$+\frac{\hbar^2 d}{r^2dr}\left(\frac{r^2}{p_0+Mc}\frac{dg}{dr}\right)+\frac{\hbar}{r^2}\frac{d(r^2f)}{dr}=0,$$
$$(p_0-Mc+mc)f \quad (3.1)$$
$$+\frac{\hbar^2}{r^2}\frac{d}{dr}\left(\frac{r^2}{p_0+Mc}\frac{df}{dr}\right)-\frac{hdg}{dr}=0.$$

The angles and spin orientations have been eliminated at this stage and only the radial motion has been left. The possibility of separating variables in this manner is not unexpected. It is, in fact, readily verified that the Hamiltonian

$$H_0=-e^2/r-c(\alpha_e\mathbf{p}_e)$$
$$-c(\alpha_M\mathbf{p}_M)-\beta_e mc^2-\beta_M Mc^2 \quad (3.15)$$

commutes with the total angular-momentum components. Thus, for instance,

$$[H_0, xp_y-yp_x+\hbar(\sigma_{ex}+\sigma_{Mx})/2]\psi=0 \quad (3.16)$$

for any ψ satisfying Eq. (1.2). In this equation σ_{ex}, σ_{Mx} are the x components of the Dirac 4-row matrix vectors σ_e, σ_M, referring to the electron and proton. The original Eq. (1), with Y omitted, can be satisfied, therefore, by a wave function for which the total momentum is zero and for which also the z component as well as the square of the total angular momentum can have eigenvalues. It will be noted that the orbital angular momentum entering the problem is that of relative motion and that the elimination of Φ does not spoil the validity of the conservation of angular momentum.

If M is made to approach ∞ in Eq. (3.1), and if p_0 is expressed in terms of ϵ by means of Eq. (1.7), the radial equations become identical with corresponding radial equations for Dirac's electron in a central field, and aside from questions connected with the polarization of a vacuum they are the correct equations for an electron in the field of a point charge within the limitations of present day theory.

It has been shown by Bechert and Meixner,[5] and by Lowen,[6] that the effect of nuclear motion on the energy is not changed by relativistic effects within the first-order correction terms of order m/M. It is to be expected, therefore, that the main effect of m/M on the wave function is that of changing the linear scale, since this is its effect for the non-relativistic Schrödinger wave function ψ_S.

The Schrödinger radial equation is obtained by replacing the quantity p_0+Mc occurring in the first line of Eq. (3.1) by $2Mc$ expressing f as approximately $(\hbar/2mc)dg/dr$ by means of the second line and substituting this value of f into the first line. One obtains in this way

$$\left(\epsilon_S+\frac{e^2}{r}\right)\psi_S+\frac{\hbar^2}{2}\left(\frac{1}{m}+\frac{1}{M}\right)\frac{d(r^2d\psi_S/dr)}{r^2dr}=0, \quad (3.2)$$

which is the non-relativistic Schrödinger equation. The largest error in this reduction is introduced by the replacement of $(p_0-Mc+mc)f$ by $2mcf$, when f is solved for in terms of g. The fractional error introduced into f is of the order $(\epsilon+e^2/r)/(2mc^2)$, and this is of the order $\alpha^2/4$ for large r. At the turning point of the Bohr orbit the error vanishes. For sufficiently small r the fractional error becomes large, but for $r\sim a_H/10$ the fractional error in f is still of the order 10^{-4}. For smaller distances the fractional error in f introduced by the approximation used here increases, and one cannot claim that this approximation is good enough on the grounds of numerical smallness of the effect everywhere. On the other hand, it is readily verified that if $M=\infty$ the approximation made in approximating f by $(\hbar/2mc)dg/dr$ is harmless and can be taken care of by the correction factor to hyperfine structure splitting having the value

$$[2(1-\alpha^2)-(1-\alpha^2)^{\frac{1}{2}}]^{-1}\cong 1+3\alpha^2/2, \quad (3.3)$$

which has to be taken into account for large atomic numbers[3] but is negligible for hydrogen. This correction factor arises as the quotient of the exact and approximate value of

$$\int_0^\infty fgdr. \quad (3.4)$$

The approximate value of the integral being obtained by replacement of g by ψ_S and of f by $(\hbar/2mc)d\psi_S/dr$. The order of magnitude of the correction factor is what one would estimate from the fact that the average value of e^2/r is -2ϵ and that $\epsilon\sim -mc^2\alpha^2/2$. The value of the correction factor cannot be correctly estimated in this manner, however, because the function g is only approximately represented by ψ_S. Aside from the normalization factor, this difference consists only in the presence of an extra factor,

$$r^{\rho-1}\cong r^{-\alpha^2/2}; \quad \rho=(1-\alpha^2)^{\frac{1}{2}},$$

in g, which results again in effects of order α^2.

The smallness of the difference between the correction factor Eq. (3.3) and unity has just been explained for $M=\infty$. The corresponding correction factor for $M\neq\infty$ will be studied next. It will be found in connection with Eqs. (5.5) that the radial integrals needed for the evaluation of the expectation value of Y are of the form listed in Eq. (3.4). The examination of the

[5] K. Bechert and J. Meixner, Ann. d. Physik **22**, 525 (1935).
[6] I. S. Lowen, Phys. Rev. **51**, 190 (1937).

radial equations will be made first, and the reduction of the expectation value to radial integrals will follow.

B. Orientation Regarding Radial Functions by the Ritz Method

Expressing energy in units $mc^2\alpha^2$, and length in $a_H=\hbar^2/me^2=$ Bohr radius, one obtains in place of Eq. (3.1)

$$\alpha\left(\epsilon+\frac{1}{r}\right)g+\frac{d(r^2f)}{r^2dr}+\alpha\frac{d}{r^2dr}\left[\frac{r^2dg/dr}{2/\beta+1+\alpha^2(\epsilon+1/r)}\right]=0, \tag{3.5}$$

$$\left[1+(\alpha^2/2)\left(\epsilon+\frac{1}{r}\right)\right]f-\frac{\alpha dg}{2dr}+\frac{\alpha^2 d}{2r^2dr}\left[\frac{r^2df/dr}{2/\beta+1+\alpha^2(\epsilon+1/r)}\right]=0,$$

where

$$\beta=m/M\ll 1. \tag{3.6}$$

These equations can be derived from the variational equation

$$\delta\int_0^\infty\{\tfrac{1}{2}[1+(\alpha^2/2)(\epsilon+1/r)]f^2-(\alpha/2)fdg/dr+(\alpha^2/4)(\epsilon+1/r)g^2-(\alpha^2/4)[(df/dr)^2+(dg/dr)^2]/[(2/\beta+1+\alpha^2(\epsilon+1/r)]\}r^2dr=0. \tag{3.7}$$

The smallness of $\alpha^2\epsilon$, in comparison with $2/\beta$, allows the replacement of ϵ by ϵ_S in the last term and the restatement of the variational equation for the ground state in the form

$$-\alpha^2\epsilon\int_0^\infty(f^2+g^2)r^2dr=\int_0^\infty\{(2+\alpha^2/r)f^2+\alpha^2g^2/r-2\alpha fdg/dr-\alpha^2[(df/dr)^2+(dg/dr)^2]/[(2/\beta)+1+\alpha^2(\epsilon_S+1/r)]\}r^2dr, \tag{3.8}$$

$$(\epsilon+\alpha^{-2})^2=\text{minimum}. \tag{3.9}$$

Minimizing the energy gives $\epsilon=-\infty$. This is a consequence of the existence of negative energy states. The problem is stated, therefore, in the form of minimizing the square of the energy.

The minimum of $(\epsilon+\alpha^{-2})^2$ for $M=\infty$ is $(1-\alpha^2)\alpha^{-1}$ and corresponds to the normal state of hydrogen.

By means of the variational equation the best values of the parameters A, σ, γ will now be determined for the trial functions

$$g=r^\sigma e^{-\gamma r},\quad f=Ar^\sigma e^{-\gamma r}, \tag{4}$$

by the Ritz method. One has

$$\int_0^\infty g^2r^2dr=A^{-2}\int_0^\infty f^2r^2dr=(2\gamma)^{-2\sigma-3}\Gamma(2\sigma+3), \tag{4.1}$$

and, similarly, the other needed integrals are readily obtained. One finds

$$1+\alpha^2\epsilon=(1-A^2)/(1+A^2)-\gamma[\alpha^2+2\alpha A/(1+A^2)]/(\sigma+1)+\alpha^2\beta\gamma^2/(2+\beta)(2\sigma+1), \tag{4.2}$$

where the approximation

$$(2/\beta)+1+\alpha^2(\epsilon_S+1/r)\cong(2/\beta)+1 \tag{4.21}$$

has been made in the last term of the integral on the right side of Eq. (3.8). Minimizing the square of the energy with respect to γ, A and σ in accordance with Eq. (3.9), one obtains, respectively,

$$\alpha^2+2\alpha A/(1+A^2)=2\alpha^2\beta\gamma(\sigma+1)/(2+\beta)(2\sigma+1), \tag{4.22}$$

$$2A+\alpha\gamma(1-A^2)/(1+\sigma)=0, \tag{4.23}$$

$$\alpha^2+2\alpha A/(1+A^2)=2\alpha^2\beta\gamma(\sigma+1)^2/(2+\beta)(2\sigma+1)^2. \tag{4.24}$$

From Eqs. (4.22) and (4.24) it follows that $\sigma=0$, and the solution of the remaining two independent relations gives

$$A=-\alpha\gamma/2+\alpha^3/8(1+\beta)^3+\cdots, \tag{4.3}$$

$$\gamma=1/(1+\beta)+\alpha^2/2+\cdots, \tag{4.31}$$

where the quantities A, γ are being represented in descending powers of $1+\beta$. It is seen that if A and γ are approximated by the first term in

the expansions on the right side of Eqs. (4.3), (4.31), the error introduced into the radial integral in Eq. (3.4) is of the order $\alpha^2\beta$ which may be neglected. It is natural that the adjustment of σ to the best value gives $\sigma=0$ rather than $-\alpha^2/2$ because the Ritz method is not sensitive to errors of the wave function close to $r=0$. It is this region that is responsible for the occurrence of the exponent $-\alpha^2/2$. On the other hand, the presence of the factor $\exp[-(\alpha^2/2)\ln r]$ in the wave function produces an error of the order of 10^{-4} in the density as r changes by a factor $2.72^2=7.4$. It is, therefore, natural to expect that the integral of Eq. (3.4), as well as the variational principle expressions for the energy, are not sensitive to the difference between $\sigma=0$ and $\sigma=-\alpha^2/2$. That the integral is not sensitive to this difference has been shown in connection with Eq. (3.3).

In view of the lack of sensitivity of the variational principle to σ, the question arises regarding the error introduced by the failure of Eqs. (4.3), (4.31) to reproduce correctly the wave function close to $r=0$ for $M=\infty$. An estimate of the error can be made by assigning to σ the value $-\alpha^2/2$ and adjusting γ and A by the Ritz method by means of Eqs. (4.22), (4.23). It is then found that A, γ have values A_σ, γ_σ given by

$$A_\sigma=-(\alpha\gamma/2)[1-\sigma-\alpha^2/4(1+\beta)^2+\cdots], \quad (4.32)$$

$$\gamma_\sigma=1/(1+\beta)-\beta\alpha^2/(1+\beta)^2+\cdots. \quad (4.33)$$

The second term of the formula for γ_σ is negligible compared with the first. The term $-\sigma$ on the right side of Eq. (4.32) changes A_σ by one part in 30,000 and is the largest correction. From the point of view of over-all adjustment by the Ritz method, with the three parameters which have been used above, the radial integral which matters for hyperfine structure is seen to be stable to within fractional errors of order α^2.

The answer just obtained for the radial integral by the variational method leads to a correction factor involving the cube of the ratio of the electronic and reduced mass ratios. Considerations will be given next, however, which show that the form of the wave function assumed in Eq. (4) is not sufficiently flexible and that a more accurate solution modifies the result for the wave function without affecting, however, the radial integrals that are important for hyperfine structure.

For larger r the last term in the second Eq. (3.5) can be neglected, and the equation just mentioned yields then an expression for f in terms of g which, when substituted into the first of the two Eqs. (3.5), gives a second-order equation in one variable g. In this one can replace the denominator $2/\beta+1+\alpha^2(\epsilon+1/r)$ by $2/\beta$ for $r>\alpha^2$ and even for smaller r. Replacing g by

$$G=rg, \quad (4.4)$$

one has

$$\frac{d^2G}{dr^2}+\frac{P'(r)}{P(r)}\frac{dG}{dr}+\left[\frac{\epsilon+1/r}{P(r)}-\frac{P'(r)}{rP(r)}\right]G=0, \quad (4.5)$$

where

$$P(r)=1/(A+\alpha^2/r)+1/(B+\alpha^2/r), \quad (4.51)$$

$$P'(r)=\alpha^2r^{-2}[(A+\alpha^2/r)^{-2}+(B+\alpha^2/r)^{-2}], \quad (4.52)$$

$$A=2+\alpha^2\epsilon, \quad B=2/\beta+\alpha^2\epsilon. \quad (4.53)$$

Equation (4.5) can be discussed by standard methods. The term in the first derivative can be removed by the transformation

$$G=v/[P(r)]^{\frac{1}{2}}, \quad (4.54)$$

and it is found from the differential equation satisfied by v that the asymptotic form of v is a constant multiple of

$$r^n\exp(-\gamma r), \quad (4.55)$$

where

$$\gamma^2\cong-2\epsilon(1+\beta)^{-1}(1+\alpha^2\epsilon/2), \quad (4.56)$$

and

$$n\cong[(1+\beta)^{-1}+\alpha^2\epsilon]/\gamma. \quad (4.57)$$

Equations (4.54), (4.55), (4.56), and (4.57) determine the asymptotic value of the logarithmic derivative of g for large r.

C. Perturbation Calculation of the Radial Functions

The calculation of g will next be made by determining first its logarithmic derivative. The latter will be found by means of a perturbation calculation in which the radial equations for $\beta=0$ serve as the reference point. The logarithmic derivative

$$y=dG/Gdr \quad (4.6)$$

is expressed in terms of

$$y_0 = dG_0/G_0 dr \tag{4.61}$$

as

$$y = y_0 + \delta y. \tag{4.62}$$

It is found from the second-order differential equation by first converting to the Riccati type of equation in y and then introducing the integrating factor corresponding to the terms linear in δy that

$$\frac{d}{dr}(G_0^2 P \delta y) + G_0^2 P\{\delta[(\epsilon+1/r)/P - P'/rP] + y_0\delta(P'/P) + (\delta y)^2\} = 0, \tag{4.63}$$

where the following conventions are employed: (a) all quantities with the exception of ϵ are functions of r, (b) the quantity P' is the derivative of P with respect to r in agreement with the notation of Eq. (4.52), (c) the symbol δ before a parenthesis or a bracket indicates that one subtracts from the quantity in parentheses or brackets the value of the quantity for $\beta = 0$. Since according to Eqs. (4.56), (4.57) the quantity δy is finite at $r = \infty$, and since G_0^2 vanishes exponentially at $r = \infty$, one can neglect the value of $G_0^2 P \delta y$ at $r = \infty$. Integration of Eq. (4.63) yields, therefore,

$$G_0^2 P \delta y = \int_r^\infty G_0^2 P\{\delta[(\epsilon+1/r)/P - P'/rP] + y_0\delta(P'/P) + (\delta y)^2\} dr. \tag{4.64}$$

The determination of the effect of β has been now put into the form of obtaining a solution of an integral equation which is suitable for iteration. The process of joining smoothly the branch of g extending to $r = \infty$ with the branch starting at $r = 0$ involves an adjustment of $\delta\epsilon$. The joining of the two branches of the curve will be made at $r = \alpha^2$, which is the value of r in units of Bohr radii, which corresponds to the classical electron radius e^2/mc^2.

The right side of Eq. (4.64) contains under the integral sign the quantity δy, which has to be determined. The practicability of employing the above equation depends on the fact that the first-order result which is obtained by neglecting $(\delta y)^2$ in the integrand yields a small value of δy if the adjustment of ϵ is made so as to secure smooth joining of the two branches of the wave function.

Neglecting $(\delta y)^2$ under the integral sign of Eq. (4.64) for the present, one obtains

$$\delta y \cong (A_0 + \alpha^2/r) r^{-2\rho} e^{2r} \int_r^\infty r^{2\rho} e^{-2r} \times \{\delta\epsilon + (\beta/2)[1 - (2/r) - \alpha^2(r^{-2} - r^{-1})] + \alpha^2\beta/[2r^2(A_0 + \alpha^2/r)]\} dr. \tag{4.65}$$

In addition to the approximation, consisting of neglecting quadratic effects, which has already been mentioned, the following approximations have been made at this stage: (a) A term in $y_0\alpha^2\beta^2/r^2$ has been omitted since it occurs side by side with a term in $y_0\beta\alpha^2/r^2$; (b) The quantity $\beta\alpha^2(1-\alpha^2)^{\frac{1}{2}}r^{-2}$ has been replaced by $\beta\alpha^2 r^{-2}$; (c) The energy ϵ_0 has been expressed as $-\frac{1}{2} - \alpha^2/8$. By means of Eq. (4.65) one finds by straightforward calculation

$$\delta y \cong (1 + \alpha^2/2r)\{(\delta\epsilon - \beta/2)[1/2r^2 + 1/r + \alpha^2 e^{2r} Ei(-2r)/2r^2 + 1 - (\alpha^2/2)(1/r + 3/2r^2)] + \beta[1 - \alpha^2/4r^2 + \alpha^4 e^{2r} Ei(-2r)/4r^2]\}, \tag{4.66}$$

where

$$-Ei(-x) = \int_x^\infty (e^{-z}/x) dx. \tag{4.67}$$

In this calculation terms of higher order than $\alpha^2\beta$ have been dropped, with the exception of those containing $\alpha^4\beta Ei/r^2$, since it is not clear without further consideration that their effect is negligible. In the evaluation of the integral of $(2+\alpha^2/r)^{-1}\exp(-2r)$ the factor $\exp(\alpha^2)$ multiplying the Ei has been dropped. This term is multiplied by $\alpha^4\beta$. Inclusion of the factor $\exp(\alpha^2)$ would amount to taking into account effects of order $\alpha^6\beta$ and it is not done for this reason.

Equations (1), (1.1) are not valid at very small r. If the interparticle distance becomes small enough, and if the Coulomb force is assumed to act at small distances, then the velocity of both the proton and the electron becomes comparable to the velocity of light, and there is no reason for expecting Eq. (1) to apply under such conditions. Equations (1.1), which are obtained from Eq. (1) by omitting the term in Y, are also not directly applicable at $r = 0$. If

one had to rely on Eq. (1) altogether, it would be impossible to obtain a solution with any certainty.

It is questionable, however, whether the Coulomb law is valid at distances much smaller than e^2/mc^2. There is a definite indication of a modification of the inverse-square law of force at this distance for two protons, and whether the origin of the specific proton-proton force at short distances be of the nature of a meson or some other type of field, it would not be surprising if the force between a proton and an electron should also turn out to be modified at distances comparable to those at which proton-proton interactions set in. In view of the likelihood of the absence of a strong increase in the velocity of the proton at distances smaller than the electronic radius and the gain in definiteness of discussion which results through the removal of the problem of finding a suitable Hamiltonian for the description of the motion of two rapidly moving point charges, *it will now be assumed* that at distances smaller than e^2/mc^2 the potential energy $-e^2/r$ is modified so as to be approximately constant. For simplicity it will be taken to have a constant value $-mc^2$ for $0<r<e^2/mc^2$. The conclusions do not depend, however, on whether one takes the potential energy to be exactly constant in this range of values of r or not.

Inasmuch as the last term in the second Eq. (3.5) is of the order $\alpha^2\beta$ of the first, it will be neglected in the calculation that will be made now. Since $f \ll g$, the effect on the term in $d(r^2f)/r^2dr$ in the first of the two Eqs. (3.5) is small. One obtains in this manner, on elimination of f, a simplified special case of Eq. (3.5)

$$d^2G/dr^2+K^2G=0, \tag{4.68}$$

with

$$K^2=(1+\alpha^2\epsilon)\alpha^{-2}[1/(3+\alpha^2\epsilon) +(\beta/2)(1+\beta+\alpha^2\beta\epsilon/2)^{-1}]^{-1}, \tag{4.69}$$

so that

$$ry=Kr\cot(Kr)=1-K^2r^2/3+\cdots. \tag{4.7}$$

Substituting K^2 and evaluating for $r=\alpha^2$, one has

$$(ry)_{r=\alpha^2}\cong 1-\alpha^2+3\alpha^2\beta/2. \tag{4.71}$$

On the other hand, the solution for the ground state corresponding to $\beta=0$ is, apart from a normalizing factor common to f and g,

$$\begin{aligned} f_0&=-(1-\rho)^{\frac{1}{2}}r^{\rho-1}e^{-r};\\ g_0&=(1+\rho)^{\frac{1}{2}}r^{\rho-1}e^{-r}, \end{aligned} \tag{4.72}$$

where ρ is as explained in the list of notations following Eq. (1). It follows that

$$y_0=\rho/r-1,\ (ry_0)_{r=\alpha^2}=(1-\alpha^2)^{\frac{1}{2}}-\alpha^2 =1-3\alpha^2/2. \tag{4.73}$$

Combining Eqs. (4.71) and (4.73), one obtains

$$(r\delta y)_{r=\alpha^2}=\alpha^2/2+3\alpha^2\beta/2. \tag{4.74}$$

In this formula the first term $\alpha^2/2$ has to do with the modification introduced by changing the inverse first-power potential to a constant in the range $0<r<\alpha^2$. It has nothing to do with the effect of the mass of the proton on δy. Its inclusion in the calculation would correspond to making a combined estimate of the effect of the proton's size and of the effect of nuclear motion. In order to keep the two effects separate from each other, only the part of δy containing β will be kept at this stage. By separating the effects in this manner one obtains the effect of changing β from 0 to its experimental value. A slight error is introduced at this point through the employment of the functions given by Eqs. (4.72) rather than functions corresponding to

$$(r\delta y)_{r=\alpha^2,\,\beta=0}=\alpha^2/2, \tag{4.75}$$

which correspond to infinite proton mass and a constant potential energy in $0<r<\alpha^2$. The difference between these functions and the functions of Eq. (4.72) is very slight, however. The right side of Eq. (4.66) is equated, therefore, to $3\beta/2$, which is the part of δy corresponding to the term containing β on the right side of Eq. (4.74). Calculation gives then

$$\begin{aligned} \delta\epsilon-\frac{\beta}{2}&=\frac{(1/4\alpha^2)-Ei(-2\alpha^2)(\exp 2\alpha^2)/4}{(1/2\alpha^4)+(1/4\alpha^2) +Ei(-2\alpha^2)(\exp 2\alpha^2)/2\alpha^2+1/2}\beta\\ &\cong(\alpha^2\beta/2)[1-2\alpha^2Ei(-2\alpha^2)-\alpha^2/2], \end{aligned} \tag{4.8}$$

and the value of the first-order effect δy corresponding to this value of $\delta\epsilon-(\beta/2)$ is obtained

from Eq. (4.66) as

$$\delta y \cong \beta\{1+\alpha^2/2+\alpha^2/r + (\alpha^4/2r^2)[e^{2r}Ei(-2r)-Ei(-2\alpha^2)] - (\alpha^4/r)Ei(-2\alpha^2)\}. \quad (4.81)$$

The factor β, which is present in all terms of the above formula, makes the result small, and the quadratic term in the integrand of Eq. (4.64) is negligible on account of the presence of the factor β^2. This is the result of making δy small at $r=\alpha^2$.

The integral which matters for the hyperfine structure splitting is

$$\int_0^\infty fg dr. \quad (4.82)$$

The effect of δy on this integral can be broken down into: (a) The presence of the factor $\exp(\int^r(\delta y)dr)$ in both f and g, which results in a net factor $\exp(2\int^r(\delta y)dr)$, (b) an extra term arising in f because it is expressible in terms of dg/dr, so that the exponential just referred to brings in an extra term on differentiation. The correction factor to the integrand resulting from both causes is

$$[1+(g_0 dr/dg_0)\delta y]\exp\left[2\int^r(\delta y)dr\right],$$

which on substituting g_0 becomes

$$[1-(1+\alpha^2/2r)^{-1}\delta y]\exp\left(2\int^r \delta y dr\right). \quad (4.83)$$

This correction factor does not include the change in the normalization constant. It will be simpler to take this change into account later. It will first be explained that in Eq. (4.81) the only important term inside the brace is 1. The other terms give effects of the order $\alpha^2\beta$. For $r=\alpha^2$ the largest additional term inside the brace is that containing α^2/r. In the exponent of Eq. (4.83) it brings in a factor, $2\alpha^2\beta \log r$, which is entirely negligible in a larger range of values of r than $\alpha^2<r<10^3$. For the factor multiplying the exponential in Eq. (4.83) the term in α^2/r has the effect of multiplying the integrand by $1-\beta\alpha^2$, which is a negligible effect. At $r=\alpha^2$ the effect is greater, but an estimate of it shows that the integral of Eq. (4.82) is changed by the fractional amount $-\alpha^2\beta \ln 2\alpha^2$, which is also negligible. The term in square brackets containing $Ei(-2r)$ vanishes at $r=\alpha^2$. The square bracket changes slowly at $r=\alpha^2$, because at small r the dependence of the Ei-function on its argument is logarithmic. The effect of the square bracket is thus also negligible.

It is thus seen that the effect of β on the integral of Eq. (4.82) is to multiply it by the factor

$$\text{correction factor} = \frac{\int(1-\beta)\exp(2\beta r)f_0 g_0 dr}{\int f_0 g_0 dr} \times \frac{\int(f_0^2+g_0^2)r^2 dr}{\int(f_0^2+g_0^2)\exp(2\beta r)r^2 dr}, \quad (4.84)$$

all integrals being taken from 0 to ∞. To within first-order terms in β this is simply $(1+\beta)^{-1}$. The justification for employing the integral of Eq. (4.82) is given in the next section.

D. The Hyperfine Structure

The expectation value $\langle Y\rangle$, of the operator Y of Eq. (1), will now be computed. One has from the first Eq. (1.1) with the aid of Eqs. (1.6) and (2.4)

$$\Phi=[(p_0+Mc)^{-1}-(p_0+Mc)^{-1}(\boldsymbol{\alpha}\mathbf{p}+\beta mc) \times(p_0+Mc)^{-1}](\boldsymbol{\sigma}_M\mathbf{p})\Psi, \quad (5)$$

where the subscript e is dropped and c.g.s. units are used. The operator cp_0 is

$$cp_0=(M+m)c^2+\epsilon+e^2/r. \quad (5.1)$$

The first term in Eq. (5) contributed the main part of the expectation value. The second term contributes a correction of order β. Relationship to familiar expressions is secured by means of the approximation

$$cp_0 \cong Mc^2. \quad (5.1')$$

This approximation is not good enough for the evaluation of contributions arising from the first

term on the right side of Eq. (5), but suffices for the calculation of effects arising from the second term. The integral representing $\langle Y\rangle$ contains Φ linearly, and the approximation made in Eq. (5.1′) is taken care of for the first term of Eq. (5) by the correction factor

$$2M/(2M+m)=1/(1+\beta/2). \tag{5.2}$$

The quantity $\epsilon+e^2/r$ in Eq. (5.1) contributes terms of the order α^2 in comparison with mc^2. The correction factor of Eq. (5.2) is, therefore, good enough. The second term of Eq. (5) can be taken into account by noting that commuting $\boldsymbol{\alpha}\mathbf{p}+\beta mc$ with $(p_0+Mc)^{-1}$ brings in terms of still higher order and

$$(\boldsymbol{\alpha}\mathbf{p}+\beta mc)\Psi\cong -mc\Psi.$$

The correction factor brought in by the second term of Eq. (5) is thus

$$1-(-mc)(2Mc)/(2Mc)^2=1+\beta/2. \tag{5.2′}$$

Combining this correction factor with that of Eq. (5.2) one obtains a correction factor of unity to within terms of order $\alpha^2\beta$. It is, therefore, good enough to calculate with the simple approximation of Eq. (5.1′), which corresponds to

$$\Phi\cong(\boldsymbol{\sigma}_M\mathbf{p})\Psi/(2Mc). \tag{5.3}$$

One obtains in this manner

$$\langle 2Y\rangle=(e^2/2Mc)\int\Psi^\dagger[(\boldsymbol{\alpha}\boldsymbol{\sigma}_M)/r$$

$$+(\boldsymbol{\alpha}\mathbf{r})(\boldsymbol{\sigma}_M\mathbf{r})/r^3](\boldsymbol{\sigma}_M\mathbf{p})\Psi+\text{comp. conj.}\}d\tau,$$

where comp. conj. stands for the complex conjugate of the immediately preceding expression. Linearizing in $\boldsymbol{\sigma}_M$ one obtains

$$\langle 2Y\rangle=(e^2/2Mc)\int\{\Psi^\dagger[r^{-1}(\boldsymbol{\alpha}\mathbf{p})+ir^{-1}\boldsymbol{\sigma}_M[\boldsymbol{\alpha}\times\mathbf{p}]$$

$$+r^{-3}(\boldsymbol{\alpha}\mathbf{r})(\mathbf{r}\mathbf{p}+i[\mathbf{r}\times\mathbf{p}]\boldsymbol{\sigma}_M)]\Psi$$

$$+\text{comp. conj.}\}d\tau. \tag{5.4}$$

The value of this quantity is calculated for the state in which the z component of $\boldsymbol{\sigma}_M/2$, which represents the nuclear spin, has the characteristic value $\frac{1}{2}$ and in which the projection of the electronic angular momentum on the z axis is also $\frac{1}{2}$. This state is one of the three magnetic levels with hyperfine-structure quantum number $f=1$. It suffices to calculate $\langle Y\rangle$ for this state because according to well-known relations it has the same value for the other magnetic levels of $f=1$; the value of $\langle Y\rangle$ for $f=0$ is known to be (-3) times the value for $f=1$. Straightforward substitution and calculation gives

$$\langle Y\rangle=-(8\pi/3)(e^2h/Mc)\int_0^\infty fg\,dr. \tag{5.5}$$

The normalization is supposed to be

$$4\pi\int_0^\infty(f^2+g^2)r^2dr=1. \tag{5.5′}$$

The integral of Eq. (4.82) is seen to occur in Eq. (5.5). The normalization integrals of Eq. (4.84) are also seen to be in agreement with Eq. (5.5′). It remains to evaluate the right side of Eq. (4.84).

The factor $(1-\beta)\exp(2\beta r)$ of the first integral in the numerator of Eq. (4.84) just suffices to change it into the first integral in the denominator by a change of variable

$$r'=r/(1+\beta), \tag{5.5″}$$

which corresponds to the non-relativistic effect of expansion of the wave-function space in the ratio $(1+\beta):1$. A slight inaccuracy is involved at this point. The factor $[1+(\alpha^2/2)(\epsilon+1/r)]^{-1}$ in the expression for f in terms of dg/dr does not have its $1/r$ changed into $1/r'$ by the transformation of Eq. (5.5″). The error involved in this inaccuracy is of the order $\alpha^2\beta$ and will be neglected. It may be well to recall here that the whole term $(\alpha^2/2)(\epsilon+1/r)$ could be omitted without affecting the result to more than terms of relative order α^2 and that Fermi's well-known result involving the Schrödinger $\psi^2(0)$ has been obtained in this manner. The ratio of the first integral of Eq. (4.84) in the numerator to the first integral in the denominator is thus unity to within terms of relative order $\alpha^2\beta$. The ratio of the second integral in the numerator to the second integral in the denominator can again be considered by means of the transformation of Eq. (5.5″). The factor $\exp(2\beta r)$ suffices for the change to r' in g_0^2 and within errors of relative order $\alpha^2\beta$ or β^2 in f_0^2. The conversion of r^2dr in the denominator brings about the appearance of

the factor $(1+\beta)^3$ in the denominator, which amounts to $1/(1+\beta)^3$ for the correction factor.

Another way of explaining the result just arrived at is to note that the factors $(1-\beta)$ and $\exp(2\beta r)$ in the first integral in the numerator of Eq. (4.84) suffice to make the integrand $(\alpha/4)dg^2/dr$ with an error of relative order $\alpha^2\beta$, while the factor $\exp(2\beta r)$ makes the second integrand of the second integral in the denominator in the same approximation as previously g^2r^2. Similarly, the integrands of the first integral in the denominator and the second integral in the numerator are f_0g_0 and g_0^2 respectively. The right side of Eq. (4.84) is thus $g^2(0)/g_0^2(0)$. The difference between $g^2(r)$ and $g_0^2(r)$, aside from normalization, is that

$$g(r)=\text{const.}g_0(r/(1+\beta)).$$

Since the normalization of g^2 is obtained by division by

$$4\pi\int g^2(r)r^2dr=4\pi(1+\beta)^3\int g_0^2(r)r^2dr,$$

the correction factor is $(1+\beta)^{-3}$.

In both explanations f_0^2/g_0^2 has been neglected in the normalization integral. The error introduced by doing so is represented according to Eq. (3.5) by the factor

$$1-(\alpha^2/4)\int(dg/dr)^2r^2dr\Big/\int g^2r^2dr\cong 1-\alpha^2/4.$$

This factor is compensated for, however, by the fact that

$$f_0\cong-(\alpha/2)(1+\alpha^2/4)g_0.$$

The remaining inaccuracy is thus represented to relative order α^2 by the factor

$$\left[\int(r^{\rho-1}e^{-r})^2dr\Big/\int r^2(r^{\rho-1}e^{-r})^2dr\right]$$

$$\times\left[\int r^2e^{-2r}dr\Big/\int e^{-2r}dr\right]$$

$$\cong[\Gamma(2\rho-1)/\Gamma(2\rho+1)][\Gamma(3)/\Gamma(2)]$$

$$=1/(2\rho^2-\rho)\cong 1+3\alpha^2/2, \quad (5.6)$$

in agreement with the exact result[3] for $\beta=0$.

A check on the validity of the factor $(1+\beta)^{-3}$ can be obtained by going to the extreme case of two equal masses. For this case the problem has been essentially worked out previously.[7] The scheme employed a limiting process in which the potential energy $-e^2/r$ was first replaced by a function $-e^2\{1/r\}$ which was kept finite at $r=0$. The range of values of r within which the function was assumed to differ from $-e^2/r$ was made to approach zero, and the value of the function at $r=0$ was made to approach ∞. At all stages in the limiting process the Laplacian of the modified function was well defined. In the limit it approached a multiple of the Dirac δ function as below,

$$\lim\Delta(-e^2\{1/r\})=4\pi e^2\delta(\mathbf{r}). \quad (6)$$

The spin interactions between the particles were brought in by a generalization of the operator Y. The expectation value of the perturbing energy for parallel spin orientations was calculated to be the same as that of

$$H'=-(e^2h^2/6M^2c^2)\Delta\{1/r\}, \quad (6.1)$$

where M is the common mass of the two particles with the understanding that the unperturbed Hamiltonian is that of the non-relativistic Schrödinger equation. The expectation value of H' is, therefore, according to Eqs. (6), (6.1)

$$\langle H'\rangle=(8\pi/3)(he/2Mc)^2\psi_S^2(0)$$

$$=(E_1-E_0)/4, \quad (6.2)$$

where ψ_S is the non-relativistic Schrödinger function for the relative motion of the two particles. The energy difference between levels having fine quantum numbers $f=1$ and 0 should be 4 times the above $\langle H'\rangle$, as is also indicated in Eq. (6.2). Since $he/2Mc$ is the magnetic moment appropriate to each particle, according to the Dirac equation which was supposed to be obeyed by each particle, this result is in agreement with Fermi's formula

$$E_{i+\frac{1}{2}}-E_{i-\frac{1}{2}}=(8\pi/3)(2+1/i)\mu\mu_0\psi_S^2(0), \quad (6.3)$$

where i is the nuclear spin and μ, μ_0 are, respectively, the magnetic moments of the nucleus and the electron. In the present case $i=\frac{1}{2}$. According

[7] G. Breit, Phys. Rev. **51**, 249 (1936), see Eqs. (17.7), (17.8). These are practically the same as the equations for spin-spin interactions of electrons referred to in reference 4. *Ibid.*, **53**, 153 (1938) pp. 159–160 discusses the relations of Casimir, Physica **3**, 936 (1936).

to Eq. (6.2) the hyperfine-structure splitting depends on the mass of one of the particles partly through μ and partly through $\psi_s^2(0)$. The latter dependence is taken care of by the transformation of Eq. (5.5″), which brings the factor $(1+\beta)^{-3}$ into the answer.

III. THE PAULI PART OF THE MOMENT. THE DEUTERON

Since the proton does not have a magnetic moment which would be expected for it according to Dirac's equation, it is necessary to take into account the additional moment of ~ 1.79 nuclear Bohr magnetons. An understanding of the origin of this addition is lacking, and the additional moment will be treated, therefore, as an intrinsic property of the proton. Pauli[8] gave an equation suitable for the representation of a particle obeying an equation of the general Dirac form but having in addition to the Bohr magneton an intrinsic moment. The excess of ~ 1.79 nuclear Bohr magnetons will be represented by a term in the Hamiltonian of the type invented by Pauli and will be referred to as the Pauli part of the proton's moment. The part of μ corresponding to it will be referred to as μ_P. The interaction with an external field is represented by an addition to the Hamiltonian

$$H_P' = \mu_P[\rho_{3M}(\mathfrak{H}\sigma_M) - \rho_{2M}(\mathcal{E}\sigma_M)], \qquad (7)$$

where for a discussion of a single particle ρ_2, ρ_3 are four row four column matrices introduced by Dirac in his original notation. The matrix ρ_3 is the same as β. The matrix ρ_2 is

$$\rho_2 = \begin{pmatrix} 0 & 0 & -i & 0 \\ 0 & 0 & 0 & -i \\ i & 0 & 0 & 0 \\ 0 & i & 0 & 0 \end{pmatrix}. \qquad (7.1)$$

In Eq. (7) the matrices σ_M are four row matrices in the proton index identical with Dirac's vector matrix σ. For two particles ρ_{2M} operates on the proton indices as though there were no electron and is diagonal in electron indices. For a single particle in an external field Eq. (7) gives a rigorously consistent relativistic description. If the electron's motion could be considered as preassigned one could substitute for $\mathcal{E}$ and $\mathfrak{H}$ the values for the electric and magnetic fields at the proton produced by the electron without bringing into question the propriety of employing Eq. (7). Since the electron's motion is not preassigned, however, one has to examine the errors introduced by borrowing an interaction Hamiltonian from single particle theory.

In employing Eq. (7) for two particles, the proton's equations of motion are still formally correct. The addition to the x component of the force on the proton brought about by H_P' is

$$\delta\dot{p}_{xM} = (i/\hbar)[H', p_{xM}] = -\mu_p[\rho_{3M}(\sigma_M \partial\mathfrak{H}/\partial x_M) - \rho_{2M}(\sigma_M \partial\mathcal{E}/\partial x_M)], \qquad (7.2)$$

corresponding to magnetic moment $-\mu_P\rho_{3M}\sigma_M$ and electric moment $\mu_P\rho_{2M}\sigma_M$. For a proton at rest the magnetic moment is represented by $\mu_P\sigma_M$, and there is no electric moment. The densities of electric- and magnetic-moment distributions can be verified to transform themselves correctly under Lorentz transformations. The relation between $\dot{x}_M$ and α_M is left undisturbed by Eq. (7). From the point of view of the correspondence principle the proton's motion is, therefore, represented satisfactorily by Eq. (7).

For the consideration of the electron's motion Eq. (7) would be exact if the proton could be considered as stationary. The operator, ρ_{3M}, would then be equivalent to multiplication by -1, the operator ρ_{2M} to multiplication by 0. The interaction Hamiltonian in this limit becomes the same form as that commonly used for a stationary nucleus. It is well known that this form represents satisfactorily the electron's motion, the expressions for $\mathfrak{H}$ at the nucleus in terms of Dirac's α matrices for the electron being just right to make the magnetic vector potential of the nucleus appear in the right linear combination with electrons momentum operator. The inaccuracies of Eq. (7) for the discussion of the electron's motion have their origin, therefore, in the finiteness of the velocity of the nucleus. For a slowly moving nucleus these inaccuracies are small, because so far as the motion of the electron is concerned only the retardation of the effects of the nucleus at the electron caused by the finiteness of the velocity of light is neglected by the employment of Eq. (7). The retardation effects of nuclear motion

[8] W. Pauli, *Handbuch der Physik* (Verlagsbuchhandlung, Julius Springer, Berlin, 1933), Vol. 24/1, p. 221.

are of relative order $(m/M)^2(v^2/c^2)$, where v is the electron velocity, and are negligible since v^2/c^2 is $\sim\alpha^2$.

In terms of the electron operators employed in Eq. (1)

$$H_p'=\mu_p e[\rho_{3M}\sigma_M[\mathbf{r}\times\boldsymbol{\alpha}_e]-\rho_{2M}(\mathbf{r}\boldsymbol{\sigma}_M)]/r^3. \quad (7.3)$$

The second term in the brackets requires special consideration. One finds by calculation that

$$\int\psi^\dagger\rho_{2M}(\mathbf{r}\boldsymbol{\sigma}_M)r^{-3}\psi d\tau=(h/Mc)\text{R.P.}\int\Psi^\dagger r^{-3}$$

$$\{(\mathbf{r}\nabla)+i\boldsymbol{\sigma}_M[\mathbf{r}\times\nabla]\}\Psi d\tau, \quad (7.31)$$

where the $\boldsymbol{\sigma}_M$ are four row matrices in the nuclear subscript when they multiply ψ and two row matrices when they multiply Ψ. The quantity Φ has been eliminated in this calculation by means of Eq. (5.3). The integrand of the right side of Eq. (7.31) depends on the orientation of the nuclear spin only through the term in $\boldsymbol{\sigma}_M$ which contains also the orbital angular-momentum operator $[\mathbf{r}\times\mathbf{p}]$. Non-relativistically the latter factor is equal to zero for s terms. In the approximation of the present paper it is

$$(h/Mc)\int_0^\infty(-8\pi/3)(f^2/r)dr, \quad (7.32)$$

the expression having been evaluated for parallel spin orientations. This expression has to be multiplied by $(-\mu_P e)$ in order to give the contribution to the expectation value of H_P'. If the integration in the last formula were carried out for a value of f corresponding to a Coulomb field, one would obtain an infinite result. For a Coulomb potential modified so as to have finite value for $0<r<e^2/mc^2$ the integral is finite, and only a logarithmic term in mc^2/e^2 is brought in. The ratio f/g being of the order α, the contribution of the term under discussion to the hyperfine structure is of the order $(m/M)\alpha^2\log\alpha$ and may be neglected.

It may be noted that the effect just discussed is that of the mutual energy of the electron's electric field and of the nuclear electric dipole produced by the nuclear motion of translation as a result of the nuclear magnetic moment. In non-quantum analogy the effect is zero for s terms. It is also zero in any approximation in which L is a good quantum number.

The first term of Eq. (7.3) differs from the interaction Hamiltonian generally employed for a fixed nucleus only through the presence of the factor ρ_{3M}. The effect introduced by this factor is that of changing the sign of the terms containing Φ and is of the relative order $(m/M)^2\alpha^2$.

The effect of the electric-dipole moment induced by nuclear translation is present also for the Dirac part of the moment. Calculation shows, in fact, that the part of the particle-density formula which is spin dependent when expressed in terms of Ψ alone gives an electric-dipole contribution of the same order as the second term in brackets in Eq. (7.3). This effect is also of order $(m/M)\alpha^2\log\alpha$.

It is seen that for the Pauli part of the proton's moment the mass effect is represented by the same factor $(1+m/M)^3$ as for the Dirac part within terms of the order $(m/M)\alpha^2\log\alpha$.

All of the deuteron's moment is reasonably represented as an intrinsic one. The magnetic moment of the Dirac type does not enter the deuteron problem because the proton contained in the deuteron is moving in the field of the neutron. The circulation of the proton's charge contributes to the magnetic moment of the deuteron, but its perturbation by recoil action from the electron is negligibly small because of the much larger force to which the proton is subjected as a result of the forces acting on it within the deuteron.

A few arguments concerned with physical plausibility will be dealt with first. It will be supposed that the neutron is not interacting with the electron in any way except through the rather small effect of its magnetic moment. If the neutron's mass were negligible and if its mass were instead assigned to the proton, one could construct a substitute model for the deuteron which would behave in weak external fields in the same way as the deuteron. To obtain this result one would have to arrange for the magnetic model of the model to be the same as that of the deuteron. It is plausible to assume that such a model will be equivalent to the deuteron in its action on the electron. For the state with magnetic-quantum number 3/2 this model shows a simple relationship to the case of magnetic-

quantum number 1 which has been worked out for the case of the proton. The spins of the proton and neutron are parallel to the angular momentum of relative electronic motion. Since the neutron does not interact with the electron except through its magnetic moment, and since in the present model the neutron's mass has been transferred to the proton, the calculations made for ordinary hydrogen are directly applicable. The only changes that have to be made are: (a) the mass of the deuteron has to be substituted for the mass of the proton, (b) the magnetic moment of the neutron has to be added to the magnetic moment of the proton. The formula for the hyperfine-structure splitting expected on the basis of the above model is, therefore, the one derived by Fermi with the modification of the factor $(1+m/M_D)^{-3}$.

The applicability of the correction to deuterium can also be demonstrated along more rigorous lines. The Hamiltonian for three particles can be written down so as to describe the system of proton, neutron, and electron. The term corresponding to Y of the present paper is neglected at first. Solutions of the proton-neutron relative motion problem are introduced. These solutions have to be modified first for the effect of the momentum of the deuteron. The magnetic momentum changes slightly, and a small electric moment results. Both of these changes are insignificant as in the case of the single proton. The wave function of the whole system is expanded in products of the internal deuteron function and the function describing the relative motion of the electron with respect to the center of mass of the deuteron. Radial equations for relative motion analogous to those dealt with for the single proton are obtained. The term in Y for the proton, the Pauli part of the proton's magnetic moment, and the magnetic moment of the deuteron combine into one term corresponding to the magnetic moment of the deuteron. The result of this consideration is the same as that of the simplified model just considered.[9]

A preliminary report on the present work was made at the conference on The Foundations of Quantum Mechanics held at Shelter Island, New York on June 2–4, 1947. The conference was sponsored by the National Academy of Sciences at the suggestion of Dr. D. A. MacInnes who has organized it. It is a pleasure to acknowledge the stimulus derived from the conference for finishing this work.

[9] After this manuscript had been completed there appeared a note on the same subject by O. Halpern in Phys. Rev. **72**, 245(L) (1947). The results obtained in the present paper differ from Halpern's.

Fluctuations of the Number of Neutrons in a Pile[1]

E. D. COURANT[2] AND P. R. WALLACE[3]
Chalk River Laboratory, Chalk River, Ontario, Canada

(Received June 16, 1947)

Statistical fluctuations in the number of neutrons in a pile which is just under critical and contains distributed neutron sources such as spontaneous fissions, $\alpha-n$ reactions, etc., are considered for the following two cases: (a) The delayed neutrons are taken into account, but the pile is assumed to be operating at a steady power, and (b), the power at which the pile operates is assumed to change periodically, but the delayed neutrons are neglected.

For both cases the expression for the standard deviation of the number of neutrons is derived, and in case (a) the expression for the coefficient of correlation between the number of neutrons and the number of excited nuclei of each particular type, which lead to the formation of the delayed neutrons, is also given.

The method used throughout the calculations is that of the probability generating function.

For the case of a steadily operating pile, the effect of a finite resolving time of the recording instrument upon the observed value of the standard deviation of the number of neutrons is also determined through a study of the spectrum of the fluctuations.

I. INTRODUCTION

WE consider a chain-reacting pile in which there is a source of neutrons (spontaneous fissions, $\alpha-n$ reactions, cosmic rays, etc.). Let N be the number of neutrons present in the pile, and let $Q_1, Q_2, Q_3 \cdots Q_m$ be the number of radioactive fission-product nuclei of decay constants $a_1, a_2 \cdots a_m$, respectively, capable of giving off delayed neutrons. The time-dependent equations for N and Q_i are

$$dN/dt = S-(1-k'/\tau)N+\sum_{i=1}^{m} a_iQ_i, \quad (1.1)$$

$$(dQ_i/dt) = (c_i/\tau)N-a_iQ_i. \quad (1.2)$$

Here S = the number of neutrons emitted by the source per unit time,

k' = the mean number of neutrons formed instantaneously per neutron lost in the pile through absorption or escape,

c_i = the mean number of radioactive nuclei of type i formed per neutron lost,

τ = the mean lifetime of a neutron in the pile.

It is also convenient to define

$c=\sum_{i=1}^{m} c_i$ = the mean number of delayed neutrons formed per neutron lost,

$k=k'+c$ = the effective multiplication factor of the system.

Equations (1.1) and (1.2) would be satisfied exactly if neutron capture and production were continuous processes. Since they are, in fact, discrete elementary processes occurring at random, the rates dN/dt and dQ_i/dt given by (1.1) and (1.2) are only *average* rates, and the true rates will fluctuate about these average rates. As a result, the actual values of N and Q_i at any given time will not be given exactly by the solution of (1.1) and (1.2), but will fluctuate at random about these solutions. It is the object of this paper to estimate the magnitude of these fluctuations in a number of cases.

Let $P(N, Q_1, Q_2, \cdots; t)$ be the probability that N neutrons, Q_1 nuclei of type 1, Q_2 nuclei of type 2, etc., are present in the system at time t. The average number of neutrons is

$$\langle N\rangle_{Av}=\sum_{N}\sum_{Q_1}\sum_{Q_2}\cdots NP(N, Q_1, Q_2\cdots; t), \quad (1.3)$$

and the average number of nuclei of type i is

$$\langle Q_i\rangle_{Av}=\sum_{N}\sum_{Q_1}\sum_{Q_2}\cdots Q_iP(N, Q_1, Q_2, \cdots; t). \quad (1.4)$$

A measure of the fluctuations in N is given by the standard deviation

$$\varphi_{NN}=\langle N^2\rangle_{Av}-\langle N\rangle_{Av}^2=\sum_{N,Q_i} N^2P(N, Q_i; t) - [\sum_{N,Q_i} NP(N, Q_i; t)]^2. \quad (1.5)$$

[1] Contribution from the Chalk River Laboratories of the National Research Council. This work was completed in April, 1946.

[2] Now at Cornell University, Ithaca, New York.

[3] Now at McGill University, Montreal, Quebec.

We also define

$$\varphi_{Nj}=\langle NQ_j\rangle_M-\langle N\rangle_M\langle Q_j\rangle_M$$
$$=\sum_{N,Q_i} NQ_jP(N,Q_i;t)$$
$$-[\sum_{N,Q_i} NP(N,Q_i;t)]$$
$$\times[\sum_{N,Q_i} Q_jP(N,Q_i;t)], \quad (1.6)$$

$$\varphi_{jk}=\langle Q_jQ_k\rangle_M-\langle Q_j\rangle_M\langle Q_k\rangle_M$$
$$=\sum_{N,Q_i} Q_jQ_kP(N,Q_i;t)$$
$$-[\sum_{N,Q_i} Q_jP(N,Q_i;t)][\sum_{N,Q_i} Q_kP(N,Q_i;t)]. \quad (1.7)$$

The problem is to obtain values for $\langle N\rangle_M$, $\langle Q_j\rangle_M$, φ_{NN}, φ_{Nj}, and φ_{jk}. To do this we define the "probability generating function"

$$F(x,y_1,y_2,\cdots;t)=\sum_N\sum_{Q_1}\sum_{Q_2}\cdots$$
$$\times x^N y_1^{Q_1}y_2^{Q_2}\cdots P(N,Q_1,Q_2,\cdots;t). \quad (1.8)$$

This function has the property that

$$F|_{x=y_i=1}=1, \quad (1.9)$$

$$\langle N\rangle_M=x\partial F/\partial x|_{x=y_i=1}, \quad (1.10)$$

$$\langle Q_j\rangle_M=y_j\partial F/\partial y_j|_{x=y_i=1}, \quad (1.11)$$

$$\varphi_{NN}=[(x\partial/\partial x)^2F-(x\partial F/\partial x)^2]_{x=y_i=1}, \quad (1.12)$$

$$\varphi_{Nj}=[x(\partial/\partial x)y_j(\partial/\partial y_j)F$$
$$-xy_j\partial F/\partial x\cdot\partial F/\partial y_j]_{x=y_i=1}, \quad (1.13)$$

$$\varphi_{jk}=[y_j(\partial/\partial y_j)y_k(\partial/\partial y_k)F$$
$$-y_jy_k\partial F/\partial y_j\cdot\partial F/\partial y_k]_{x=y_i=1}, \quad (1.14)$$

as is easily verified by differentiation of (1.8), since

$$\sum_{N,Q_i} P(N,Q_i;t)=1.$$

In the next section, a partial differential equation for F will be derived. From this equation it is possible to obtain expressions for the derivatives of F when x and all the y_i are equal to unity, and from Eqs. (1.9) to (1.14) we can then obtain the mean values and mean deviation of N and Q_i.

II. DIFFERENTIAL EQUATION FOR THE GENERATING FUNCTION

We wish to establish equations for the rates of variation of the probabilities $P(N,Q_1,Q_2,\cdots;t)$ and, consequently, for the probability generating function F defined by (1.8). To do this, let us suppose that we know the probabilities at time t, and let us try to determine what they become at time $t+dt$, i.e., after an infinitesimal time interval.

The probability that in such an interval *two* fundamental processes occur is $O(dt^2)$; we need only consider, therefore, the effect of a single process (emission by the source, capture with possible fission, or emission by excited fission-product nuclei).

Let us introduce the function

$$f(x,y_1,y_2\cdots)=\sum_{n,m_i} p_{nm_1m_2\cdots}x^ny_1^{m_1},y_2^{m_2}\cdots, \quad (2.1)$$

in which $p_{nm_1m_2\cdots}$ is the probability that a capture process will lead to formation of n instantaneous fission neutrons, and m_i radioactive fission-product nuclei of type i. $p_{nm_1m_2\cdots}$ will certainly be zero for $\sum m_i>2$, and perhaps even for $\sum m_i>1$, i.e., at most one or two delayed neutrons are emitted in one fission. We note the identity

$$f|_{x=y_i=1}=1.$$

The multiplication factor (i.e., the average number of neutrons released in the system per neutron lost through escape or absorption) is

$$k=\sum_{nm}(n+\sum_i m_i)p_{nm_1m_2\cdots}$$
$$=(x\partial/\partial x+\sum y_i\partial/\partial y_i)f|_{x,y_i=1}. \quad (2.2)$$

The mean square of the number of neutrons formed per neutron lost is

$$k_2=\sum_{nm}[n+\sum_i m_i]^2p_{nm_1m_2\cdots}$$
$$=[x/\partial x+\sum y_i\partial/\partial y_i]^2f|_{x,y_i=1}. \quad (2.3)$$

We may then write

$$k_2-k=\frac{\partial^2f}{\partial x^2}+2\sum_i\frac{\partial^2f}{\partial x\partial y_i}+\sum_{i,j}\frac{\partial^2f}{\partial y_i\partial y_j}. \quad (2.4)$$

In the notation of paragraph 1, we may break k down into its component parts:

$$k'=\partial f/\partial x|_{x,y_i=1} \quad (2.5)$$

due to instantaneous neutrons, and

$$c_i=\partial f/\partial y_i|_{x,y_i=1} \quad (2.6)$$

due to delayed neutrons of class i, where

$$k=k'+\sum c_i=k'+c. \tag{2.7}$$

Let us also introduce the abbreviation

$$c'=[2\sum_i \partial^2 f/\partial x\partial y_i+\sum_{ij} \partial^2 f/\partial y_i\partial y_j]_{x=y_i=1}, \tag{2.8}$$

so that

$$k_2-k=\partial^2 f/\partial x^2+c'. \tag{2.9}$$

For the source emission, we may introduce a similar function,

$$g(x, y_1, y_2\cdots)=\sum q_{nm_1m_2\cdots}x^n y_1^{m_1}y_2^{m_2}\cdots, \tag{2.10}$$

where the $q_{nm_1m_2\cdots}$ are source emission probabilities similar to the $p_{nm_1m_2\cdots}$. We shall, however, for simplicity, assume that the source produces only one neutron at a time, i.e., that $g(x, y_i\cdots)=x$. It can be shown that this assumption does not seriously affect any of the results of this paper.

Given the probabilities for different numbers of neutrons and radioactive fission-product nuclei at time t, what is the probability that there are N neutrons, Q_i nuclei of type i, at time $t+dt$? It is made up of four terms:

(i) the probability that there are $(N-1)$ neutrons, Q_i nuclei of type i at time t, multiplied by the probability that a source emission gives rise to one neutron in time dt. This is

$$P(N-1, Q_1, Q_2, \cdots; t)Sdt.$$

(ii) the probability that there are $(N-n+1)$ neutrons, (Q_i-m_i) nuclei at time t, multiplied by the probability that a neutron loss gives rise to the production of n neutrons and m_i nuclei in time dt. This is

$$\sum_{n,m_i} P(N-n+1, Q_1-m_1, Q_2-m_2, \cdots; t)\cdot\frac{(N-n+1)dt}{\tau}\cdot p_{nm_1m_2\cdots}.$$

(iii) the probability that there are $(N-1)$ neutrons, (Q_I+1) nuclei of a particular type I and $Q_i(i\neq I)$ of all others, multiplied by the probability that a nucleus of type I decays in time dt. This is

$$\sum_I P(N-1, Q_1, \cdots Q_I+1, \cdots; t)(Q_I+1)a_I dt,$$

where a_I is the decay exponent of radioactive nuclei of type I.

(iv) the probability that no source emission, neutron loss, or radioactive decay takes place in time dt, multiplied by the probability that there were at the beginning of this time N neutrons, Q_i nuclei. This is

$$\left(1-Sdt-N\frac{dt}{\tau}-\sum a_I Q_I dt\right)P(N, Q_1, Q_2\cdots; t).$$

Combining the above results we get

$$\begin{aligned}&P(N, Q_1, Q_2\cdots; t+dt)\\&=P(N-1, Q_1, Q_2, \cdots; t)Sdt\\&+\sum_{nm_i} P(N-n+1, Q_1-m_1, Q_2-m_2, \cdots; t)\\&\times((N-n+1)dt/\tau)p_{nm_1m_2\cdots}\\&+\sum_I P(N-1, Q_1, \cdots, Q_I+1, \cdots; t)a_I(Q_I+1)dt\\&+[1-Sdt-N(dt/\tau)-\sum_I a_I Q_I dt]\\&\qquad\times P(N, Q_1, Q_2, \cdots; t).\end{aligned}$$

Let us now multiply both sides of the above by

$$x^N y_1^{Q_1}y_2^{Q_2}\cdots,$$

and sum over N, Q_1, Q_2, $\cdots$. The left-hand side becomes $F(t+dt)$, and the terms on the right become, respectively,

$$SdtxF,\quad \frac{dt}{\tau}f(x, y_i)\partial F/\partial x,\quad x\sum_i a_i\partial F/\partial y_i,$$

and

$$\left[F(t)-SFdt-\frac{dt}{\tau}x\frac{\partial F}{\partial x}-\sum_i a_i y_i\frac{\partial F}{\partial y_i}dt\right].$$

By equating the two sides, dividing by dt, and letting $dt\to 0$, we get

$$\begin{aligned}\partial F/\partial t&=(x-1)SF+\tau^{-1}(f(x, y_i)-x)\partial F/\partial x\\&\quad+\sum_i a_i(x-y_i)\partial F/\partial y_i.\end{aligned} \tag{2.11}$$

It should be noted that the derivation of this equation does not demand the assumption of the constancy in time of S, $f(x, y_i)$, or τ. We shall, in fact, in later sections, deal with cases in which some of these quantities vary with time.

From the equation for F, it is possible, by differentiating successively and putting x, $y_i=1$, to obtain equations for $\langle N\rangle_{Av}$, $\langle Q_i\rangle_{Av}$, φ_{NN}, φ_{Nj}, φ_{ij}, and also, if desired, the higher moments of the

probability distribution. In simple particular cases it may even be possible to solve Eq. (2.11) completely for F.

III. STEADILY OPERATING PILE

In the case of a pile operating at a constant mean intensity, all the probabilities $P(N, Q_i; t)$ are independent of time, and therefore

$$\partial F/\partial t=0.$$

The differential equation (2.11) thus becomes

$$S(x-1)F+\tau^{-1}[f(x, y_i)-x]F_x +\sum_{i=1}^{m} a_i(x-y_i)F_i=0, \quad (3.1)$$

where the subscripts x, i indicate differentiation with respect to x, y_i, respectively.

Differentiating (3.1) in turn by x and each of the y_i, adding the resulting equations, and setting $x=y_i=1$, we obtain, with the help of (1.10), (2.2), and (2.6),

$$\begin{aligned}\langle N\rangle_{\text{Av}}&=F_x=S\tau/(1-k);\\ \langle Q_i\rangle_{\text{Av}}&=F_i=c_iS\tau/\epsilon_i(1-k),\end{aligned} \quad (3.2)$$

where $\epsilon_i=a_i\tau$.

Differentiating (3.1), in turn, by all sets of two of the variables x and y_i and setting $x=y_i=1$, we obtain the following set of equations for the moments φ_{NN}, φ_{Ni}, φ_{ik}:

$$(1-k+c)\varphi_{NN}-\sum \epsilon_i\varphi_{Ni} =[\tfrac{1}{2}f_{xx}+(1-k+c)]\langle N\rangle_{\text{Av}}, \quad (3.3)$$

$$-c_i\varphi_{NN}+(1-k+c+\epsilon_i)\varphi_{Ni}-\sum_j \epsilon_j\varphi_{ij} =(f_{xi}-2c_i)\langle N\rangle_{\text{Av}}, \quad (3.4)$$

$$-c_i\varphi_{Nk}-c_k\varphi_{Ni}+(\epsilon_i+\epsilon_k)\varphi_{ik} =(f_{ik}+2c_i\delta_{ik})\langle N\rangle_{\text{Av}}. \quad (3.5)$$

We shall solve these equations for the case when there are no delayed neutrons, for one delayed-neutron period, and for many delayed-neutron periods.

A. No Delayed Neutrons

When the delayed neutrons are neglected, Eqs. (3.3) to (3.5) reduce to the single equation

$$(1-k)\varphi_{NN}=[\tfrac{1}{2}(k_2-k)+(1-k)]\langle N\rangle_{\text{Av}}, \quad (3.6)$$

so that

$$\begin{aligned}\varphi_{NN}&=[1+(k_2-k)/2(1-k)]\langle N\rangle_{\text{Av}}\\ &=[(k_2-k)/2S\tau]\langle N\rangle_{\text{Av}}^2+\langle N_{\text{Av}}\rangle. \quad (3.7)\end{aligned}$$

Thus when the power level is changed by varying k, the mean square fluctuations are essentially proportional to the square of the number of neutrons; in other words the mean fractional deviation of the number of neutrons from the mean is independent of the number. We shall see in the following sections how this conclusion is modified when the delayed neutrons are taken into account.

B. One Delayed-Neutron Period

Let us assume that only one type of fission-product nucleus gives rise to delayed neutrons. Equations (3.3) to (3.5) then become

$$(1-k+c)\varphi_{NN}-\epsilon\varphi_{NQ} =[\tfrac{1}{2}f_{xx}+(1-k+c)]\langle N\rangle_{\text{Av}}, \quad (3.8)$$

$$-c\varphi_{NN}+(1-k+c+\epsilon)\varphi_{NQ}-\epsilon\varphi_{QQ} =(f_{xy}-2c)\langle N\rangle_{\text{Av}}, \quad (3.9)$$

$$-c\varphi_{NQ}+\epsilon\varphi_{QQ}=(c+\tfrac{1}{2}f_{yy})\langle N\rangle_{\text{Av}}. \quad (3.10)$$

Adding (3.8), (3.9), and (3.10), we obtain

$$(1-k)(\varphi_{NN}+\varphi_{NQ}) =[\tfrac{1}{2}(k_2-k)+(1-k)]\langle N\rangle_{\text{Av}}. \quad (3.11)$$

Solving (3.8), (3.10), and (3.11), we find

$$\varphi_{NN}=\langle N\rangle_{\text{Av}}\left[1+\frac{(1-k+\epsilon)(k_2-k)}{2(1-k)(1-k+\epsilon+c)} -\frac{\tfrac{1}{2}c'}{1-k+\epsilon+c}\right], \quad (3.12)$$

$$\varphi_{NQ}=\langle N\rangle_{\text{Av}}\left[\frac{c(k_2-k)}{2(1-k)(1-k+\epsilon+c)} +\frac{\tfrac{1}{2}c'}{1-k+\epsilon+c}\right], \quad (3.13)$$

$$\varphi_{QQ}=(\langle N\rangle_{\text{Av}}/\epsilon)\left[\frac{c^2(k_2-k)}{2(1-k)(1-k+\epsilon+c)} +\frac{\tfrac{1}{2}cc'}{1-k+\epsilon+c}+c^2+\tfrac{1}{2}cf_{yy}\right]. \quad (3.14)$$

In practice the second term in the bracket of (3.12) will be large compared to the first and third, so that we have, approximately,

$$\varphi_{NN}=\langle N\rangle_{Av}\frac{(1-k+\epsilon)(k_2-k)}{2(1-k)(1-k+\epsilon+c)}$$
$$=\langle N\rangle_{Av}^2\frac{(k_2-k)(1-k+\epsilon)}{2S\tau(1-k+\epsilon+c)}. \quad (3.15)$$

When $1-k\gg c$ and $1-k\gg\epsilon$, this is identical with the expression (3.7) for the case in which there are no delayed neutrons. However, when the number of neutrons is increased by bringing k closer to unity, (3.15) increases more slowly than (3.7), i.e., the delayed neutrons tend to smooth out the fluctuations.

In practice ϵ will be much smaller than c: ($c\approx 0.01$; $\epsilon=\tau/$(lifetime of delayed-neutron emitters) $\approx 10^{-3}$ sec./10 sec. $=10^{-4}$). There will, therefore, be a range of values of k for which $\epsilon\ll(1-k)\ll c$, so that

$$\varphi_{NN}\approx((k_2-k)/2c)\langle N\rangle_{Av}, \quad (3.16)$$

i.e., in this range the fluctuations increase with the square root of $\langle N\rangle_{Av}$. Finally, if $1-k\gg\epsilon$, (3.15) becomes

$$\varphi_{NN}=\langle N\rangle_{Av}^2\frac{(k_2-k)\epsilon}{2S\tau(c+\epsilon)}, \quad (3.17)$$

i.e., the fluctuations are again proportional to $\langle N\rangle_{Av}$, but with a smaller constant of proportionality than in the case of no delayed neutrons.

C. Several Delayed-Neutron Groups

When there are m distinct groups of delayed neutrons, the equations to be solved are (3.3), the m equations (3.4), and the $\frac{1}{2}m(m+1)$ equations (3.5). These equations determine the $\frac{1}{2}(m+1)(m+2)$ quantities φ_{NN}, φ_{Ni}, and φ_{ik}. Adding (3.3), all Eq. (3.4), and all Eq. (3.5) multiplied by $\frac{1}{2}$, we obtain

$$(1-k)(\varphi_{NN}+\sum_i\varphi_{Ni})$$
$$=\langle N\rangle_{Av}[\tfrac{1}{2}(k_2-k)+(1-k)]. \quad (3.18)$$

Let us define ϵ^* by

$$\sum_i\epsilon_i\varphi_{Ni}=\epsilon^*\sum_i\varphi_{Ni}. \quad (3.19)$$

Equations (3.3) and (3.18) for φ_{NN} and $\sum\varphi_{Ni}$ are now exactly similar to Eqs. (3.8) and (3.11) for φ_{NN} and φ_{NQ}, with ϵ^* taking the place of ϵ. The solutions are, therefore,

$$\varphi_{NN}=\langle N\rangle_{Av}\left[1+\frac{(1-k+\epsilon^*)(k_2-k)}{2(1-k)(1-k+c+\epsilon^*)}-\frac{c'}{2(1-k+c+\epsilon^*)}\right], \quad (3.20)$$

$$\sum\varphi_{Ni}=\langle N\rangle_{Av}\left[\frac{c(k_2-k)}{2(1-k)(1-k+c+\epsilon^*)}+\frac{c'}{2(1-k+c+\epsilon^*)}\right]. \quad (3.21)$$

The problem is to find ϵ^*. To do this, in other words to determine the proper weight function to be used in averaging the ϵ_i, we have to solve Eqs. (3.3) to (3.5) numerically. This can be done if the number of delayed-neutron periods is not too great.

In the special case where $1-k$ is small enough, it is possible to obtain approximate explicit expressions for the φ's.

We first solve (3.5) for φ_{ik}, obtaining

$$\varphi_{ik}=[c_i\varphi_{Nk}+c_k\varphi_{Ni}+\langle N\rangle_{Av}(f_{ik}+2c_i\delta_{ik})]/(\epsilon_i+\epsilon_k). \quad (3.22)$$

Equation (3.4) becomes

$$(1-k+\epsilon_i)\varphi_{Ni}-\sum_k\frac{\epsilon_kc_i\varphi_{Nk}-\epsilon_ic_k\varphi_{Ni}}{\epsilon_i+\epsilon_k}$$
$$=c_i\varphi_{NN}+\langle N\rangle_{Av}[f_{xi}-c_i+\sum_i\epsilon_kf_{ik}/(\epsilon_i+\epsilon_k)]. \quad (3.23)$$

Let us now assume

$$(1-k)/\epsilon_i=\mu_i\ll 1. \quad (3.24)$$

Since $\varphi_{NN}\gg\langle N\rangle_{Av}$ and $\varphi_{NN}\gg S\tau$, the right-hand side of (3.23) is approximately equal to $c_i\varphi_{NN}$. Let us assume for a moment that the summation on the left-hand side may be neglected. Equation (3.23) then becomes, approximately,

$$\varphi_{Ni}\approx[c_i/\epsilon_i(1+\mu_i)]\varphi_{NN}\approx(c_i/\epsilon_i)\varphi_{NN}(1-\mu_i). \quad (3.25)$$

We now substitute this into the summation to see whether the assumption that the summation

may be neglected is justified. We find

$$\sum_j (\epsilon_j c_i \varphi_{Nj} - \epsilon_i c_j \varphi_{Ni})/(\epsilon_i+\epsilon_j) = c_i \varphi_{NN} \sum_j (\mu_i-\mu_j)c_j/(\epsilon_i+\epsilon_j). \quad (3.26)$$

Our assumption is justified if

$$|\sum_j (\mu_i-\mu_j)c_j/(\epsilon_i+\epsilon_j)| \ll 1 \quad (3.27)$$

for all i. This will be true if

$$\mu_i \ll 1/\sum(c_j/\epsilon_j) \text{ for all } i.$$

Neglecting μ_i in (3.25), we have

$$\varphi_{Ni} \approx c_i \varphi_{NN}/\epsilon_i; \quad (3.28)$$

substituting in (3.19), we find

$$\epsilon^* = \sum c_i / \sum (c_i/\epsilon_i). \quad (3.29)$$

Since we have assumed $1-k \ll \epsilon_i$, we must have $1-k \ll \epsilon^*$, so that (3.20) becomes

$$\varphi_{NN} \approx \frac{\epsilon^*(k_2-k)}{2(c+\epsilon^*)(1-k)}\langle N\rangle_{Av} = \frac{\epsilon^*(k_2-k)}{2(c+\epsilon^*)S\tau}\langle N\rangle_{Av}^2 \quad (3.30)$$

for the limiting case $1-k \ll \epsilon_i/\sum(c_j/\epsilon_j) = \epsilon_i\epsilon^*/c$, i.e., for sufficiently high power levels.

IV. CASE OF VARIABLE k IN THE ABSENCE OF DELAYED NEUTRONS

Let us consider the problem of fluctuations in intensity, in the absence of delayed neutrons, in a pile in which the relative probabilities of loss and reproduction of neutrons varies with time. Such a time variation will be met in a "pulse generator," or in the application of cyclical variations for determining the operating characteristics of any pile.

It will be justifiable in a first approximation to neglect the delayed-neutron term, and include the contribution of delayed neutrons in the source, if the period of time variation of the function f is short compared to the delayed-neutron periods. This will of course give a constant source only if the *mean* level of operation of the pile is held constant.

The derivation of the differential equations for $\langle N\rangle_{Av}$ and φ_{NN} does not differ from that when the function f has constant coefficients. The equations are

$$d\langle N\rangle_{Av}/dt = S - \kappa\langle N\rangle_{Av} \quad (\kappa=(1-k)/\tau), \quad (4.1)$$

$$d\varphi_{NN}/dt = -2\kappa\varphi_{NN} + \kappa_2\langle N\rangle_{Av} + S, \quad (4.2)$$

where $\kappa_2 = (k_2-2k+1)/\tau \approx (k_2-1)/\tau$. This is very nearly constant if k remains near unity.

The solution of (4.1) is

$$\langle N\rangle_{Av} = \exp\left(-\int_0^t \kappa dt'\right) \times \left\{S\int_0^t \exp\left(\int_0^{t'} \kappa dt''\right)dt' + \langle N(0)\rangle_{Av}\right\}. \quad (4.3)$$

Inserting this into (4.2) we get

$$\varphi_{NN} = \exp\left(-2\int_0^t \kappa dt'\right) \times \left\{\int_0^t [\langle N(t')\rangle_{Av}\kappa_2 + S] \times \exp\left(2\int_0^{t'} \kappa dt''\right)dt' + \varphi_{NN}(0)\right\}. \quad (4.4)$$

Let us consider the case in which k is constant. We find then that

$$\langle N(t)\rangle_{Av} - S/\kappa = e^{-\kappa t}[\langle N(0)\rangle_{Av} - S/\kappa], \quad (4.5)$$

i.e., any excess of $\langle N(0)\rangle_{Av}$ over the steady-state value will decay or grow exponentially, according to whether $k<1$ or $k>1$.

Substituting (4.5) into (4.2) and simplifying, we obtain

$$\varphi_{NN}(t) - (S/2\kappa)(1+\kappa_2/\kappa) = [\varphi_{NN}(0) - (S/2\kappa)(1+\kappa_2/\kappa)]e^{-2\kappa t} + (\kappa_2/\kappa)[\langle N(0)\rangle_{Av} - S/\kappa](e^{-\kappa t} - e^{-2\kappa t}). \quad (4.6)$$

Thus, in addition to a decay or growth of the excess of the initial value of φ_{NN} over the steady-state value, there is another term which is due to the deviation of $\langle N(0)\rangle_{Av}$ from its steady-state value.

Case of Periodic "k"

Let us consider now the case in which k, and consequently κ, is periodic with period T, i.e.,

$$\kappa(t+T)=\kappa(t). \tag{4.7}$$

Let us introduce the following notations:

$$\int_0^t \kappa dt' = \sigma(t), \tag{4.8}$$

$$\sigma(T)=I. \tag{4.9}$$

Now suppose $mT \leq t' \leq (m+1)T$. Then

$$\int_0^{t'} \kappa dt'' = mI+\sigma(t'-mT). \tag{4.10}$$

Now put

$$\int_0^t e^{\sigma(t')}dt' = \chi(t), \tag{4.11}$$

$$\chi(T)=A. \tag{4.12}$$

We then find that, for $nT \leq t \leq (n+1)T$,

$$\int_0^t \exp\left(-\int_0^{t'} \kappa dt''\right)$$
$$= A(1+e^I+e^{2I}+\cdots e^{(n-1)I})+e^{nI}\chi(t-nT)$$
$$= A\frac{e^{nI}-1}{e^I-1}+e^{nI}\chi(t-nT).$$

It follows that, if we put $\eta = t-nT$ (that is, if η is time elapsed since the end of the last completed period)

$$\langle N\rangle_{Av}(t) = e^{-nI-\sigma(\eta)}$$
$$\times\left\{\langle N\rangle_{Av}(0)+S\left[A\frac{e^{nI}-1}{e^I-1}+e^{nI}\chi(\eta)\right]\right\}.$$

As $n\to\infty$, that is, when the oscillation has been in effect for a sufficient length of time so that the effect of starting has disappeared, this reduces to

$$\langle N\rangle_{Av}(T) = Se^{-\sigma(\eta)}\left\{\frac{A}{e^I-1}+\chi(\eta)\right\}. \tag{4.13}$$

If we now substitute into Eq. (4.4), and, as above, make use of the periodicity of κ, we get

$$\varphi_{NN} = e^{-(2nI+2\sigma(\eta))}\Big\{(1+e^{2I}+e^{4I}+\cdots+e^{2(n-1)I})S$$
$$\times\int_0^T\left[\kappa_2 e^{-\sigma(\eta')}\left(\frac{A}{e^I-1}+\chi(\eta')\right)+1\right]e^{2\sigma(\eta')}d\eta'$$
$$+Se^{2nI}\int_0^\eta\left[\kappa_2 e^{-\sigma(\eta')}\left(\frac{A}{e^I-1}+\chi(\eta')\right)+1\right]$$
$$\times e^{2\sigma(\eta')}d\eta'+\varphi_{NN}(0)\Big\}.$$

We must again let $n\to\infty$ to neglect the transient effects. We then obtain

$$\varphi_{NN}(t) = Se^{-2\sigma(\eta)}\left\{\frac{1}{e^{2I}-1}\left[\kappa_2 A^2\left(\frac{1}{e^I-1}+\tfrac{1}{2}\right)+A_2\right]\right.$$
$$\left.+\kappa_2\chi(\eta)\left[\frac{A}{e^I-1}+\tfrac{1}{2}\chi(\eta)\right]+\chi_2(\eta)\right\}, \tag{4.14}$$

where

$$\chi_2(\eta) = \int_0^\eta e^{2\sigma(\eta')}d\eta', \tag{4.15}$$

$$\chi_2(T)=A_2. \tag{4.16}$$

V. EFFECT OF RESOLVING TIME OF THE MEASURING INSTRUMENT ON THE MEASUREMENT OF STATISTICAL FLUCTUATIONS IN A PILE

Any practical measurement of fluctuations will be subject to limitations imposed by the resolving time of the measuring instrument and by the fact that the measurements will extend over only a finite time interval.

The effect of a resolving time of the measuring instrument is that the quantity measured is not an instantaneous value of N (or of the neutron intensity), but rather a value averaged over an interval of length Δt, where Δt is the resolving time.

Thus fluctuations whose period is appreciably shorter than Δt will not be observed. Similarly, if the measurements extend over a time T, fluctuations whose period are appreciably longer than T will not be observed. In order to interpret experimental measurements, it is therefore neces-

sary to know the frequency distribution of the fluctuations.

Let $\varphi_{NN}{}^{(\Delta t)}$ be the standard deviation of the number of neutrons averaged over an interval Δt, i.e., the standard deviation observed when measurements with an instrument of resolving time Δt extend over an infinite time. If sharp measurements (resolving time zero) could be taken over a finite interval, T, the standard deviation observed would be then, on the average,

$$\varphi_{NN(T)} = \varphi_{NN} - \varphi_{NN}{}^{(T)}.$$

For

$$\varphi_{NN} = \langle N^2\rangle_{Av} - \langle N\rangle_{Av}{}^2;$$

$$\varphi_{NN}{}^{(T)} = \langle\langle N\rangle_{AvT}{}^2\rangle_{Av} - \langle N\rangle_{Av}{}^2,$$

where "AvT" denotes averaging over the time interval, T, and

$$\varphi_{NN(T)} = \langle\langle N^2\rangle_{AvT} - \langle N\rangle_{AvT}{}^2\rangle_{Av} = \langle N^2\rangle_{Av} - \langle\langle N\rangle_{AvT}{}^2\rangle_{Av}.$$

The standard deviation observed when measurements with resolving time Δt extend over an interval T is then

$$\varphi_{NN}\,|_T{}^{\Delta t} = \varphi_{NN}{}^{(\Delta t)} - \varphi_{NN}{}^{(T)}.$$

We now determine the function $\varphi_{NN}{}^{(\Delta t)}$. The quantity $\langle N^2\rangle_{Av}$, which was used in Section II for the calculation of fluctuations in the case of sharp measurements, must be replaced by

$$\langle N^2\rangle_{Av\Delta t} = \frac{1}{(\Delta t)^2}\sum_{N', N'', Q_i', Q_i''} N'N'' \int_{t-\Delta t}^{t} dt' \times \int_{t-\Delta t}^{t} dt'' R(N', N''; Q_i', Q_i''; t', t''), \quad (5.1)$$

where $R(N', N''; Q_i', Q_i''; t', t'')$ is the probability that there are N' neutrons, Q_i' excited nuclei at time t', and N'' neutrons, Q_i'' excited nuclei at time t''. Equation (5.1) may be transformed to

$$\langle N^2\rangle_{Av\Delta t} = \frac{2}{(\Delta t)^2}\sum_{N', N'', Q_i', Q_i''} N'N'' \int_{t-\Delta t}^{t} dt' \times \int_{0}^{t-t'} d\xi \cdot R^*(N', N''; Q_i', Q_i''; t', \xi), \quad (5.2)$$

where R^* is the probability that there are N' neutrons, Q_i' excited nuclei at time t', and N'' neutrons, Q_i'' excited nuclei at a time ξ later (i.e., at the time $t'+\xi$). We may write

$$R^*(N', N''; Q_i', Q_i''; t', \xi) = (\text{the probability } P(N', Q_i'; t') \text{ of } N' \text{ neutrons, } Q_i' \text{ excited nuclei at } t') \times (\text{the probability } P_{N'Q_i'}{}^{N''Q_i''}(\xi) \text{ that } N', Q_i' \text{ give rise to } N'', Q_i'' \text{ in time } \xi). \quad (5.3)$$

We may introduce the probability-generating function

$$G(x, x'; y_i, y_i'; t, \xi) = \sum_{N, N', Q_i, Q_i'} R^*(N, N'; Q_i, Q_i'; t, \xi) \times x^N x'^{N'} \Pi_i\{y_i^{Q_i} y_i'^{Q_i'}\}, \quad (5.4)$$

where the $\Pi_i\{\ \}$ indicates a product over the y's corresponding to the various delayed-neutron periods. Then

$$\langle N^2\rangle_{Av\Delta t} = (2/(\Delta t)^2)\int_{t-\Delta t}^{t} dt' \times \int_{0}^{t-t'} d\xi \partial^2 G/\partial x \partial x'\,|_{x=x'=y_i=y_i'=1}. \quad (5.5)$$

This may be written alternatively, on interchanging the order of integrations,

$$\langle N^2\rangle_{Av\Delta t} = (2/(\Delta t)^2)\int_{0}^{\Delta t} d\xi \times \int_{t-\Delta t}^{t-\xi} dt' \partial^2 G/\partial x \partial x'\,|_{x=x'=y_i=y_i'=1}. \quad (5.6)$$

Our problem is now to find the function G.

Let us now introduce the following probability-generating functions:

(a) Let

$$\varphi(x, y_i, t) = \sum_{N'Q_i'} \varphi_{N'Q_i'}(t) x^{N'} \Pi_i y_i^{Q_i'} \quad (5.7)$$

be the function whose coefficients are the probabilities that, in the absence of sources, 1 neutron at time 0 will give rise to N' neutrons, Q_i' excited nuclei at time t.

(b) Let

$$\psi^{(j)}(x, y_i, t) = \sum_{N'Q_i'} \psi_{N'Q_i'}{}^{(j)}(t) x^{N'} \Pi_i y_i^{Q_i'} \quad (5.8)$$

be the function whose coefficients are the probabilities that, in the absence of sources, one excited

nucleus of type j at time 0 will give rise to N' neutrons, Q_i' excited nuclei at time t.

(c) Let

$$F_s(x, y_i, t) = \sum_{N', Q_i'} P_{N'Q_i'^{(s)}}(t) x^{N'} \Pi_i y_i^{Q_i'} \quad (5.9)$$

be the function whose coefficients are the probabilities that N' neutrons, Q_i' excited nuclei are produced by a source of strength S in time t, there being no neutrons or excited nuclei present at $t=0$. It is then easily demonstrated that in the absence of sources, φ^N is the probability-generating function for the initial condition of N neutrons alone present at $t=0$; $\psi^{(j)Q_j}$ is that for the initial condition of Q_j excited nuclei of type j alone present at $t=0$. The function $\varphi^N \Pi_j \psi^{(j)Q_j}$ is the probability-generating function corresponding to N neutrons, Q_1 excited nuclei of type 1, etc., at $t=0$. Finally, the function

$$\Omega_{NQ_1Q_2\cdots}(x, y_i; t) = F_s \varphi^N \Pi_j \psi^{(j)Q_j} \quad (5.10)$$

is the probability-generating function for the same problem when sources are present.

It is easily verified that Ω satisfies the appropriate differential equation (2.11).

We may now write down the function

$$G(x, x'; y_i, y_i'; t, \xi).$$

It is, in fact, equal to

$$F_s(x', y_i', \xi) F[x\varphi(x', y_i', \xi) \cdot y_1 \psi^{(1)}(x', y_i', \xi), \cdots t], \quad (5.11)$$

where $F(x, y_1, y_2, \cdots; t)$ is the probability-generating function for the number of neutrons and excited nuclei in the system at time t, as defined in Section II. For this is equal to

$$F_s \sum P(N, Q_i; t)(x\varphi)^N (y_1\psi^{(1)})^{Q_1} \cdots = \sum P(N, Q_i; t) \Omega_{NQ_i}(x', y_i'; \xi) x^N y_i^{Q_i}. \quad (5.12)$$

Comparison with (5.4) enables us to identify this function with G.

Differentiating (5.11) with respect to x and x', and setting all the x, x', y_i, y_i' equal to unity, we find

$$\partial^2 G/\partial x \partial x' \,|_{x=x'=y_i=y_i'=1} = \langle N_s(\xi)\rangle_{Av}\langle N(t)\rangle_{Av} + \langle N_n(\xi)\rangle_{Av}\langle N^2(t)\rangle_{Av} + \sum \langle N_j(\xi)\rangle_{Av}\langle NQ_j(t)\rangle_{Av}, \quad (5.13)$$

where $\langle N_s(\xi)\rangle_{Av}$ is the mean number of neutrons present at time ξ arising from the action of the source if $N(0)=Q_i(0)=0$; $\langle N_n(\xi)\rangle_{Av}$ is the mean number of neutrons at time ξ if $S=0$, $N(0)=1$, $Q_i(0)=0$; $\langle N_j(\xi)\rangle_{Av}$ is the mean number of neutrons at time ξ if $S=0$, $N(0)=0$, $Q_i(0)=0$ for $i \neq j$, and $Q_j(0)=1$.

In the steady state $G(x, y_i, \cdots; t, \xi)$ does not depend on t, and (5.6) becomes

$$\varphi_{NN}{}^{(\Delta t)} = (2/(\Delta t)^2) \int_0^{\Delta t} (\Delta t - \xi) \times [\langle N_n(\xi)\rangle_{Av}\langle N^2\rangle_{Av} + \sum \langle N_j(\xi)\rangle_{Av}\langle NQ_j\rangle_{Av} - \langle N\rangle_{Av}(\langle N\rangle_{Av} - \langle N_s(\xi)\rangle_{Av})] d\xi. \quad (5.14)$$

But $\langle N\rangle_{Av} - \langle N_s(\xi)\rangle_{Av}$ is the average number of neutrons which would exist at time t if $S=0$, $N(0)=\langle N\rangle_{Av}$, $Q_j(0)=\langle Q_j\rangle_{Av}$:

$$\langle N\rangle_{Av} - \langle N_s(\xi)\rangle_{Av} = \langle N\rangle_{Av}\langle N_n(\xi)\rangle_{Av} + \sum_j \langle Q_j\rangle_{Av}\langle N_j(\xi)\rangle_{Av}. \quad (5.15)$$

Substituting in (5.14) we get

$$\varphi_{NN}{}^{(\Delta t)} = (2/(\Delta t)^2) \int_0^{\Delta t} (\Delta t - \xi) \times [\varphi_{NN}\langle N_n(\xi)\rangle_{Av} + \sum_j \varphi_{Nj}\langle N_j(\xi)\rangle_{Av}] d\xi. \quad (5.16)$$

$\langle N_n\rangle_{Av}(t)$ is determined by Eqs. (1.1) and (1.2), with $S=0$ and the initial conditions $\langle N\rangle_{Av}(0)=1$, $\langle Q_i\rangle_{Av}(0)=0$. Let us look for solutions of the form

$$\langle N\rangle_{Av} = \langle N\rangle_{Av}(0) e^{-\gamma t},$$
$$\langle Q_i\rangle_{Av} = \langle Q_i\rangle_{Av}(0) e^{-\gamma t}.$$

We find that γ must satisfy the equation

$$\kappa' - \gamma = (1/\tau) \sum_{i=1}^{n} a_i c_i/(a_i - \gamma), \quad (5.17)$$

which has $(n+1)$ solutions γ_s. Here $\kappa' = (1-k')/\tau$. The general solution is then

$$\langle N\rangle_{Av} = \sum_{s=0}^{n} \rho_s e^{-\gamma_s t}, \quad (5.18)$$

$$\langle Q_i\rangle_{Av} = (c_i/\tau) \sum_{s=0}^{n} \rho_s e^{-\gamma_s t}/(a_i - \gamma_s). \quad (5.19)$$

With the initial condition $N(0)=1$, $Q_i(0)=0$,

we get the equations for ρ_s:

$$\sum_{s=0}^{n} \rho_s = 1, \tag{5.20}$$

$$\sum_{s=0}^{n} \rho_s/(a_i-\gamma_s) = 0, \quad (i=1, 2, \cdots, n). \tag{5.21}$$

Alternatively, the ρ_s's may be determined by solving (1.1) and (1.2) above, for the case $S=0$, by Laplace transforms. It is then easily verified that

$$\rho_s = \gamma_s\tau/[\kappa\tau+\sum_i c_i/(1-a_i/\gamma_s)^2]. \tag{5.22}$$

Since if there is only an excited nucleus present at $\xi=0$, it must first decay, and this is followed by the decay of the resulting neutron, we have

$$\langle N_j(\xi)\rangle_{Av} = a_j\int_0^\xi e^{-a_jt'}\langle N_n(\xi-\xi')\rangle_{Av}d\xi'. \tag{5.23}$$

Explicitly,

$$\begin{aligned}\langle N_j(\xi)\rangle_{Av} &= a_j\sum_s [\rho_s/(a_j-\gamma_s)](e^{-\gamma_s\xi}-e^{-a_j\xi}) \\ &= a_j\sum_s \rho_s e^{-\gamma_s\xi}/(a_j-\gamma_s),\end{aligned} \tag{5.24}$$

because of (5.21). Substituting from (5.17) and (5.20) into (5.16), we get

$$\varphi_{NN}^{(\Delta t)} = \sum_{s=0}^{n} \frac{2\rho_s}{(\gamma_s\Delta t)^2}(\gamma_s\Delta t-1+e^{-\gamma_s\Delta t}) \times\left[\varphi_{NN}^{(0)}+\sum_{j=1}^{n}\frac{a_j\varphi_{Nj}^{(0)}}{a_j-\gamma_s}\right]. \tag{5.25}$$

Expression (5.25) may be simplified for the case of very small or very large values of Δt. If $\gamma_s\Delta t \ll 1$ for all γ_s, we may write

$$2(\gamma_s\Delta t-1+e^{-\gamma_s\Delta t})/(\gamma_s\Delta t)^2 = 1-\tfrac{1}{3}\gamma_s\Delta t. \tag{5.26}$$

With the help of (5.20) and (5.21) and the relation

$$\sum_{s=0}^{m} \rho_s\gamma_s = \kappa' \tag{5.27}$$

(which follows from (5.17)), we can transform (5.25) to

$$\varphi_{NN}^{(\Delta t)} = \varphi_{NN}(1-\tfrac{1}{3}\kappa'\Delta t)+(\Delta t/3\tau)\sum_l \epsilon_l\varphi_{Nl}. \tag{5.28}$$

From (3.19), (3.20), and (3.21) we have

$$\varphi_{NN} = (1-k+\epsilon^*)\Phi/(1-k+\epsilon^*+c);$$
$$\sum \epsilon_l\varphi_{Nl} = \epsilon^*c\Phi/(1-k+\epsilon^*+c),$$

where

$$\Phi = \tfrac{1}{2}(k_2-k)\langle N\rangle_{Av}/(1-k),$$

so that

$$\varphi_{NN}^{(\Delta t)}/\varphi_{NN} = 1 - \tfrac{1}{3}\kappa\Delta t(1-k+c+\epsilon^*)/(1-k+\epsilon^*). \tag{5.29}$$

Similarly, it can be shown that, if $\gamma_s\Delta t \gg 1$ for all γ_s, i.e., if Δt is longer than the longest relaxation period of the pile,

$$\begin{aligned}\varphi_{NN}^{(\Delta t)}/\varphi_{NN} &= 2\Phi/\kappa\Delta t\varphi_{NN} \\ &= 2(1-k+\epsilon^*+c)/\kappa\Delta t(1-k+\epsilon^*).\end{aligned} \tag{5.30}$$

In practice Δt will often be longer than the shortest relaxation period and shorter than the longest. Let us assume that the various relaxation periods are well separated, and that

$$\gamma_{r+1}\Delta t \ll 1 \ll \gamma_r\Delta t.$$

Then, by writing

$$(2/(\gamma_s\Delta t)^2)(\gamma_s\Delta t-1+e^{-\gamma_s\Delta t}) = \begin{cases} 1, & s \geqslant r+1 \\ 2/\gamma_s\Delta t, & s \leqslant r \end{cases},$$

we obtain

$$\varphi_{NN}^{(\Delta t)}/\varphi_{NN} = \sum_{s=r+1}^{m} \rho_s[1+\sum_{l=1}^{m} a_l\varphi_{Nl}/(a_l-\gamma_s)\varphi_{NN}]. \tag{5.31}$$

In particular, if $r=0$, i.e., Δt is large compared to the shortest period but small compared to all others, (5.31) can be transformed to

$$\varphi_{NN}^{(\Delta t)}/\varphi_{NN} = 1 - (1-k)\epsilon^*/(1-k+c)(1-k+c+\epsilon^*), \tag{5.32}$$

and for $r=m-1$, i.e., for Δt large compared to all except the longest relaxation period of the pile,

$$\varphi_{NN}^{(\Delta t)}/\varphi_{NN} = \rho_m(1-k+\epsilon^*+c)/(1-k+\epsilon^*). \tag{5.33}$$

We may further deduce the "normalized spectrum" of the fluctuations. For, if $S(\sigma)d\sigma$ is the proportion of fluctuations corresponding to the

frequency σ, it follows from a theorem of Wang and Uhlenbeck,[4] that $S(\sigma)$ is the Fourier cosine transform of

$$[\langle N(t)N(t+\xi)\rangle_{Av}-\langle N\rangle_{Av}^2]/\varphi_{NN};$$

in fact, according to Wang and Uhlenbeck,

$$S(\sigma)=4\int_0^\infty \frac{\langle N(t)N(t+\xi)\rangle_{Av}-\langle N\rangle_{Av}^2}{\varphi_{NN}} \times\cos 2\pi\sigma\xi d\xi. \quad (5.34)$$

Using the relation

$$\langle N(t)N(t+\xi)\rangle_{Av}-\langle N\rangle_{Av}^2 = \varphi_{NN}\langle N_n(\xi)\rangle_{Av}+\sum_l \varphi_{Nl}\langle N_l(\xi)\rangle_{Av},$$

we get

$$S(\sigma)=\frac{4}{\varphi_{NN}}\left\{\varphi_{NN}\sum_{s=0}^{n}\frac{\rho_s\gamma_s}{\gamma_s^2+4\pi^2\sigma^2} +\sum_{l=1}^{n}a_l\varphi_{Nl}\frac{\rho_s}{a_l-\gamma_s} \times\left[\frac{\gamma_s}{\gamma_s^2+4\pi^2\sigma^2}-\frac{a_l}{a_l^2+4\pi^2\sigma^2}\right]\right\}. \quad (5.35)$$

[4] M. C. Wang and G. E. Uhlenbeck, Rev. Mod. Phys. 17, 326 (1945).

One can easily calculate the proportion of fluctuations of period greater than T; it is

$$\int_0^{1/T} S(\sigma)d\sigma=\frac{2}{\varphi_{NN}\pi}\left\{\varphi_{NN}\sum_{s=0}^{n}\rho_s\tan^{-1}\frac{2\pi}{\gamma_s T} +\sum_{l=1}^{n}a_l\varphi_{Nl}\sum_{s=0}^{n}\frac{\rho_s}{a_l-\gamma_s} \times\left[\tan^{-1}\frac{2\pi}{\gamma_s T}-\tan^{-1}\frac{2\pi}{a_l T}\right]\right\}. \quad (5.36)$$

The terms for which $\gamma_s T\ll 1$ are approximately equal to the corresponding term in the expression (5.25) for $\varphi_{NN}^{(\Delta t)}/\varphi_{NN}$ if

$$T=\pi^2\Delta t/3;$$

the terms with $\gamma_s T\gg 1$ are approximately equal to the corresponding terms in (5.25) if

$$T=2\Delta t.$$

In other words, one can get the order of magnitude of the ratio by which the resolving time cuts down the fluctuations by omitting those fluctuations whose period is more than two or three times the resolving time.

Such a result is to be expected, since the effect of resolving time and finite measuring time is, approximately, to eliminate from observation those fluctuations of periods shorter than the resolving time or longer than the measuring time.

Decay Scheme of $_{45}Rh^{106}$*

W. C. PEACOCK
Clinton Laboratories, Monsanto Chemical Company, Oak Ridge, Tennessee

(Received August 14, 1947)

The decay scheme of $_{45}Rh^{106}$ (30*s*) is proposed as a complex beta-spectra with end points at 3.55±0.10 and 2.30±0.10 Mev. The latter is 18±2 percent abundant and is followed by two gamma-rays 0.51±0.02 and 0.73±0.02 Mev in cascade, or a single 1.25±0.05-Mev gamma. The 1.25-Mev gamma is present in 1–2 percent of the disintegrations. Evidence in support of the Gamow-Teller selection rules for beta-decay is given.

I. INTRODUCTION

IN 1942 B. L. Goldschmidt and I. Perlman[1] found two isotopes of Ru with half-lives of about 1 month and 3 months in U bombarded for 45 days with neutrons from 14-Mev deuterons on Be. The longer-lived one had associated with it a hard beta-ray which they reported as about 2.7 Mev from absorption measurements in aluminum.

L. E. Glendenin and E. P. Steinberg[2,3] made an investigation of the Ru from U bombarded at the Clinton Laboratories pile. They reported the longer-lived Ru as having a 330 d half-life and a 30 sec. daughter of Rh which gave beta-radiation with approximately 4-Mev maximum and gamma-radiation. Further work by Glendenin[1,4] characterized the radiation from the 30 sec. Rh as 20 percent of 2.8-Mev and 80 percent of 3.9-Mev betas as measured by absorption in aluminum and coincidence techniques, and also 0.3- and 0.8-Mev gamma-rays as measured by absorption in lead. According to Sleight *et al.*,[5] the radiations from the Ru have not yet been detected and hence are probably less than 5-kev maximum energy.

The mass assignment of 106 was made by Dempster[6] with a mass spectrometer.

Grummitt and Wilkinson[7] report a beta-ray maximum of 3.3 Mev and half-lives of 290 d and 30 sec. for Ru^{106} and Rh^{106}, respectively. The former differs from the current Project value of 1.0*y* as given in reference 3.

II. SOURCES AND APPARATUS

Rh^{106} in the sample used was in secular equilibrium with Ru^{106} and had been separated from other fission products in November 1945 by sulfide precipitation and two subsequent distillations. All observations here reported were made during May, 1947 so that all activities

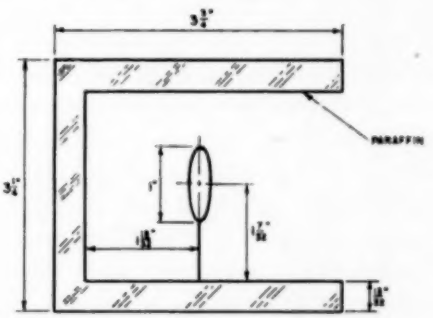

FIG. 1. Beta-ray source holder for spectrometer. (A beta-ray source is mounted on 50 g/cm² film and supported by the aluminum ring shown in the center of the figure.)

* This document is based on work performed under Contract No. W-35-058-eng-71 for the Atomic Energy Project at the Clinton Laboratories.

[1] From the Plutonium Project Report (PPR) Vol. 9B to be published shortly. This volume contains a complete report of Project information on the isotopes of Ru and Rh obtained in fission. B. L. Goldschmidt and I. Perlman, CC-295, Sept. 1942; PPR Vol. 9B, 7.18.1 (1946). A reference like the first refers to wartime reports of the Manhattan Project and one like the second reference is to papers prepared for the Plutonium Project Record (PPR), Vol. 9B, *Radiochemistry of the Fission Products*, in the process of being declassified and prepared for publication as part of the National Nuclear Energy Series, under the auspices of the United States Atomic Energy Commission.

[2] L. E. Glendenin and E. P. Steinberg, CC-579, p. 11, April 1943; CC-680, p. 9, May 1943; CC-920, p. 43, September 1943; Vol. 9B, 7.18.2 (1946).

[3] The numerical data bearing on decay characteristics, fission yields, and chain relationships of all known fission products are given by the Plutonium Project, Rev. Mod. Phys., **18**, 513–44 (1946) and also J.A.C.S., **68**, 2411–42 (1946).

[4] Plutonium Project Report, Rev. Mod. Phys. **18**, 526 (1946).

[5] N. R. Sleight, T. B. Novey, and L. E. Glendenin, PPR, Vol. 9B, 7.18.14 (1946).

[6] R. J. Hayden (working under the direction of A. J. Dempster), CP-3383, p. 4, December 1945.

[7] W. E. Grummitt and G. Wilkinson, Nature **158**, 163 (1946).

except Ru^{106} and Rh^{106} should have decayed to less than 1 percent of the total activity.

Approximately 50-μ curies of this activity were dried (at temperatures well below 150°C at which the Ru volatilizes) on to the center of a laminated film of polystyrene and Formvar one inch in diameter, and approximately 50-μ g/cm^2. The film was supported by a thin aluminum ring mounted as shown in Fig. 1. This served as a beta-source for a thin lens-type beta-ray spectrometer similar to that described by Deutsch *et al.*[8]

A spectrometer source was also prepared for the study of the gamma-rays by evaporating approximately 2 mc of the solution into a lead cup. This cup was thick enough to stop all the beta-rays at the source (1.8 g/cm^2). Electrons resulting from gamma-ray interactions in the lead were also analyzed in the spectrometer, and for a part of the time a thin uranium foil was put over the lead cup in order to increase the number of photo-electron interactions.

Annihilation radiation from the positrons of Cu^{64} (12.8 h) were used to calibrate the spectrometer. Thereafter, the beta-rays from P^{32} (14.3 d), mounted as in Fig. 1, were analyzed and found to form a straight line on a Kurie plot from their end point (1.72 Mev) to the point where the absorption caused by the counter window became appreciable (<150 kev).

Absolute gamma-counter efficiency as a function of gamma-ray energy was determined prior to the coincidence measurements using[9] Na^{24}, Co^{60}, I^{131}, and Au^{198}.

Beta-gamma, and gamma-gamma coincidence measurements were made using samples dried on 3 g/cm^2 polystyrene. The coincidence techniques used were similar to those used elsewhere.[9–11]

Coincidence and individual counting rates were recorded continuously on separate scaling circuits. The coincidence circuit had a resolving time of approximately one microsecond.

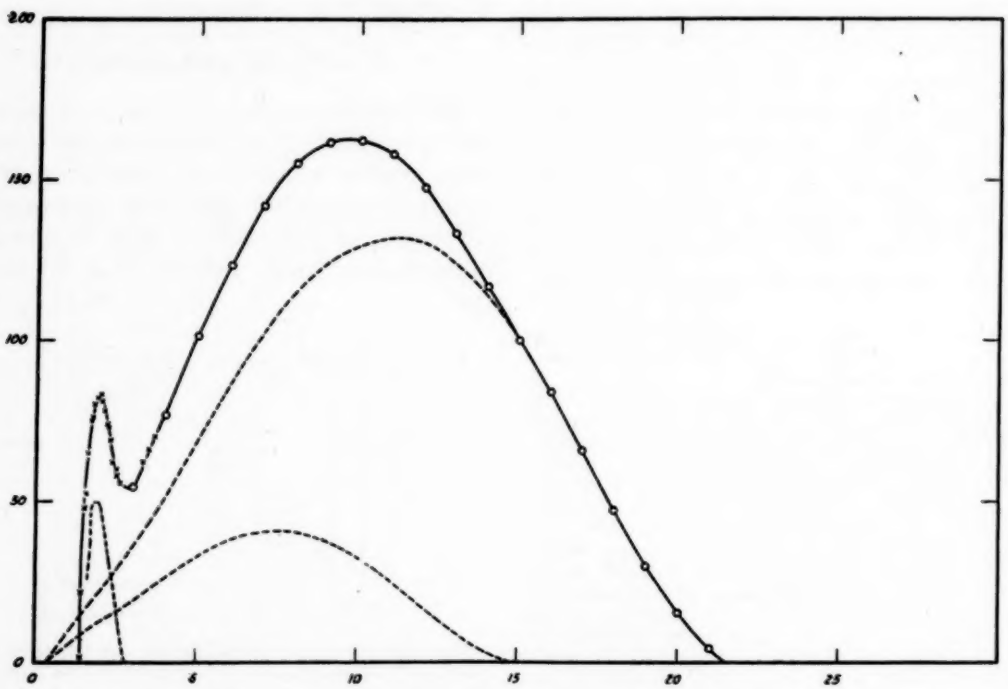

FIG. 2. Distribution of beta-rays from Rh^{106}. (The beta-spectra of Rh^{106} (30 sec.). Counting rate per unit momentum is plotted against coil current in amperes.)

[8] M. Deutsch, L. G. Elliott, and R. D. Evans, Rev. Sci. Inst. **15**, 178 (1944).
[9] A. Roberts, L. G. Elliott, J. R. Downing, W. C. Peacock, and M. Deutsch, Phys. Rev. **64**, 268 (1943).
[10] J. V. Dunworth, Rev. Sci. Inst. **11**, 167 (1940).
[11] A. Roberts, J. R. Downing, and M. Deutsch, Phys. Rev. **60**, 544 (1941).

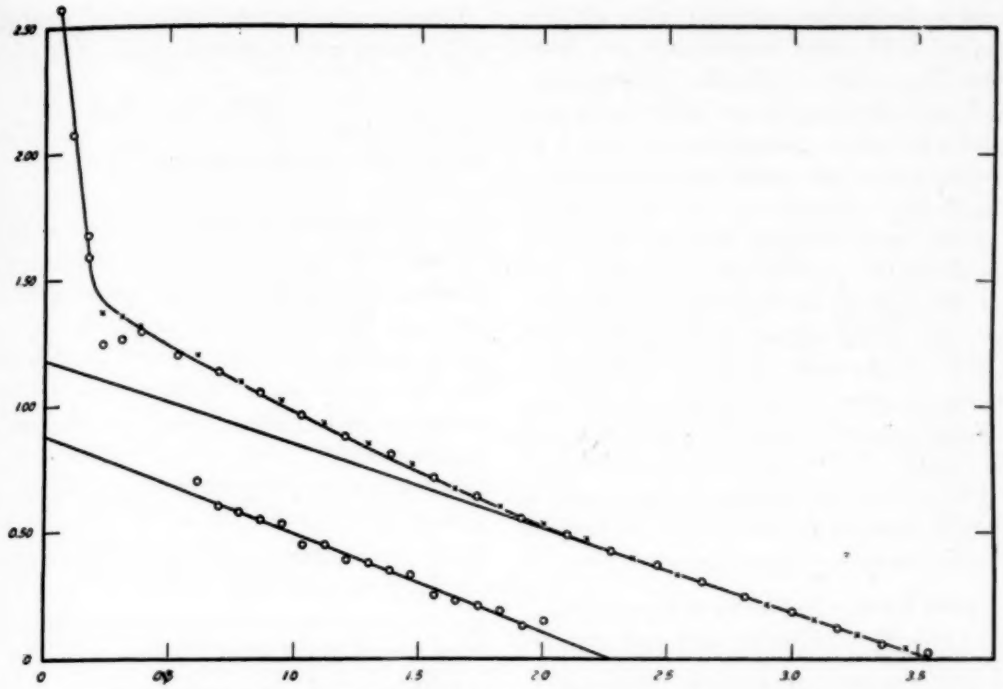

FIG. 3. Kurie plot of Rh^{106} beta-rays. (Kurie plot, $\sqrt{N/FI^2}$ *vs.* energy, E, where N is net counting rate, F is the Fermi function and I is coil current (α momentum of the electrons).)

III. RESULTS

The solid curve of Fig. 2 is a plot of the counts per minute per unit momentum interval, N/I *vs.* the current, I, in the spectrometer coil. (I is proportional to the momentum of the electrons.) The counter window for the run was 2.7 g/cm.[2] Figure 3 shows a Kurie plot taken from the same data. Above about 0.2 Mev this seems to be resolved into two beta-spectra with end points at 2.30±0.10 Mev and 3.55±0.10 Mev. The two spectra plotted as dotted lines in Fig. 2 are taken from points along the straight lines of Fig. 3. Relative areas under these two curves indicate 82±2 percent of the beta-rays are related to the higher energy spectra and 18±2 percent to the lower.[12]

Figure 4 shows the N/I *vs.* I curve for the electrons resulting from the interactions of the gamma-rays associated with Rh^{106} in lead. Points of particular interest are at A and B, where one sees K and L photo-electron peaks from a 0.51 ±0.02-Mev gamma-ray, C, where one sees the K line from a 0.73±0.02-Mev gamma-ray, and D, just beyond the Compton end point for a third gamma-ray, found to have an energy of 1.25±0.05 Mev. The region between 4.5 and about 5.25 amperes includes Compton electrons from the 0.73-Mev gamma-ray as well as the peak from the photo-electron line of the 0.51-Mev gamma-ray. Uranium foil used as a radiator over the lead cup produced photo-electrons at C and D, making it possible to determine more accurately the energies of the 0.73- and 1.25-Mev gamma-rays. Relative intensities of the 0.51- and 0.73-Mev gammas are approximately the same, and that of the 1.25-Mev one is approximately 5–10 percent as abundant as either of them.

Coincidences between betas and gammas using 428 mg/cm² of Al before the beta-counter gave 0.19±0.03 coincidence per 1000 betas, while using 6 mg/cm² of polystyrene and mica gave 0.44±0.04 coincidences per 1000 betas.

These measurements indicate that as the ratio of lower to higher energy beta-rays entering to the beta-counter is increased (absorber decreased) the number of gamma-rays coinciding with the betas increases. This is confirmation that the beta-spectra is complex.

[12] The broad peak at 1 to 3 amperes seems to depend on source backing and is ascribed to back scattering.

From the known gamma-counter efficiency one would expect 0.71 ± 0.03 coincidence per 1000 betas coinciding with a 0.51-Mev gamma-ray, γ_1, 1.35 ± 0.06 coincidences per 1000 betas coinciding with 0.73-Mev gamma-ray, γ_2, and 3.37 ± 0.14 coincidences per 1000 betas coinciding with a 1.25-Mev gamma-ray, γ_3. If only 18 percent of the betas coincide with gamma-rays, of which about 10 percent are 1.25 Mev and the other 90 percent are 0.51 in cascade with 0.73 Mev, one would expect $(0.71+1.35)\times0.18\times0.90+3.37\times0.18\times0.10=0.40$ per 1000 betas. Gamma-counter efficiency under these conditions (with negligible absorber before the beta-counter) should be: $(0.71+1.35)\times10^{-3}\times0.90+3.37\times10^{-3}\times0.10=2.19\times10^{-3}$. Beta-counter efficiency is 0.166 ± 0.015. The net counting rate divided by efficiency, i.e., disintegration rate, would be

$$4405/0.166=26{,}500 \text{ by beta-emission,}$$
$$(10\pm1)/2.19\times10^{-3}=4560 \text{ by beta and gamma,}$$

or about 17 ± 2 percent of the disintegrations include gamma-rays.

Gamma-gamma coincidences per 1000 gammas with a cross-over gamma-ray should be given by

$$\frac{N_c}{N_\gamma/1000}=\frac{2KN_0\cdot e_1e_2\times1000}{N_0[K(e_1+e_2)+(1-K)e_3]}=0.80.$$

K is the fraction of gammas not in coincidence (taken as 10 percent) and the e's are the efficiencies of the counter for gammas of 0.51, 0.73, and 1.25 Mev, respectively. N_c and N_γ are the net coincidence and net gamma-counting rate, and N_0 is the disintegration rate by gamma-emission (lower beta-energy component of the disintegration). The value of $N_c/(N_\gamma/1000)$ found was 0.62 ± 0.05. This value is not in good agreement with the values to be expected, but may be accounted for by the bremstrahlung from the high energy, more abundant, beta-ray that was counted in the counters. (It would not be in coincidence with the gamma-rays and hence would decrease the coincidence rate per 1000 gammas.)

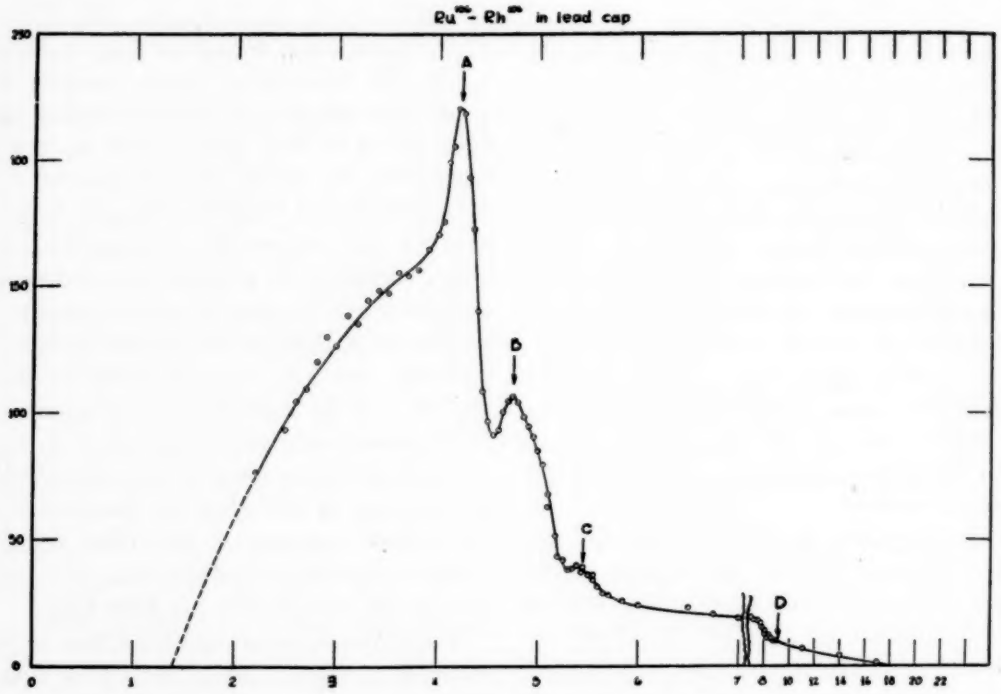

FIG. 4. Compton and photo-electrons from the Rh^{106} gamma-rays. (Electrons resulting from interactions of the Rh^{106} gamma-rays with lead. Counting rate per unit momentum is plotted against coil current in amperes. K photo-electrons are to be seen at A and C from 0.51- and 0.73-Mev gamma-rays. The end point for the Compton electrons from the latter gamma-ray and the L photo-electrons from the former are near B. D lies just beyond the Compton end-point for a 1.25-Mev gamma-ray.)

IV. DISCUSSION

It would seem that the decay scheme for Rh^{106} is probably as shown in Fig. 5.

If one computes the product *ft*, that is, Fermi function times the partial half-life, for the two beta-spectra, 3.55 Mev and 2.30 Mev,[13] one obtains 3310×36.6 sec. $=12.1\times10^4$ sec., and 533×167 sec. $=8.9\times10^4$ sec., respectively. Both of these values are in the range of values for allowed spectra (see reference 11, page 222).

One might further assume that the matrix elements for both processes were essentially the same, thus that both *ft* values would be approximately the same. Because of the errors in determining the beta-ray energies (ratio of relative abundances goes approximately as the fifth power of the energy ratio) and relative abundances, the *ft* values obtained cannot be considered significantly different.

Since the beta-spectra are allowed, they are accompanied by no nuclear-spin change if Fermi selection rules are obeyed. Now $_{46}Pd^{106}$ is an even-even nucleus, hence its ground state probably has zero total nuclear angular momentum ($J=0$). Fermi selection would seem, then, to require the 1.25-Mev gamma-ray to occur between two states with $J=0$. Such a $0\rightarrow0$ transition is completely forbidden for gamma-rays. According to the Gamow-Teller selection rules a spin change of 0, or 1 (no $0\rightarrow0$ change) can accompany either beta-decay. If one assumes, as before, that the ground state of the product nucleus has zero total nuclear angular momentum, then the state at 1.25 Mev above the ground level could have $J=1$ or 2. The value $J=0$ for the upper state is to be ruled out (gamma-transition $0\rightarrow0$ is completely forbidden as mentioned before). In either of the latter cases the 1.25-Mev gamma, γ_3, would be expected to be more abundant than the 0.51- and 0.73-Mev cascade, $\gamma_1+\gamma_2$, if both modes of decay involved the same spin and parity changes.

With either Fermi or Gamow-Teller selection rules an allowed beta-transition involves no parity change, so both the upper and lower states have the same parity. If $\Delta J=1$ between the upper and lower states, no parity change is forbidden for electric-dipole radiation and hence γ_3 must be magnetic-dipole radiation, if $\Delta J=2$ is electric-quadrupole radiation. Whether γ_3 is magnetic dipole or electric quadrupole, the only lower energy gamma-transition competing more favorably is electric dipole involving a parity change.[14] The transition $\gamma_1+\gamma_2$ (whichever is emitted first),[15] must then involve a spin change of $J=1$, and the intermediate excited state must have $J=1$, 2 or 3. (Here again the $J=0$ level would require the second gamma-ray to be a $0\rightarrow0$ transition.)

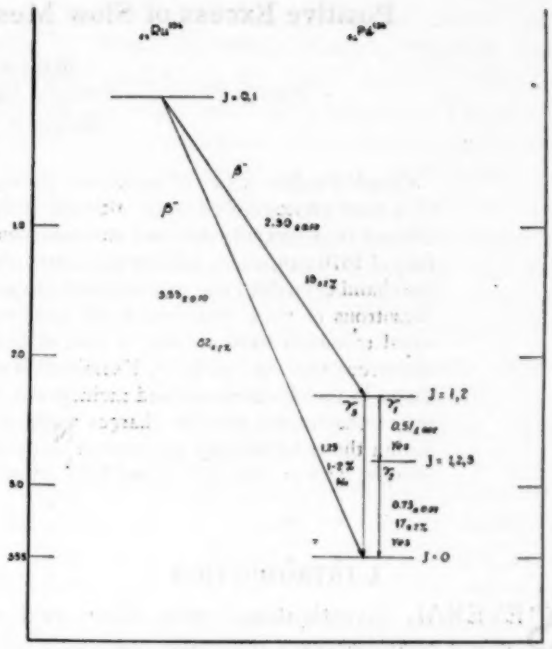

FIG. 5. Proposed decay scheme for Rh^{106}.

We wish to acknowledge the assistance of L. M. Gunning, J. W. Jones, and R. T. Overman.

[13] See for example, Eq. (24a) of E. J. Konopinski, Rev. Mod. Phys. 15, 209 (1943).

[14] Magnetic 2^l-pole radiation is approximately as much less likely than electric 2^l-pole radiation as electric 2^{l+1}-pole radiation. Both such less-favored transitions should result in longer partial lifetimes with a ratio to the electric 2^l-pole radiation about the same.

[15] We have as yet no information about the order of emission of γ_1 and γ_2.

Positive Excess of Slow Mesotrons at an Altitude of 3.5 km

MALCOLM CORRELL
Ryerson Physical Laboratory, University of Chicago, Chicago, Illinois
(Received August 6, 1947)

Cloud-chamber tracks of mesotrons having momenta between 1.25×10^8 ev/c and 2.5×10^8 ev/c were photographed at an altitude of 3.5 km. Mesotrons in this momentum range were selected by a specially designed anticoincidence circuit. The tracks were curved by a magnetic field of 1670 gausses. A 1.25-cm lead plate above the chamber and two 1-cm lead plates within the chamber enabled one to distinguish electrons from mesotrons by multiplication phenomena. Mesotrons of these momenta easily penetrate several centimeters of lead, while protons of equal momenta have a range in lead of less than 0.2 mm. Thus, confusion of protons with mesotrons was very unlikely. Examination of 320 mesotron tracks which traversed both lead plates in the chamber and had momenta in the selected range showed that 47.2 percent of the mesotrons carried positive charges while the remaining 52.8 percent were negative. Hence, within the ±5.6 percent precision of this experiment, positive and negative mesotrons having energies between 0.6×10^8 ev and 1.7×10^8 ev occur in equal numbers at an elevation of 3.5 km.

I. INTRODUCTION

SEVERAL investigators,[1] who have used a cloud chamber in a magnetic field to study the charge carried by cosmic-ray mesotrons, have reported that there is an excess of those bearing a positive charge. The best measurements seem to indicate that, of the mesotrons at sea level having energies $E>5\times10^8$ ev, the ratio of the number of positive to that of negative mesotrons is about 1.2, or the positive excess is about 20 percent. Recently Bernardini[2] and his collaborators confirmed a positive excess of about 20 percent by deflecting the mesotrons in magnetized iron. In this system only mesotrons capable of traversing at least 40 cm of iron were registered; therefore, this measurement of the positive excess likewise pertained to mesotrons of energy $E>5\times10^8$ ev.

According to Carlson and Schein[3] the observed 20 percent positive-mesotron excess may be explained by supposing that the primary cosmic radiation consists of protons which interact with nucleons of air nuclei close to the top of the atmosphere. In their explanation each collision with a nucleon on the average produces several mesotrons and, in order that the positive charge of the primary proton be conserved, more positive than negative mesotrons are produced. In such an act the proton loses an appreciable amount of its kinetic energy and is finally changed into a neutron. If an average of 11 mesotrons is created in these events, and if all of them are of sufficiently high energy to reach sea level before decaying, the ratio of the number of positive to the number of negative mesotrons would be 6:5, or the positive excess would be 20 percent.

The assumptions of Carlson and Schein regarding the production of mesotrons in multiple processes to account for the 20 percent positive mesotron excess are based on the work of Schein, Jesse, and Wollan.[4] These investigators used a coincidence system, which included from 4 to 18 cm of lead, to measure the intensity of mesotrons as a function of altitude up to about 2-cm Hg. Their intensity-*vs.*-pressure curve showed no maximum up to the highest altitudes attained. This result, in conjunction with the fact that mesotrons themselves cannot be the primary radiation, since they decay spontaneously with a mean life of $\sim2\times10^{-6}$ second, led to the conclusion that most of the mesotrons observed in this experiment are produced close to the top of the atmosphere. Schein, Jesse, and Wollan also concluded from the results of their experiment that it is highly unlikely that the primary radiation consists of electrons. They decided that the primary radiation is probably composed of protons.

[1] P. M. S. Blackett, Proc. Roy. Soc. **A159**, 1 (1937); L. LePrince-Ringuet and J. Crussard, J. de phys. et rad. **8**, 207 (1937); H. Jones, Rev. Mod. Phys. **11**, 235 (1939); D. J. Hughes, Phys. Rev. **57**, 592 (1940).
[2] Bernardini, Conversi, Pancini, Scrocco, and Wick, Phys. Rev. **68**, 109 (1945).
[3] J. F. Carlson and M. Schein, Phys. Rev. **59**, 840 (1941).
[4] M. Schein, W. P. Jesse, and E. O. Wollan, Phys. Rev. **59**, 615 (1941).

Johnson[5] also concluded that part of the primary radiation consists of protons. In attempting to explain the east-west asymmetry of the hard component, observed near the equator at sea level, he attributed the origin of the hard component to these primary protons and showed that the deflection of the incoming protons in the earth's magnetic field could account for the observed asymmetry.

The assumption that mesotrons are produced in multiple is supported by the experiments of Schein, Iona, and Tabin.[6] At altitudes corresponding to 3-cm Hg they have found several penetrating particles ejected from paraffin, and they thought that these were probably mesotrons produced in a multiple act.

Heitler and Walsh[7] have used different assumptions to describe the elementary process of mesotron production. However, the positive excess predicted by their theory is smaller than that observed by a factor of from 3 to 5.

A detailed theory of collisions between protons and air nuclei to account for the observed positive mesotron excess is yet to be developed. Nevertheless, the existence at sea level of a positive excess among mesotrons having energies $E>5\times10^8$ ev is qualitatively consistent with the hypothesis that such mesotrons are produced multiply close to the top of the atmosphere by the interaction of primary protons with air nuclei and that the excess conserves the positive charge of the protons.

There are, however, lower energy mesotrons, existing at higher elevations, which are apparently not formed by the mechanism described above. Several investigations have confirmed the fact that, as the altitude of observation increases, the relative number of mesotrons of energies $E<5\times10^8$ ev is rapidly augmented. The best sea-level measurement of the mesotron differential energy spectrum is probably the one reported recently by Wilson.[8] Using a cloud chamber in a magnetic field, he found a definite maximum at an energy $E\sim6.1\times10^8$ ev. The approximate shape of the mesotron differential energy spectrum has been determined at an elevation of 3.24 km by Rossi, Greisen, Stearns, Froman, and Koontz,[9] at 4.35 km by Hall,[10] and at 6.7 km by Schein, Wollan, and Groetzinger.[11] These investigations were made with counter configurations which included various thicknesses of absorbers between the counters. Hall, at Mt. Evans (4.35 km), found that his spectrum showed a maximum for mesotrons of energy $E\sim10^8$ ev. He used this spectrum to compute the mesotron energy spectrum at 3.24 km, the altitude of Echo Lake, and found good agreement with the measurements made there by Rossi, Greisen, Stearns, Froman, and Koontz. Schein, Wollan, and Groetzinger found that, at an altitude of 6.7 km, about 33 percent of the total mesotron intensity was comprised of mesotrons having energies $E<5.2\times10^8$ ev. Bhabha, Aiya, Hoteko, and Saxena[12] used counter telescopes to measure mesotron intensity-*vs.*-altitude curves at 3.3° N mag. lat. under 5.5, 20, and 30 cm of lead. They too have found a large increase of low energy mesotrons with increasing altitude.

A comparison of these spectra shows that the maximum of the mesotron differential energy spectrum becomes considerably more prominent

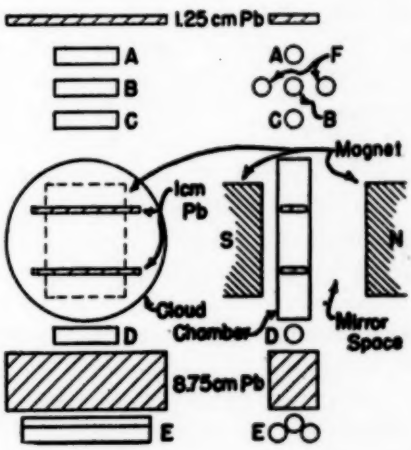

FIG. 1. Arrangement of apparatus. A mirror, set vertically in the mirror space at 45° with the magnetic-field direction, permitted a camera to take pictures in a plane perpendicular to the magnetic field. Counters *ABCD* were connected in coincidence, while *EF* were in anticoincidence.

[5] T. H. Johnson, Rev. Mod. Phys. **11**, 208 (1939).
[6] M. Schein, M. Iona, Jr., and J. Tabin, Phys. Rev. **64**, 253 (1943).
[7] W. Heitler and P. Walsh, Rev. Mod. Phys. **17**, 252 (1945).
[8] J. G. Wilson, Nature **158**, 414 (1946).
[9] B. Rossi, K. Greisen, J. C. Stearns, D. K. Froman, and P. G. Koontz, Phys. Rev. **61**, 678 (1942).
[10] D. B. Hall, Phys. Rev. **66**, 321 (1944).
[11] M. Schein, E. O. Wollan, and G. Groetzinger, Phys. Rev. **58**, 1027 (1940).
[12] H. J. Bhabha, S. V. C. Aiya, H. E. Hoteko, and R. C. Saxena, Phys. Rev. **68**, 147 (1945).

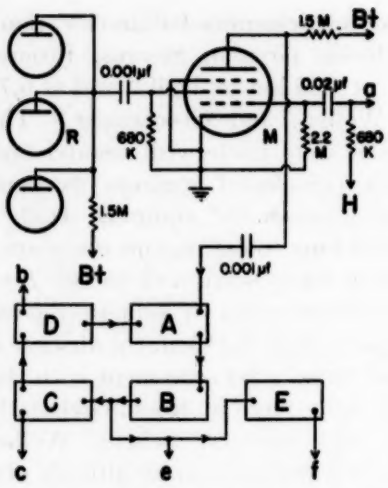

FIG. 2. Block diagram of timing circuits. Coincidence tubes R furnish positive pulse to screen of pentode mixer M when coincidence occurs. This makes M conduct unless anticounters at a simultaneously supply a strong bias to the control grid. Differentiation at plate of M supplies triggering pulse to trigger circuit A (detail in Fig. 3a). B, C, D, and E are unbalanced multi-vibrators (detail in Fig. 3b) and serve to delay the original pulse. A feeds pulse to B; B, after delay, feeds pulse to C; etc. Pulse e expands chamber, f flashes lamps, c compresses chamber and rewinds camera, and pulse from D to A retriggers A to original condition for next cycle of operation. b supplies a sustained boosted clearing-field voltage. $B+$ is 225 v and H is the high voltage for the anticounters. Tubes R and M were of type 9001.

and shifts toward lower energies as the altitude increases. This increase cannot easily be explained by the mechanism which Carlson and Schein proposed in accounting for the positive excess observed at sea level in mesotrons of energies $E>5\times10^8$ ev. It is, therefore, probable that at least some of these mesotrons are produced by another mechanism. Several different experiments have already indicated the production of mesotrons with energies $\sim10^8$ ev by *non-ionizing* radiation.[13] Such mesotrons would not be expected to show an excess of either charge. Hence, it is pertinent to ask whether the low energy mesotrons, which are increasingly prevalent as the altitude is increased, show a positive excess.

The present investigation is confined to mesotrons of energies 0.6×10^8 ev $<E<1.7\times10^8$ ev at an altitude of 3.5 km and attempts to determine the relative numbers of positive and negative mesotrons.

[13] See summary in M. Schein and D. Montgomery, *Problems in Cosmic Ray Physics* (Princeton University Press, Princeton. 1946), Chapter VIII.

II. APPARATUS

The apparatus consisted of a counter-controlled cloud chamber of the rubber diaphragm type mounted vertically against the south pole face of a permanent magnet (see Fig. 1). The cloud chamber was 10 inches in diameter and 2 inches deep. The chamber was filled in its compressed condition with commercial argon to a pressure of 20- to 24-cm Hg more than that of the atmosphere.

The magnet was made of Alnico V and weighed 1000 lb. It was designed as a horseshoe to provide an air gap 7 inches long, wherein the field strength would be fairly uniform over an area 7 inches high and 5 inches wide. The field was carefully mapped along the central plane of the photographable region of the chamber. It was found that the field strength was 1670 gausses at the center of the $5''\times7''$ area and was down about 10 percent at the edges. Since the heat treatment process in the manufacture of Alnico V makes it impossible to cast magnets of this size in one piece, this magnet was designed to be assembled as a horseshoe out of 11 castings of Alnico V, two soft steel corner blocks, and two soft-steel pole faces. These pieces were held together by threaded bronze tie-rods and by a rigid casing made of $\frac{1}{2}$-inch aluminum plates.

The chamber, when mounted in the air gap, occupied approximately $3\frac{1}{2}$ inches of the gap length. A plane mirror aluminized on the front surface was mounted in the remaining $3\frac{1}{2}$ inches of the air gap at 45° with the magnetic axis. By this arrangement a camera aimed into the mirror could take pictures through the front wall of the chamber. The photographable volume within the chamber was 4 inches wide, one inch deep, and 10 inches high. The pictures were taken by a specially designed, automatic camera, which was provided with a coated Kodak Ektar f:2 lens and which used 35-mm Super-XX perforated movie film. The illumination was furnished by two FT-26 General Electric Flash tubes, each operating from 45 microfarads charged up to 1400 volts. It was found in practice that, with the illumination provided, a lens speed of f:3 was sufficient and, of course, the focus was then less critical. The magnet, the chamber, the camera, and the counter telescope were all enclosed in a light-tight box so that the camera could be operated without using a shutter.

As may be seen from Fig. 1, the chamber expansions were controlled by a fourfold coincidence telescope composed of 4 GM counters (*ABCD*) one inch in diameter and 4 inches long. These counters were filled with argon and alcohol. A particle which discharged these 4 counters had traversed the chamber and, if it was unable to emerge from the 8.75-cm lead filter below the fourth counter, it was within the energy range selected for the experiment and its track was photographed. However, if it also discharged the anticounters (*E*) below the lead, its energy was too great and the chamber did not expand. The counters (*F*) also were connected as anticounters; their function was to protect the coincidence set (*ABCD*) from the effects of showers.

A block diagram of the timing circuits is shown in Fig. 2. The detail of the trigger circuit *A* is shown in Fig. 3a. The delay- or interval-timing circuits *B*, *C*, *D*, and *E* were all unbalanced multi-vibrators or "flip-flop" circuits. The detail of these circuits is shown in Fig. 3b, except for the particular values of the components *R* and *C* which determine the duration of the delay or of the interval and are optional within wide limits. Circuits of the types shown in Fig. 3 can easily be made sensitive to negative pulses only,[14] and this feature makes it possible to connect several such circuits in series about a closed ring, as is illustrated in the block diagram by the connections between blocks *A*, *B*, *C*, and *D*. When the counter telescope registered the occurrence of a suitable event, a positive pulse from the coincidence tubes, *R*, applied screen voltage to the pentode mixer, *M*, (Fig. 2). Normally, the bias on the control grid of this tube was zero, so that the sudden application of screen voltage resulted in a sudden rise in plate current; i.e., a negative pulse could be obtained from the plate of this tube. However, if the event registered by the coincidence set also discharged an anticounter, a negative pulse from this counter was applied to the control grid of the pentode mixer, so that no rise in the plate current of this tube could occur.

The negative pulses appearing on the plate of the mixer tube, *M*, were applied to the trigger circuit and caused it to trigger to the other stable condition. As long as this circuit remained so triggered it acted as a barrier to pulses from succeeding cosmic-ray events, which might interfere with the cycle of operation of the cloud chamber if the chamber were not yet ready for the next expansion. At the close of the cycle of operation, the trigger circuit was triggered back to its normal condition by a negative pulse from the circuit represented by block *D*.

Block *A* was so connected that a negative pulse from the plate of the mixer tube was passed immediately to block *B*. Block *B*, which was an unbalanced multi-vibrator, produced a single square wave of a duration adjustable from 0.001 to 0.1 second. The falling side of this wave was differentiated to obtain a sharp negative pulse for triggering blocks *C* and *E*, both of which were unbalanced multi-vibrators; this pulse also caused

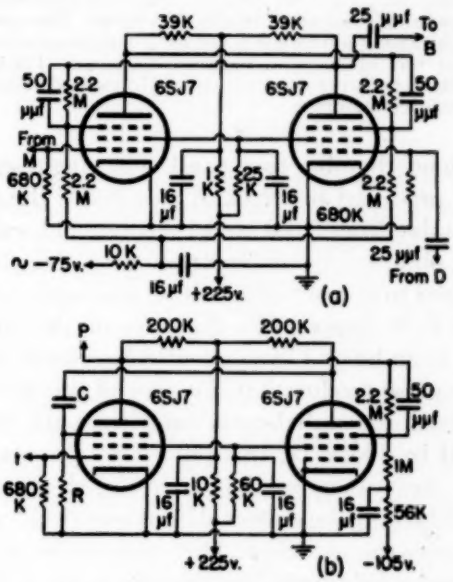

FIG. 3. Detail of blocks in Fig. 2. (a) shows trigger circuit (block *A*). Circuit is very sensitive to negative pulses on control grids and relatively insensitive to all other pulsings. Left tube is normally "on" and negative pulse from *M* is passed directly to block *B* by 25 μμf from right plate. At end of cycle, pulse from block *D* onto right control grid triggers circuit back to original condition. (b) shows unbalanced multi-vibrator circuits (blocks *B*, *C*, *D*, and *E*) which, upon being triggered, produce single, very square waves whose durations are determined by particular values of *R* and *C*. Left tube is normally "on" and negative triggering pulse is introduced at *t*; circuit is relatively insensitive to all other pulsings. The successive triggering pulse and pulses *c*, *e*, and *f* were obtained by differentiating the single square waves as they appeared at *P*; this produced sharp, delayed, negative pulses as the circuits returned to normal. Sustained positive voltage *b* was obtained from *P* directly. Where desirable, as on thyratron grids, the negative pulse was changed in sign by a stage of amplification.

[14] H. J. Reich, *Theory and Application of Electron Tubes* (McGraw-Hill Book Company, Inc., New York, 1939).

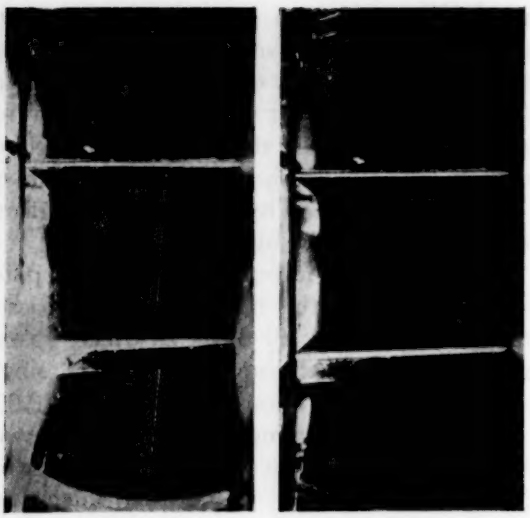

FIG. 4. Typical pictures. Each of these tracks is visible in all three sections of the chamber, and there is no evidence of cascade multiplication in the lead plates. The track in the right-hand picture has a radius of curvature of ~200 cm and was made by a negative mesotron. The other track has a radius of curvature of ~175 cm and was made by a positive mesotron.

the cloud chamber to expand. The single square wave produced by block E also had a duration adjustable from 0.001 to 0.1 second, and a sharp pulse obtained by differentiation as this circuit returned to its normal condition was used to flash the FT-26 lamps. The duration of the square wave from block C was about 3.5 seconds, and a sharp pulse produced at the close of this interval triggered the unbalanced multi-vibrator represented by block D; this pulse was also used to close the valves, so that compressed air introduced behind the rubber diaphragm could again compress the chamber. This same pulse started the motor for turning up the film in the camera. The circuit in block D remained in its triggered condition for about 30 seconds, and throughout this interval 180 volts was applied to the chamber as a field for clearing old ions from the interior. As was mentioned before, a sharp negative pulse obtained at the close of this interval returned the trigger circuit (block A) to its normal condition, and the entire apparatus was then ready to make the next picture.

The apparatus was installed at Climax, Colorado, in a small portable house,[15] whose roof was made of $\frac{1}{4}$-inch plywood. It was found necessary to control the temperature inside of the house to within 1°F to insure reliable operation of the chamber.

[15] This house was constructed by Lewis and used in his experiments at Echo Lake: L. G. Lewis, Phys. Rev. **67**, 228 (1945).

III. DISCUSSION OF THE ACCEPTABLE TRACKS

Two 1-cm lead plates were mounted 8.5 cm apart within the chamber, and a 1.25-cm lead plate was placed above the counter telescope ($ABCD$), (see Fig. 1). Any mesotron capable of causing a coincidence in the fourfold coincidence set must have had sufficient energy to traverse at least 3.25 cm of lead, since the fourth counter of the set was just below the cloud chamber. If, however, the mesotron had sufficient energy to traverse not only the 3.25 cm of lead but also the 8.75 cm of lead below the chamber, it also discharged one of the anticounters (E). Thus, in order to initiate automatic operation of the cloud chamber, a mesotron had to be able to pass through 3.25 cm of lead but be unable to pass through 12 cm of lead. From the curves given by Rossi and Greisen[16] it can be seen that such mesotrons must be in the momentum range 1.25×10^8 ev/c$<p<2.5\times10^8$ ev/c; this corresponds to a range in kinetic energy of 0.6×10^8 ev $<E<1.7\times10^8$ ev.[17]

The radius of curvature ρ of the path of a charged particle which travels with momentum p in a plane normal to a magnetic field of strength H is given by the relation,

$$p=300H\rho.$$

From this equation it is seen that an electron and a mesotron having equal momenta cannot be distinguished by the curvatures of their tracks. Furthermore, as long as the lower limit of the momentum range is well above 10^8 ev/c, the ionization produced by the passage of electrons and mesotrons through a gas is nearly the same, so that their tracks will be equally heavy and will not serve to distinguish the two kinds of particles. It was necessary, therefore, to employ the three lead plates in the upper part of the telescope in order to enable one to distinguish events involving

[16] B. Rossi and K. Greisen, Rev. Mod. Phys. **13**, 240 (1941).

[17] For converting momenta to energies the mesotron mass was taken as 10^8 ev/c^2 or 200-electron masses. This is in close agreement with Fretter's recent measurement of mesotron mass ~202-electron masses: W. B. Fretter, Phys. Rev. **70**, 625 (1946).

electrons from those involving mesotrons, since, in general, electrons produce cascade showers in traversing lead, and hence should show many tracks, while mesotrons do not.

There is a small probability, however, that some incident electrons with energies of approximately 10^8 ev traversed the first lead plate (2.5-radiation lengths of matter) without multiplication.[18] For these electrons there is again a small probability that some of them traversed the second lead plate (2-radiation lengths) without multiplication. But the probability that an incident electron with energy $\sim 10^8$ ev traversed both of the first two plates without having initiated a shower is proportional to the product of two small probabilities. Furthermore, for the electrons which emerged from both the first and second lead plates without having multiplied, there is yet a small probability that some of them passed through the third lead plate without producing a shower. But the total probability that such an electron traversed all three lead plates (6.5-radiation lengths) without multiplication in any one of them is proportional to the product of three small probabilities. The likelihood that many such electrons will be mistaken for mesotrons is, therefore, negligibly small.

Electrons incident with considerably greater energies (up to 10^{10} ev at which energy they begin to affect the anticounters (E)) than that considered above would have produced showers of a large number of particles in traversing 2.5-radiation lengths and also 4.5-radiation lengths of matter. Hence, they should be definitely identifiable at any stage of their traversal of the telescope.

It is also well to note that the three lead plates make it practically impossible to confuse protons with mesotrons in the photographable region. This is true since those protons which would travel along an arc of measurable curvature, say 300-cm radius, have a range in lead of less than 0.2 mm.

Before the results are discussed it should be mentioned that a calculation was made to ascertain whether the scattering in the gas of the chamber might introduce apparent radii of curvature of such magnitude as to confuse the results. In order to make the hypothetical case severe, the calculation was carried out for a mesotron of momentum $p=4.8\times10^7$ ev/c, which is considerably below the range of momenta considered in the experiment. This mesotron would travel along an arc having a radius of 100 cm. The probable "scattering radius" for such a mesotron was calculated according to the recent formula given by Bethe[19] and is 950 cm. This is entirely negligible within the precision of this experiment, particularly since this research concerns only the determination of the kind of charge carried by the mesotron. Typical pictures are shown in Fig. 4.

IV. RESULTS

The curvature of a track was measured by projecting the image of the 35-mm negative onto a table top and then using a micrometer stage to determine sagitta measurements. There were 320 tracks which were visible in all three sections of the chamber. Of these 169 showed curvatures corresponding to negatively-charged particles. The remaining 151 tracks showed the opposite curvature and, consequently, had been made by positively-charged particles. It would thus appear that 52.8 percent of the mesotrons in the energy range 0.6×10^8 ev $<E<1.7\times10^8$ ev are negatively charged, while the other 47.2 percent of these mesotrons were positively charged. The statistical error for 320 observations is ±5.6 percent, so it would seem that the numbers of positive and negative slow mesotrons are equal within the precision of this experiment. At any rate, it is apparent that at an altitude of 3.5 km a positive mesotron excess as large as 20 percent does not exist for mesotrons of this energy range.

At present there are two possible explanations for the lack of a 20 percent positive excess among the slow mesotrons occurring abundantly at high elevations. These mesotrons may be produced in the atmosphere by a neutral radiation, which

[18] On the average, the energy E of an electron after traversing a layer of matter of thickness t, measured in radiation lengths, is given with good approximation by

$$E=E_0e^{-t},$$

where E_0 is the energy with which the electron entered the layer. For lead the radiation length is about 0.5 cm. Thus, on the average, after having traversed the first lead plate in this experiment, an electron would have radiated, very approximately, all but 8 percent of its incident energy. This radiated energy, of course, should have initiated a shower provided E_0 is greater than the critical energy in lead, which is 7×10^8 ev.

[19] H. A. Bethe, Phys. Rev. **70**, 821 (1946).

might be either neutrons or γ-rays, in which case no positive mesotron excess would be expected. Or it may be that they are produced with very high multiplicity at the top of the atmosphere by a mechanism similar to that described by Heitler and Walsh.[7] According to their theoretical calculations, the excess should be 3 to 5 times smaller than that observed at higher energies. However, it is difficult to understand why this small excess is limited only to the lowest energies in the mesotron spectrum and does not extend to energies above 5×10^8 ev, where the observed excess is as high as 20 percent.

Bernardini and his collaborators,[2] using their magnetized iron at 3.3 km, have tried to investigate the positive-mesotron excess as a function of mesotron energy. They have concluded that their arrangement is not particularly suited to this use, but that, if the 20 percent excess persists down into the low energy regions, they should have obtained a larger effect at their lowest energies ($\sim5\times10^8$ ev) than they actually found.

ACKNOWLEDGMENTS

The author desires to express his deep appreciation to Prof. Marcel Schein, who suggested the problem and whose interest, encouragement, and advice were an indispensable factor in the successful execution of the experiment. The continuing support of Dr. Walter Orr Roberts and Dr. John W. Evans, both of the Harvard College Observatory at Climax, which was always available to the expedition, is gratefully acknowledged. The hospitality of Supt. C. J. Abrams of the Climax Molybdenum Company, who placed many facilities of his company at the disposal of the expedition, is deeply appreciated. Thanks are also due Mr. Ivar Kalberg for the machining of the metal parts of the cloud chamber and camera and for the assembly of the magnet.

PHYSICAL REVIEW VOLUME 72, NUMBER 11 DECEMBER 1, 1947

The Production of a Positron-Electron Pair in the Electrostatic Field of an Electron

K. M. WATSON
Physics Department, University of Iowa, Iowa City, Iowa

(Received August 14, 1947)

The production of positron-electron pairs in the electrostatic field of an electron is considered. In spite of the light mass of the recoil electron and the exchange effect between the two electrons, the process is quite similar to ordinary pair production. For the limiting case of high energy γ-rays, the ratio of triplet production to pair production should vary as $1/Z$. For $h\nu/mc^2<30$, pair production will have a relatively greater cross section for all values of Z, the nuclear charge.

It is found that in general (except near the γ-ray energy threshold of $4mc^2$) the positron and one electron will have relatively high energy compared to the second electron.

1. INTRODUCTION

THE production of "triplets," that is, pair creation in the vicinity of an electron, has been reported by Kruger.[1] This process is essentially equivalent to ordinary pair production, but differs from the latter in two details. First, an appreciable amount of the energy of the incident γ-ray can be carried away by the initial electron (as a matter of-fact, the energy threshold occurs at γ-ray energies of $4mc^2$ instead of at $2mc^2$ as for ordinary pair creation). Second, the process is complicated by the equivalence of the two electrons involved, which permits their roles to be interchanged.

2. THE CROSS SECTION FOR TRIPLET PRODUCTION

The differential cross section for a process initiated by γ-rays, and in which two particles

[1] Private communication to Professor Jauch. See also J. A. Phillips and P. G. Kruger, Phys. Rev. 72, 164 (1947).

are emitted into solid angles $d\Omega_1$ and $d\Omega_2$, respectively, is

$$d\sigma = 2\pi |H_{FA}|^2 \rho_F d\Omega_1 d\Omega_2 \tag{1}$$

when a third particle carries off the excess momentum and energy. Here H_{FA} is the matrix element corresponding to a transition from the initial state A to the final state F, and ρ_F is the density of energy levels per unit energy interval of the final state. (We use units in which the magnitudes of $\hbar$ and c are unity.)

The calculation of H_{FA} is similar to that for pair creation, if we include the exchange terms due to the similarity of the two electrons. We choose for our initial state that in which there is one electron with positive energy E_0 and momentum $\mathbf{P}_0$ and a second electron with negative energy, $\epsilon_0 = -|\epsilon_0|$, and momentum $\mathbf{p}_0$. There will also be an incident γ-ray with energy and momentum, k and $\mathbf{k}$. We assume that we can use plane wave eigenfunctions for the particles, as the energies involved are high compared to the binding energy of the electrons within an atom. Furthermore, the momentum $\mathbf{P}_0$ will be small compared to the other momenta involved, so we set it equal to zero and E_0 equal to m, the electron rest-mass.

The wave function for the initial state will be

$$\chi_A = \frac{1}{\sqrt{2}}[\psi_1(r_1)\psi_2(r_2) - \psi_2(r_1)\psi_1(r_2)] \tag{2}$$

where

$$\psi_1 = \exp i(\mathbf{p}_0 \cdot \mathbf{r}_1)\mu_1(s_1),$$

$$\psi_2 = \exp i(\mathbf{P}_0 \cdot \mathbf{r}_2)\mu_2(s_2)$$

and $\mu_1(s_1)$ and $\mu_2(s_2)$ are the matrices for the corresponding Dirac wave functions for free particles of energies ϵ_0 and E_0, respectively.

In the final state, the two electrons both have positive energies E and ϵ_- with respective momenta $\mathbf{P}$ and $\mathbf{p}_-$. The matrices in the plane wave functions will be designated by $\mu_2''(s_2)$ and $\mu_1''(s_1)$ respectively.

The interaction terms in the Hamiltonian for the system will be

$$V = e^2/(|\mathbf{r}_1 - \mathbf{r}_2|) \tag{3}$$

for the electrostatic repulsion of the two electrons and

$$U = e(\boldsymbol{\alpha}, \mathbf{A}) \tag{4}$$

for the interaction between the γ-ray and either electron, where e is the magnitude of the electronic charge, $\boldsymbol{\alpha}$ is the Dirac matrix vector, and $\mathbf{A}$ is the vector potential of the γ-ray field.

In terms of standard perturbation theory, the transition from initial to final state must occur through one intermediate state in the first approximation. If we designate the parameters in the intermediate state by the same symbols as for the initial state with primes, the schemes for the transition from initial to final state will be

$$\mathbf{k}, \mathbf{P}_0, \mathbf{p}_0 \rightarrow \mathbf{k}, \mathbf{P}_0', \mathbf{p}_0' \rightarrow \mathbf{P}, \mathbf{p}_- \tag{5}$$

and

$$\mathbf{k}, \mathbf{P}_0, \mathbf{p}_0 \rightarrow \mathbf{P}_0', \mathbf{p}_0' \rightarrow \mathbf{P}, \mathbf{p}_- \tag{6}$$

H_{FA} is then

$$H_{FA} = \sum_{II} \frac{U_{FII} V_{IIA}}{E_A - E_{II}} + \sum_{I} \frac{V_{FI} U_{IA}}{E_A - E_I} \tag{7}$$

where subscripts "I" and "II" refer to the intermediate steps of Eqs. (6) and (5), respectively.

The matrix elements occurring in Eq. (7) will then be of the form

$$V_{IIA} = 4\pi e^2 \left\{ \frac{1}{|\mathbf{p}_0 - \mathbf{p}_0'|^2} (\mu_1^{*\prime} \mu_1)(\mu_2^{*\prime} \mu_2) - \frac{1}{|\mathbf{p}_0 - \mathbf{P}_0'|^2} (\mu_1^{*\prime} \mu_2)(\mu_2^{*\prime} \mu_1) \right\} \tag{8}$$

and

$$U_{FII} = \tfrac{1}{2}[e(2\pi/k)^{\frac{1}{2}}](\mu_i^{*\prime\prime} \alpha \mu_j'), \quad (i, j = 1, 2) \tag{9}$$

where $\alpha = (\boldsymbol{\alpha}, \hat{\mathbf{e}})$, and $\hat{\mathbf{e}}$ is a unit vector in the direction of the polarization of the γ-ray. Also

$$(\mu^{*\prime} Q \mu) \equiv \sum_s \mu^{*\prime}(s) Q \mu(s)$$

where Q is any operator acting on μ. (μ^* designates the complex conjugate of μ.)

The conditions for conservation of energy and momentum give the equations

$$\begin{aligned} m + k + \epsilon_0 &= \epsilon_- + E, \\ \mathbf{p}_0 + \mathbf{k} &= \mathbf{p}_- + \mathbf{P} \end{aligned} \tag{10}$$

as well as those for momentum conservation for the intermediate states.

On evaluation of Eq. (7) by well-known

methods,[2] we obtain the following four terms

$$W_{II_a}=-\frac{\lambda}{2[\epsilon_- k-\mathbf{p}_-\cdot\mathbf{k}]}\times\left\{\frac{1}{P^2}(\mu_1^{*''}\alpha Q\mu_1)(\mu_2^{*''}\mu_2)-\frac{1}{|\mathbf{p}_--\mathbf{k}|^2}(\mu_1^{*''}\alpha Q\mu_2)(\mu_2^{*''}\mu_1)\right\} \quad (11)$$

where

$$Q=\epsilon_- -k+(\boldsymbol{\alpha},\mathbf{p}_--\mathbf{k})+\beta m$$

(β is the Dirac matrix, and $\lambda\equiv 4\pi e^3(2\pi/k)^{\frac{1}{2}}$).

$$W_{II_b}=-\frac{\lambda}{2[Ek-\mathbf{k}\cdot\mathbf{P}]}\times\left\{\frac{1}{|\mathbf{P}-\mathbf{k}|^2}(\mu_2^{*''}\alpha Q'\mu_2)(\mu_1^{*''}\mu_1)-\frac{1}{p_-^2}(\mu_2^{*''}\alpha Q'\mu_1)(\mu_1^{*''}\mu_2)\right\} \quad (12)$$

where

$$Q'=E-k+(\boldsymbol{\alpha},\mathbf{P}-\mathbf{k})+\beta m.$$

$$W_{I_a}=\frac{\lambda}{2[\epsilon_0 k-\mathbf{p}_0\cdot\mathbf{k}]}\times\left\{\frac{1}{P^2}(\mu_1^{*''}N\alpha\mu_1)(\mu_2^{*''}\mu_2)-\frac{1}{p_-^2}(\mu_2^{*''}N\alpha\mu_1)(\mu_1^{*''}\mu_2)\right\} \quad (13)$$

where

$$N=\epsilon_0+k+(\boldsymbol{\alpha},\mathbf{p}_0+\mathbf{k})+\beta m.$$

$$W_{I_b}=\frac{\lambda}{2mk}\left\{\frac{1}{|\mathbf{k}-\mathbf{P}|^2}(\mu_2^{*''}N'\alpha\mu_2)(\mu_1^{*''}\mu_1)-\frac{1}{|\mathbf{k}-\mathbf{p}_-|^2}(\mu_1^{*''}N'\alpha\mu_2)(\mu_2^{*''}\mu_1)\right\} \quad (14)$$

where

$$N'=m+k+(\boldsymbol{\alpha},\mathbf{k})+\beta m.$$

Then

$$H_{FA}=W_{II_a}+W_{II_b}+W_{I_a}+W_{I_b}. \quad (15)$$

According to Dirac's theory of the negative energy states for an electron, the "hole" left by the electron leaving the negative energy state acts as a positively charged particle, or positron. The momentum and energy of the positron are $\mathbf{p}_+=-\mathbf{p}_0$ and $\epsilon_+=-\epsilon_0$, respectively. We make this substitution in Eqs. (10) and (15). The final energy, E_F, is given by

$$E_F=(p_+^2+m^2)^{\frac{1}{2}}+(p_-^2+m^2)^{\frac{1}{2}}+(P^2+m^2)^{\frac{1}{2}}. \quad (16)$$

Then

$$\rho_F dE_F=-[Pp_+E\epsilon_+ d\epsilon_+/(2\pi)^6]\times(\partial E/\partial E_F)dE_F d\Omega_+ d\Omega,$$

where $d\Omega_+$ and $d\Omega$ are solid angle increments about the directions of $\mathbf{p}_+$ and $\mathbf{P}$, respectively. But from Eq. (16),

$$\partial E/\partial E_F\cong P\epsilon_-/(P\epsilon_- -\mathbf{P}\cdot\mathbf{p}_-)$$

when $P\cong E$, so

$$\rho_F=\frac{Pp_+E\epsilon_+ d\epsilon_+}{(2\pi)^6}\left(\frac{P\epsilon_-}{P\epsilon_- -\mathbf{P}\cdot\mathbf{p}_-}\right)d\Omega_+ d\Omega \quad (17)$$

(when $P\cong E$, which will be justified later for the case we are considering).

We have yet to square the magnitude of H_{FA}. As we are not interested in the effect of relative spin orientation or the direction of polarization of the γ-ray, we must average over the initial spin and polarization directions and sum over the final spin directions. The resulting expression is quite complicated. However, in the case of a γ-ray whose energy is large compared with the electron rest-mass, we can obtain a considerable simplification.

Let us first suppose that the outgoing particles are all fast. We can then write their energies, E, as $E\cong P+\frac{1}{2}m^2/P$. This gives (Eqs. (11) to (14))

$$\begin{aligned}
W_{II_a}&\cong-\frac{\lambda p_-}{p_-^2\theta_-^2+m^2}\left\{\frac{\Gamma_1}{P^2}-\frac{\Gamma_2}{|\mathbf{p}_++\mathbf{P}|^2}\right\},\\
W_{II_b}&\cong-\frac{\lambda P}{P^2\theta^2+m^2}\left\{\frac{\Gamma_3}{|\mathbf{p}_++\mathbf{p}_-|^2}-\frac{\Gamma_4}{p_-^2}\right\},\\
W_{I_a}&\cong-\frac{\lambda p_+}{p_+^2\theta_+^2+m^2}\left\{\frac{\Gamma_5}{P^2}-\frac{\Gamma_6}{p_-^2}\right\},\\
W_{I_b}&\cong(\lambda/2m)\left\{\frac{\Gamma_7}{|\mathbf{p}_-+\mathbf{p}_+|^2}-\frac{\Gamma_8}{|\mathbf{p}_++\mathbf{P}|^2}\right\}
\end{aligned} \quad (18)$$

[2] W. Heitler, *Quantum Theory of Radiation* (Oxford University Press, London, 1936), p. 149.

where θ_- is the angle between $\mathbf{k}$ and $\mathbf{p}$, θ is the angle between $\mathbf{P}$ and $\mathbf{k}$, θ_+ is the angle between $\mathbf{k}$ and $\mathbf{p}_+$, and the θ's are small enough angles that we have replaced $\cos\theta$ by $1-\frac{1}{2}\theta^2$. (The conservation Eqs. (10) require that the angles θ be small when k is large and the particles are fast.) The quantities Γ are functions involving the angles between the particles and ratios of their energies to k. Thus the Γ's will be of the order of unity when averaged over the angles.

If the momenta are all of about the same order of magnitude, the W's will also be of about the same order of magnitude. If, however, one or two of the particles are slow, some of the terms involving

$$1/P^2,\ 1/p_-^2,\ 1/|\mathbf{p}_+ + \mathbf{P}|^2,\ 1/|\mathbf{p}_- + \mathbf{p}_+|^2$$

will become considerably larger than the others. When two of the particles are slow, the density factor (Eq. (17)) will become proportionately much smaller than when the particles are fast. If, however, only one of the electrons, say p_-, is slow, then the terms involving $1/p_-^2$ will still be large compared to the other terms, and the density factor, ρ_F, will be much larger than when two of the particles are slow. Therefore, the cross section will be greatest when p_- or P, say p_-, is slow with the other two particles fast (energy of the order of k), and in this case we can neglect all the terms in H_{FA} not involving a factor of $1/p_-^2$. We can also conclude that the total cross section is negligible except when p_- is small if we can show that the contribution from the two terms involving $1/p_-^2$ to the total cross section (integral over the angles) is appreciable only for values of p_- which are very small compared to P and p_+. This follows, since the neglected terms are of the same order of magnitude as the part of the integral over the angles which will be shown to be negligible.

The expression for H_{FA}, when we neglect all but the two terms having $1/p_-^2$ as a factor, is the same as the corresponding expression for pair production,[3] except for the common factor $(\mu_1^{*\prime\prime}\mu_2)$. This latter term gives only a factor

$$(m+\epsilon_-)/2\epsilon_- \tag{19}$$

multiplying the matrix H_{FA} for pair production when one has averaged over the directions of polarization and summed over the spin directions.

Then from Eqs. (1), (12), (13), (17), and (19) we obtain[3]

$$\begin{aligned} d\sigma = -\left(\frac{e^6}{2\pi k}\right)\Bigg[& P p_+ d\epsilon_+ \\ & \times\left(\frac{P\epsilon_-}{P\epsilon_- - \mathbf{P}\cdot\mathbf{p}_-}\right)\sin\theta d\theta \sin\theta_+ d\theta_+ d\phi\Bigg] \\ & \times\left[\frac{(m+\epsilon_-)}{2\epsilon_- p_-^4}\right]\Bigg\{\frac{P^2\sin^2\theta}{[Ek-\mathbf{P}\cdot\mathbf{k}]^2}(4\epsilon_+^2) \\ & + \frac{p_+^2\sin^2\theta}{[\epsilon_+ k - \mathbf{p}_+\cdot\mathbf{k}]^2}(4E^2) \\ & + [2Pp_+\sin\theta\sin\theta_+\cos\phi(4E\epsilon_+ - 2k^2) \\ & - 2k^2(P^2\sin^2\theta + p_+^2\sin^2\theta_+)] \\ & \times\left[\frac{1}{[Ek-\mathbf{P}\cdot\mathbf{k}][\epsilon_+ k - \mathbf{p}_+\cdot\mathbf{k}]}\right]\Bigg\} \end{aligned} \tag{20}$$

where ϕ is the angle between the $(\mathbf{P},\mathbf{k})$ plane and the $(\mathbf{p}_+,\mathbf{k})$ plane. Except for some terms in Eq. (19) involving p_-, which are negligible when p_- is small, the expression in the brackets $\{\ \}$ is the same as the corresponding one for pair production. The density factor differs from that for pair production by the term

$$P\epsilon_-/(P\epsilon_- - \mathbf{P}\cdot\mathbf{p}_-),$$

which is unity in the case of pair production. This term occurs because the initial positive-energy electron can carry away an appreciable part of the energy of the γ-ray.

Returning to our considerations concerning the relative magnitudes of the energies of the particles, we can write the energy and momentum conservation equations as

$$\begin{aligned} m + k \cong (p_-^2 + m^2)^{\frac{1}{2}} + p_+ + P & \\ + \tfrac{1}{2}m^2[1/P + 1/p_+], & \\ \mathbf{k} = \mathbf{P} + \mathbf{p}_+ + \mathbf{p}_- & \end{aligned} \tag{21}$$

when $\mathbf{P}$ and $\mathbf{p}_+$ are large compared to m. We can also write

$$\begin{aligned} \mathbf{P} &= r_2\mathbf{k}\cos\theta + \check{\mathbf{u}} r_2 k \sin\theta, \\ \mathbf{p}_+ &= r_1\mathbf{k}\cos\theta_+ + \hat{\mathbf{u}} r_1 k \sin\theta_+ \end{aligned} \tag{22}$$

[3] W. Heitler, reference 2, p. 196.

where $\check{\mathbf{u}}$ and $\hat{\mathbf{u}}$ are unit vectors orthogonal to $\mathbf{k}$, and r_1 and r_2 are numerical constants defined by

$$P=r_2k, \quad p_+=r_1k. \tag{23}$$

As θ and θ_+ must be small angles when P and p_+ are large compared to m, we obtain from Eqs. (21)

$$\epsilon\cong(1/2m)\{\delta^2+k^2[r_2^2\theta^2+r_1^2\theta_+^2 +2r_1r_2\theta\theta_+\check{\mathbf{u}}\cdot\hat{\mathbf{u}}]+\delta k(r_1\theta_+^2+r_2\theta^2)\} \tag{24}$$

where

$$\epsilon\equiv(p_-^2+m^2)^{\frac{1}{2}}-m, \tag{25}$$

$$\delta\equiv m^2k/2E\epsilon_+. \tag{26}$$

Equation (24) is valid when $\theta, \theta_+\ll(m/k)^{\frac{1}{2}}$. With this restriction on θ and θ_+, we have also

$$P\epsilon_-/(P\epsilon_- -\mathbf{P}\cdot\mathbf{p}_-)\cong\epsilon_-/m,$$
$$[Ek-\mathbf{P}\cdot\mathbf{k}]\cong\tfrac{1}{2}Pk[\theta^2+(m/P)^2], \tag{27}$$
$$[\epsilon_+k-\mathbf{p}_+\cdot\mathbf{k}]\cong\tfrac{1}{2}p_+k[\theta_+^2+(m/p_+)^2].$$

If we solve Eq. (25) for p_-, substituting the value for ϵ from Eq. (24) and use Eqs. (27), we can write the factor of $d\sigma$ which depends on the angles as

$$\frac{r^5dr d\lambda\cos^3\lambda\sin\lambda d\phi}{\left[r^2\cos^2\lambda+\left(\frac{m}{k}\right)^2\right]^2\left[\frac{k^4}{4m^2}r^4a^2+k^2r^2a+\delta^2\right]^2} \tag{28}$$

plus three similar terms. In Eq. (28) we have written

$$r_2\theta\equiv r\cos\lambda,$$
$$r_1\theta_+\equiv r\sin\lambda,$$
$$a\equiv 1+2\cos\lambda\sin\lambda\cos\phi +(\delta/k)(r_1^{-1}\sin^2\lambda+r_2^{-1}\cos^2\lambda). \tag{29}$$

Equation (28) becomes small rapidly when r (and thus θ, θ_+) are larger than m/k. Therefore, if m/k is sufficiently small, the contribution to the integral over the angles will come from values of r which are less than $(m/k)^{\frac{1}{2}}$, and thus only for small values of p_-. This gives the justification for dropping the terms in H_{FA} which did not contain $1/p_-^2$ as a factor.

If we neglect the relatively small variation of the term

$$(m+\epsilon_-)/2m\cong 1$$

we can integrate Eq. (28) (and the three other terms). It should be noted that our differential cross section in this approximation differs from that for pair production only by the expression for p_-, which in that case is the momentum of the recoil nucleus and is given by

$$p_-^2\cong[k^2r^2a_0+\delta^2]$$

where

$$a_0\equiv 1+2\cos\lambda\sin\lambda\cos\phi.$$

However, in the limit of large k/m (small δ), the integral over the angles gives the same cross section as for pair production. (The substitutions made in Eq. (28) were used, with the limits zero and infinity for the integration over r. Terms which were small compared to $\ln(2k/m)$ were neglected.) This is

$$\sigma_{\epsilon_+}d\epsilon_+=8(e^6/m^2k^2) \times(E^2+\epsilon_+^2+\tfrac{2}{3}\epsilon_+E)\ln(2\epsilon_+E/mk)d\epsilon_+ \tag{30}$$

for the cross section for ϵ_+ lying between ϵ_+ and $\epsilon_++d\epsilon_+$. The total cross section is the integral of this, or

$$\sigma_t=(58e^6/9m^2)\ln(2k/m). \tag{31}$$

(Our cross section is twice that for pair production, since the terms in Eq. (15) involving $1/P^2$ give the same contribution to the cross section when P is small.)

The cross section per atom for pair production

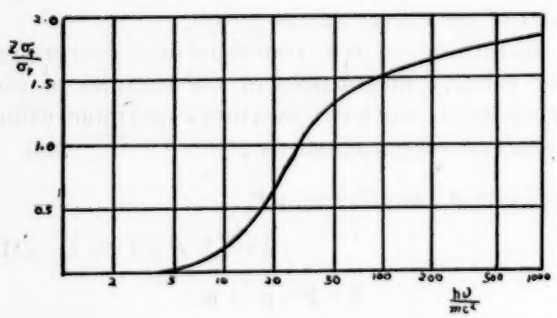

FIG. 1. The ratio of the cross section for triplet production to that for pair production multiplied by the nuclear charge Z is plotted against the ratio of the incident γ-ray energy to the rest-mass energy of the electron. The curve reaches the limiting value of $Z(\sigma_t/\sigma_p)=2$ for high γ-ray energies. The results are extrapolated between $(h\nu/mc^2)=4$ and $(h\nu/mc^2)=16$.

varies as the nuclear charge, Z, squared over a considerable energy range. We can expect the triplet production cross section per atom to vary directly with Z for energies which are low enough that screening of the electrons by each other and by the nucleus is negligible. We can thus expect the ratio of pair production to triplet production to vary as Z for the limiting case of high energies.

The limiting Eqs. (30) and (31) are of little practical use, however, as the effect of screening will become important before they are rigorously valid. As it did not appear possible to integrate Eq. (20) in closed form, it was evaluated numerically for the case of a large ratio of k/m. Figure 1 shows the result for the ratio of the total cross section for triplet production, σ_t, to that for pair production, σ_p, multiplied by the nuclear charge Z. *The curve has been extrapolated between* $k/m=4$ *and* 16 (the slope of the curve can be shown to vanish at the threshold, $k=4m$). It should be noted that the asymptotic value of $2/Z$ for the ratio of σ_t/σ_p is approached very slowly.

3. DISCUSSION OF RESULTS

From Eq. (28) we can expect to draw some qualitative conclusions concerning the distribution of energies and directions of the particles when $k>10m$. We can expect the positron and one electron to have high energies compared to the second electron, and to recoil in the forward direction with angles of the order of m/k with respect to the direction of k. We can also expect the energy of the slow particle to be distributed about the value m for moderate γ-ray energies. For increasing γ-ray energies the energy of the slow electron will tend toward zero.

Our results seem to be in general agreement with the preliminary observations reported by Kruger.[1]

The author would like to express his appreciation to Dr. J. M. Jauch for suggesting the problem to him and for several suggestions concerning its solution.

4. APPENDIX

To obtain the energy threshold for which triplet production can occur, we must satisfy the energy and momentum-conservation equations

$$m+k=(p_1^2+\alpha_1^2+m^2)^{\frac{1}{2}}+(p_2^2+\alpha_2^2+m^2)^{\frac{1}{2}}+(p_3^2+\alpha_3^2+m^2)^{\frac{1}{2}},$$
$$k=p_1+p_2+p_3,$$
$$0=\alpha_1+\alpha_2+\alpha_3$$

where p_1, p_2, p_3 are the components of momentum of the three particles parallel to k and α_1, α_2, α_3 are the components orthogonal to k. The minimum value of k will obviously occur only when $\alpha_1=\alpha_2=\alpha_3=0$. Then, because of the symmetry of the equation in p_1, p_2, and p_3, for the minimum value of k we must have $p_1=p_2=p_3$ (this is easily verified by imposing the usual conditions for the minimum value of a function). This gives

$$m+k=3((k/3)^2+m^2)^{\frac{1}{2}}$$

or

$$k=4m.$$

The finite momentum of the initial electron will, of course, modify the value of the threshold, but we can in any case expect the cross section to be negligibly small when $k<4m$.

Note added in proof: The author's attention has been called to a discussion of "triplet" production by P. Nemirovsky, Journal of Physics of the U.S.S.R., 11, 94 (1947). Nemirovsky has evaluated the cross section for the low energy γ-ray range from 4 to 6 mc^2. His results seem to be in general agreement with ours. It should be noted that in our approximation it was not necessary to consider the retarded interaction of the particles because of the slowness of the recoil electron.

The Double Current Sheet in Diffraction

W. R. SMYTHE
California Institute of Technology, Pasadena, California

(Received August 1, 1947)

The electromagnetic radiation from an aperture in a plane-conducting screen is identical with that which would exist if screen and aperture were replaced by a double current sheet fitting the aperture. The current density i is equal and opposite in the two layers of the sheet and is determined by the original tangential electric field E over the opening so that E is $-\frac{1}{2}j\omega\mu\delta i$. The distance δ between layers is infinitesimal. A rigorous expression for the vector potential of the emergent radiation in terms of E is given. This is the expression used by Bethe in finding the diffraction from small holes. It is shown to provide a simpler method of getting the results of Stratton and Chu for rectangular openings. It is then applied to the calculation of the excitation of a rectangular wave guide by a coaxial line termination in one side. An expression for the output resistance is given.

THERE is a simple but apparently little used method of setting up certain electromagnetic boundary value problems. It applies to the radiation from apertures in plane-conducting surfaces such as the wall of a rectangular wave guide. The uniqueness theorem[1a] for electromagnetic waves, when modified to fit the steady-state condition, asserts that an electromagnetic field is uniquely determined within an empty bounded region by the values of the tangential component of the electric vector (or of the magnetic vector) over the boundary. Evidently with conducting boundaries the electric field, whose tangential component over the screen is zero, must be used because the tangential magnetic field, which is not in general zero, is unknown. To use this theorem we need a source giving a tangential electric field that has any desired arbitrary value over an area S of an infinite plane and is zero over the remainder. Consider a thin plane, double current sheet in which the distance δ between layers is very small and the current densities in the two layers at any point of the sheet are equal and opposite. Such a sheet, with the thickness exaggerated, and with the dotted portion cut away along a line of flow is shown in Fig. 1(a). If the sheet is uniform in the direction of flow all the current passes around the edge, but if it is stronger in the center, as shown in Fig. 1(b), part will turn back before reaching the edge. Because the sheet is very thin the external magnetic induction is negligible compared with its value B_i between layers. Hence an application of the magnetomotance law to the rectangle $abcd$, which is normal to i and fits closely a section of the upper layer, shows[1b] B_i to be μi. The changing flux $N=B_i\delta dl$ through the rectangle $a'b'c'd'$ produces an electromotance $-dN/dt=\int \boldsymbol{E}\cdot d\boldsymbol{s}$ around it. As $\delta\rightarrow 0$ half of this appears along the side $a'b'$ so that the electric field strength E just above the sheet is $-\frac{1}{2}j\omega\mu\delta i$. Clearly a double current sheet giving any desired values of E can be built up out of infinitesimal solenoids of cross-sectional area δdl and length dc whose magnetic moment is $\boldsymbol{n}\times i\delta dl dc$ or $-2(j\omega\mu)^{-1}\boldsymbol{n}\times\boldsymbol{E}dS$. It is evident from symmetry that $\boldsymbol{E}$ is normal to the plane of the sheet outside the hole's boundaries. The vector potential[2] at P of the radiation from a small, oscillating current loop is normal to the loop axis and proportional to the sine of the angle between this axis and the radius vector $\boldsymbol{r}$ from the loop to P. Thus for the diffracted field, in m.K.S. units, the vector potential is

$$\boldsymbol{A}=\frac{1}{2\pi\omega}e^{j\omega t}\int_S \frac{(\beta r-j)(\boldsymbol{n}\times\boldsymbol{E})\times\boldsymbol{r}_1}{r^2}e^{-i\beta r}dS \quad (1)$$

where $\boldsymbol{r}_1$ is a unit vector in the direction of $\boldsymbol{r}$, β is the wave number and ω the angular frequency. The electric and magnetic fields are given by

$$\boldsymbol{E}=-j\omega\boldsymbol{A}, \quad \boldsymbol{B}=\nabla\times\boldsymbol{A}. \quad (2)$$

[1a] J. A. Stratton, *Electromagnetic Theory* (McGraw-Hill Book Company, Inc., New York, 1941), p. 487.

[1b] Throughout this paper m.K.S. units are used and $j=(-1)^{\frac{1}{2}}$.

[2] W. R. Smythe, *Static and Dynamic Electricity* (McGraw-Hill Book Company, Inc., New York, 1939), p. 477.

If Φ is written for $r^{-1}e^{-i\beta r}$ then the factors multiplying $n\times E$ in the integrand can be replaced by $\nabla\Phi$. In this form the integral is seen to be twice one of those obtained by Stratton (reference 1, p. 466) by direct integration of the field equations. It is the only one used by Bethe[3] in his rigorous calculation of the diffraction from a small hole. When the correct value of E is used the expression is exact. This double current shell replaces the fictitious magnetic currents and charges used by Stratton.

The few cases in which the value of E over the aperture can be calculated rigorously are those in which at least one dimension of the aperture and the thickness of the screen are small compared with a wave-length. These include small circular holes in thin sheets and narrow slits. The first of these has been worked out by Bethe[3] who assumes that near the hole phase differences are negligible so static field values, multiplied by $e^{i\omega t}$, can be used. He shows that any incident wave can be broken up into an electric field E_z, normal to the sheet, and a magnetic induction B_z, tangent to it. Both static problems are very simple in the spheroidal coordinate system (reference 2, p. 156) ξ, ζ, ϕ in which the sheet is $\xi=0$ and the hole of radius c is $\zeta=0$. Positive values of ζ cover the space on the incident side and negative values that on the emergent side. The electric field component in the hole in the plane of the sheet due to E_z is radial, and is found from the potential function (reference 2, p. 160, Eq. 6) for a sheet bounding a uniform static field, thus

$$E_\rho=-\frac{1}{h_1}\frac{\partial V}{\partial\xi}\bigg|_{\zeta=0}=-\frac{Ec}{\pi h_1}\bigg|_{\zeta=0}=\frac{-E\rho}{\pi(c^2-\rho^2)^{\frac{1}{2}}}. \quad (3)$$

It is easily verified that a scalar magnetic potential Ω that gives a uniform induction B_z parallel to the sheet when ζ is $+\infty$, zero induction when ζ is $-\infty$, and makes B everywhere tangential to the sheet is

$$\mu\Omega=B_z c[jP_1^1(j\zeta)+\pi^{-1}Q_1^1(j\zeta)]P_1^1(\xi)\cos\phi$$
$$=-(B_z x/\pi)[\tfrac{1}{2}\pi+\tan^{-1}\zeta+\zeta/(1+\zeta^2)].$$

The normal component of B on the emergent side of the hole is

$$\frac{\mu\partial\Omega}{h_2\partial\zeta}\bigg|_{\zeta=0}=\frac{-2B_z x}{\pi(c^2-\rho^2)^{\frac{1}{2}}}=\frac{1}{j\omega}\frac{\partial E_y}{\partial x}.$$

This relation between B_z and E_y on the emergent face of the hole follows because $\partial E_y/\partial x$ equals the time derivative of the flux leakage $\partial N/\partial x$ or $-B_z$ in the double current sheet. Integration gives

$$E_y=-(2j\omega B_z/\pi)(c^2-\rho^2)^{\frac{1}{2}}. \quad (4)$$

Insertion of (3) and (4), suitably weighted according to polarization and incident angle, in (1) gives Bethe's results.

When the tangential electric field over the aperture is unknown, distant radiation patterns can usually be found with considerable accuracy by using its unperturbed value. This is surprising in view of Andrews'[4] measurements on circular apertures. Unlike Kirchhoff's method this makes no assumption that the magnetic and normal electric fields are unperturbed. Neither does it neglect the currents and charges on the emergent face of the screen. For these reasons it gives good results where Kirchhoff's formula breaks down at wave-lengths comparable with the aperture dimensions. An example proving this was worked out by Stratton and Chu[5] whose results compare favorably with such rigorous solutions as are known. Their results for the distant radiation from a rectangular aperture in a thin plane-conducting sheet, upon which a plane wave impinges at any angle, can be derived

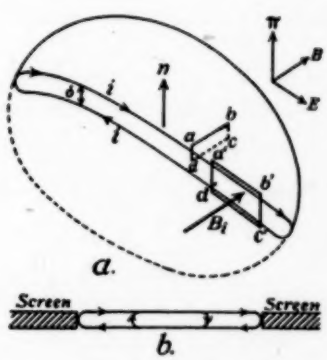

FIG. 1. Schematic diagram of the double current sheet.

[3] H. A. Bethe, Phys. Rev. 66, 163 (1944).

[4] C. L. Andrews, Phys. Rev. 71, 777 (1947).

[5] J. A. Stratton and L. J. Chu, Phys. Rev. 56, 106 (1939).

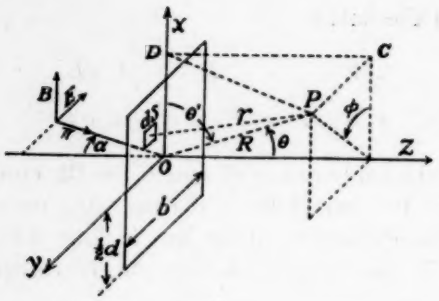

FIG. 2. Relations for an incident plane wave. (The notation $\frac{1}{2}d$ should read $\frac{1}{2}a$.)

much more simply by using the double current sheet.

Consider a plane wave whose electric vector lies in the plane of incidence and which is incident at any angle α on an aperture in the $z=0$ plane bounded by $x=\pm\frac{1}{2}a$ and $y=\pm\frac{1}{2}b$, as shown in Fig. 2. Let x_1 and y_1 be the coordinates of an area element dS in the aperture, and let x and y be those of the field point P at a distance z from the screen. Let $\boldsymbol{r}$ be the radius vector from dS to P and $\boldsymbol{R}$ that from O to P. Then if $R\gg a$ and $R\gg b$, we may take $\boldsymbol{r}$ parallel to $\boldsymbol{R}$ and

$$r\approx R-x_1\cos\phi\sin\theta-y_1\sin\phi\sin\theta.$$

The tangential component of $\boldsymbol{E}$ varies in phase at $z=0$, so that

$$E_t=E\cos\alpha\exp j(\omega t-y_1\sin\alpha).$$

Since $\boldsymbol{n}\times\boldsymbol{E}_t$ parallels the x axis, $(\boldsymbol{n}\times\boldsymbol{E}_t)\times\boldsymbol{R}$ is normal to DP and $\boldsymbol{R}$, parallel to the yz plane and proportional to $\sin\theta'$. Thus

$$(\boldsymbol{n}\times\boldsymbol{E}_t)\times\boldsymbol{r}_1=E_t(-\boldsymbol{j}\cos\theta+\boldsymbol{k}\sin\theta\sin\phi).$$

Substitution of these values in (1) gives A_y and A_z. The spherical components are given by the equations

$$A_\theta=A_y\sin\phi\cos\theta-A_z\sin\theta,\quad A_\phi=A_y\cos\phi,\quad A_r=0.$$

If we write

$$P=\beta\cos\phi\sin\theta,\quad Q=\beta(\sin\phi\sin\theta-\sin\alpha),$$

the resultant expression for A_θ is

$$\frac{-\beta E\cos\alpha\sin\phi}{2\pi\omega R}e^{j(\omega t-\beta R)}\int_{-\frac{1}{2}a}^{+\frac{1}{2}a}e^{jPx_1}dx_1\int_{-\frac{1}{2}b}^{+\frac{1}{2}b}e^{jQy_1}dy_1.$$

A straightforward integration gives

$$A_\theta=\frac{2\beta E\cos\alpha\sin\phi\sin(\frac{1}{2}Pa)\sin(\frac{1}{2}Qb)}{\pi\omega RPQ}e^{j(\omega t-\beta R)},\quad(5)$$

$$A_\phi=-A_\theta\cot\phi\cos\theta.\quad(6)$$

Stratton and Chu[5] obtained this formula by quite a different method which involved the superposition or "reflection" of two solutions of Maxwell's equations, each of which assumed unperturbed electric and magnetic fields over the openings. This was necessary to eliminate the tangential electric field over the screen, and is exactly equivalent to discarding the three integrals derived from the tangential magnetic field and doubling the remaining integral. Six figures[5] comparing their formulas with the rigorous ones of Morse and Rubenstein[6] for a slit

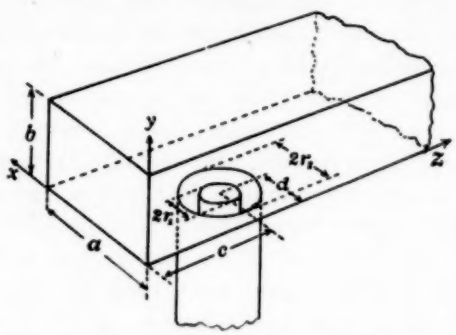

FIG. 3. Coaxial line attached to a rectangular wave guide.

show that the initial assumption of an unperturbed tangential electric field gives surprisingly accurate results. They also show the total failure of Kirchhoff's formula, which ignores polarization when the slit width is much less than a wave-length.

It has been shown that the double current sheet yields correct known solutions; it can now be applied to a new problem. Suppose that the propagation space of a coaxial line, which has internal and external radii r_1 and r_2, terminates in an annular opening whose center is at $x=d$, $y=0$, $z=c$ in the bottom of a rectangular wave guide closed at $z=0$. The walls of the guide are at $x=0$, $x=a$, $y=0$, and $y=b$ and the frequency is such that only the TE_{10} mode is transmitted. The arrangement is shown in Fig. 3. At some

[6] P. M. Morse and Pearl J. Rubenstein, Phys. Rev. **54**, 898 (1938).

positive value of z the transmitted wave is completely absorbed and we desire to find the output resistance of the coaxial line. To make E_y zero when z is zero requires two double current sheets of opposite sign, one at $z=c$ and one at $z=-c$. Each consists of a flat torus in the xz plane of a guide bounded by $x=0$, $x=a$, $y=-b$, and $y=b$. To calculate the excitation of the TE_{10} mode, whose electric field is everywhere parallel to the y axis, the thickness δ of the torus is exaggerated as shown in Fig. 4. The exact value of E over the annular opening is unknown but the field of the principal coaxial mode, which carries the energy and is the only field far from the opening, is inversely proportional to r. If the potential of the center conductor is V and the current density in the double layer in amperes per radian is i, then

$$E=\tfrac{1}{2}j\omega\mu i\delta/r=V/[r\ln(r_2/r_1)],$$

so that

$$i=2V/[j\omega\mu\delta\ln(r_2/r_1)]. \tag{7}$$

Thus all currents encircle the entire section of the torus. The only current elements that excite the TE_{10} mode are parallel to the y axis and so are those of length δ that form the curved edges of the torus. The TE_{10} term, A_{10}, in the vector potential of the waves excited in an a by $2b$ guide, extending from $z=-\infty$ to $z=+\infty$, by a current element Idy_0 at $x=x_0$, $z=z_0$, is in the y direction.

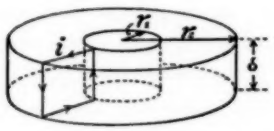

FIG. 4. Form of the toroidal current sheet for the wave guide.

$$A_{10}=(\mu Idy_0/2\beta' ab)\sin(\pi x_0/a)\times\sin(\pi x/a)\exp j[\omega t-\beta'(z-z_0)],$$

where

$$\beta'^2=\omega^2\mu\epsilon-\pi^2/a^2=4\pi^2/\lambda_{10}^2,$$

and λ_{10} is the guide wave-length. This is easily verified by multiplication of B_x by $\sin(\pi x/a)dxdy$ and integration over one face of the z_0 plane. The integral vanishes except over the element where its value is $\frac{1}{2}\mu Idy_0\sin(\pi x_0/a)$ by the magnetomotance law. We shall calculate first the contribution from four similarly directed current elements of width $d\theta$, whose x and z coordinates are $d\pm r_2\sin\theta$ and $c\pm r_2\cos\theta$, as shown by crosses in Fig. 5. The resultant dA_{10} is

$$[2\mu i\delta/(\beta' ab)]\sin(\pi x/a)\{\exp j[\omega t-\beta'(z-c)]\}\times\sin(\pi d/a)f(\theta)d\theta,$$

where

$$f(\theta)=\cos[(\pi r_2/a)\sin\theta]\cos(\beta' r_2\cos\theta).$$

If we write βr_2 for $(\pi^2/a^2+\beta'^2)^{\frac{1}{2}}r_2$, where $\beta^2=\omega^2\mu\epsilon$, and $\tan\phi$ for $\pi/(\beta' a)$, the integral of the θ terms takes the form

$$\tfrac{1}{2}\int_0^{1\pi}\{\cos[\beta r_2\cos(\theta-\phi)]+\cos[\beta r_2\cos(\theta+\phi)]\}d\theta.$$

Both terms in the integrand have a period of $\frac{1}{2}\pi$ so that the value of the integral is independent of ϕ. By choosing $\phi=0$ the integral takes the standard Bessel integral form

$$\tfrac{1}{2}\int_0^{\pi}\cos(\beta r_2\cos\theta)d\theta=\tfrac{1}{2}\pi J_0(\beta r_2)=\tfrac{1}{2}\pi J_0(2\pi r_2/\lambda),$$

where λ is the free-space wave-length. Addition of a similar expression for the currents at the inner edge of the torus and for the edges of the image sheet and substitution for i from (7) give

$$A_{10}=C\sin(\pi x/a)\exp j(\omega t-\beta' z), \tag{8}$$

where

$$C=\frac{4\pi V\sin(\pi d/a)\sin(\beta' c)}{j\omega\beta' ab\ln(r_2/r_1)}\times[J_0(2\pi r_2/\lambda)-J_0(2\pi r_1/\lambda)].$$

The TE_{10} electric field and magnetic induction are

$$B_x=-\partial A_{10}/\partial z=j\beta' A_{10},\quad E_y=-j\omega A_{10}.$$

The mean Poynting vector $\langle\Pi_z\rangle_{Av}$ is

$$\langle\Pi_z\rangle_{Av}=\tfrac{1}{2}EB^*/\mu=(\tfrac{1}{2}\omega\beta'/\mu)|C|^2\sin^2(\pi x/a). \tag{9}$$

The upper half of the tube, from $y=0$ to $y=b$,

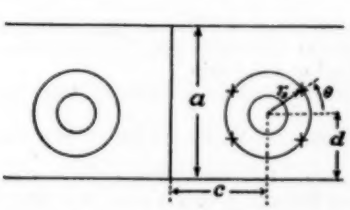

FIG. 5. Arrangement of associated current elements.

satisfies the boundary conditions of the original guide of Fig. 3, so that integration of $\langle \Pi_z \rangle_{Av}$ over its area gives the rate of power dissipation or $\frac{1}{2}V^2/R$ where R is the radiation resistance. Thus we find

$$R=\frac{\mu\omega\beta' ab \ln^2(r_2/r_1)}{8\pi^2 \sin^2(\pi d/a) \sin^2\beta' c \times[J_0(2\pi r_2/\lambda)-J_0(2\pi r_1/\lambda)]^{-2}}. \quad (10)$$

The same result is obtained by the integration of Poynting's vector over the coaxial opening, using $r_1 V[r \ln(r_2/r_1)]^{-1}$ for $\boldsymbol{E}$ and $\nabla\times\boldsymbol{A}_{10}$ for $\boldsymbol{B}$, but the integration is a little more difficult. The integration of Poynting's vector for the other non-transmitted modes over the annular opening should give the output reactance of the line. Unfortunately it does not seem possible to evaluate the resultant integrals analytically.

PHYSICAL REVIEW VOLUME 72, NUMBER 11 DECEMBER 1, 1947

X-Ray Emitting Isotopes of Radioactive Sb and Sn

K. D. COLEMAN* AND M. L. POOL
Mendenhall Laboratory, Ohio State University, Columbia, Ohio

(Received August 8, 1947)

Three new x-ray emitting activities in Sb with half-lives of 2.8 hours, 5.1 hours and 39 hours have been found by the use of the curved crystal camera in conjunction with the x-ray decay curves. The assignments are Sb^{117}, Sb^{118}, and Sb^{119} respectively. All three decay by K-electron capture giving characteristic Sn x-rays. The 2.8-hour Sb^{117} also emits 0.46-Mev electrons while the 5.1-hour Sb^{118} gives 0.20-Mev electrons and 1.5-Mev gamma-rays.

X-ray periods of 1.25 days and 9 days have been found in Sn. The reported decay scheme for Sn^{113} was verified but the 0.085-Mev gamma-ray was not found.

1. INTRODUCTION

OF the several activities which have been attributed to radioactive Sb isotopes, those of half-lives of 2.8 days,[1] 60 days[2] and 17 minutes[1] have been assigned to Sb^{122}, Sb^{124} and Sb^{120}, respectively. The first two activities emit beta-rays and gamma-rays, while the third emits positrons. These three periods have been made by four different reactions.[3]

A 2.7-year activity, emitting low energy electrons and gamma-rays, has been obtained from fission,[4] and tentatively assigned to Sb^{125}. A 3.6-minute positron activity obtained from $In+\alpha$ activation[5] has been assigned to either Sb^{116} or Sb^{118}. In addition, several Sb activities are found in fission fragments[4] with masses greater than 125.

Approximately fifteen activities have been reported as belonging to Sn isotopes.[4,6] Because of the large number of stable isotopes and because of the limited possibilities for making these activities by use of different bombarding particles and target materials, the only one which has been assigned with certainty is the 105-day[7] activity of Sn^{113}.

The present investigation was undertaken to study the application of the Cauchois curved-crystal camera, to the x-ray activities induced in Sn when activated with 10-Mev deuterons. Bombardments were also made using 5-Mev protons on Sn and 20-Mev alpha particles on In.

2. EXPERIMENTAL PROCEDURE

Characteristic x-ray lines were photographed by using a pair of Cauchois cameras[8] equipped

* Major, U. S. Army Air Corps, Research under auspices of Air University, Maxwell Field, Alabama. Now stationed Wright Field, Dayton, Ohio.

[1] J. J. Livingood and G. T. Seaborg, Phys. Rev. **55**, 414 (1939).

[2] E. B. Hales and E. B. Jordon, Phys. Rev. **64**, 202 (1943).

[3] G. T. Seaborg, Rev. Mod. Phys. **16**, 1 (1944).

[4] Plutonium Project, J. Am. Chem. Soc. **68**, 2411 (1946).

[5] J. R. Risser, K. Lark-Horovitz, and R. N. Smith, Phys. Rev. **57**, 355 (1940).

[6] J. J. Livingood and G. T. Seaborg, Phys. Rev. **55**, 667 (1939).

[7] S. W. Barnes, Phys. Rev. **56**, 414 (1939).

[8] J. E. Edwards, M. L. Pool, and F. C. Blake, Phys. Rev. **67**, 150 (1945).

with mica crystals curved to a radius of 15 inches. The two cameras were mounted with their optical axes inclined at an angle of 30°, so that simultaneous photographs could be taken from the same sample. Each camera could be removed independently for calibration and alignment. On photographs taken with the 15-inch cameras, the linear separation between the K_α lines of adjacent elements in the Sn region is 1.8 mm. Because of this wide separation, lines were identified by comparison to a standard film prepared by fluorescence, rather than placing calibration lines on each individual film. Two index marks were placed on each film, to assure proper alignment for comparison.

Because of its low melting point, Sn foil, placed on a standard Cu target holder, melted when exposed to the full deuteron beam. A hollow Sn block was cast and soldered directly to a probe. During bombardment, ice water was circulated through the Sn block for cooling. After bombardment, the surface of the block was scraped to remove the active portion. With this target, the full intensity of the deuteron beam could be utilized.

Chemical separations were performed by fractional distillation using variations of a published procedure.[9] HCl gas was bubbled through the distillation flask, instead of adding HCl dropwise in an atmosphere of CO_2. The Sn and Sb fractions were precipitated as sulfides. Because of the time required for chemical separation, no activities shorter than two hours were studied. For the activities of major interest in this investigation, the distillation method was found to give more certain and complete separation than selective precipitation.

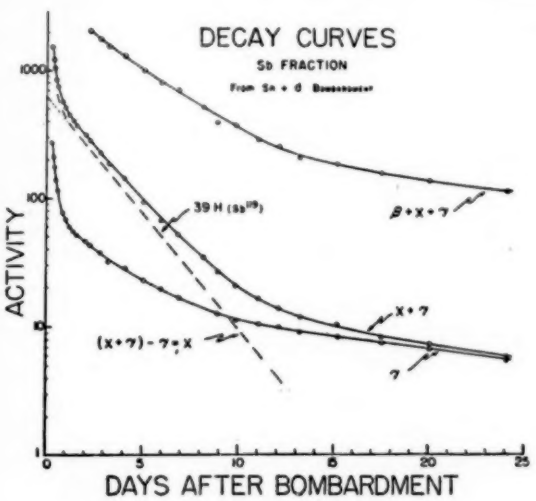

FIG. 1. Decay curve of Sb^{119} from Sn+d.

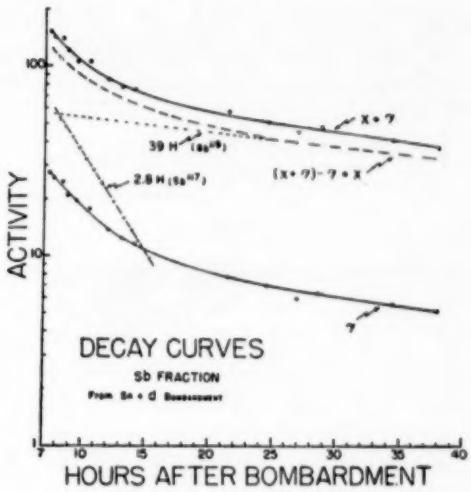

FIG. 2. Decay curve of Sb^{117} from Sn+d.

Sb^{117} AND Sb^{119}

When Sn was activated by deuterons, the Sb fraction was found to carry the major portion of the activity, including two strong x-ray periods. Figure 1 shows the decay of this fraction for the first 25 days after bombardment. Analysis of the x-ray decay curve shows the long period to be 39±1 hours. No electrons or gamma rays were found associated with this period. Since the x-ray plus gamma-ray ($x+\gamma$) curve and the gamma (γ) curve are seen to merge after some

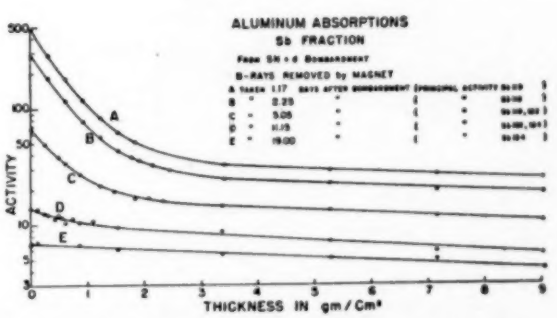

FIG. 3. Al-absorption curves of Sb^{117} and Sb^{119} showing decay of x-ray activity. X-rays have disappeared in curve *E*.

[9] J. A. Scherrer, J. Res., National Bureau of Standards 16, 253 (1936).

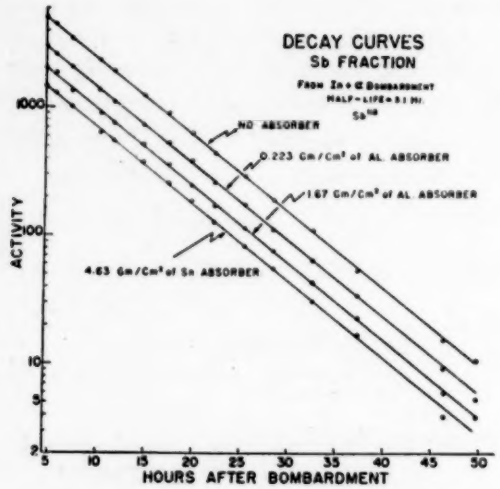

FIG. 4. Decay curves of Sb^{118} from $In+\alpha$.

20 days, there were no x-rays of a period longer than 39 hours of sufficient intensity to be measured.

Figure 2 shows the decay of the Sb fraction for the first 40 hours after bombardment. When the 39-hour x-ray activity is subtracted from the total x-ray decay curve, the short period x-ray activity is found to be 2.8 ± 0.3 hours. From successive aluminum-absorption measurements made with an open ionization chamber, a 0.46-Mev electron was found associated with this period.

Aluminum-absorption measurements, taken at intervals after bombardment, are shown in Fig. 3. In these curves, the beta rays have been removed by an electromagnet. The x-rays are seen to have disappeared after 19 days. By absorption in aluminum, the x-rays were found to be characteristic of the Sn region.

Both the 2.8-hour and 39-hour x-ray activities

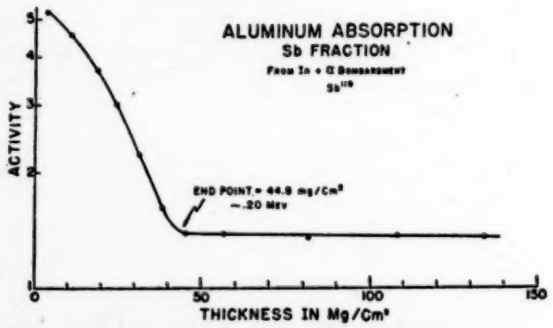

FIG. 5. Al-absorption curve of Sb^{118} showing 0.20-Mev end-point.

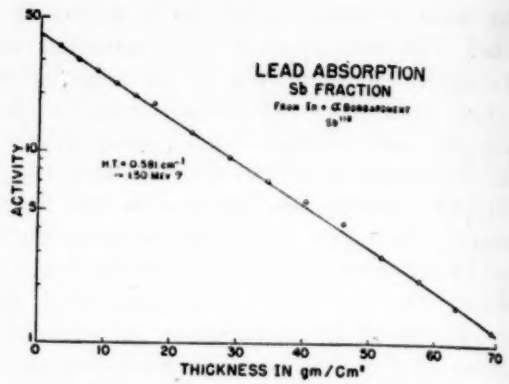

FIG. 6. Pb-absorption curve of Sb^{118} from $In+\alpha$.

were also produced by $Sn+p$ bombardment but not by $In+\alpha$ bombardment. The x-ray saturation intensity ratio of the 39-hour activity to the 2.8-hour activity is 1.70 to 1. By photographing the emission lines, the x-rays have been shown to be characteristic of Sn. Hence the decay process in both cases is by K-electron capture. This decay process indicates an isotopic assignment less than 121. Since the 17-minute positron activity has been assigned to Sb^{120}, and since an $In+\alpha$ bombardment does not produce the x-ray activities, assignment cannot be made to Sb^{116}, Sb^{118} or Sb^{120}. The low percentages of stable Sn^{112}, Sn^{114}, and Sn^{115} present, make the assignment to mass number 115 or less very improbable. This leaves Sb^{117} and Sb^{119} as the logical possibilities. In view of the relative abundances of the stable Sn isotopes, it seems more probable to assign the

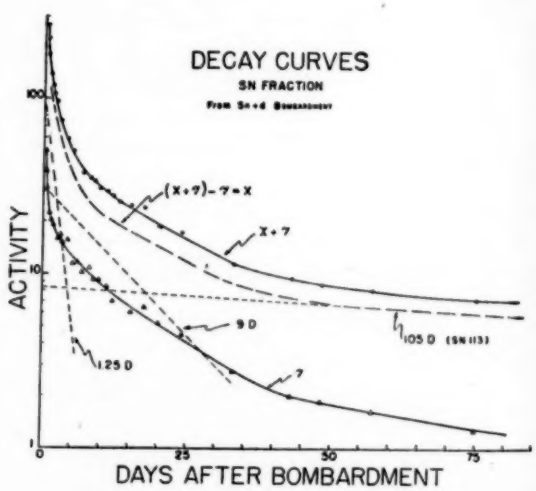

FIG. 7. Decay curves for Sn fraction of $Sn+d$ showing three x-ray periods.

2.8-hour activity to Sb^{117} and the 39-hour activity to Sb^{119}.

Sb^{118}

The Sb fraction of In activated by 20-Mev alpha particles yielded a single activity of 5.1 ± 0.3 hours. The decay curves for this period. extending over 9 half-lives are shown in Fig. 4, The small decrease in activity, as greater amounts of absorber are introduced, show that the emission is principally hard gamma-rays with some x-rays present. The Sb activity has been obtained from In furnished by the Indium Corporation of America and by Adam Hilger, Ltd., Laboratory No. 10,874.

Figure 5 shows an aluminum-absorption measurement made with the open ionization chamber. The end point is found at 0.20 Mev. The relatively large amount of x-ray and γ-ray activities indicates that, in most cases, decay does not involve beta-ray or electron emission. The x-rays have been found, by absorption in aluminum, to be characteristic of the Sn region. The energy of the gamma-ray was found by absorption in lead to be 1.5 Mev, as shown in Fig. 6.

This 5.1-hour activity is observed in the decay curves of the Sb fraction of the $Sn+d$ bombardment only by the gamma radiation. Successive absorption measurements made with the open ionization chamber show the 0.20-Mev end point. The 5.1-hour activity may be due to Sb^{116} or Sb^{118}, of which Sb^{118} seems to be the most probable.

Sn

The x-ray plus gamma-ray ($x+\gamma$) and gamma-ray (γ) decay curves for the Sn fraction of the $Sn+d$ activation are shown in Fig. 7. Analysis of the subtracted x-ray decay curve shows x-ray periods of 105 days, 9 ± 1 days and 1.25 ± 0.2 days. A beta-ray of 2.5 Mev and a gamma-ray are associated with the 9-day period. A beta-ray and gamma-ray are also associated with the 1.25-day period. The latter two periods are perhaps identified with the previously reported beta emitting 26-hour[6] period, and, beta and gamma emitting 10-day[4] period.

The Sn fraction of $In+d$ showed only the 105-day period assigned to Sn^{113}. This activity was followed through more than 5 half-lives. The decay and energy data previously reported[7] were verified except for the 0.085-Mev γ, which was not found. No evidence was found for a Sn^{113} isomer.

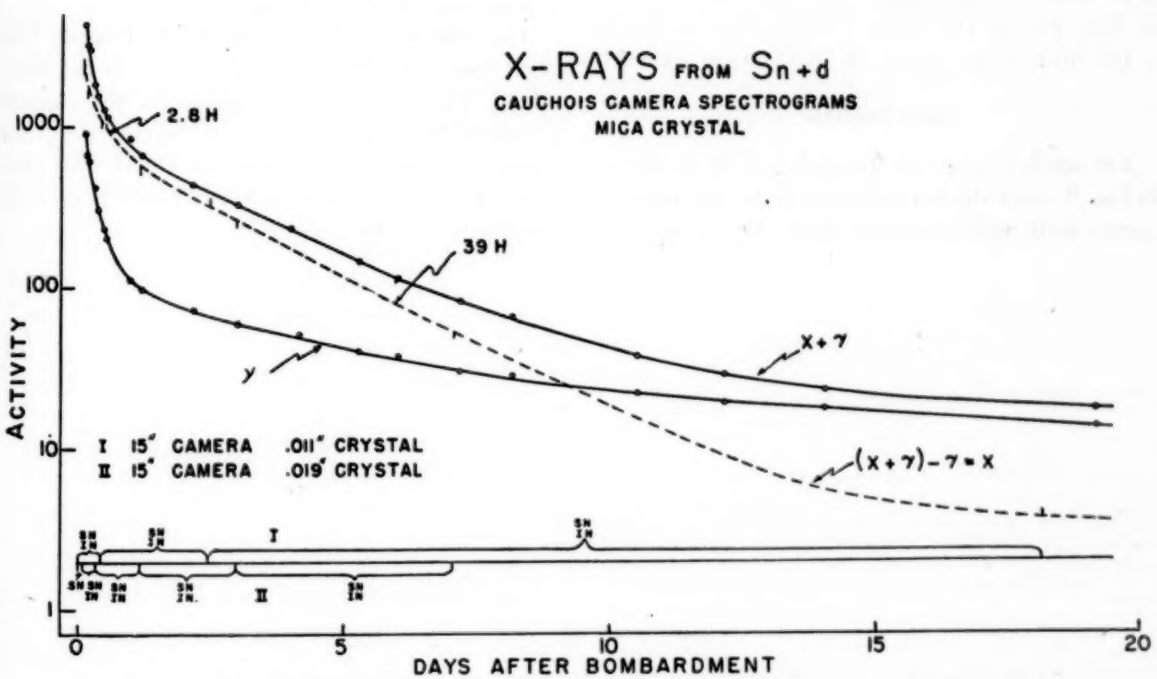

FIG. 8. Photographic analysis of x-rays from $Sn+d$ activation. Exposure periods shown on scale.

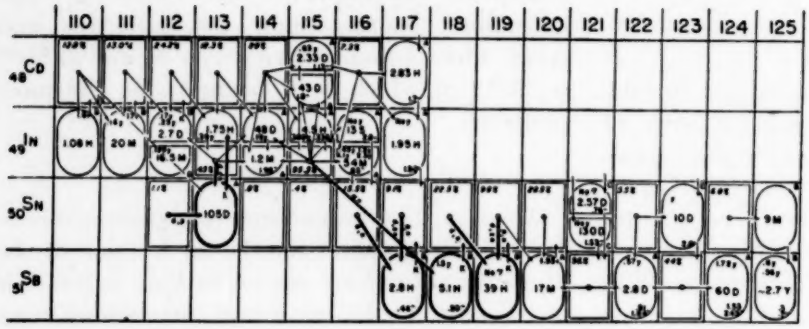

FIG. 9. Nuclear chart in the region of Sn, mass numbers against atomic numbers. The activities studied are indicated by heavy lines. Arrows represent nuclear reactions.

PHOTOGRAPHIC ANALYSIS OF X-RAYS

Figure 8 shows the results of a curved-crystal camera analysis of the x-ray decay of a Sn+d sample. The K_α lines of Sn and In appear in all except the first film on Camera II. The Sn line was initially much stronger than the In line. As exposure time was increased for successive films, the In line remained faintly visible while the Sn line became progressively weaker. An exposure of 60 days following the last one shown in Fig. 8 failed to record either line.

None of the films showed an Sb line. The x-rays from the Sb fraction of a Sn+d bombardment were photographed and showed only the Sn line. Hence the three x-ray activities found in the Sb fraction decay by K-electron capture.

DISCUSSION

The nuclear chart in the region of Sn is shown in Fig. 9, with the periods studied in this investigation indicated by heavy lines. By application of the Cauchois curved-crystal camera, in conjunction with x-ray decay curves, three previously unreported periods of 2.8 hours, 5.1 hours, and 39 hours, are assigned to Sb^{117}, Sb^{118}, and Sb^{119}, respectively. All decay by K-electron capture to Sn, giving characteristic Sn x-rays. In addition, the 5.1-hour period emits a 1.5-Mev gamma-ray.

X-ray periods of 1.25 days and 9 days have been found in the Sn fraction of Sn+d but no assignment is made. However, the latter period is perhaps identified with the previously reported 10-day period shown in the chart. The decay scheme for Sn^{113} was verified but the 0.085-Mev gamma-ray was not found.

The able assistance of Mr. H. L. Finston who performed the chemical separations is acknowledged. The authors are grateful for the support received from Mr. Julius F. Stone, the Ohio State University Development Fund, the Ohio State University Research Foundation and the Graduate School.

The Radiofrequency Spectra of the Sodium Halides

W. A. NIERENBERG AND N. F. RAMSEY
Columbia University, New York, New York

(Received August 11, 1947)

The radiofrequency spectra of $Na^{23}Br$, $Na^{23}Cl$, and $Na^{23}I$ have been investigated by use of the molecular-beam resonance method. In external fields of approximately 10,000 gausses, the spectra are about 1 Mc/sec. wide, continuous, and of a characteristic form with a deep central minimum and two smaller side minima. The central minimum agrees in frequency to 0.2 percent with the Larmor frequency for a decoupled Na^{23} nucleus. At this field the orientation-dependent interaction of the Na^{23} nucleus with the molecule is small compared to the interaction of the nuclear magnetic moment with the external magnetic field. Comparison of the observed spectra with the statistical theory of Feld and Lamb suggests that the effect is due to the interaction of an electric quadrupole moment of the sodium nucleus with the inhomogeneous electric field of the other charges in the molecule. In this theory, the continuous nature of the spectrum is a result of the large number, $2J+1$, of magnetic states of the molecule for large rotational quantum numbers, J. The triple minima are characteristic of nuclear spin $\frac{3}{2}$. The spectra were further studied in progressively lower fields. The marked loss of character of the spectra for intermediate fields is explained by extending the analysis of the $\cos^2(\mathbf{I}, \mathbf{J})$ coupling. In the limit of zero field (resonance minima of a type not heretofore observed) a single resonance is observed for each compound at a frequency equal to the frequency difference between the side minima observed in strong fields for the same compound. This is in good agreement with the predictions of Feld and Lamb. These frequencies are 1.22, 1.42, and 0.99 Mc/sec. for NaBr, NaCl, and NaI, respectively. The theory of the behavior of the central minimum as a function of the external field, and the effect of the finite resolution of the apparatus are developed more fully, particularly insofar as they affect the ultimate precision of measurements of nuclear g-factors and nuclear quadrupole interactions. The analysis of the spectra indicates the possibility of still an additional interaction of the form $c\mathbf{I}\cdot\mathbf{J}$, whose average value is 0.05 Mc/sec. This is about 25 times larger than the interaction which would be caused by the magnetic field of a charge of one electron rotating at the internuclear distance of the molecule and with its average angular velocity. This possibility is supported by the need for introducing a term of this nature in the Hamiltonian for LiF in order to explain the observed width of 0.5 Mc/sec. for the F resonance.

I. INTRODUCTION

THE molecular-beam radiofrequency resonance method[1-3] has been extensively used to measure the magnetic moments of a large number of nuclei with precisions ranging from 0.5 to 0.02 percent. With this method, the absorption and stimulated emission spectrum of a molecule in a homogeneous magnetic field is obtained by observing the reduction in beam intensity resulting from the failure of magnetic refocusing for molecules which have made a transition accompanied by a change in the effective component of magnetic moment along the field direction. Analysis of the discrete minima observed in the radiofrequency spectrum of HD and D_2[2,4] has yielded the quadrupole moment of the deuteron and the rotational magnetic moment of the hydrogen molecule. Broadening of the minima of other spectra has been reported by Millman and Kusch[5] for cases of rotational $J \gg 1$, but further investigation was limited by the lack of a statistical theory at the time.

A preliminary report of the investigations of the spectrum of Na^{23} in NaBr, NaCl, and NaI has already been published.[6] This paper gives a

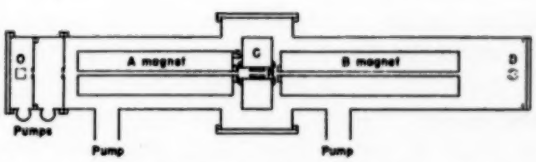

FIG. 1. Block diagram of the molecular-beam apparatus. The A and B magnets supply the inhomogeneous focusing fields, C indicates the homogeneous field, and R the oscillating field. The first chamber on the left, O, is the oven or source chamber, the slit marked S is the collimator, and D indicates the position of the hot-wire detector.

[1] Rabi, Millman, Kusch, and Zacharias, Phys. Rev. **55**, 526 (1939).
[2] Kellogg, Rabi, Ramsey, Jr., and Zacharias, Phys. Rev. **56**, 728 (1939).
[3] J. M. B. Kellogg and S. Millman, Rev. Mod. Phys. **18**, 323 (1946).
[4] Kellogg, Rabi, Ramsey, and Zacharias, Phys. Rev. **57**, 677 (1940).
[5] P. Kusch, S. Millman, and I. I. Rabi, Phys. Rev. **55**, 1176 (1939).
[6] W. A. Nierenberg, N. F. Ramsey, and S. B. Brody, Phys. Rev. **70**, 773 (1946).

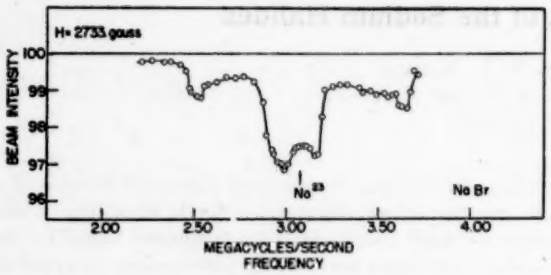

FIG. 2. Radiofrequency spectrum of NaBr. The radiofrequency current is 10 amperes. The arrow indicates the position at which the resonance of the Na^{23} nucleus would appear if there were no orientation—dependent interaction. Note that even at this low field the two side minima and the deeper central minimum are in evidence. At this field the interaction of the Na^{23} nucleus with the external field is larger than the orientation-dependent interaction of the nucleus with the molecule.

more complete account of the work on the spectra. Particularly, the experimental and theoretical arguments justifying the assumption of a sufficiently large electrical quadrupole interaction to cause the observed spectrum are developed.

II. APPARATUS AND METHOD

The apparatus is basically one built in 1938 by Millman and Kusch.[1] Figure 1 is a block diagram of the apparatus. The important dimensions are the lengths of the A and B inhomogeneous magnetic fields, 53 cm and 59 cm, respectively, and the C homogeneous field, 10 cm. The distance from the oven slit to the collimator slit is 68 cm and from the collimator to the detector is 96 cm. The oven slit is 0.025 mm wide, the collimator 0.035 mm wide, and the detector is a tungsten wire 0.025 mm in diameter. The "throwout" power of the apparatus for the sodium halides is 60 percent. It is measured by observing the decrease in beam intensity caused by the deflecting A field when the refocusing B field is zero. The oscillating magnetic field is 10 cm long. A typical oven operating temperature is 1000°K, and for this temperature the average velocity of a molecule of NaCl in the beam is 50,000 cm/sec. This corresponds to a resolution (half-width of a line) of 5000 cycles/sec. The homogeneous field was calibrated to 0.2 percent, using the resonance of Li^7 in LiBr and LiF^7.

The regions in which spectra are observed are approximately 10^6 sec.$^{-1}$ wide. Assuming these spectra arise from broadening of the nuclear resonance in the external field caused by internal interactions, then even at the strongest fields available (corresponding to a Na^{23} nuclear resonant frequency of 10^7 sec.$^{-1}$) the internal interaction is about 10 percent of the magnetic interaction and hence varying the magnetic field would change the coupling by several percent. Therefore, all runs in this research were made with a fixed magnetic field and variable oscillator frequency. The observations were made by switching the oscillator on and off and observing the resultant change in beam intensity.

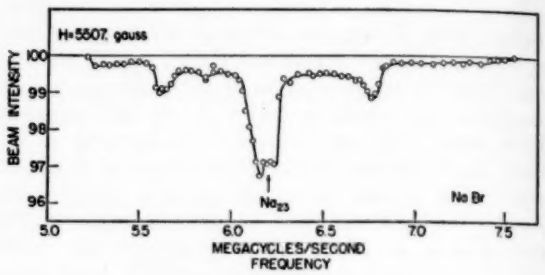

FIG. 3. Radiofrequency spectrum of NaBr at approximately double the field of Fig. 2 and 8-amperes radiofrequency current. The minima are more clearly in evidence. The central minimum in particular is deeper and narrower. Note the appearance of the plateaus on either side of the side minima (compare Fig. 14).

Since the throwout factor is appropriately 0.5 and the resolution width is 5000 sec.$^{-1}$, a spectrum 1 Mc/sec. wide will result in an average reduction in beam intensity of approximately 0.2 percent. In the course of the experiments changes as small as 0.1 percent were measured. Therefore, the oscillator and the detector were isolated to the extent that the oscillator impulse on switching was less than 0.1 percent of the total signal. However, the fluctuations of individual readings, caused by unsteadiness of the beam, were sufficiently large to require the average of four readings for each experimental point.

III. EXPERIMENTAL RESULTS

In an unpublished experiment performed in February, 1939, Kusch and Millman, while investigating the g-factors of Br^{79} and Br^{81}, found a broad and unexplained series of resonances in NaBr. The present experiments result from a further study of this phenomenon.

Figure 2 is the spectrum of NaBr observed at

2733. gausses (approximately the field values used in the previous experiments). The spectrum is essentially the same in detail as that observed by Millman and Kusch, with the principal difference being the use of the variable frequency and fixed field. The chief features of the spectrum are the broad central minimum (of width about 0.35 Mc/sec.), the large total extent of the spectrum (about 1.2 Mc/sec.), and the appearance of other subsidiary minima. As a reference, the frequency at which an uncoupled Na^{23} nucleus ($g=+1.4765 \pm 0.0015$ nuclear magnetons)[7] would show a resonance minimum at the same field, is shown on the figure. It is observed to be roughly in the center of the spectrum. The obvious next step is to observe the same spectrum at approximately double the field strength. Figure 3 shows the results for a field of 5507. gausses. A simplification in the spectrum is discernible. The central minimum is approximately half the width and twice as deep and still shows the same structure which has the appearance of two unresolved

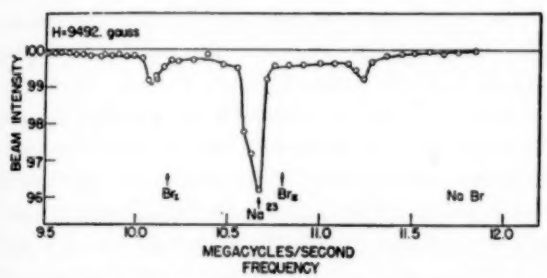

FIG. 4. Radiofrequency spectrum of NaBr at approximately double the field of Fig. 3 and 4-amperes radiofrequency current. There are no features that are different from those observed in Fig. 3, but again the central minimum is deeper and narrower. The additional arrows indicate the resonance positions of the two bromine isotopes that are not observed in this spectrum.

minima. There are two plateaus which terminate in lesser minima at approximately 0.6 Mc/sec. on either side of the central minimum. These subsidiary minima cut off sharply into residual plateaus which are 0.002 deep and which extend for 0.5 Mc/sec. on either side of the spectrum. Finally, Fig. 4 is the spectrum at approximately double the field (9492. gausses) for that of Fig. 3, and it is clear that aside from the central minimum becoming twice as deep and one-half again as narrow, there is no significant difference between this spectrum and that of Fig. 3. Apparently, the low frequency minimum of the pair composing the central minimum in Figs. 2 and 3 has been submerged in Fig. 4. In order to study the detail of the central minimum (For the sake of completeness, a run (Fig. 5) was taken at one-half the field value (1367. gausses) of Fig. 2. The complete deterioration of the pattern is clear. There is a mass of structure that shows very little characteristic feature.), its spectrum was repeated at lower radiofrequency current and correspondingly smaller intervals. Figure 6 is the curve. The general features are the same. In particular, the upper frequency side shows a very sharp cut-off.

These first results offer some immediate conclusions. Inasmuch as the average frequency of the observed spectrum is proportional to the field, the spectrum must be associated with some effective magnetic moment. That this moment is that of Na^{23} is clear from the close agreement of the resonant frequency of the Na^{23} nucleus and the position of the sharp central minimum in Fig. 4. They agree to 0.2 percent, which is within the experimental error. The resonant frequencies for Br^{79} and Br^{81} are also shown in Fig. 4. No evidence of these resonances exists in NaBr. This is undoubtedly due to the low intensity of the effect for bromine.[8] The frequencies of the side minima are not proportional to the field but remain at a constant frequency difference from the central minimum. This implies some orientation-dependent interaction

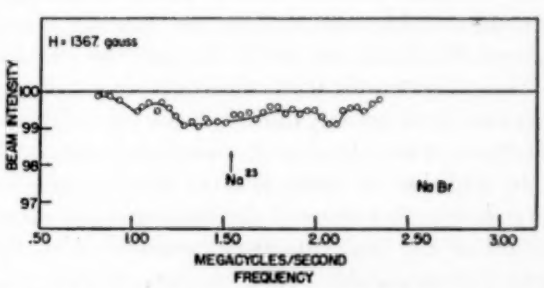

FIG. 5. Radiofrequency spectrum of NaBr at approximately one-half the field of Fig. 2. At this field the orientation-dependent interaction of the Na^{23} nucleus with the external field is approximately equal to its orientation-dependent interaction with the molecule. Note the complete degeneracy of the spectrum (compare Figs. 2, 3, and 4).

[7] S. Millman and P. Kusch, Phys. Rev. **60**, 91 (1941).

[8] S. B. Brody, W. A. Nierenberg, and N. F. Ramsey, Phys. Rev. **72**, 258 (1947).

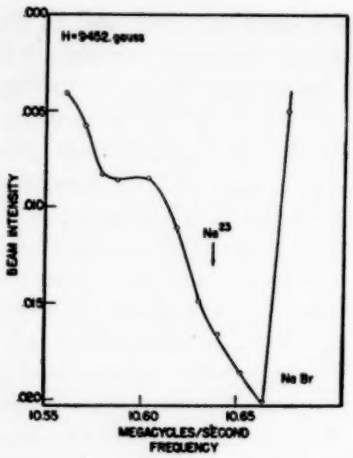

FIG. 6. Detail of the central minimum of the radiofrequency spectrum of NaBr at greater resolution. The field is approximately the same as for Fig. 4 but the radiofrequency current is one ampere, corresponding to the best resolution of the apparatus for this g-factor. Note the sharp asymmetry. The maximum reduction in intensity is one-half that for Fig. 4. This is in good agreement with the theory which predicts a variation of the maximum reduction in intensity proportional to the square root of the radiofrequency current in this region.

between the nucleus and the rest of the molecule in addition to the interaction between the nucleus and the external field. If this be so, it can be expected that NaCl and NaI would show similar spectra under approximately the same conditions. Figures 7 and 8 are the spectra of NaCl and NaI at fields corresponding to NaBr in Fig. 4. The general features of the spectra are the same. The frequency difference between the side minima of NaBr is greater than that for NaI and less than that for NaCl. The low plateaus beyond the side minima were not directly investigated for NaCl and NaBr because the effect is so close to the noise level. However, in a separate experiment at greater radiofrequency current the existence of the plateaus was confirmed for NaCl.

In addition to these spectra which were observed at such values of the field that the interaction of the Na^{23} magnetic moment with the field is comparable with, or larger than, the internal interaction, a type of spectrum new to molecular-beam research was undertaken. Observations were made at fields such that the nuclear interaction with the field is small compared to the orientation dependent interaction with the molecule. The most important case occurs when the field is nearly zero. (The demagnetization procedure is such that the field is 4 gausses or less.) There is some *a priori* question of the feasibility of such experiments because the absence of a homogeneous field allows non-adiabatic transitions of the molecules undergoing the abrupt change in field on passing from the focusing field to the low field region and on to the refocusing field. The fact that a spectrum is observed is sufficient proof that all the molecules do not undergo non-adiabatic transitions, and the remainder are responsible for the observed spectra. Figures 9–11 are the spectra of NaBr, NaI, and NaCl, respectively, at fields that are less than 4 gausses. One minimum is observed for each substance, and the center of each minimum corresponds very closely in frequency with the difference in frequency between the side minima of the corresponding strong-field spectra. The three spectra agree in general detail. They are broad (0.15–0.20 Mc/sec. in half-width) and they are asymmetrical. The upper frequency side rises more sharply than the lower frequency side.

While it is clear that the zero-field spectra will be of primary importance in the discussion, it is instructive to examine the behavior of the pattern in weak fields. Figures 12 and 13 are the spectra for NaBr at fields of 139 and 282 gausses, respectively. At these low fields there is considerable uncertainty in values of the field (~5 percent). Experimentally these spectra are the connection between the zero-field spectra and the intermediate- and strong-field spectra of NaBr. Figures 2–5, 9, 12, and 13 show the radiofrequency spectrum associated with Na^{23} in NaBr over a wide range of magnetic fields. Without a suitable theory of the interaction responsible for the zero-field minimum, it is

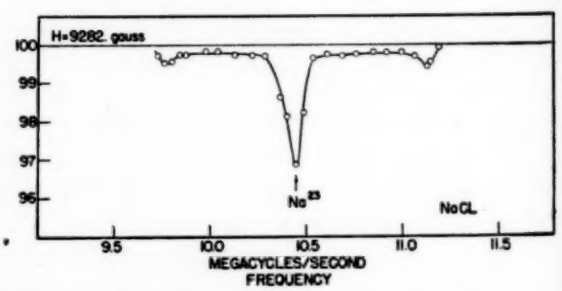

FIG. 7. Radiofrequency spectrum of NaCl at the strongest field available and radiofrequency current at 10 amperes (compare Fig. 4).

difficult to discuss Figs. 12 and 13 in any general way. However, it can be observed that the spectrum is broadened roughly proportionally to the field, and, in particular, the stronger field shows three resolved minima. Further discussion of the weak-field spectra will be given in Section VI.

IV. GENERAL DISCUSSION

One problem of this paper is to find the correct interaction between the nucleus in question and the remainder of the molecule to explain the observed spectra. The usual Hamiltonian for the orientation-dependent nuclear interactions assumed for a rotating diatomic molecules in a $^1\Sigma$ state[2,4] is

$$\begin{aligned}\mathcal{H}=&-g_1\mu_N\mathbf{I}_1\cdot\mathbf{H}-g_2\mu_N\mathbf{I}_2\cdot\mathbf{H}-g_J\mu_N\mathbf{J}\cdot\mathbf{H}\\&-g_1\mu_N H_1'\mathbf{I}_1\cdot\mathbf{J}-g_2\mu_N H_2'\mathbf{I}_2\cdot\mathbf{J}\\&+(g_1g_2\mu_N^2/r_J^3)[\mathbf{I}_1\cdot\mathbf{I}_2-3(\mathbf{I}_1\cdot\mathbf{r}_J)(\mathbf{I}_2\cdot\mathbf{r}_J)/r_J^2]\\&+\sum_{i=1,2}e^2q_iQ_i/2J(2J-1)I_i(2I_i-1)\\&\times[3(\mathbf{I}_i\cdot\mathbf{J})^2+\tfrac{3}{2}(\mathbf{I}_i\cdot\mathbf{J})\\&\qquad-I_i(I_i+1)J(J+1)].\quad(1)\end{aligned}$$

μ_N is the nuclear magneton, H is the external magnetic field, J the rotational angular momentum, I is the nuclear spin and g the corresponding g-factor. The quantity r_J is the internuclear distance, Q the quadrupole moment of the nucleus defined[4] as $eQ=\int(3z^2-r_1^2)de$, and q is defined by $eq=\int(3\cos^2\theta-1)/r_e^3de$, where the integral is carried over all charges in the molecule outside of a small sphere containing the nucleus for the rotational state $J_z=J$. H' is the magnetic field at the position of the nucleus caused by the molecular rotation. The first two terms of the Hamiltonian represent the interaction of the nuclear magnetic moments with the external field. This interaction corresponds to a frequency of 0.76 Mc/sec. for $g_i=1$ in an external field of 1000 gausses. The third term is the interaction of the magnetic moment of the rotation of the molecule with the external field. This term would have an estimated $g_J=0.1$. However, in strong fields the transitions observed correspond to $\Delta m_J=0$, and therefore this term contributes nothing to the spectrum. The fourth and fifth terms are the interactions of the nuclear moments with the field at the nuclei caused by the rotation of the molecule. This field can be estimated by considering the other nucleus and surrounding electrons as one electron charge rotating about the nucleus in question and causing an estimated frequency difference of $4g_I\mu_N^2/hr_J^3$ for an average value $J=40$. If $r_J=2.5\times10^{-8}$ cm (a good assumption for most diatomic molecules), then the corresponding frequency is 1000 cycles/sec. As discussed in Section VI, this estimate of the $\mathbf{I}\cdot\mathbf{J}$ interaction is too naive and must be replaced by more detailed consideration of the rotation. Similarly, the sixth term, the dipole-dipole interaction of the two nuclei, is of the same order. Finally, the

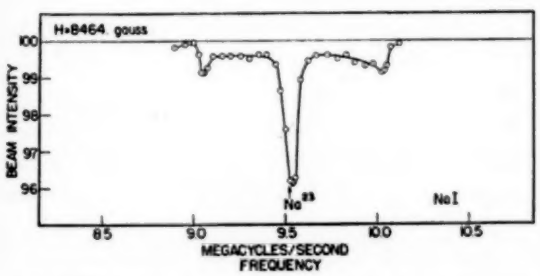

FIG. 8. Radiofrequency spectrum of NaI at the strongest field available and radiofrequency current at 10 amperes (compare Fig. 4).

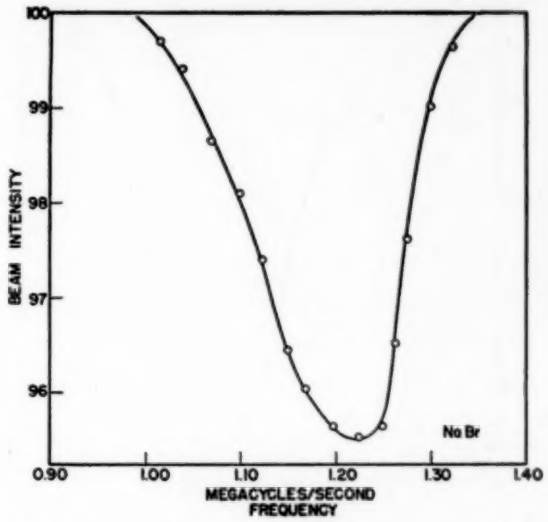

FIG. 9. "Zero"-field radiofrequency spectrum of NaBr. The radiofrequency current is 3 amperes. This spectrum is essentially due to the interaction of the nucleus with the molecule only. Note that the position of the minimum is almost exactly at a frequency equal to the difference between frequencies of the side minima of Fig. 4. The width is much larger than the natural width.

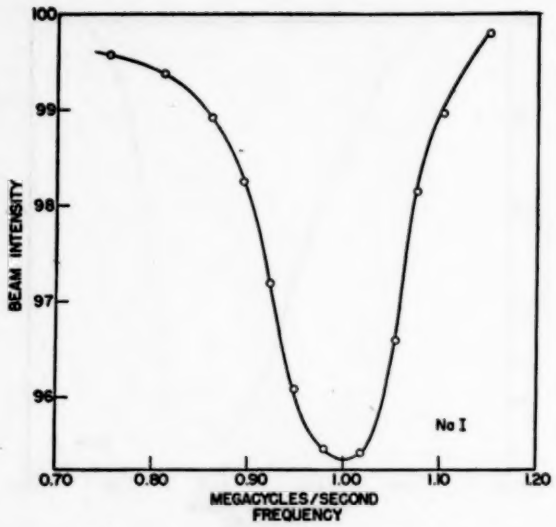

FIG. 10. "Zero"-field radiofrequency spectrum of NaI at 3-amperes radiofrequency current (compare Figs. 9 and 8).

last two terms represent the interaction of the quadrupole moments of the nuclei with the gradient of the electric field. This interaction is of the order of e^2Q/hr_J^3. If the quadrupole moment be taken as 10^{-25} cm^2, then for $r_J=2.5\times10^{-8}$ cm, the corresponding frequency is 0.23 Mc/sec.

In the HD and D_2 molecular-beam radiofrequency experiments,[2,4] all the minima observed were interpreted using the Hamiltonian of Eq. (1). The relative sizes of the interactions differ from the above estimates because of the small internuclear distance (10^{-8} cm) for D_2 and the small quadrupole moment of the deuteron (2.7×10^{-27} cm^2). The spectrum consisted of a series of discrete minima because the source was at liquid nitrogen temperature and therefore only the lowest rotational state contributed appreciably. The spectra reported here were observed under completely different experimental conditions. The dipole-dipole and the nuclear-rotation interactions are not observable because they are considerably less than the resolution of the apparatus (5000 sec.$^{-1}$). Therefore, these terms in the Hamiltonian may be neglected. For the typical sodium halide, the beam-source (oven) temperature is such that there are effectively 100 rotational states excited with the corresponding $2J+1$ values of J_z for each state. It is clear then that the strong-field spectrum will not, in general, be a series of discrete peaks whose width is the resolution width, but, instead, will be a continuum whose extent in frequency will be measured by the largest internal interaction. Assuming the estimates made above to be valid, a sufficiently large quadrupole interaction of Na^{23} in the sodium halides will be assumed.

A statistical theory of the effect of a nuclear-electrical quadrupole moment in the molecular-beam radiofrequency spectrum, including the contribution to the Hamiltonian of the rotational magnetic moment has been developed by Feld and Lamb.[9] Figure 14 is a copy of their Fig. 5, redrawn to show the spectrum as a reduction in beam intensity. The assumptions and approximations that were made in arriving at Fig. 14 are the following: (1) The nuclear spine in $\frac{3}{2}$, (2) The rotational angular momentum $J\gg1$, (3) H is large, so that $\mu_N g_i H\gg e^2qQ/4$. (4) The central minimum is drawn in arbitrary fashion to correspond to the resolution width of the apparatus. (This minimum, corresponding to a nuclear reorientation $m_I=\frac{1}{2}\leftrightarrow m_I=-\frac{1}{2}$, shows no quadrupole effect to the first order in the perturbation calculation.) (5) The spectrum is calculated as the product of the density of transitions in energy and the transition probability. The actual depths of the minima are determined by the resolution of the apparatus. This approximation is very

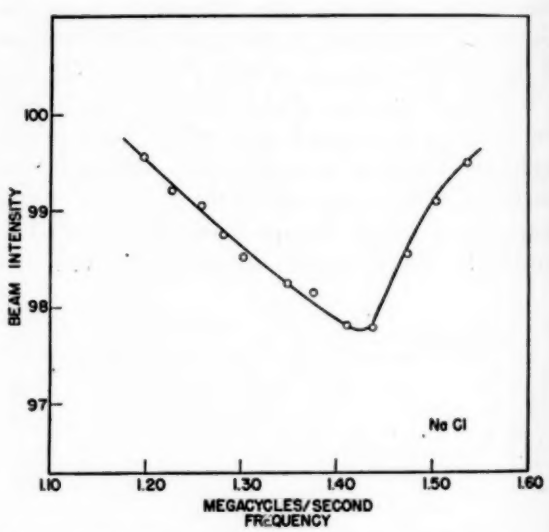

FIG. 11. "Zero"-field radiofrequency spectrum of NaCl at 3 amperes (compare Figs. 9 and 7).

[9] B. T. Feld and W. E. Lamb, Jr., Phys. Rev. 67, 15 (1945).

good. (6) The other nucleus has spin zero. It is assumed that the results for the strong-field spectra of the sodium halides will be unaffected by the spin of the halogens concerned. In the case of homonuclear molecules such as Na_2, there is a definite effect of the spins of both nuclei which has been calculated by H. M. Foley.[10]

The spectra of Figs. 4, 7, and 8, were observed under conditions suitable for comparison with Fig. 14 (the largest fields available). The value of $e^2qQ/4\mu_N gH$ is approximately 0.05 for each. The general agreement with the theory is very good. There are three minima with the central minimum corresponding to the Larmor frequency of the Na nucleus. The side minima cut off relatively sharply into the side plateaus which the theory also predicts. When these experiments were performed the g-values of Br^{79} and Br^{81} were not known. They have since been measured,[8] and their spectra do fall within the spectrum of Fig. 4. (A careful search for these minima confirmed their absence and the cause is undoubtedly lack of intensity.) The Cl^{35} and Cl^{37} resonances are far removed from the Na resonance and the I^{127} g-factor is still unknown. Figure 14 shows that $e^2qQ/2h$ can be estimated from the actual spectrum as the frequency difference of the side minima.

In the absence of an external field, and assuming a negligible contribution from the halide nucleus in first approximation, the Hamiltonian of Eq. (1) will consist of one term, the quadrupole interaction of the Na nucleus. The energy levels have been computed by Feld and Lamb,[9] and the only non-vanishing transition is at a frequency $e^2qQ/2h$. The zero-field spectra were observed at these frequencies (Figs. 9, 10, 11).

Table I gives the comparison of $e^2qQ/2h$ obtained from the strong-field and the zero-field spectra. They agree to better than 5 percent. However, the differences are systematic, the weak-field values being the larger, and the differences are beyond experimental error. This difference is not yet explained. An estimate of $e^2qQ/2h=0.13$ Mc/sec. (corrected for resolution) has been made from the strong-field spectrum of Na_2^{23} reported by Millman and Kusch. In this case, the theory of Lamb and Feld does not apply because of spin degeneracy. Foley[10] has developed the correct theory for homonuclear diatomic molecules, which is the basis of the above estimate.

[10] H. M. Foley, Phys. Rev. 71, 747 (1947).

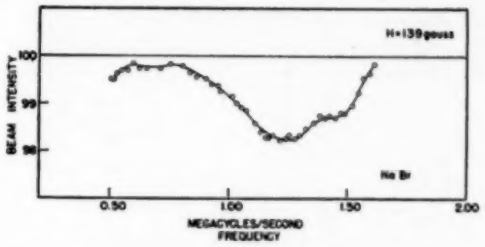

FIG. 12. Radiofrequency spectrum of NaBr in weak fields. The interaction of the Na^{23} nucleus with the external field is less than the orientation-dependent interaction of the nucleus with the molecule. Note that the spectrum is broadened but still situated about the central frequency of Fig. 9.

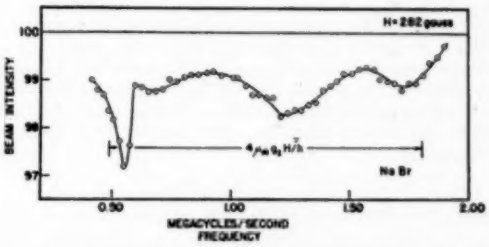

FIG. 13. Radiofrequency spectrum of NaBr in a field approximately double that of Fig. 12. The spectrum is broadened approximately proportionately to the field and still is approximately centered about the central frequency of Fig. 9. Three minima are observed in agreement with theory. $4\mu_N g_I H/h$ is calculated equal to 1.3 Mc/sec., and compared with the separation of the outer minima. Again there is approximate agreement with experiment.

Feld and Lamb also discuss the Zeeman broadening of the zero-field line. The theory predicts a broadening of the line proportional to $\mu_N g_I H$. It also predicts a possible resolution into three minima. Figures 12 and 13 are the actual spectra for weak fields. The broadening of the zero-field lines is clearly proportional to the fields, and for the stronger field (Fig. 13) three minima are actually observed. The frequency difference between the three extreme peaks is less than the predicted value of $4\mu_N g_I H/h$ by 10 percent. The discrepancy is due in part to poor field calibration at low fields and in part to the fact that at this value of the field the magnetic interaction is not small compared to the internal interaction, and hence the first-order theory cannot be expected to give very accurate results.

The conclusion to be drawn from this general discussion is that the radiofrequency spectrum

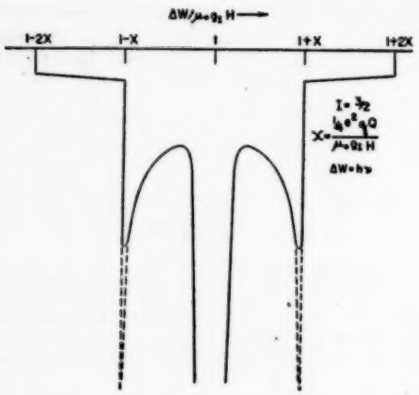

FIG. 14. This is a copy of Fig. 5 from Feld and Lamb's paper.[9] This is the predicted radiofrequency spectrum of a nucleus of spin $\frac{3}{2}$ in a diatomic molecule, where an electrical-quadrupole interaction with the molecule is assumed but is very small compared to the interaction of the nucleus with the external magnetic field. The ordinate is proportional to the beam intensity, the abscissa is a dimensionless frequency.

of the Na halides is to be explained in gross detail on the assumption of a sufficiently large nuclear-electric quadrupole interaction of about 1 Mc/sec. The succeeding sections of this paper are devoted to an analysis of the finer details to ascertain the limits of application of the theory and the completeness of the Hamiltonian of Eq. (1). The width of the central minimum in strong fields as a function of the field is explained on the basis of a quadrupole interaction. The effect of the finite resolution of the apparatus and the finiteness of J are introduced into the theory and compared with observation. These are found to be insufficient to explain all the detail observed, and a term $-c\mathbf{I}\cdot\mathbf{J}$ is added to the Hamiltonian to explain this insufficiency.

V. ANALYSIS OF HIGH FIELD RESULTS

The frequency differences of a nucleus in a strong magnetic field are, from the Hamiltonian of Eq. (1), including only the first and last terms for one nucleus of spin $\frac{3}{2}$, to second order in x_0,

$$\bar{\nu}(\tfrac{3}{2},\tfrac{1}{2})/\nu_I=1-x_0[1-3(1-1/J)z^2]+6x_0^2z^2(1-z^2). \quad (2a)$$

$$\bar{\nu}(\tfrac{1}{2},-\tfrac{1}{2})/\nu_I=1-\tfrac{3}{4}x_0^2[(1-z^2)(9z^2-1)]-(3x_0^2/2J)(9z^4-5z^2), \quad (2b)$$

$$\bar{\nu}(-\tfrac{1}{2},-\tfrac{3}{2})/\nu_I=1+x_0[1-3(1-1/J)z^2]+6x_0^2z^2(1-z^2). \quad (2c)$$

The matrix elements of the Hamiltonian giving rise to these frequency differences are explicitly calculated by Kellogg, Rabi, Ramsey, and Zacharias.[4] The expressions for the transition frequencies are expanded to the first term in $1/J$. $\bar{\nu}(m_I, m_I-1)$ is the frequency observed in the transition $m_I-1\rightarrow m_I$. ν_I is the Larmor frequency $\mu_N g_I H/h$; z is the cosine of the angle between J and H (J large) or $z=m_J/J$; $x_0=e^2q'Q/4\mu_N g_I H$; $q=-2Jq'/2J+3$ and q' is independent[11] of J. For J large, $q'=-q$. These equations are similar to those derived by Feld and Lamb. The only difference is the expansion to the first power in $1/J$. The $1/J$ terms are included only for the leading term in the perturbation series with respect to x_0. Figure 14 was calculated from these equations neglecting second-order terms in x_0 and the terms in $1/J$. The quantity actually plotted was the product of the density of transitions $dz/d\bar{\nu}$ and the transition probability for small perturbations of the oscillating field. In the experiments reported here the oscillating field is not a small perturbation, since a large fraction of the molecules capable of undergoing transitions actually do so, although all are not observable because of lack of perfect defocusing, but the transition probabilities are independent of z in strong field and hence the complete spectrum will retain its symmetry although the strengths of the various minima will differ. This is not true for the weak-field experiments and therefore the spectrum in this case is considerably less than ideal.

The central minimum of Figs. 3–5 corresponds to the transition $m_I=\frac{1}{2}\leftrightarrow-\frac{1}{2}$ because the term in x_0 vanishes for that transition. The widths of the observed central minimum at different fields are due to the effect of the term in x_0^2. Figure

TABLE I. Comparison of weak-field and strong-field interactions.

Substance	External magnetic field (gausses)	$e^2qQ/2h$ (Mc/sec.)
NaBr	9490	1.17
NaBr	4	1.22
NaCl	9282	1.35
NaCl	4	1.42
NaI	8494	0.97
NaI	4	0.99

[11] A. Nordsieck, Phys. Rev. **58**, 310 (1940).

15a is the theoretical plot of $\bar{\nu}/\nu_I$ *versus* z, neglecting terms of order $1/J$. There are two extremes which define the limits of $\bar{\nu}/\nu_I$. Here z is a multi-valued function of $\bar{\nu}/\nu_I$, and therefore the density of transitions is computed as $|dz_1/d\bar{\nu}|+|dz_2/d\bar{\nu}|$ *versus* z. Figure 15b is the plot of the density of transition, omitting the $1/J$ terms. The two extremes are represented here as two peaks separated in frequency by $25x_0^2\nu_I/12$. The corresponding minima were actually observed in Figs. 3 and 4. The lower frequency minimum is the more prominent, judging from the area underneath the associated peak in Fig. 15b. The observed widths are also in good agreement with the theory. The quantity $2x_0\nu_I$ is the separation of the subsidiary minima. Using the values of x_0 from the curves at different fields, we construct Table II, which compares the widths of the central minima for various fields *versus* $25x_0^2\nu_I/12$. The width of the minimum for 9500 gausses is taken from Fig. 6 rather than from Fig. 4 because of the increased broadening by the radiofrequency current. The agreement is again good within the chief approximation still to be considered; namely, the effect of the finite resolving power of the apparatus. This is responsible for the systematic deviations in Table II. However, aside from this difference, the widths of the central minima are inversely proportional to the field.

This theory of the structure of the central minimum is important when considered from the viewpoint of the precision measurement of nuclear magnetic moments. The quadrupole moment introduces asymmetries which are proportional to the square of the ratio of the quadrupole and the magnetic interactions. If the center of the minimum is used, a fractional error proportional to x_0^2 is introduced in the measurement of the nuclear g for half-integral

TABLE II. Comparison of the half-widths of the central minimum with theory for NaBr.

Field (gausses)	x_0	$(25/12)x_0^2\nu_I$ (Mc/sec.)	Measured half-width Mc/sec.
9452	0.055	0.07	0.08
5507	0.094	0.11	0.16
2733	0.187	0.22	0.31

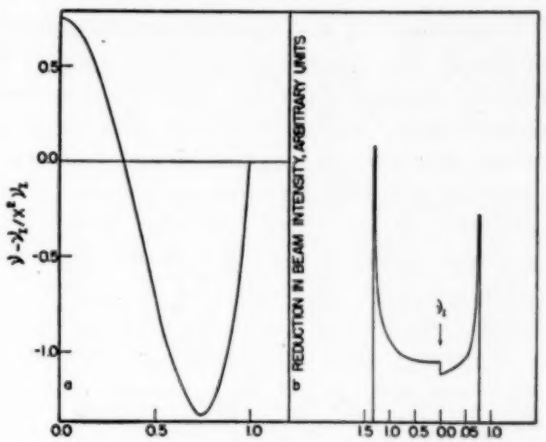

FIG. 15. Theoretical shape of the central minimum in strong fields. ν is the transition frequency between levels, and ν_I is the Larmor frequency for the nucleus. Figure 15a is, therefore, a plot of the reduced frequency difference $\nu/\nu_I/x^2\nu_I$ *versus* z, the cosine of the angle between **J** and **H** for $J\gg1$. Using this function, the line shape, uncorrected for finite resolution, is plotted in 15b as a reduction in beam intensity *versus* the reduced frequency difference. Note that the two peaks correspond to the two stationary points of Fig. 15a (compare Figs. 2 and 3).

spin. If the spin is $\frac{3}{2}$, this yields an underestimate $7x_0^2/24$. The error that would be made in measurement of the value of g for Na^{23} from Fig. 4 is 0.1 percent. In Figs. 2–4 and 6 the position of the Na^{23} resonance frequency is indicated, and its relative position is correct within the precision of the measurement of the field. It should be noted that these asymmetries are proportional to the square of the perturbation parameter and therefore independent of the sign of the quadrupole moment.

At still lower values of the field, Fig. 5 (where $x_0=0.4$), the central minimum has practically disappeared. The entire structure becomes complicated. In fact, for $x=0.5$, additional minima are predicted. Despite the increasing complexity of the spectrum, the over-all width remains the same. This is due to the vanishing of the second-order terms for $z=0$ in Eqs. (2a) and (2c). The positions of the side minima are therefore unaffected by the second-order perturbation term. This has two effects: the width of the spectrum remains constant over a very wide range of x_0 (experimentally, down to 0.5 where the weak-field representation is the more appropriate) and it prevents the determination of the sign of the quadrupole interaction from this statistical data.

Comparison of the experiments with theory disclosed one discrepancy. The values for $e^2qQ/2h$ obtained from the zero-field data were approximately 5 percent greater than those obtained from the strong-field data. A possible explanation of this difference is the effect of the resolution of the apparatus. The theory until now has neglected the effect of the apparatus resolution, with the result that the minima observed experimentally in strong fields are infinite in the theory. The finite resolving power of the apparatus will cut off these minima and shift their positions. The shape of the resonance curve for a single level is given by[12]

$$P_{\frac{1}{2},-\frac{1}{2}}=[\Delta^2/(1-q)^2+\Delta^2]\times\sin^2\pi ft[(1-q)^2+\Delta^2]^{\frac{1}{2}}. \quad (3)$$

$\Delta=H_1/2H_0$, one-half the ratio of the amplitudes of the oscillating and static fields, q is the ratio of the applied to the resonant frequency, f is the applied frequency, and t is the time interval the system has been in the magnetic field. The Rabi formula has the usual resonance denominator, but, since the resolution widths are different for different molecular velocities and the narrowest structure to be interpreted is ten times this average width, it is sufficiently representative to choose this function as

$$F(\bar{\nu},\nu)=K_1K_2, \quad \nu-\Delta\bar{\nu}\leqslant\bar{\nu}\leqslant\nu+\Delta\bar{\nu}, \quad (4)$$

and $F(\bar{\nu},\nu)=0$ for all other values of $\bar{\nu}$. $\Delta\bar{\nu}$ is half the resolution width and is to be estimated in a particular case from Eq. (3). K_1 is a factor introduced to compensate for the lack of complete defocusing of the apparatus. K_2 is introduced to compensate for the different final magnetic states of the nucleus caused by the spread in times t that (Eq. (3)) the various molecules of the Maxwellian beam spend in the oscillating field. Both K_1 and K_2 are less than unity. The method of calculation of the line shape for the transitions $m_I=\frac{3}{2}\leftrightarrow\frac{1}{2}$ and $m_I=\frac{3}{2}\leftrightarrow\frac{1}{2}$, including the effect of the resolution and the term in $1/J$, is outlined in Appendix I (Eqs. (14), (15), and (16)). The result is

$$R(\nu)=\frac{K_1K_2}{3(3x_0\nu_I)^{\frac{1}{2}}}[\nu+\Delta\bar{\nu}-(1-x_0)\nu_I]^{\frac{1}{2}}\times(1+a^{\frac{1}{2}}\sqrt{\pi}),$$
$$(1-x_0)\nu_I-\Delta\bar{\nu}\leqslant\nu\leqslant(1-x_0)\nu_I+\Delta\bar{\nu}, \quad (5a)$$
$$R(\nu)=\frac{K_1K_2}{3(3x_0\nu_I)^{\frac{1}{2}}}\{[\nu+\Delta\bar{\nu}-(1-x_0)\nu_I]^{\frac{1}{2}}-[\nu-\Delta\bar{\nu}-(1-x_0)\nu_I]^{\frac{1}{2}}\}(1+a^{\frac{1}{2}}\sqrt{\pi}),$$
$$\nu\geqslant(1-x_0)\nu_I+\Delta\bar{\nu}.$$

$$R(\nu)=\frac{K_1K_2}{3(3x_0\nu_I)^{\frac{1}{2}}}[(1+x_0)\nu_I-\nu+\Delta\bar{\nu}]^{\frac{1}{2}}(1+a^{\frac{1}{2}}\sqrt{\pi}),$$
$$(1+x_0)\nu_I-\Delta\bar{\nu}\leqslant\nu\leqslant(1+x_0)\nu_I+\Delta\bar{\nu}, \quad (5b)$$
$$R(\nu)=\frac{K_1K_2}{3(3x_0\nu_I)^{\frac{1}{2}}}\{[(1+x_0)\nu_I-\nu+\Delta\bar{\nu}]^{\frac{1}{2}}-[(1+x_0)\nu_I-\nu-\Delta\bar{\nu}]^{\frac{1}{2}}\}(1+a^{\frac{1}{2}}\sqrt{\pi}),$$
$$(1+x_0)\nu_I-\Delta\bar{\nu}\geqslant\nu.$$

Equation (5a) is the spectrum of the transition $\frac{3}{2}\leftrightarrow\frac{1}{2}$. Equation (5b) is the spectrum of the transition $-\frac{3}{2}\leftrightarrow-\frac{1}{2}$. $R(\nu)$ is the fractional reduction in beam intensity or depth of resonance minima with respect to the total beam and

$$a^2=h^2/8\pi^2IkT=\pi/4J^2,$$

where I is the moment of inertia of the molecule. The value of a is about 0.02. Examination of Eq. (5) shows that J finite but large (J affects Eq. (5) through a which is of the order of $1/J$) does not affect the position of the minima but increases the over-all reduction in beam intensity by ~ 2 percent. The maximum depth of resonance minima becomes $\frac{1}{3}K_1K_2[2\Delta\bar{\nu}/3x_0\nu_I]^{\frac{1}{2}}$ for both minima and occurs at frequencies $(1+x_0)\nu_I-\Delta\bar{\nu}$ and $(1-x_0)\nu_I+\Delta\bar{\nu}$. This is a difference between the minima of $2x_0\nu_I-2\Delta\bar{\nu}$. In the experiments at the strongest fields $2\Delta\bar{\nu}=0.02$ Mc/sec. This is in the right direction and accounts for approximately one-third of the discrepancy. The remainder is still beyond the experimental error (0.015 Mc/sec.). The experimental arrangement is such that $K_1=0.6$ and $K_2=0.5$. When applied to the experiment in the strongest field, this yields 0.011 for the fractional reduction in intensity at the side minima of NaBr, which compares

[12] I. I. Rabi, Phys. Rev. 51, 652 (1937).

well within the approximations to the observed value 0.012 if the value of $2\Delta\bar{\nu}$ is taken as 0.02 Mc/sec. The corresponding calculation for the central minimum is more tedious principally because of the averaging over J. However, it is not necessary to complete it for the points of major importance. Examination of Eq. (2b) shows that in the neighborhood of $z=0$ the term in $1/J$ vanishes $\sim z^2$, and therefore this term will have a negligible effect in broadening and lowering the higher frequency component of the central minimum. This minimum will be equal to $\frac{1}{3}K_1K_2[4\Delta\bar{\nu}/15x_0^2\nu_I]^{\frac{1}{2}}$ after averaging over the resolution (Appendix I). This gives a value of 0.03 which compares favorably with that of 0.04 observed (Fig. 4).

The reason for the experimental disappearance of the lower frequency component of the central minimum at the field of 9000 gausses is obscure. In principle the term in $1/J$ in Eq. (2b) could cause the necessary broadening of this minimum. However, the contribution of this term to the Hamiltonian vanishes at $z=(5/9)^{\frac{1}{2}}$, the value corresponding to this minimum. At this point in the discussion it is convenient to introduce the possibility of adding an additional term to the Hamiltonian to explain this broadening. Stronger arguments in favor of this additional interaction will be discussed later. For the present, it will only be noted that this interaction must satisfy the requirement that it submerge the lower frequency component of the central minimum at sufficiently strong fields. The simple operator $-c\mathbf{I}\cdot\mathbf{J}$ satisfies this condition. If this term be added to the Hamiltonian, then in strong fields the equation equivalent to (2b) becomes (Appendix II, Eq. (20))

$$\bar{\nu}(\tfrac{1}{2},-\tfrac{1}{2})/\nu_I=1-\tfrac{3}{4}x_0^2[(1-z^2)(9z^2-1)] +yz+\tfrac{1}{2}y^2(1-z^2), \quad (6)$$

where, for convenience, the dimensionless parameter $y=cJ/\mu_N g_I H$ is introduced. The calculation is to the second order in x_0 and y. To fix ideas, at a field $H=10{,}000$ gausses, $x_0\cong 0.05$, and y will be assumed $\cong 0.005$, which is equivalent to an average $(J=40)$ $cJ/h=0.05$ Mc/sec. If $y=0$, Eq. (6) reduces to Eq. (2) (neglecting terms of order $1/J$). Just as before, values of $\bar{\nu}$ are sought for which $d\bar{\nu}/dz$ vanishes. The result, to sufficient approximation, is

$$\bar{\nu}/\nu_I=1+3x_0^2/4+y^2/30x_0^2. \quad (7a)$$

$$\bar{\nu}/\nu_I=1-4x_0^2/3-y^2/30x_0^2+(5/9)^{\frac{1}{2}}y. \quad (7b)$$
$$\bar{\nu}/\nu_I=1-4x_0^2/3-y^2/30x_0^2-(5/9)^{\frac{1}{2}}y.$$

If $y=0$, there are but two distinct values, corresponding to the two minima in Fig. 15. The effect of the additional interaction is to shift the position of the minima in frequency by $(y^2/30x_0^2)\nu_I$ and to split the lower frequency minimum into two minima whose separation is $2(5/9)^{\frac{1}{2}}y\nu_I$. $(y^2/30x_0^2)\nu_I\cong 3000$ sec.$^{-1}$ which is less than the resolution width of the apparatus and therefore not observable. Hence the higher frequency minimum will remain sharp. The lower frequency minimum will be broadened by an amount equal to the separation of its two components for an average value of J. For the values of the interaction cited, the corresponding width is 0.07 Mc/sec. or of the same magnitude as the x_0^2 broadening. The splitting, as such, is not observable, because the position of the lines are still to be averaged over J. The net result of the $\mathbf{I}\cdot\mathbf{J}$ interaction is to submerge the lower frequency minimum at a field $H=10{,}000$ gausses. At appreciably smaller values of the field (5000 gausses), the relative effect of this term on the lower component disappears. The addition of this term will have a negligible effect on the spectrum corresponding to the transitions $\pm\frac{3}{2}\leftrightarrow\pm\frac{1}{2}$, because it is small compared to the first order terms in x_0.

VI. ANALYSIS OF WEAK-FIELD RESULTS

In a weak field the chief unexplained feature is the anomalous width of the lines ($\sim$0.15 Mc/sec.). The Hamiltonian for the quadrupole interaction in zero fields is (from Eq. (1))

$$\mathcal{H}=\frac{e^2qQ}{2J(2J-1)I(2I-1)}\{3(\mathbf{I}\cdot\mathbf{J})^2 +\tfrac{3}{2}(\mathbf{I}\cdot\mathbf{J})-I(I+1)J(J+1)\}, \quad (8a)$$

and the energy levels are given by[13]

$$W_F=\frac{e^2qQ}{2J(2J-1)I(2I-1)}\{\tfrac{3}{4}K^2+\tfrac{3}{4}K -I(I+1)J(J+1)\}, \quad (8b)$$

[13] H. B. G. Casimir, *On the Interaction Between Atomic Nuclei and Electrons* (Teyler's Tweede Genootshap., 1936).

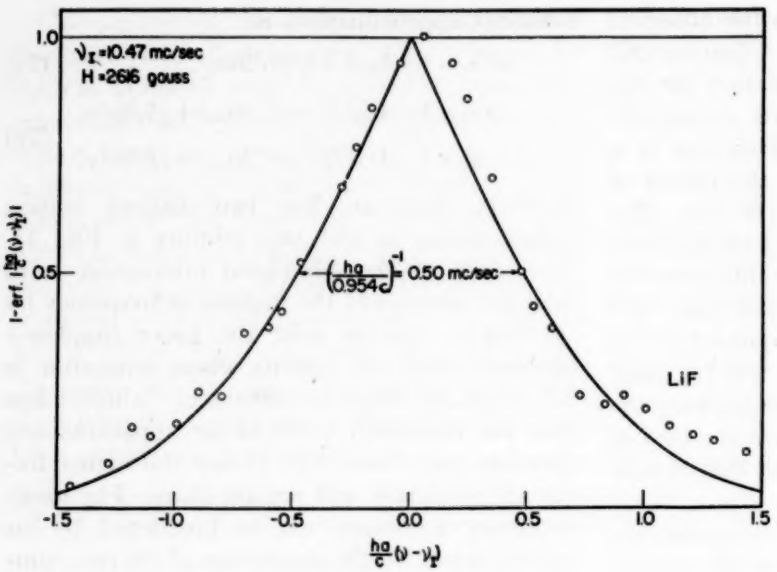

FIG. 16. Comparison of theory and experiment for the radio-frequency spectrum of LiF. The experimental points are plotted as reduction in beam intensity (normalized to unity for the maximum) *versus* the difference in frequency from the Larmor frequency for fluorine normalized by the factor $ha/c=1.91\times10^6$ sec. The solid line is the calculated line shape for a total orientation-dependent Hamiltonian, equal to $-\mu_N g_I \mathbf{I}\cdot\mathbf{H}-c\mathbf{I}\cdot\mathbf{J}$.

where

$$K=F(F+1)-I(I+I)-J(J+1)$$

and $F=J+i$ and $i=I,\ I-1,\ \cdots,\ -I$. For J infinite and $I=\frac{3}{2}$ the energy differences are given by

$$\begin{aligned} W_{3/2}-W_{\frac{1}{2}}&=e^2qQ/2,\\ W_{\frac{1}{2}}-W_{-\frac{1}{2}}&=0,\\ W_{-\frac{1}{2}}-W_{-3/2}&=-e^2qQ/2. \end{aligned} \tag{9}$$

For J finite, the level differences are

$$\begin{aligned} W_{3/2}-W_{\frac{1}{2}}&=-e^2q'Q/2,\\ W_{\frac{1}{2}}-W_{-\frac{1}{2}}&=\frac{3e^2q'Q}{2}\,\frac{2J+1}{(2J-1)(2J+3)}\\ &\cong 3e^2q'Q/4J, \end{aligned} \tag{10}$$

$$W_{-\frac{1}{2}}-W_{-3/2}=e^2q'Q/2.$$

(Note the introduction of q', as in Eq. (2) which is independent of J.) The result is that the line at $\nu=e^2q'Q/2h$ is completely unaffected by the distribution of rotational states when $I=\frac{3}{2}$. The spectrum due to $W_{\frac{1}{2}}-W_{-\frac{1}{2}}$ is not observable because of the presence of non-adiabatic transitions near zero frequency.

In the preceding section the possibility of an interaction of the type $-c\mathbf{I}\cdot\mathbf{J}$, whose order of magnitude is $(cJ/h)_M=0.05$ Mc/sec. was introduced. This term is diagonal in the same $\mathbf{F}=\mathbf{I}+\mathbf{J}$, M_F representation. (In fact any power series in $(\mathbf{I}\cdot\mathbf{J})$ is diagonal in this representation, and its set of eigenvalues is the series with the eigenvalues of $\mathbf{I}\cdot\mathbf{J}$ replacing $\mathbf{I}\cdot\mathbf{J}$ in the series.) In Appendix III (Eq. (23)) it is shown that the addition of this term to the Hamiltonian will cause a splitting and broadening of the zero-field peak with an over-all half-width equal to $2\pi^{-\frac{1}{2}}2.64(cJ/h)_M$ or 0.15 Mc/sec. This value is in good agreement with experiment, but there was no resolution into twin lines. This is not a fundamental difficulty because the effect of the first few excited vibrational states and of the centrifugal expansion of the rotating molecule on q' can easily be such as to smear out the structure and produce the observed asymmetries.

The splitting of the zero-field lines, Figs. 12 and 13, are not in as clear agreement with theory. It will be recalled that the frequency difference between the extreme minima was 10 percent too low, and there was lack of symmetry about the center of the spectrum. The reasons are probably several. The first is the uncertainty in the calibration of the field at low fields, the second the fact that the approximations used in the theory are not completely applicable. The perturbation introduced by the oscillating field is not small, and the only circumstance under which the Zeeman splitting is resolved (Fig. 13) is at a field where the perturbation of the fixed C-field is too large compared

to the quadrupole term and a more exact calculation would need to be made.

VII. GENERAL INTERACTIONS

Results similar to those found with the alkali halides and interpretable as quadrupole interactions are found in the spectra of other molecules. In fact, data of this nature were published by Millman and Kusch[5] prior to the development of the theory by Feld and Lamb. Examination of this data shows that the quadrupole interpretation is possible for Li_2^7 and K_2^{39} as well. The high spin and relatively narrow width of the Cs_2^{133} spectrum agree with the lack of structure observed. However, in no case do the halogens show structure that is easily interpretable as a quadrupole interaction. Cl^{35} and Cl^{37}, for example, show shallow, broad (~0.4 Mc/sec.), featureless resonances in NaCl. The radiofrequency spectrum of I^{127} has not yet been observed despite a number of searches, and this is presumably because of the extreme width of its spectrum.

A possible reason for this phenomenon can be inferred from the spectrum of F^{19}. F^{19}, having spin $\frac{1}{2}$ has no quadrupole moment, and therefore a quadrupole interaction is impossible. The sharpest F resonance observed, however, was reported by Millman and Kusch[3] for NaF where the half-width is 0.08 Mc/sec. The F resonance in CsF and LiF, however, reveal half-widths of about 0.5 Mc/sec. Fig. 16 is the plot of the relative change of beam intensity *versus* the relative difference in frequency from the Larmor frequency of a fluorine nucleus in LiF. An attempt to explain this width can be made by assuming an additional term in the Hamiltonian of the form $-c\mathbf{I}\cdot\mathbf{J}$, so that the Hamiltonian for F is therefore

$$\mathcal{H}=-\mu_N g_I \mathbf{H}\cdot\mathbf{I}-c\mathbf{I}\cdot\mathbf{J}. \qquad (11)$$

The additional term assumes a cosine coupling of the spin to the rotation which is proportional to the rotation. (The first power of the cosine operator is the maximum the symmetry of spin $\frac{1}{2}$ will allow.) This is similar in form to the operator for the interaction of the nuclear moment and the magnetic field because of the rotation of the molecular-charge distribution, but the order of magnitude assumed for c is greater. (The simpler interaction, $c\mathbf{I}\cdot\mathbf{J}/J$, whose strength is largely independent of the rotation, yields a result that is clearly not in agreement with experiment. The spectrum is rectangular with width $2c/h$.) In strong fields (Appendix III) the line-shape function derived from Eq. (11) is

$$dN/d\bar{\nu}=(ha\sqrt{\pi}/2c)\{1-\mathrm{erf}[(ha/c)|\bar{\nu}-\nu_I|]\}. \qquad (12)$$

The effect of resolution of the apparatus is not included in Eq. (12) because the large structure and absence of infinities make it relatively small. The solid curve of Fig. (16) is the theoretical curve computed from Eq. (12). The half-width of the line of Fig. 16 is 0.954 c/ha, and c/ha was evaluated by comparison with the observed value of 0.50 Mc/sec. Assuming an internuclear distance of 2.5A, the moment of inertia of the LiF molecule equals 52.6×10^{-40} g cm^2 and $a=2.57\times10^{-2}$ at the oven temperature of 1150°K. Therefore, $c=8.93\times10^{-23}$ erg and $c/g_I\mu_N$, the equivalent field at the nucleus per unit rotation, is 3.4 gausses in contrast to a value of 0.3 gauss per unit rotation to be, expected from a one-electron charge rotating at a distance of 2.5A from the F nucleus with the angular velocity of the molecule (Section IV).

The spectrum associated with Eq. (11) can be observed in weak fields. In Appendix III (Eq. 24) it is shown that the corresponding zero-field spectrum is

$$dN/d\bar{\nu}=2(ha/c)^2\bar{\nu}\exp[-(ha/c)^2\bar{\nu}^2]. \qquad (13)$$

The maximum R occurs at $\bar{\nu}=0.707c/ha$, and the spectrum has a half-width equal to 1.05

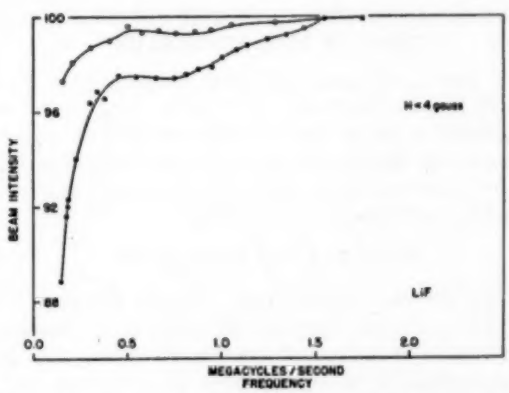

FIG. 17. "Zero"-field spectrum of LiF. The circled points correspond to a radiofrequency current of 3 amperes, and the squared points correspond to a radiofrequency current of 10 amperes.

c/ha. It is therefore broad. Figure 17 is the experimental weak-field spectrum. Qualitatively there is agreement. Unfortunately, the large fraction of the adiabatic transitions at near-zero frequency obscures the results. The expected minimum should be observed at 0.37 Mc/sec. Actually, it is observed at 0.7 ± 0.2 Mc/sec.

J. H. Van Vleck has offered the valuable suggestion that this cosine interaction may arise from second-order couplings between the nuclear spin and the electronic angular momenta even though the molecule is in a $^1\Sigma$ state. It is possible for such a second-order interaction also to introduce a quadrupole-like term. In this case the observed quadrupole interaction may be the sum of two parts: one attributable to a nuclear quadrupole moment and the other attributable to the second-order nuclear-electronic coupling. This effect and its probable magnitude are being further studied theoretically by J. H. Van Vleck and H. M. Foley. G. C. Wick is investigating this interaction using an approach similar to that adopted for the analogous interaction in H_2.[14,15]

This work has been facilitated by the contributions of present and past members of the molecular-beam laboratories. In particular, Professor I. I. Rabi suggested the initial line of research that led to the problem and also suggested the possibility of a cosine coupling of the nuclear spin to the rotational moment. Dr. S. Millman provided valuable advice in re-activating the apparatus. Drs. S. Brody and J. Trischka were of considerable help in the laboratory.

APPENDIX I. THE EFFECT OF THE FINITE RESOLUTION OF THE APPARATUS

Feld and Lamb have calculated the density of levels $|dz/d\tilde{\nu}|$ for the transitions $\pm\frac{3}{2}\leftrightarrow\pm\frac{1}{2}$, using first-order perturbation terms. If $F(\tilde{\nu},\nu)$ is there solution function for the apparatus (the specific one used is defined by Eq. (4)), then for a fixed but large value of J, the reduction in beam intensity at a frequency ν is given by

$$R(\nu,J)=\int_0^\infty F(\tilde{\nu},\nu)\,|dz/d\tilde{\nu}|\,d\tilde{\nu} \tag{14}$$

if $dz/d\tilde{\nu}$ nowhere changes sign. (In the problems considered $\tilde{\nu}=f(z^2)$, and therefore the range of z is restricted to $0\leqslant z\leqslant 1$.) For the special function, F, chosen, (Eq. (4)) the spectral curve for any transition is

$$R(\nu,J)=(K_1K_2/2I)\,|z(\nu+\Delta\tilde{\nu})-z(\nu-\Delta\tilde{\nu})|. \tag{15}$$

This yields Eq. (5) with $a=0$. The coefficient $1/2I$ is an approximate normalization factor arising from the consideration that there are $2I$ different allowed transitions for a molecule in a given rotational state. The result of summing $R(\nu,J)$ for all J is as follows:

$$R(\nu)=2a^2\int_0^\infty R(\nu,J)J\exp(-a^2J^2)dJ. \tag{16}$$

If Eq. (15) is used in Eq. (16) with z determined by Eq. (2a) and (2c), Eq. (5) follows.

For the transition $\frac{1}{2}\leftrightarrow-\frac{1}{2}$ the second-order terms (Eq. (2b)) need be considered. This calculation is different in that z is a multi-valued function of $\tilde{\nu}$. The calculation is of sufficient complexity to warrant the neglect of the term in $1/J$. For a given value of $\tilde{\nu}$ there are in general two allowable values of $z(|z|\leqslant 1)$, z_+ and z_-. Equation (15) then becomes

$$R(\nu)=(K_1K_2/2I)\,|[z_-(\nu+\Delta\tilde{\nu})-z_-(\nu-\Delta\tilde{\nu})]-[z_+(\nu+\Delta\tilde{\nu})-z_+(\nu-\Delta\tilde{\nu})]|. \tag{17}$$

(Equations (15) and (17) may be used explicitly for all values of ν, if the convention be adopted that z, z_+, or z_- is to be taken as zero whenever it becomes imaginary, or to be taken as unity whenever it exceeds unity.) Substitution of $\nu=\nu_I+\frac{3}{4}x_0^2\nu_I-\Delta\tilde{\nu}$ and $I=\frac{3}{2}$ in Eq. (17), together with z determined by Eq. (2b), yields for the intensity at the upper frequency minimum of the central minimum

$$R(\nu_I+\tfrac{3}{4}x_0^2\nu_I-\Delta\tilde{\nu})=\tfrac{1}{2}K_1K_2(4\Delta\tilde{\nu}/15x_0^2\nu_I)^{\frac{1}{2}}.$$

APPENDIX II. ENERGY LEVELS IN STRONG AND WEAK FIELDS

The Hamiltonian used to analyze the results of the experiments reported is:

$$\mathcal{H}=-\mu_N g_I\mathbf{I}\cdot\mathbf{H}+\frac{e^2qQ}{2I(2I-1)J(2J-1)}\{3(\mathbf{I}\cdot\mathbf{J})^2+\tfrac{3}{2}(\mathbf{I}\cdot\mathbf{J})-I(I+1)J(J+1)\}-c\mathbf{I}\cdot\mathbf{J}. \tag{18}$$

Strong Field

The matrix elements of each term of the Hamiltonian in the m_I and m_J representation are most conveniently stated in reference 4. The calculation of the energy levels to the second order in e^2qQ and c, considering $-\mu_N g_I\mathbf{I}\cdot\mathbf{H}$ the unperturbed Hamiltonian, yields for J large and $I=\frac{3}{2}$:

$$W_{3/2}=-\tfrac{3}{2}\mu_N g_I H+\tfrac{1}{2}b(3z^2-1)-\tfrac{3}{2}cJ_z-\frac{[\sqrt{3}bz-c\frac{1}{2}\sqrt{3}J]^2(1-z^2)}{\mu_N g_I H}-\frac{\frac{3}{4}b^2(1-z^2)^2}{2\mu_N g_I H} \tag{19a}$$

$$W_{\frac{1}{2}}=-\tfrac{1}{2}\mu_N g_I H-\tfrac{1}{2}b(3z^2-1)-\tfrac{1}{2}cJ_z+\frac{[\sqrt{3}bz-c\frac{1}{2}\sqrt{3}J]^2(1-z^2)}{\mu_N g_I H}-\frac{c^2J^2(1-z^2)}{\mu_N g_I H}-\frac{\frac{3}{4}b^2(1-z^2)^2}{2\mu_N g_I H} \tag{19b}$$

$$W_{-\frac{1}{2}}=\tfrac{1}{2}\mu_N g_I H-\tfrac{1}{2}b(3z^2-1)+\tfrac{1}{2}cJ_z-\frac{[-\sqrt{3}bz-c\frac{1}{2}\sqrt{3}J]^2(1-z^2)}{\mu_N g_I H}+\frac{c^2J^2(1-z^2)}{\mu_N g_I H}+\frac{\frac{3}{4}b^2(1-z^2)^2}{2\mu_N g_I H} \tag{19c}$$

$$W_{-3/2}=\tfrac{3}{2}\mu_N g_I H+\tfrac{1}{2}b(3z^2-1)+\tfrac{3}{2}cJ_z+\frac{[-\sqrt{3}bz-c\frac{1}{2}\sqrt{3}J]^2(1-z^2)}{\mu_N g_I H}+\frac{\frac{3}{4}b^2(1-z^2)^2}{2\mu_N g_I H} \tag{19d}$$

with $b=e^2qQ/4$.

[14] G. C. Wick, Zeits. f. Physik 85, 25 (1933).
[15] N. F. Ramsey, Phys. Rev. 58, 226 (1940).

The energy differences are

$$W_{3/2}-W_{1/2}=-\mu_N g_I H-cJ_z+b(3z^2-1) -\frac{6b^2z^2(1-z^2)}{\mu_N g_I H}-\frac{1}{2}\frac{c^2J^2(1-z^2)}{\mu_N g_I H}+\frac{6bcJ_z(1-z^2)}{\mu_N g_I H} \quad (20a)$$

$$W_{1/2}-W_{-1/2}=-\mu_N g_I H-cJ_z +\frac{3}{4}\frac{b^2(1-z^2)(9z^2-1)}{\mu_N g_I H}-\frac{1}{2}\frac{c^2J^2(1-z^2)}{\mu_N g_I H}, \quad (20b)$$

$$W_{-1/2}-W_{-3/2}=-\mu_N g_I H-cJ_z-b(3z^2-1) -\frac{6b^2z^2(1-z^2)}{\mu_N g_I H}-\frac{1}{2}\frac{c^2J^2(1-z^2)}{\mu_N g_I H}-\frac{6bcJ_z(1-z^2)}{\mu_N g_I H}. \quad (20c)$$

Equation (6) of the text follows by dividing through by $-\mu_N g_I H$.

Zero Field

The Hamiltonian is diagonal in the $\mathbf{F}=\mathbf{I}+\mathbf{J}$ and m_F representation. The energy differences are, for large J

$$W_{3/2}-W_{1/2}=-\tfrac{1}{2}e^2q'Q-cJ, \quad (21a)$$

$$W_{1/2}-W_{-1/2}=(3e^2q'Q/4J)-cJ, \quad (21b)$$

$$W_{-1/2}-W_{-3/2}=\tfrac{1}{2}e^2q'Q-cJ. \quad (21c)$$

Neglecting the transition $\frac{1}{2}\leftrightarrow-\frac{1}{2}$ the spectrum will be situated about the frequency $\nu_I^0=e^2q'Q/2h$, and the transition frequency is given by

$$\bar{\nu}=e^2q'Q/2h\pm cJ/h. \quad (22)$$

APPENDIX III. EFFECT OF THE $cI\cdot J$ TERM ON THE LINE SHAPE

Zero Field

Assuming $e^2q'Q\gg(cJ)_{Av}$, the line shape can be calculated in a straightforward fashion. $d\bar{\nu}/dJ=c/h$ and $dN/dJ=2a^2J\exp(-a^2J^2)$, and, therefore,

$$dN/d\bar{\nu}=\tfrac{2}{3}(ah/c)^2|\bar{\nu}-\nu_I^0|\exp[-(ha/c)^2(\bar{\nu}-\nu_I^0)^2]. \quad (23)$$

The factor $\frac{2}{3}$ is inserted to normalize the total transitions to unity. If there is no quadrupole interaction $\nu_I^0=0$. Repeating the calculation for $e^2qQ=0$, the line shape is given by

$$dN/d\bar{\nu}=2(ah/c)^2\bar{\nu}\exp[-(ha/c)^2\bar{\nu}^2]. \quad (24)$$

This is Eq. (13) of the text.

Strong Field

In the absence of a quadrupole moment, $(b=0)$, the strong-field frequencies are given, from Eq. (20), by

$$\bar{\nu}=\nu_I+cm_J/h. \quad (25)$$

Again, $d\bar{\nu}/dm_J=c/h$, but

$$dN/dm_J=a^2\int_{m_J}^{\infty}\exp(-a^2J^2)dJ$$

for $m_J\gtrless 0$ or,

$$dN/d\bar{\nu}=(ha/c)\int_{am_J}^{\infty}\exp(-v^2)dv, \quad m_J\gtrless 0, \quad (26)$$

and therefore

$$dN/d\bar{\nu}=(ha\sqrt{\pi}/2c)\{1-\mathrm{erf}[(ha/c)|\bar{\nu}-\nu_I|]\} \text{ all } m_J. \quad (27)$$

PHYSICAL REVIEW VOLUME 72, NUMBER 11 DECEMBER 1, 1947

Relativistic Invariance of the Quantum Theory of Radiation

S. T. MA
The Institute for Advanced Study, Princeton, New Jersey
(Received June 30, 1947)

It is shown that the current formulation of the quantum theory of radiation, which is concerned solely with the quantization of the transverse part of the electromagnetic field, is in conformity with the principle of relativity. The relativistic invariance of the quantum theory of the neutral-vector meson field is also discussed.

1. INTRODUCTION

THE quantum theory of the electromagnetic field is relativistically invariant so far as its general postulates, the commutation relations, and supplementary conditions are concerned; but the invariance of the subsequent deductions from these postulates, which are concerned with the transverse part of the field alone, is not obvious at first sight because the separation of the transverse part of the field is not a relativistically invariant procedure. Recently Dirac[1] has shown the relativistic invariance of the quantum theory of electromagnetic field by means of his theory of expansors, which treats each Fourier component of the field as a four-dimensional oscillator. In view of the current formulation of the theory, it is of interest to consider also the question whether the ordinary theory concerned with two-dimensional radiation oscillators is in conformity with the principle of relativity. It is the purpose of the present paper to discuss a few aspects of this problem.

For the discussion of this problem it is convenient to introduce in each Lorentz frame of reference for each Fourier component of the field a system of mutually perpendicular space axes with one axis pointing in the direction of the propagation of the plane wave. The orthogonal transformation of the coordinates of a 4-vector referred to these systems of axes will be discussed in Section 2. With the help of the general relations thus obtained we shall discuss in Section 3 the relativistic invariance of the quantization of the transverse waves. The investigation in Section 2 also makes it possible to construct emission and absorption operators for the transverse photons having invariant properties, which, as will be shown in Section 4, are closely related to the invariant operators introduced by Kramers.[2] In Section 5 we shall replace the transverse electromagnetic waves by a discrete set of radiation oscillators and discuss the problem from the point of view of Fock's representation of the quantized field.

Finally our considerations will be generalized in Section 6 to the neutral-vector meson field, the theory of which differs from that of the electromagnetic field mainly in that the former is associated with a non-vanishing rest mass.

2. A SPECIAL TYPE OF FOUR-DIMENSIONAL ORTHOGONAL TRANSFORMATION

Consider an arbitrary real Lorentz transformation of the coordinates of a 4-vector referred to two frames of reference S and S',

$$x_\mu=\alpha_{\mu\nu}x'_\nu, \quad x'_\mu=x'_\nu\alpha_{\nu\mu} \quad (\mu, \nu=0, 1, 2, 3). \quad (1)$$

The coefficients $\alpha_{\mu\nu}$ satisfy the orthogonality relations

$$\alpha_{\mu\nu}\alpha^{\mu\rho}=\alpha_{\nu\mu}\alpha^{\rho\mu}=g_\nu{}^\rho, \quad (2)$$

where $g_\nu{}^\rho$ is equal to 1 when $\nu=\rho$ and is equal to zero otherwise. If the magnitude of the propagation vector $\mathbf{k}$ is denoted by k_0, the four quantities (k_0, k_1, k_2, k_3) transform like the components of a 4-vector according to Eq. (1). We shall denote the 4-vector $(k_0, \mathbf{k})$ by the symbol $\mathbf{K}$.

Let us introduce a new frame of reference S^* whose four axes are parallel to four unit vectors $\mathbf{u}_0$, $\mathbf{u}_I$, $\mathbf{u}_{II}$, $\mathbf{u}_{III}$, with $\mathbf{u}_0$ in the direction of the time axis[2a] and $\mathbf{u}_{III}$ in the direction of $\mathbf{k}$. The transformation of the coordinates referred to the

[1] P. A. M. Dirac, Proc. Roy. Soc. **A183**, 284 (1945), Princeton Lectures, 1946.

[2] H. A. Kramers, *Quantentheorie des Elektrons und der Strahlung* (Akademische Verlagsgesellschaft, Leipzig, 1938), p. 435.

[2a] As the unit vector $\mathbf{u}_0$ is taken to be in the direction of the time axis, there is no difference between x_0 and x_0.

two systems S and S^* is that of a three-dimensional rotation, namely,

$$x_N=\sum_{n=1}^{3}\omega_{Nn}x_n \quad (N=I, II, III), \tag{3}$$

which is a special case of the four-dimensional orthogonal transformation. There are an infinite number of ways of choosing S^* because of the arbitrariness in the choice of the axes $\mathbf{u}_I$, $\mathbf{u}_{II}$. Let S'^* be a similar system of axes obtained from the frame of reference S'. Since orthogonal transformations applied in succession are equivalent to a single orthogonal transformation, it follows that the transformation of the coordinates referred to S^* and S'^* is again an orthogonal transformation of the form

$$x_\mu=\beta_{\mu\nu}x'^\nu, \quad x'_\mu=x^\nu\beta_{\nu\mu} \quad (\mu, \nu=0, I, II, III), \tag{4}$$

with the coefficients $\beta_{\mu\nu}$ satisfying the orthogonality relations

$$\beta_{\mu\nu}\beta^{\mu\rho}=\beta_{\nu\mu}\beta^{\rho\mu}=g_\nu^{\ \rho}. \tag{5}$$

Referred to S^* and S'^* the 4-vector $\mathbf{K}$ has the components

$$(k_0, 0, 0, k_0), \quad (k'_0, 0, 0, k'_0), \tag{6}$$

respectively. The relation between the values of k_0 and k'_0 is given by the transformation Eq. (1) alone, since these values are invariant under the three-dimensional rotations.

There are a few relations between the coefficients $\beta_{\mu\nu}$ which can be obtained from general considerations. Substituting the components of $\mathbf{K}$ in formulae (6) into Eqs. (4) with μ equal to I and II, respectively, we see that

$$\begin{aligned}\beta_{I0}-\beta_{I\,III}&=\beta_{II0}-\beta_{II\,III}=0,\\ \beta_{0I}-\beta_{III\,I}&=\beta_{0II}-\beta_{III\,II}=0.\end{aligned} \tag{7}$$

Similarly from Eqs. (4) applied with μ equal to 0 and III, respectively, we have

$$\begin{aligned}\beta_{00}-\beta_{0III}&=\beta_{III0}-\beta_{III\,III}=k_0/k'_0,\\ \beta_{00}-\beta_{III0}&=\beta_{0III}-\beta_{III\,III}=k'_0/k_0.\end{aligned} \tag{8}$$

Equations (7) enable us to deduce from the general orthogonality relations given by Eqs. (5) similar relations for the coefficients $\beta_{\mu\nu}$ related to the transverse directions alone, namely,

$$\sum_{L=I}^{II}\beta_{ML}\beta_{NL}=\sum_{L=I}^{II}\beta_{LM}\beta_{LN}=\delta_{MN} \quad (M, N=I, II). \tag{9}$$

The coefficients $\beta_{\mu\nu}$ can be specified a step further by making the choice of the system of axes S^* and S'^* more definite. This can be done in a relativistic way by introducing a new space-like 4-vector $\mathbf{E}$ orthogonal to the 4-vector $\mathbf{K}$, i.e., a 4-vector with components satisfying the relations

$$e_\mu k^\mu=0, \tag{10}$$

$$e_\mu e^\mu<0. \tag{11}$$

Denoting the space part of $\mathbf{E}$ by $\mathbf{e}$, which is a 3-vector, and the transverse part of $\mathbf{e}$ by $\mathbf{e}_T$, we have

$$\begin{aligned}|\mathbf{e}_T|^2&=|\mathbf{e}-\mathbf{k}(\mathbf{k}\cdot\mathbf{e})/k_0^2|^2=\mathbf{e}^2-(\mathbf{k}\cdot\mathbf{e})^2/k_0^2\\ &=\mathbf{e}^2-e_0^2=-e_\mu e^\mu,\end{aligned} \tag{12}$$

by Eq. (10). It will be convenient to choose $\mathbf{E}$ such that

$$|\mathbf{e}_T|=1. \tag{13}$$

In order to specify the choice of the systems S^* and S'^* we shall take

$$\mathbf{u}_I=\mathbf{e}_T, \qquad \mathbf{u}'_I=\mathbf{e}'_T, \tag{14}$$

$$\mathbf{u}_{II}=\mathbf{k}\times\mathbf{e}_T/k_0, \quad \mathbf{u}'_{II}=\mathbf{k}'\times\mathbf{e}'_T/k'_0. \tag{15}$$

Let the systems chosen in this way be denoted by S^{**} and S'^{**}, respectively. Referred to these systems of axes, the components of the 4-vector, $\mathbf{E}$ are

$$(e_0, 1, 0, e_0), \quad (e'_0, 1, 0, e'_0), \tag{16}$$

the longitudinal component being equal to the time component in each case on account of Eq. (10). Substituting these values into Eqs. (4) with μ equal to I and II, respectively, and making use of the orthogonality relations and continuity considerations, we have

$$\beta_{I\,II}=\beta_{II\,I}=0, \tag{17}$$

$$\beta_{I\,I}=\beta_{II\,II}=-1. \tag{18}$$

The coefficients $\beta_{\mu\nu}$ can be explicitly given in terms of the coefficients $\alpha_{\mu\nu}$ and the direction cosines ω_{Nn}, $\omega_{N'n}$ $(N=I, II, III, n=1, 2, 3)$ of the

unit vectors $\mathbf{u}_N$, $\mathbf{u}'_N$ relative to the space axes of S and S'. We have

$$x_0=\alpha_{00}x'_0-\sum_{n=1}^{3}\alpha_{0n}x'_n$$

$$=\alpha_{00}x'_0-\sum_{n=1}^{3}\alpha_{0n}\sum_{N=I}^{III}x'_N\omega'_{Nn},$$

$$x_M=\sum_{m=1}^{3}\omega_{Mm}x_m$$

$$=\sum_{m=1}^{3}\omega_{Mm}\left(\alpha_{m0}x'_0-\sum_{n=1}^{3}\alpha_{mn}\sum_{N=1}^{III}x'_N\omega'_{Nn}\right),$$

so that

$$\left.\begin{aligned}\beta_{00}&=\alpha_{00},\\ \beta_{0N}&=\sum_n\alpha_{0n}\omega'_{Nn},\\ \beta_{M0}&=\sum_m\omega_{Mm}\alpha_{m0},\\ \beta_{MN}&=\sum_{m,n}\omega_{Mm}\alpha_{mn}\omega'_{Nn}.\end{aligned}\right\}(M,N=I,II,III). \quad (19)$$

It can easily be verified that the coefficients $\beta_{\mu\nu}$ in Eq. (19) satisfy Eqs. (7) and (8) for any choice of systems of axes S^*, S'^* and also satisfy Eqs. (17) and (18) in the case of the systems S^{**}, S'^{**}.

For comparison with later results it will be convenient to write

$$\beta_{MN}=-\gamma_{MN} \quad (M,N=I,II). \quad (20)$$

The Eqs. (9) for S^* and S'^* become then

$$\sum_{L=I}^{II}\gamma_{ML}\gamma_{NL}=\sum_{L=I}^{II}\gamma_{LM}\gamma_{LN}=\delta_{MN}$$

$$(M,N=I,II), \quad (21)$$

and the Eqs. (17), (18) for S^{**}, S'^{**} becomes

$$\gamma_{MN}=\delta_{MN} \quad (M,N=I,II). \quad (22)$$

3. QUANTIZATION OF THE TRANSVERSE ELECTROMAGNETIC FIELD

The electromagnetic potentials are expressible as Fourier integrals of the form

$$A_\mu(\mathbf{X})=\int\{\eta_\mu(\mathbf{k})\exp i(\mathbf{K},\mathbf{X})+\bar{\eta}_\mu(\mathbf{k})\exp -i(\mathbf{K},\mathbf{X})\}d^3k/k_0$$

$$(\mu=0,1,2,3), \quad (23)$$

where $\bar{\eta}_\mu$ is the Hermitian conjugate of the operator η_μ and $(\mathbf{K},\mathbf{X})$ denotes the scalar product $k_\mu x^\mu$. The η_μ and $\bar{\eta}_\mu$ transform like the components of a 4-vector.

In quantum theory the operators η_μ, $\bar{\eta}_\mu$ satisfy the invariant commutation relations[3]

$$\eta_\mu(\mathbf{k}')\bar{\eta}_\nu(\mathbf{k}'')-\bar{\eta}_\nu(\mathbf{k}'')\eta_\mu(\mathbf{k}')=g_{\mu\nu}(hk_0'/4\pi^2)\delta(\mathbf{k}'-\mathbf{k}'')$$

$$(\mu,\nu=0,1,2,3). \quad (24)$$

The Lorentz relation

$$\partial A_\mu/\partial x_\mu=0 \quad (25)$$

in the classical theory is replaced in the quantum theory by the supplementary conditions

$$k_\mu\eta^\mu|\rangle=0, \quad k_\mu\bar{\eta}^\mu|\rangle=0, \quad (26)$$

which should be satisfied by any $|\rangle$ representing a state that occurs in nature, in the absence of charged particles. In the system of reference S^* these conditions become

$$(\eta_0-\eta_{III})|\rangle=0, \quad (\bar{\eta}_0-\bar{\eta}_{III})|\rangle=0. \quad (27)$$

The axes of the system S^* point in different directions for different values of $\mathbf{k}$. We shall take the unit vectors $\mathbf{u}_N$ $(N=I,II,III)$ to be continuous functions of $\mathbf{k}$.

As a result of these conditions the only physical observables that have non-vanishing expectation values involve only the operators related to the transverse directions, which satisfy the commutation relations

$$\eta_M(\mathbf{k}')\bar{\eta}_N(\mathbf{k}'')-\bar{\eta}_N(\mathbf{k}'')\eta_M(\mathbf{k}')=-\delta_{MN}(hk'_0/4\pi^2)\delta(\mathbf{k}'-\mathbf{k}'')$$

$$(M,N=I,II). \quad (28)$$

The current scheme of quantum theory of radiation is concerned solely with the operators η_I, η_{II}, $\eta_0-\eta_{III}$, and their Hermitian conjugates.

The questions we shall consider are (i) whether these operators are transformed by a Lorentz transformation into functions of the same operators in the new system of reference, and (ii) whether they are transformed in such a way that the Eqs. (27) and (28) are invariant. It is obvious that the operators $\eta_0-\eta_{III}$, $\bar{\eta}_0-\bar{\eta}_{III}$ are

[3] P. A. M. Dirac, Ann. Inst. Poincaré 9, 13 (1939).

transformed into the same operators multiplied by a numerical factor in the new frame of reference and Eqs. (27) are invariant. For the other operators we have, by Eqs. (4), (7), and (20),

$$\left.\begin{aligned}\eta_N&=\beta_{N0}(\eta_0'-\eta_{III}')+\sum_{M=I}^{II}\gamma_{NM}\eta_M'\\ \eta_N'&=(\eta_0-\eta_{III})\beta_{0N}+\sum_{M=I}^{II}\eta_M\gamma_{MN}\end{aligned}\right\}$$
$$(N=I,\ II). \quad (29)$$

This settles the first question. Concerning the second question we note that, if the expressions for η_N given by the first equation of Eqs. (29) together with their Hermitian conjugates are substituted into Eqs. (28), terms involving the operators $\eta_0'-\eta_{III}'$, $\bar{\eta}_0'-\bar{\eta}_{III}'$ will in general appear. These new terms give vanishing results, however, when operating on a $|\rangle$ satisfying the supplementary conditions. From Eqs. (27) and (29) it follows that

$$\left.\begin{aligned}\left(\eta_N-\sum_{M=I}^{II}\gamma_{NM}\eta_M'\right)|\rangle&=0\\ \left(\eta_N'-\sum_{M=I}^{II}\eta_M\gamma_{MN}\right)|\rangle&=0\end{aligned}\right\}(N=I,\ II). \quad (30)$$

For this reason we replace Eq. (28) by the equation

$$\{\eta_M(\mathbf{k}')\bar{\eta}_N(\mathbf{k}'')-\bar{\eta}_N(\mathbf{k}'')\eta_M(\mathbf{k}')\}|\rangle$$
$$=-\delta_{MN}(\hbar k_0'/4\pi^2)\delta(\mathbf{k}'-\mathbf{k}'')|\rangle, \quad (31)$$

which is to hold for any $|\rangle$ satisfying Eqs. (27). The invariance of this equation follows from the orthogonality relations for the coefficients γ_{MN} expressed by Eqs. (21).

4. "INVARIANT" OPERATORS

Equations (29) in the preceding section take the simplest form in the systems of reference S^{**}, S'^{**} introduced in Section 2, namely,

$$\left.\begin{aligned}\eta_N&=\eta_N'+\beta_{N0}(\eta_0'-\eta_{III}')\\ \eta_N'&=\eta_N+(\eta_0-\eta_{III})\beta_{0N}\end{aligned}\right\}(N=I,\ II). \quad (32)$$

For any $|\rangle$ representing an actual state we have, therefore,

$$(\eta_N-\eta_N')|\rangle=0 \quad (N=I,\ II). \quad (33)$$

Similarly,

$$(\bar{\eta}_N-\bar{\eta}_N')|\rangle=0 \quad (N=I,\ II). \quad (34)$$

For this reason the operators η_N, $\bar{\eta}_N$ $(N=I,\ II)$ may be regarded as invariant.

These "invariant operators" are closely connected with similar operators introduced by Kramers. In the notation of the present paper, Kramers' result may be expressed as follows. Let $\mathfrak{E}$ and $\mathfrak{H}$ be the operators representing the electric and magnetic field strengths and write

$$\mathfrak{F}=\mathfrak{E}+i\mathfrak{H}, \quad \bar{\mathfrak{F}}^+=\mathfrak{E}-i\mathfrak{H}. \quad (35)$$

Then from Eq. (23)

$$\mathfrak{F}=\int\{(-ik_0\boldsymbol{\eta}+i\mathbf{k}\eta_0+\mathbf{k}\times\boldsymbol{\eta})\exp i(\mathbf{K},\mathbf{X})$$
$$+(ik_0\bar{\boldsymbol{\eta}}-i\mathbf{k}\bar{\eta}_0-\mathbf{k}\times\bar{\boldsymbol{\eta}})$$
$$\times\exp -i(\mathbf{K},\mathbf{X})\}d^3k/k_0, \quad (36)$$

where $\boldsymbol{\eta}$ and $\bar{\boldsymbol{\eta}}$ denote the space parts of the 4-vectors η_μ, $\bar{\eta}_\mu$. Now denoting the transverse part of $\boldsymbol{\eta}$ by $\boldsymbol{\eta}_T$ we have

$$-ik_0\boldsymbol{\eta}+i\mathbf{k}\eta_0+\mathbf{k}\times\boldsymbol{\eta}$$
$$=i\mathbf{k}(\eta_0-\eta_{III})-ik_0(\boldsymbol{\eta}_T+i\mathbf{k}\times\boldsymbol{\eta})$$
$$=i\mathbf{k}(\eta_0-\eta_{III})-ik_0(\boldsymbol{\eta}_I-i\boldsymbol{\eta}_{II})(\mathbf{u}_I+i\mathbf{u}_{II}),$$

and similarly,

$$ik_0\bar{\boldsymbol{\eta}}-i\mathbf{k}\bar{\eta}_0-\mathbf{k}\times\bar{\boldsymbol{\eta}}=-i\mathbf{k}(\bar{\eta}_0-\bar{\eta}_{III})$$
$$+ik_0(\bar{\boldsymbol{\eta}}_I-i\bar{\boldsymbol{\eta}}_{II})(\mathbf{u}_I+i\mathbf{u}_{II}),$$

so that

$$\mathfrak{F}=i\int\{[(\eta_0-\eta_{III})\exp i(\mathbf{K},\mathbf{X})$$
$$-(\bar{\eta}_0-\bar{\eta}_{III})\exp -i(\mathbf{K},\mathbf{X})]\mathbf{k}$$
$$-[(\boldsymbol{\eta}_I-i\boldsymbol{\eta}_{II})\exp i(\mathbf{K},\mathbf{X})$$
$$-(\bar{\boldsymbol{\eta}}_I-i\bar{\boldsymbol{\eta}}_{II})\exp -i(\mathbf{K},\mathbf{X})]k_0$$
$$\times(\mathbf{u}_I+i\mathbf{u}_{II})\}d^3k/k_0. \quad (37)$$

Similarly,

$$\bar{\mathfrak{F}}^+=i\int\{[(\eta_0-\eta_{III})\exp i(\mathbf{K},\mathbf{X})$$
$$-(\bar{\eta}_0-\bar{\eta}_{III})\exp -i(\mathbf{K},\mathbf{X})]\mathbf{k}$$
$$-[(\boldsymbol{\eta}_I+i\boldsymbol{\eta}_{II})\exp i(\mathbf{K},\mathbf{X})-(\bar{\boldsymbol{\eta}}_I+i\bar{\boldsymbol{\eta}}_{II})$$
$$\times\exp -i(\mathbf{K},\mathbf{X})]k_0(\mathbf{u}_I-i\mathbf{u}_{II})\}d^3k/k_0. \quad (38)$$

Apart from minor differences in numerical factors, the operators $\eta_I \pm i\eta_{II}$, $\bar{\eta}_I \pm i\bar{\eta}_{II}$ here are just Kramers' emission and absorption operators of right and left quanta and the vectors

$$k_0(\mathbf{u}_I + i\mathbf{u}_{II}) \equiv \mathbf{c}, \quad k_0(\mathbf{u}_I - i\mathbf{u}_{II}) \equiv \bar{\mathbf{c}} \tag{39}$$

are the complex null vectors denoted by $\mathbf{c}_\lambda$, $\mathbf{c}_\lambda^*$ in Kramers' book. It follows immediately from Eqs. (39) that

$$\begin{gathered}(\mathbf{c}\cdot\mathbf{c}) = (\bar{\mathbf{c}}\cdot\bar{\mathbf{c}}) = 0, \quad (\mathbf{c}\cdot\bar{\mathbf{c}}) = k_0^2, \\ \mathbf{c}\times\mathbf{k} = ik_0\mathbf{c}, \quad \bar{\mathbf{c}}\times\mathbf{k} = -ik_0\bar{\mathbf{c}}.\end{gathered} \tag{40}$$

It is also easy to show that the components of the vectors $\mathbf{c}$, $\bar{\mathbf{c}}$ are subjected to a three-dimensional orthogonal transformation when an arbitrary real orthogonal transformation is applied to the coordinates of a 4-vector. Like the unit vectors $\mathbf{u}_I$, $\mathbf{u}_{II}$ the vectors $\mathbf{c}$, $\bar{\mathbf{c}}$ are not unique owing to the arbitrariness in the choice of the 4-vector $\mathbf{E}$ satisfying the Eqs. (10), (11), and (13). We can obtain a new set of axes $\mathbf{u}_I$, $\mathbf{u}_{II}$ by making a rotation about the vector $\mathbf{k}$, say through an angle φ. Then the vectors $k_0(\mathbf{u}_I \pm i\mathbf{u}_{II})$ become multiplied by the factors $\exp \mp i\varphi$, respectively, which do not affect the relations in Eqs. (40).

The terms in Eqs. (37), (38) involving the factors $(\eta_0 - \eta_{III})$, etc., may be discarded when the operators $\mathfrak{F}$, $\bar{\mathfrak{F}}^+$ operate on a $|\rangle$ satisfying the supplementary conditions. From the fact that the transverse parts of $\mathfrak{F}$ and $\bar{\mathfrak{F}}^+$ transform in the same way as $\mathbf{c}$ and $\bar{\mathbf{c}}$, respectively, Kramers came to the conclusion that the operators $\eta_I \pm i\eta_{II}$, $\bar{\eta}_I \pm i\bar{\eta}_{II}$ are invariant. This is clearly equivalent to the invariance of the operators η_N, $\bar{\eta}_N$ $(N = I, II)$. We have thus obtained an independent proof of Kramers' result.

5. WAVE FUNCTIONS OF RADIATION OSCILLATORS

For the purpose of further discussion it will be convenient to replace the radiation field by a discrete set of oscillators. Let the $\mathbf{k}$-space be divided into regions of small size $\Delta^{(1)}$, $\Delta^{(2)}$, $\Delta^{(3)}$, $\cdots$, and let

$$\left[\int_{\Delta^{(i)}} \eta_\mu(\mathbf{k}) d^3k/k_0\right] \Big/ \left[(h/4\pi^2)\int_{\Delta^{(i)}} d^3k/k_0\right]^{\frac{1}{2}} = \xi_\mu^{(i)} \quad (i = 1, 2, 3, \cdots). \tag{41}$$

The quantities $\xi_\mu^{(i)}$ transform like the components of a 4-vector and satisfy the commutation relations

$$\xi_\mu^{(i)}\xi_\nu^{(j)} - \xi_\nu^{(j)}\xi_\mu^{(i)} = \delta_{ij}g_{\mu\nu}. \tag{42}$$

We replace the supplementary conditions expressed by Eqs. (26) by the conditions

$$k_\mu^{(i)}\xi^{\mu(i)}|\rangle = 0, \quad k_\mu^{(i)}\xi^{\mu(i)}|\rangle = 0 \quad (i = 1, 2, 3, \cdots) \tag{43}$$

where the $\mathbf{K}^{(i)}$ form a discrete set of 4-vectors. In the following we shall confine our attention to a particular radiation oscillator and drop the indices (1), (2), $\cdots$. As in Section 3, we have referred to the frame of reference S^*

$$(\xi_M\xi_N - \xi_N\xi_M)|\rangle = -\delta_{MN}|\rangle \quad (M, N = I, II), \tag{44}$$

$$(\xi_0 - \xi_{III})|\rangle = 0, \quad (\xi_0 - \xi_{III})|\rangle = 0. \tag{45}$$

Under a Lorentz transformation from S^* to S'^* we have

$$\left(\xi_N - \sum_{M=I}^{II} \gamma_{NM}\xi_{M'}\right)|\rangle = 0, \quad \left(\xi_{N'} - \sum_{M=I}^{III} \xi_M\gamma_{MN}\right)|\rangle = 0 \quad (N = I, II). \tag{46}$$

The Lorentz transformation of Eqs. (44), (45) is the same as in Section 3.

It follows from Eqs. (44), (45) that

$$(\xi_{III}\xi_{III} - \xi_0\xi_0)|\rangle = 0. \tag{47}$$

The operators $\xi_I\xi_I$ and $\xi_{II}\xi_{II}$ commute and their eigenvalues n_I, n_{II} both take on the integral values 0, 1, 2, $\cdots$. The normalized vector representing a state corresponding to a given set of values of n_I, n_{II} is of the form

$$|n_I, n_{II}\rangle = (n_I!n_{II}!)^{-\frac{1}{2}}\xi_I^{n_I}\xi_{II}^{n_{II}}|0\rangle, \tag{48}$$

where $|0\rangle$ represents the state with no quanta present. These vectors may be taken to be the basic vectors of a representation in which the operators $\xi_I\xi_I$ and $\xi_{II}\xi_{II}$ are diagonal. An arbitrary state of the radiation oscillator is a superposition of the states represented by these basic

vectors, thus

$$|\rangle=\sum_{n_I,\,n_{II}}|n_I,\,n_{II}\rangle\langle n_I,\,n_{II}|\rangle. \tag{49}$$

From Eq. (47) we have

$$(-\xi_\mu\xi^\mu+1)\,|n_I,\,n_{II}\rangle=(\xi_I\xi_I+\xi_{II}\xi_{II})\,|n_I,\,n_{II}\rangle$$
$$=(n_I+n_{II})\,|n_I,\,n_{II}\rangle, \tag{50}$$

showing that

$$n_I+n_{II}=\text{invariant}, \tag{51}$$

which means physically that the total number of transverse photons polarized in two mutually orthogonal directions of polarization is an invariant quantity.

Now according to the general scheme of quantum theory the square of the modulus of the wave function $\langle n_I,\,n_{II}|\rangle$ represents the probability that the radiation oscillator is in the state $(n_I,\,n_{II})$. From the invariance of n_I+n_{II} we should therefore expect the invariance of the sum

$$\sum_{n_I+n_{II}=n}|\langle n_I,\,n_{II}|\rangle|^2 \tag{52}$$

extending over all values of n_I and n_{II}, such that n_I+n_{II} is equal to a positive integer n (the total number of transverse photons). This can be proved by the method used by Dirac in the theory of expansors. Putting

$$\langle n_I,\,n_{II}|\rangle=(n_I!n_{II}!)^{\frac{1}{2}}A_{n_I,\,n_{II}}, \tag{53}$$

we see that the transformation of the quantities $A_{n_I\,n_{II}}$ under a Lorentz transformation is determined by the equations

$$\sum_{n_I,\,n_{II}}A_{n_I,\,n_{II}}\xi_I^{n_I}\xi_{II}^{n_{II}}=\sum_{n_I,\,n_{II}}A'_{n_I,\,n_{II}}\xi'_I{}^{n_I}\xi'_{II}{}^{n_{II}}, \tag{54}$$

$$\xi_N=\sum_{M=I}^{III}\gamma_{NM}\xi_M'. \tag{55}$$

The invariance of the sum in formula (52) is equivalent to the invariance of the sum

$$\sum_{n_I+n_{II}=n}n_I!n_{II}!|A_{n_I,\,n_{II}}|^2, \tag{56}$$

which can be proved by considering an infinitesimal transformation with coefficients γ_{MN} satisfying the orthogonality relations.

6. NEUTRAL-VECTOR MESON FIELD

The theory of the neutral-vector meson field differs from the theory of the electromagnetic field mainly in the fact that the meson has a finite rest mass $m=\hbar\kappa/c$, so that, as a consequence, the time component of the 4-vector $\mathbf{K}$ becomes

$$k_0=(k^2+\kappa^2)^{\frac{1}{2}}, \tag{57}$$

where $k=|\mathbf{k}|$.

The supplementary conditions in the quantum theory are still given by Eqs. (26), but the requirement of commutability of the operators $k_\mu\eta^\mu$, $k_\mu\bar{\eta}^\mu$ makes it necessary to change the commutation relations into

$$\eta_\mu(\mathbf{k}')\bar{\eta}_\nu(\mathbf{k}'')-\bar{\eta}_\nu(\mathbf{k}'')\eta_\mu(\mathbf{k}')$$
$$=(g_{\mu\nu}-k_\mu k_\nu/\kappa^2)(\hbar/4\pi^2)k'_0\delta(\mathbf{k}'-\mathbf{k}'')$$
$$(\mu,\,\nu=0,\,1,\,2,\,3), \tag{58}$$

by substituting the factor $g_{\mu\nu}-k_\mu k_\nu/\kappa^2$ for the factor $g_{\mu\nu}$ in Eq. (24).[4]

As in Section 2, we can introduce a system of axes S^* with one axis parallel to the propagation vector $\mathbf{k}$. Referred to S^* the 4-vector $\mathbf{K}$ has the components

$$(k_0,\,0,\,0,\,k), \tag{59}$$

so that the supplementary conditions may be written

$$(k_0\eta_0-k\eta_{III})\,|\rangle=0,\quad(k_0\bar{\eta}_0-k\bar{\eta}_{III})\,|\rangle=0. \tag{60}$$

Let ζ_I, ζ_{II}, ζ_{III} be three operators defined by

$$\eta_I=\zeta_I,\quad\eta_{II}=\zeta_{II},\quad\kappa\eta_{III}/k_0=\zeta_{III}. \tag{61}$$

From Eq. (58) the ζ's satisfy the commutation relations

$$\zeta_M(\mathbf{k}')\bar{\zeta}_N(\mathbf{k}'')-\bar{\zeta}_N(\mathbf{k}'')\zeta_M(\mathbf{k}')$$
$$=-\delta_{MN}(\hbar/4\pi^2)k'_0\delta(\mathbf{k}'-\mathbf{k}'')$$
$$(M,\,N=I,\,II,\,III), \tag{62}$$

and commute with the operators in Eqs. (60).

It can be shown that

$$\sum_{N=I}^{III}\zeta_N\bar{\zeta}_N|\rangle=-\eta_\mu\bar{\eta}^\mu|\rangle \tag{63}$$

for any $|\rangle$ satisfying the supplementary conditions.

[4] W. Pauli, Rev. Mod. Phys. 13, 203 (1941).

In a system of axes S'^* we can define three operators ζ_N' $(N=I, II, III)$ in terms of the operators η_μ' in the same way as in Eq. (61). From the equation

$$\eta_\mu=\alpha_{\mu\nu}\eta'^\nu$$

we obtain

$$\zeta_N|\rangle=\{-\beta_{NI}\zeta_I'-\beta_{NII}\zeta_{II}' -\kappa^{-1}(\beta_{NIII}k'_0-\beta_{NO}k')\zeta_{III}'\}|\rangle \quad (N=I, II), \tag{64}$$

$$\zeta_{III}|\rangle=\kappa k_0^{-1}\{-\beta_{III\ I}\zeta_I'-\beta_{III\ II}\zeta_{II}' -\kappa^{-1}(\beta_{III\ III}k'_0-\beta_{III O}k')\zeta_{III}'\}|\rangle.$$

And from the equation

$$\eta_\mu'=\eta^\nu\alpha_{\nu\mu},$$

we have

$$\zeta_N'|\rangle=\{-\zeta_I\beta_{IN}-\zeta_{II}\beta_{IIN} -\zeta_{III}(k_0\beta_{IIIN}-k\beta_{ON})\kappa^{-1}\}|\rangle \quad (N=I, II), \tag{65}$$

$$\zeta_{III}'|\rangle=\kappa k'^{-1}_0\{-\zeta_I\beta_{I\ III}-\zeta_{II}\beta_{II\ III} -\zeta_{III}(k_0\beta_{III\ III}-k\beta_{OIII})\kappa^{-1}\}|\rangle.$$

It remains for us to show that Eqs. (64) and (65) are equivalent and that the transformation of the ζ's is orthogonal.

For this purpose we have to repeat the study in Section 2, bearing in mind the difference between k_0 and k. Instead of Eqs. (7) and (8) we have now

$$\begin{aligned} &\beta_{IO}k'_0-\beta_{I\ III}k'=0, \quad \beta_{IIO}k'_0-\beta_{II\ III}k'=0,\\ &\beta_{OO}k'_0-\beta_{OIII}k'=k_0, \quad \beta_{IIIO}k'_0-\beta_{III\ III}k'=k. \end{aligned} \tag{66}$$

$$\begin{aligned} &k_0\beta_{OI}-k\beta_{III\ I}=0, \quad k_0\beta_{OII}-k\beta_{III\ II}=0,\\ &k_0\beta_{OO}-k\beta_{IIIO}=k_0', \quad k_0\beta_{OIII}-k\beta_{III\ III}=k'. \end{aligned} \tag{67}$$

From these equations it can be seen that Eqs. (64) and (65) may be written in the form

$$\zeta_N|\rangle=\sum_{M=1}^{III}\gamma_{NM}\zeta_M'|\rangle, \quad (N=I, II, III), \tag{68}$$

$$\zeta_N'=|\rangle=\sum_{M=I}^{III}\zeta_M\gamma_{MN}|\rangle$$

with

$$\begin{bmatrix} \gamma_{I\ I}, & \gamma_{I\ II}, & \gamma_{I\ III} \\ \gamma_{II\ I}, & \gamma_{II\ II}, & \gamma_{II\ III} \\ \gamma_{III\ I}, & \gamma_{III\ II}, & \gamma_{III\ III} \end{bmatrix} = \begin{bmatrix} -\beta_{I\ I}, & -\beta_{I\ II}, & -\kappa k'^{-1}_0\beta_{I\ III} \\ -\beta_{II\ I}, & -\beta_{II\ II}, & -\kappa k'^{-1}_0\beta_{II\ III} \\ -(\kappa/k_0)\beta_{III\ I}, & -(\kappa/k_0)\beta_{III\ II}, & -(\kappa^2/k_0k_0')\beta_{III\ III}+kk'/k_0k'_0 \end{bmatrix}. \tag{69}$$

It can also be shown that the coefficients γ_{MN} satisfy the orthogonality relations

$$\sum_{L=I}^{III}\gamma_{ML}\gamma_{NL}=\sum_{L=I}^{III}\gamma_{LM}\gamma_{LN}=\delta_{MN} \quad (M, N=I, II, III). \tag{70}$$

It is no longer convenient to consider the system of axes S^{**} introduced in Section 2. This system of axes is useful only when $\kappa=0$, in which case the matrix in Eq. (69) reduces to

$$\begin{bmatrix} -\beta_{I\ I}, & -\beta_{I\ II}, & 0 \\ -\beta_{II\ I}, & -\beta_{II\ II}, & 0 \\ 0, & 0, & 1 \end{bmatrix}.$$

I am indebted to Professor P. A. M. Dirac for a comment on this work. I wish also to thank Dr. E. M. Corson for his help in the publication of this paper.

Energy of Beta-Radiation from S^{35} and C^{14}

A. K. SOLOMON, R. G. GOULD, AND C. B. ANFINSEN
Biophysical Laboratory and Department of Biological Chemistry, Harvard Medical School, Boston, Massachusetts

(Received August 18, 1947)

Aluminum-absorption curves have been obtained for C^{14} and S^{35}. The ranges in aluminum, measured as suggested by Feather, are 27.9 ± 0.3 mg/cm² for C^{14} and 31.4 ± 0.5 mg/cm² for S^{35}. The energies deduced from these ranges are 154 ± 4 kev for C^{14} and 167 ± 4 kev for S^{35}. Measurements have also been made of the self-absorption of $BaC^{14}O_3$, yielding an absorption coefficient $\alpha=0.29$.

1. INTRODUCTION

WITH the intense sources of radioactive S^{35} and C^{14} now available from the Atomic Energy Commission, it is possible to assay the maximum energy of the emitted beta-radiation by the absorption method with a high degree of accuracy. Feather[1] has developed the technique of absorption measurements to give precise values of the maximum energy of several beta-emitting isotopes. His method depends upon comparison of the unknown range with the known range (476 mg/cm² of aluminum) and spectrum of RaE, which he chose because it is free from gamma-emission. In particular, the radiation transmitted through aluminum foil from the source being studied is compared with that transmitted by RaE at several absorber thicknesses. In practice the net count per minute from the source is plotted against absorber weight expressed as mg/cm². From the RaE absorption curve, obtained with identical geometry, the percent of RaE radiation transmitted can be obtained at absorber thicknesses chosen as 0.1, 0.2, 0.3 up to 1.0 times the maximum thickness for RaE, i.e., 47.6, 95.2, etc., mg/cm² of aluminum. Then, by comparison with the unknown source, say $BaC^{14}O_3$, the thickness of absorber corresponding to these transmission percentages for C^{14} can be obtained. Finally these values, multiplied by $10/n$, i.e., 10, 5, 3.33, etc., are plotted against n, the number of tenths of absorber. These points lie along a smooth curve called a *Feather plot*, a curve which can easily be extrapolated to a good end point in case the sample is too weak or too gamma-active to permit a complete beta-absorption curve. If the unknown source should have a spectrum identical with that of RaE, the Feather plot would be a straight line, parallel to the abscissa.

2. EXPERIMENTAL DETAILS

A low background thin-window counter sketched in Fig. 1 has been devised for use in these measurements and also for the routine measurement of $BaC^{14}O_3$ samples in biochemical research. Counters of this type give stable low backgrounds; indeed, throughout all the absorption experiments reported here, the average background varied only between 4.3 and 5.3 counts/min. Thin mica windows about 2.0 to 2.5 mg/cm² are sealed onto the counter with

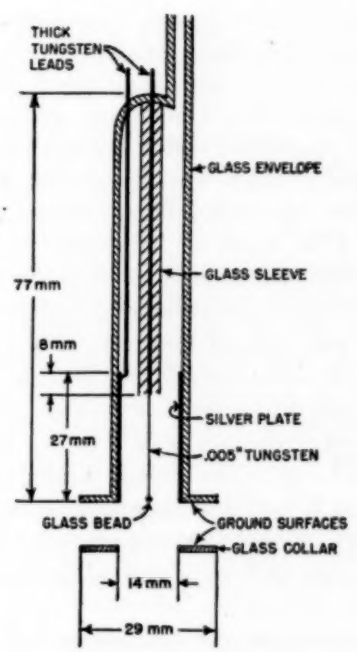

FIG. 1. End-window counter.

[1] Feather, Proc. Camb. Phil. Soc. **35**, 599 (1938).

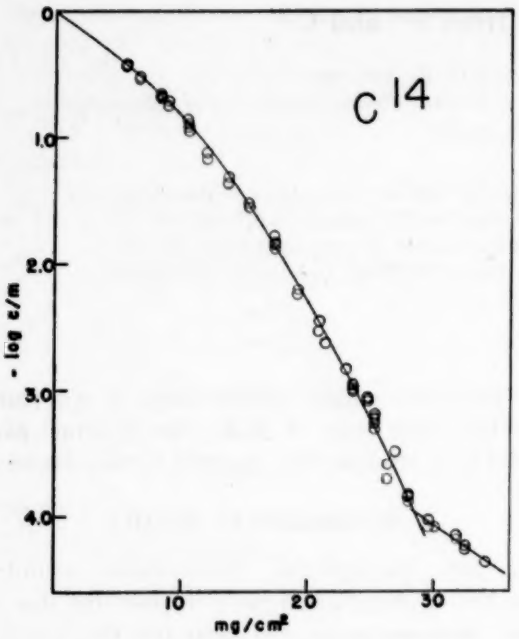

FIG. 2. Absorption of C^{14} by aluminum.

Vinyl-seal AYAB resin in acetone (70 percent).* Using so small an area there would appear to be no difficulty in sealing on windows as thin as 1.0 to 1.5 mg/cm²; in practice we have had more trouble with faulty cementing than with window thickness.

For counting, the samples were placed in thin (0.017 inch) aluminum-stamped cups, which fit into an accurately machined dural slide. The slides in turn were placed on shelves in an accurately machined dural housing. For these experiments a shelf was chosen in which the base of the cup was 2.18 cm below the mica window. This large air gap was required to accommodate the aluminum foils used for the RaE absorption experiments. The whole counting assembly was housed inside a dural-lined lead chamber, one inch in thickness. All three sources, C^{14}, S^{35}, and RaE, were very thin; by visual estimate total weights of 0.1 to 0.5 mg in an area of 3.1 cm². The initial strength of the sources was C^{14}: 13,100 counts/min., S^{35}: 11,800 counts/min., RaE: 8800 counts/min. The contribution due to γ-rays and other unabsorbed contaminants was: C^{14}: 2.5 counts/min., S^{35}: 15 counts/min., RaE: 2.0 counts/min.

For RaE, the visual range in aluminum was found to be 476 mg/cm² in agreement with the value accepted by Feather.[1] The visual ranges for C^{14} and S^{35} are, respectively, 28.5±0.3 mg/cm² and 31.4±0.6 mg/cm²; the data from which these conclusions are drawn are plotted in Figs. 2 and 3. The Feather ranges are 27.9 ±0.3 mg/cm² for C^{14} and 31.4±0.5 mg/cm² for S^{35}; the Feather plots are given in Fig. 4.

3. SELF-ABSORPTION

In the course of biological experiments it is of particular interest to measure self-absorption so that samples of varying weight may be compared exactly. With elements having radiation as soft as those of C^{14} and S^{35}, the self-absorption correction becomes very large even with thin samples. For the biological work and, incidentally, for the determination of self-absorption correction, samples were deposited in stainless-steel cups accurately machined to provide wells measuring 1.4 cm in diameter by 1 mm deep. Initially, considerable difficulty was experienced in forming a $BaC^{14}O_3$ precipitate flat and uniform

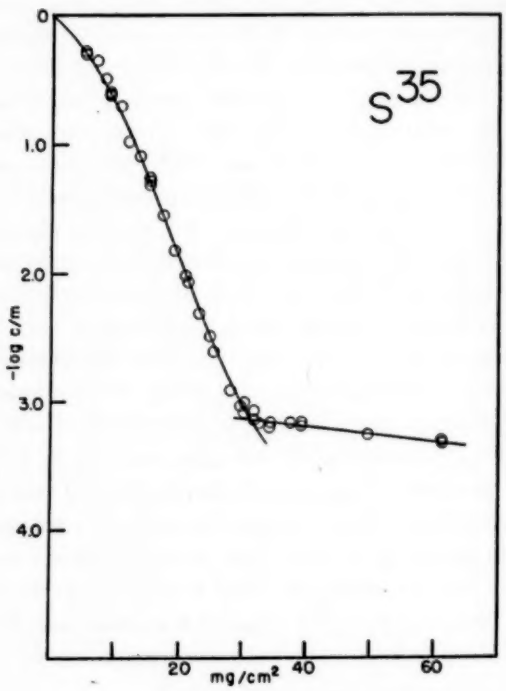

FIG. 3. Absorption of S^{35} by aluminum.

* In order to obtain good seals, it is necessary to let the solvent evaporate almost completely before attaching the mica.

enough to give reproducible counting rates. Finally, we adopted a technique of transferring precipitates by micro-pipette. After precipitation in a 15-ml centrifuge tube, the $BaC^{14}O_3$ is centrifuged. The excess $Ba(OH)_2$ is removed and the precipitate washed by suspension in a mixture of 1 ml of CO_2-free water and 2–3-ml alcohol (to prevent creeping). After centrifugation, the wash solution is poured off and the precipitate drained. The precipitate is then suspended in a few drops of water (less than 0.3 ml) and transferred to the stainless-steel cups with a micro-pipette (an eye dropper with the tip drawn to a capillary). During evaporation to dryness over a hot plate maintained at 45–60°C in a hood, the suspension is stirred with a thin rod to make it more uniform. A set of ten identical measurements showed that this technique gave results reproducible to better than 1.5 percent, including errors in counting. Some effort was made to extend the absorption experiments to densities lower than 1 mg/cm², but it was found that recovery is apparently incomplete when the total amount of solid is less than 1 mg corresponding to a density of 0.65 mg/cm².**

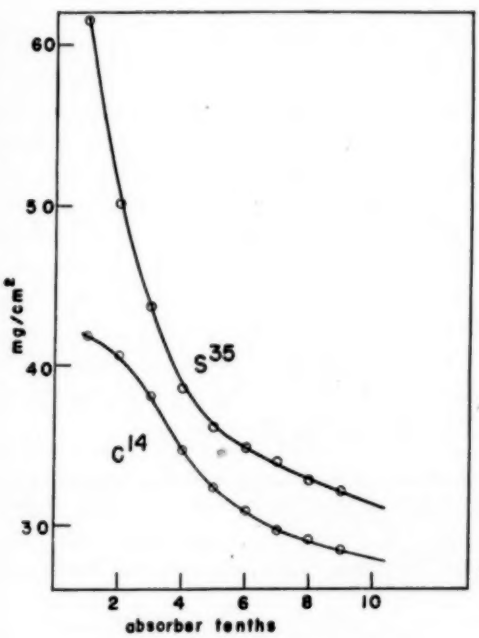

FIG. 4. Feather plot for C^{14} and S^{35}.

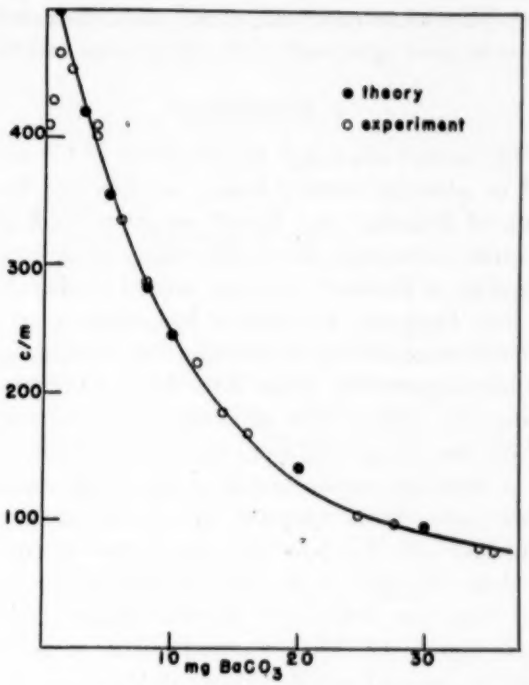

FIG. 5. Self-absorption of $BaC^{14}O_3$.

The simple equation governing self-absorption is given by Henriques[2] *et al.*, and also by Libby.[3] Derived from a simple absorption law, $I = I_0 e^{-\alpha d}$, the self-absorption equation is:

$$I = I_0 \frac{I - e^{-\alpha d}}{\alpha d}$$

where I = intensity transmitted, I_0 = intensity before absorption, α = absorption coefficient, and d = thickness in mg/cm².

The self-absorption results obtained in the course of this research are shown in Fig. 5. With a value of α of 0.29 cm²/mg, a good fit can be obtained from 0.65 mg/cm² to 13.0 mg/cm², a somewhat surprising result in view of the oversimplifications of the theory, and the fact that, as shown in Fig. 2, the absorption of C^{14} electrons in aluminum does not follow a simple exponential

** Note added in proof: I am indebted to L. E. Glendenin for pointing out that this effect is due to a hitherto unpublished phenomenon called "self-scattering." Apparently, sizable precipitates of the order of 5% of maximum range expressed as mg/cm²—exert a focussing effect on the beta particles, and scatter more particles up and down at the expense of those that emerge in a horizontal direction, thereby increasing the counting rate of the source. A. K. S.

[2] Henriques, Kistiakowsky, Margnetti, and Schneider, Ind. and Eng. Chem. (Anal. Ed.) 18, 349 (1946).

[3] Libby, Ind. Eng. Chem. (Anal. Ed.) 19, 2 (1947).

law. Yankwich[4] obtains a value of 0.285 ± 0.008 for α in good agreement with the present results.

4. DISCUSSION

To convert the range in aluminum of C^{14} and S^{35} to absolute energy values is difficult. The data of Marshall and Ward[5] on monoenergetic electron absorption cover this range, though the equation of Feather[1] does not extend to energies so low. However, Glendenin[6] has constructed a smooth empirical curve covering the whole range of beta-absorption, from 0.01 Mev to 3 Mev using the values from monoenergetic electrons in the low range and beta-particles determined in a beta-ray spectrograph in the high range. This curve flows smoothly from the data of Marshall and Ward for monoenergetic electrons to data obtained with beta-ray spectrometers, and does not leave the Marshall-Ward curve until above 0.5 Mev. Consequently, it seems valid to assign from the Marshall-Ward curve a value of 154 ± 4 kev for C^{14} and 167 ± 4 kev for S^{35}.

The value for C^{14} is in good agreement with the original absorption limit of 145 ± 15 kev given by Ruben and Kamen.[7] The recent report of Stephens and Lewis[8] gives a value of 150 ± 20 kev determined by the beta-ray spectrometer, also in good agreement as is the value of 154 kev obtained by Levy.[9] The S^{35} value differs by more than the experimental error from the value of 107 ± 20 kev given by Libby and Lee,[10] but is in better agreement with Kamen's[11] determination of 120 ± 15 kev. Recent unpublished work by Osborne[12] gives a beta-ray spectrometer value of 169 ± 3 kev in good agreement with the result given here.

Since the experimentally determined self-absorption curve follows a simple exponential closely, it is tempting to try to correlate the self-absorption coefficient obtained for $BaC^{14}O_3$ with the aluminum-absorption coefficient for C^{14}. Such a comparison should be valid since, as is well-known, the composition of the absorber is of small importance in these low energy regions, where density of absorber is the major factor. However, examination of Fig. 2 shows that in the case of C^{14} no single unequivocal absorption coefficient can be picked since the aluminum absorption is so far from exponential. In the case of S^{35}, the aluminum absorption is more nearly exponential, and an absorption coefficient, $\alpha = 0.29$ can be obtained in good agreement with the value of 0.27 given by Henriques[13] for S^{35}.

The radical difference in shape between the absorption curves for S^{35} and C^{14} is immediately apparent from Figs. 2, 3 and 4. This difference may well be attributed to the difference in the forbidden characters of the transitions, as evidenced by the great difference between the 87.1-day half-life[14] of S^{35} and the 4700-year half-life[15] of C^{14}.

In spite of this difference, the values for α are remarkably uniform, and it is probable that the equation proposed by Libby[3] that $\alpha l_0 = k$, where l_0 is the maximum range, and k is a constant, can serve as a guide to the estimation of α. From this research, the value of k would appear to be 8.6, higher than the value of $k = 5$ chosen by Libby from earlier data on the S^{35} range.

This work has been supported with funds from the Office of Naval Research under contract N5ori-76. The authors wish to express their appreciation to Miss Jacqueline Becker for her assistance in making the counts.

[4] Yankwich, private communication.
[5] Marshall and Ward, Can. J. Research **15**, 29 (1939).
[6] L. E. Glendenin, private communication; Glendenin and Coryell, report at American Chem. Soc. Meeting, Atlantic City, April, 1946.
[7] Ruben and Kamen, Phys. Rev. **59**, 349 (1941).
[8] Stephens and Lewis, Bull. Am. Phys. Soc. **22**, 6 (1947).
[9] Levy, Phys. Rev. **72**, 248 (1947).
[10] Libby and Lee, Phys. Rev. **55**, 245 (1939).
[11] Kamen, Phys. Rev. **60**, 537 (1941).
[12] R. K. Osborne, private communication.
[13] Henriques, private communication. Results obtained for benzidine sulfate absorption with counter with mica window 1.8 mg/cm² thick.
[14] Seaborg, Rev. Mod. Phys. **16**, 4 (1944).
[15] Reid, Dunning, Weinhouse, and Von Grosse, Phys. Rev. **70**, 431 (1946).

Anomalous Values of Certain of the Fine Structure Lines in the Ammonia Microwave Spectrum

HARALD H. NIELSEN
Mendenhall Laboratory of Physics, Ohio State University, Columbus, Ohio

AND

DAVID M. DENNISON
Randall Laboratory of Physics, University of Michigan, Ann Arbor, Michigan

(Received August 18, 1947)

The anomalous positions in the microwave spectrum of ammonia of the lines originating with the rotational levels $K=3$ are explained on the basis of a K-type splitting of these levels. The splitting is due to a fourth-order perturbation originating with the first-order correction terms to the moments of inertia, $I_{zz}^{(a)}=I_{yy}^{(a)}$, and the first-order coriolis correction terms. The Pauli exclusion principle permits only one of the two components to be present. Thus in the lower vibration state when J is even only the lower component of the levels $K=3$ is present, but when J is odd only the upper component is permitted. Similarly, for the upper vibration state when J is even only the upper component of the levels $K=3$ may exist while for J odd only the lower component may exist. Since in this spectrum $\Delta J=\Delta K=0$, the lines originating in levels where J is even will be displaced to shorter wave-lengths, while the lines originating in levels where J is odd will be displaced to longer wave-lengths. The agreement between computed shifts and measured shifts is satisfactory.

1. INTRODUCTION

RECENT measurements[1] of the microwave spectrum of ammonia gas have shown that the lines may be correlated by means of an empirical formula containing the rotational quantum numbers J and K. The simplest form of function consists of a power-series development in the variables J^2+J and K^2. It is found that such a formula will account accurately for the positions of nearly all of the lines, the exceptions being those lines originating in levels where the number K is equal to 3. (The line $J=6$, $K=6$ seems also to deviate from its predicted position. The reason for the anomaly of this single line is at present obscure.) When J is even and $K=3$, the observed line possesses a higher frequency than that predicted by the empirical formula, while when J is odd it has a lower frequency. The magnitude of the deviation increases steadily as J increases. The effect occurs in the spectrum of $N^{15}H_3$ as well as in that of $N^{14}H_3$ and the lines are displaced by nearly the same amount. It is, therefore, clearly a property of the molecule and not of the nitrogen nucleus.

The qualitative explanation of the phenomenon may be readily understood and has been discussed by us in an earlier communication.[2] It is well known that the rotational levels for which $K\neq 0$ are each double corresponding to the two wave functions (that part depending upon φ, the angle of rotation about the symmetry axis) $e^{iK\varphi}$ and $e^{-iK\varphi}$. The wave functions for the levels where K is not a multiple of 3 possess a mixed symmetry denoted by the symbol E. It has been rigorously proved that no perturbation, providing it has threefold symmetry, can ever remove the degeneracy of such a pair of levels. Since the three protons in NH_3 are identical particles, no perturbation whose origin lies within the ammonia molecule itself can split these levels apart.

When $K\neq 0$ and is a multiple of 3, the symmetry classification is quite different. One of the two originally coincident levels will be symmetrical (denoted by A_1) for an interchange of any two of the protons while the other is anti-

[1] W. E. Good and D. K. Coles, Phys. Rev. 71, 383 (1947); M. W. P. Strandberg, R. Kyhl, T. Wentink, Jr., and R. E. Hilliger, Phys. Rev. 71, 639 (1947); B. Bleaney and R. P. Pinrose, Nature 157, 339 (1946). We are also indebted to Dr. Good and Dr. Coles for the numerical results stated in this work which were sent to us in a private communication.

[2] H. H. Nielsen and D. M. Dennison, Phys. Rev. 72, 86 (1947).

symmetric (denoted by A_2). A perturbation having the threefold symmetry is able to undegenerate the levels and split them apart. The source of a perturbation having the threefold symmetry lies in the fact that the Hamiltonian is not separable, except in zero-order approximation, into one part containing rotational coordinates only and a second part containing vibrational coordinates only. It is customary to express the Hamiltonian by means of a series expansion. All orders, with the exception of the zero-order, contain both sets of coordinates and hence constitute an interaction between vibration and rotation. Since these functions are derived from the properties of the molecule itself, they must necessarily possess threefold symmetry about the axis of the molecule.

For the lowest of the vibration states and for J odd, it will be shown that the perturbation separates the two levels where $K=3$ and that the upper member of the pair has the antisymmetrical character A_2 while the lower one is symmetrical or A_1. For the next higher vibration state (these two vibration states constitute the levels giving rise to the microwave spectrum) the situation is reversed, the upper level being A_1 and the lower A_2. From the Pauli principle and from the fact that the nuclear-spin wave functions of three protons have the symmetry characters A_1 and E, but not A_2, it is evident that the states which are A_1 as regards vibration and rotation will not exist, whereas the A_2 states will. Thus the transition $J\rightarrow J$, $K=3\rightarrow K=3$ will consist of a single line. The displacement of this line from its expected position will be just equal to the splitting of one of the levels caused by the threefold perturbation. (It should be remarked that in the microwave spectrum of ND_3, the lines of $K=3$ will not be displaced, but will consist of doublets. In the case of NDH_2 or ND_2H every line will be doubled with the exception of those where $K=0$. This splitting occurs already in zero-order and is a consequence of the fact that these molecules are asymmetric rotators.)

2. QUALITATIVE CONSIDERATIONS

Certain qualitative features of the perturbation may be obtained easily. The perturbed energy levels will be computed in the usual manner by seeking the roots of the determinant

$$|(J,K|H|J',K')-E\delta_{JJ'}\delta_{KK'}|=0,$$

where $(J,K|H|J',K')$ are the elements of the perturbed Hamiltonian expressed through the wave functions of the unperturbed system (i.e., the zero-order Hamiltonian). The problem is greatly simplified by three facts. (1) $(J,K|H|J',K')=0$ unless $J=J'$ (i.e., H is diagonal in J) and consequently the originally infinite determinant factors into a product of determinants each with its own value of J. (2) From the symmetry considerations given earlier $(J,K|H|J,K')=0$ unless $K-K'$ is a multiple of 3. (3) Since the only levels which can possibly be split by a threefold perturbation are those where K itself is a multiple of 3, it will not be necessary to consider any of the other levels. As an example consider the case when J is equal to 3, 4 or 5. The determinant reduces to:

$$\begin{vmatrix} A-E & b & a \\ b & B-E & b \\ a & b & A-E \end{vmatrix}=0 \qquad (1)$$

in which the quantities A and B are, respectively, $(J,3|H|J,3)$ and $(J,0|H|J,0)$. They are large since these elements contain the zero-order terms. a and b are $(J,3|H|J,-3)$ and $(J,3|H|J,0)$ and are small quantities produced by the perturbing terms.

It has been shown by Shaffer[3] that for a molecule of the ammonia type, the first contributions which can be made to a and b are of third order. It will appear later from the analysis that in the case of a, the first non-vanishing contribution comes from the fourth-order perturbation.

The roots of the secular determinant may be designated as E_3^+, E_3^- and E_0. E_3^+ and E_3^- are very close together and differ only slightly from A, while E_0 is nearly equal to B. An elementary study of the determinant shows that E_3^+-A or E_3^--A will depend upon a to the first power but only upon b^2 as well as upon higher powers of a and b. Since b is already at least a third-order term, its influence upon E_3^+ and E_3^- will be, at best, only of sixth order. It may therefore

[3] W. H. Shaffer, J. Chem. Phys. 9, 607 (1941).

be neglected.[4] In that case the determinant becomes very simple and the two roots are,

$$E_3^+ = A + a, \quad E_3^- = A - a. \tag{2}$$

The stabilized wave functions (those parts depending upon φ) for E_3^+ and E_3^- are, respectively, $\psi_3^+ = (e^{3i\varphi} + e^{-3i\varphi})$ and $\psi_3^- = (e^{3i\varphi} - e^{-3i\varphi})$. The symmetry properties of these wave functions may be readily obtained by performing a transformation in which two of the hydrogen nuclei are interchanged.[5] It is found that when J is an even integer ψ_3^+ is symmetrical (has the character A_1) and ψ_3^- is antisymmetrical, or A_2. If J is odd, the symmetries are interchanged and ψ_3^+ is A_2 while ψ_3^- is A_1.

It has already been pointed out that the wave functions of the protons have characters A_1 and E, but not A_2. The total wave function must be antisymmetric or A_2. Thus for the lower of the pair of vibrational states giving rise to the inversion frequency and for J even, only the state defined by the wave function ψ_3^- exists. For the higher of the two vibrational levels only ψ_3^+ exists. The observed absorption line will therefore be displaced towards *higher* frequencies by the amount $2a$. The analysis will show that a is a positive quantity and is a function of J. In a similar fashion one can show that when J is odd the observed line will be displaced towards *lower* frequencies. These qualitative results are in complete agreement with the experimental observations.

3. ANALYSIS OF THE SPLITTING OF LEVELS WHERE $K=3$

The problem of the vibration-rotation energies of the pyramidal XY_3 molecule has been studied by Shaffer[3] who expanded the quantum-mechanical Hamiltonian to include second-order terms and evaluated relations for the energies to this approximation. As has been mentioned, Shaffer demonstrated that to second order the energy matrix contained elements only along the principal diagonal. This is equivalent to stating that to this order the molecule remains a symmetric rotator and that none of the degeneracies in K are removed. It is therefore necessary in our case to investigate the energies to approximations beyond the second. We have, moreover, seen that no degeneracies in K except for those states where K is an integer equal to a multiple of 3 can be removed by any perturbation which lies within the molecule itself. It is only necessary to consider, therefore, the elements $(K=\pm 3 \,|\, K=\mp 3)$ to the energy in a given approximation. It has been pointed out that elements of the kind $(K=\pm 3 \,|\, K=0)$ may be neglected, since they can only introduce exceedingly high order terms. Since the expansion of the quantum-mechanical Hamiltonian contains the angular-momentum operators at most quadratically in any approximation the elements $(K=\pm 3 \,|\, K=\mp 3)$ cannot arise before in third order of approximation. It is readily shown that these will be equal in nth order to:

$$\begin{aligned}
&(\tau, K=\pm 3 \,|\, H^{(n)} \,|\, \tau, K=\mp 3) \\
&= \sum_{\tau'} \sum_{\tau''} \cdots \sum_{\tau^{(n-1)}} \frac{(\tau, K=\pm 3 \,|\, H^{(1)} \,|\, \tau', K')(\tau' K' \,|\, H^{(1)} \,|\, \tau'' K'') \cdots (\tau^{(n-1)} K^{(n-1)} \,|\, H^{(1)} \,|\, \tau, K=\mp 3)}{(hc)^{n-1} \omega(\tau, \tau') \omega(\tau, \tau'') \cdots \omega(\tau, \tau^{(n-1)})} \\
&+ \sum_{\tau'} \sum_{\tau''} \cdots \sum_{\tau^{(n-2)}} \frac{(\tau, K=\pm 3 \,|\, H^{(2)} \,|\, \tau', K')(\tau' K' \,|\, H^{(1)} \,|\, \tau'', K'') \cdots (\tau^{(n-2)} K^{(n-2)} \,|\, H^{(1)} \,|\, \tau, K=\mp 3)}{(hc)^{n-2} \omega(\tau, \tau') \omega(\tau, \tau'') \cdots \omega(\tau, \tau^{(n-2)})} \\
&+ \sum_{\tau'} \sum_{\tau''} \cdots \sum_{\tau^{(n-2)}} \frac{(\tau, K=\pm 3 \,|\, H^{(1)} \,|\, \tau', K')(\tau', K' \,|\, H^{(2)} \,|\, \tau'', K'') \cdots (\tau^{(n-2)} K^{(n-2)} \,|\, H^{(1)} \,|\, \tau, K=\mp 3)}{(hc)^{n-2} \omega(\tau, \tau') \omega(\tau, \tau'') \cdots \omega(\tau, \tau^{(n-2)})} + \cdots \\
&+ \sum_{\tau'} \sum_{\tau''} \cdots \sum_{\tau^{(n-2)}} \frac{(\tau, K=\pm 3 \,|\, H^{(1)} \,|\, \tau', K')(\tau', K' \,|\, H^{(1)} \,|\, \tau'', K'') \cdots (\tau^{(n-2)} K^{(n-2)} \,|\, H^{(2)} \,|\, \tau, K=\mp 3)}{(hc)^{n-2} \omega(\tau, \tau') \omega(\tau, \tau'') \cdots \omega(\tau, \tau^{(n-2)})} + \cdots,
\end{aligned} \tag{3}$$

where τ is made to embrace all the vibration quantum numbers.

[4] Although our example was for $J=3$, 4 or 5 in order not to introduce the complication of K equalling higher multiples of 3, it is evident that the argument may be extended to include any value of J.

[5] The total wave function is a product of the vibrational wave function ψ_v and a rotational wave function containing the quantum numbers J, K, and M. Since the symmetry cannot depend upon the magnetic quantum number M it

Shaffer made use of a method whereby the quantum-mechanical Hamiltonian is transformed by a contact transformation such that the first order transformed Hamiltonian, $H^{(1)\prime}$, will contain no terms to second order except the coriolis terms arising from the twofold degenerate oscillations. He does not, therefore, state explicitly the quantum-mechanical Hamiltonian before transformation, but gives only the first- and second-order transformed Hamiltonians. Since these are good only to second order it becomes necessary here to expand the quantum-mechanical Hamiltonian to the second order of approximation. This may be accomplished by using the method of Howard and Wilson,[6] or what is actually simpler, the method of Nielsen[7] for the general polatomic molecule.

Retaining the notation of Shaffer except in minor respects we obtain

$$H^{(0)}=(\hbar/2)\{\sum_{i=1,3}\lambda_i^{\frac{1}{2}}(p_i^2/\hbar^2+q_i^2)+\sum_{k=2,4}\lambda_k^{\frac{1}{2}}(p_{k,1}^2/\hbar^2+p_{k,2}^2/\hbar^2+q_{k,1}^2+q_{k,2}^2)\}$$
$$+(1/2)\{(P_x^2+P_y^2)/I_{xx}^{(e)}+(P_z^2/I_{zz}^{(e)})\}, \quad (4a)$$

$$H^{(1)}=\cdots-\{\sum_{i=1,2}\sum_{k=2,4}\xi_{ik}[(\omega_i/\omega_k)^{\frac{1}{2}}q_{k,2}p_i-(\omega_k/\omega_i)^{\frac{1}{2}}q_ip_{k,2}]+\xi_{24}[(\omega_2/\omega_4)^{\frac{1}{2}}(q_{4,2}p_{2,1}+q_{4,1}p_{2,2})$$
$$-(\omega_4/\omega_2)^{\frac{1}{2}}(q_{2,1}p_{4,2}+q_{2,2}p_{4,1})]\}(P_x/I_{xx}^{(e)})+\{\sum_{i=1,3}\sum_{k=2,4}\xi_{ik}[(\omega_i/\omega_k)^{\frac{1}{2}}q_{k,1}p_i-(\omega_k/\omega_i)^{\frac{1}{2}}q_ip_{k,1}]$$
$$-\xi_{2,4}[(\omega_2/\omega_4)^{\frac{1}{2}}(q_{4,1}p_{2,1}-q_{4,2}p_{2,2})-(\omega_4/\omega_2)^{\frac{1}{2}}(q_{2,1}p_{4,1}-q_{2,2}p_{4,2})]\}(P_y/I_{xx}^{(e)})$$
$$-\tfrac{1}{2}\sum_{i=1,3}(\hbar^2/\lambda_i)^{\frac{1}{2}}\{2[(I_{xx}^{(e)}-\tfrac{1}{2}I_{zz}^{(e)})^{\frac{1}{2}}\alpha_i-\tfrac{1}{2}\beta_i(I_{zz}^{(e)})^{\frac{1}{2}}](P_x^2+P_y^2)/(I_{xx}^{(e)})^2\}q_i$$
$$+\tfrac{1}{2}\sum_{k=2,4}(\hbar^2/\lambda_k)^{\frac{1}{2}}\{(I_{zz}^{(e)})^{\frac{1}{2}}\delta_k(P_x^2-P_y^2)/(I_{xx}^{(e)})^2\}q_{k,1}$$
$$-\tfrac{1}{2}\sum_{k=2,4}(\hbar^2/\lambda_k)^{\frac{1}{2}}\{(I_{zz}^{(e)})^{\frac{1}{2}}\delta_k(P_xP_y+P_yP_x)/(I_{xx}^{(e)})^2\}q_{k,2}$$
$$+\tfrac{1}{2}\sum_{k=2,4}(\hbar^2/\lambda_k)^{\frac{1}{2}}\{(2I_{zz}^{(e)})^{\frac{1}{2}}(1-I_{zz}^{(e)}/2I_{xx}^{(e)})\delta_{k'}(P_yP_z+P_zP_y)/(I_{xx}^{(e)})(I_{zz}^{(e)})\}q_{k,2}$$
$$+\tfrac{1}{2}\sum_{k=2,4}(\hbar^2/\lambda_k)^{\frac{1}{2}}\{(2I_{zz}^{(e)})^{\frac{1}{2}}(1-I_{zz}^{(e)}/2I_{xx}^{(e)})\delta_{k'}(P_zP_x+P_xP_z)/(I_{xx}^{(e)})(I_{zz}^{(e)})\}q_{k,1}+V_1, \quad (4b)$$

$$H^{(2)}=\cdots\tfrac{1}{2}\{\sum_{k=2,4}(\hbar^4/\lambda_k^2)^{\frac{1}{2}}(3\delta_k^2I_{zz}^{(e)}/4I_{xx}^{(e)})(q_{k,1}^2+q_{k,2}^2)+3\sum_{i=1,3}(\hbar^4/\lambda_i^2)^{\frac{1}{2}}[(1-(I_{zz}^{(e)}/2I_{xx}^{(e)})^{\frac{1}{2}})\alpha_i$$
$$-(\beta_i/\sqrt{2})(I_{zz}^{(e)}/2I_{xx}^{(e)})^{\frac{1}{2}}]^2q_i^2\}(P_x^2+P_y^2)/(I_{xx}^{(e)})^2-\tfrac{1}{2}\{\textstyle\sum_k(\hbar^4/\lambda_k^2)^{\frac{1}{2}}[\delta_k^2-3(I_{zz}^{(e)}/2I_{xx}^{(e)})\delta_{k'}^2$$
$$+4(I_{zz}^{(e)}/2I_{xx}^{(e)})^2\delta_{k'}^2-(I_{zz}^{(e)}/2I_{xx}^{(e)})^2\delta_{k'}^4-(1+(I_{zz}^{(e)}/2I_{xx}^{(e)})^2)\delta_k\delta_{k'}-\delta_k^4](q_{k,1}^2+q_{k,2}^2)$$
$$-3\textstyle\sum_i(\hbar^4/\lambda_k^2)^{\frac{1}{2}}\alpha_iq_i^2\}(P_z/I_{zz}^{(e)})^2+\tfrac{1}{2}\textstyle\sum_k(\hbar^4/\lambda_k^2)^{\frac{1}{2}}\{2\delta_{k'}^2(1-I_{zz}^{(e)}/2I_{xx}^{(e)})q_{k,1}^2$$
$$-[\delta_{k'}^2(I_{zz}^{(e)}/2I_{xx}^{(e)})-(\xi_{k,1}^2+\xi_{k,3}^2)]q_{k,2}^2\}(P_z/I_{xx}^{(e)})^2+\tfrac{1}{2}\textstyle\sum_k(\hbar^4/\lambda_k^2)^{\frac{1}{2}}$$
$$\times\{2\delta_{k'}^2(1-I_{zz}^{(e)}/2I_{xx}^{(e)})q_{k,2}^2-[\delta_{k'}^2(I_{zz}^{(e)}/2I_{xx}^{(e)})-(\xi_{k,1}^2+\xi_{k,3}^2)]q_{k,1}^2\}(P_y/I_{xx}^{(e)})^2$$
$$-\tfrac{1}{2}\sum_{k=2,4}(\hbar^4/\lambda_k^2)^{\frac{1}{2}}\{2\delta_{k'}^2(1-I_{zz}^{(e)}/2I_{xx}^{(e)})+[\delta_{k'}^2(I_{zz}^{(e)}/2I_{xx}^{(e)})-(\xi_{k,1}^2+\xi_{k,3}^2)]\}$$
$$\times q_{k,1}q_{k,2}(P_xP_y+P_yP_x)/(I_{xx}^{(e)})^2+V_2+\cdots. \quad (4c)$$

To test the relation H against computational errors, we may specialize it for the case of the planar XY_3 model by letting the height of the pyramid go to zero, i.e., then $I_{zz}^{(e)}=2I_{xx}^{(e)}$. Inspection reveals that (4) reduces to the relations (14) in the work of Silver and Shaffer.[8]

will be convenient to chose $M=0$. In that case, one has $\Psi=\psi_v\sin^3\theta F(\cos\theta)f(\varphi)$. When J is even, $F(\cos\theta)$ is an odd function of $\cos\theta$ while for J odd it is even. For the level E_3^+, $f(\varphi)=\cos3\varphi$ while for E_3^-, $f(\varphi)=\sin3\varphi$. The process of interchanging two of the protons may be accomplished through the following steps. (1) Invert the molecule. For the lowest of the vibrational levels $\psi_v\rightarrow\psi_v$ while for the higher one $\psi_v\rightarrow-\psi_v$. (2) Let $\theta\rightarrow\pi-\theta$. Clearly $F\rightarrow-F$ when J is even and $F\rightarrow F$ when J is odd. (3) Let $\varphi\rightarrow\pi-\varphi$. In this process $\cos3\varphi\rightarrow-\cos3\varphi$, but $\sin3\varphi\rightarrow\sin3\varphi$. (4) Let $\psi\rightarrow\pi+\psi$. The angle ψ is the third Eulerian angle and does not appear in the wave functions since M has been set equal to zero.

[6] E. B. Wilson, Jr. and J. B. Howard, J. Chem. Phys. **4**, 262 (1936).

[7] H. H. Nielsen, Phys. Rev. **60**, 794 (1941).

[8] S. Silver and W. H. Shaffer, J. Chem. Phys. **9**, 599 (1941).

It is convenient to replace the coordinates $q_{k,1}$ and $q_{k,2}$ by $r_k \cos\chi_k$ and $r_k \sin\chi_k$, respectively, and the conjugate momenta, $p_{k,1}$ and $p_{k,2}$, by their equivalents $(\cos\chi_k p_{r_k} - (\sin\chi_k/r_k)p_{\chi_k})$ and $(\sin\chi_k p_{r_k} + (\cos\chi_k/r_k)p_{\chi_k})$ where $p_{r_k} = -i\hbar\partial/\partial r_k$ and $p_{\chi k} = -i\hbar\partial/\partial\chi_k$. When this is accomplished the relations become:

$$H_0 = (\hbar/2)\{\sum_{i=1,3}\lambda_i^{\frac{1}{2}}(p_i^2/\hbar^2+q_i^2)+\sum_{k=2,4}\lambda_k^{\frac{1}{2}}[((1/r_k)p_{r_k}r_k p_{r_k})/\hbar^2+(p_{\chi_k}^2/r_k^2)+r_k^2]\}$$
$$+(1/2)\{(P_x^2+P_y^2)/I_{xx}^{(e)}+(P_z^2/I_{zz}^{(e)})\}, \quad (5a)$$

$$H_1 = \cdots\{\sum_{\substack{i=1,3\\k=2,4}}(i\xi_{ik}/2)e^{i\chi_k}[(\omega_i/\omega_k)^{\frac{1}{2}}r_k p_i-(\omega_k/\omega_i)^{\frac{1}{2}}q_i(p_{r_k}+ip_{\chi_k}/r_k)]$$
$$-(i\xi_{2,4}/2)e^{-i(\chi_2+\chi_4)}[(\omega_2/\omega_4)^{\frac{1}{2}}r_4(p_{r_2}-ip_{\chi_2}/r_2)-(\omega_4/\omega_2)^{\frac{1}{2}}r_2(p_{r_4}-ip_{\chi_4}/r_4)]\}(P_x-iP_y)/I_{xx}^{(e)}$$
$$-\{\sum_{\substack{i=1,3\\k=2,4}}(i\xi_{ik}/2)e^{-i\chi_k}[(\omega_i/\omega_k)^{\frac{1}{2}}r_k p_i-(\omega_k/\omega_i)^{\frac{1}{2}}q_i(p_{r_k}-ip_{\chi_k}/r_k)]+(i\xi_{2,4}/2)e^{i(\chi_2+\chi_4)}$$
$$\times[(\omega_2/\omega_4)^{\frac{1}{2}}r_4(p_{r_2}+ip_{\chi_2}/r_2)-(\omega_4/\omega_2)^{\frac{1}{2}}r_2(p_{r_4}+ip_{\chi_4}/r_4)]\}(P_x+iP_y)/I_{xx}^{(e)}$$
$$-(\hbar^{\frac{1}{2}}/2)\{\sum_{i=1,3}2[(I_{xx}^{(e)}-\tfrac{1}{2}I_{zz}^{(e)})\alpha_i-\tfrac{1}{2}\beta(I_{zz}^{(e)})^{\frac{1}{2}}](q_i/\lambda_i^{\frac{1}{2}})\}(P_x^2+P_y^2)/(I_{xx}^{(e)})^2$$
$$+(\hbar^{\frac{1}{2}}/4)(I_{zz}^{(e)})^{\frac{1}{2}}\{\sum_{k=2,4}(\delta_k/\lambda_k^{\frac{1}{2}})r_k e^{i\chi_k}(P_x+iP_y)^2/(I_{xx}^{(e)})^2+\sum_{k=2,4}(\delta_k/\lambda_k^{\frac{1}{2}})r_k e^{-i\chi_k}(P_x-iP_y)^2/(I_{xx}^{(e)})^2\}$$
$$+(\hbar^{\frac{1}{2}}/4)(2I_{xx}^{(e)})^{\frac{1}{2}}(1-I_{zz}^{(e)}/2I_{xx}^{(e)})\{(\gamma_k/\lambda_k^{\frac{1}{2}})r_k e^{i\chi_k}[(P_x-iP_y)P_z+P_z(P_x-iP_y)]/(I_{xx}^{(e)})(I_{zz}^{(e)})\}$$
$$+(\hbar^{\frac{1}{2}}/4)(2I_{xx}^{(e)})^{\frac{1}{2}}(1-I_{zz}^{(e)}/2I_{xx}^{(e)})\{(\gamma_k/\lambda_k^{\frac{1}{2}})r_k e^{-i\chi_k}$$
$$\times[(P_x+iP_y)P_z+P_z(P_x+iP_y)]/(I_{xx}^{(e)})(I_{zz}^{(e)})\}^9+V_1+\cdots, \quad (5b)$$

$$H_2 = \cdots(\sum_{i=1,3}a_i q_i^2+\sum_{k=2,4}a_k r_k^2)(P_x^2+P_y^2)/(I_{xx}^{(e)})^2+(\sum_{i=1,3}b_i q_i^2+\sum_{k=2,4}b_k r_k^2(P_z/I_{zz}^{(e)})^2$$
$$+\tfrac{1}{4}\sum_{k=2,4}(\hbar^4/\lambda_k^2)^{\frac{1}{2}}r_k^2 e^{2i\chi_k}[(3\gamma_k^2/4)(1-I_{zz}^{(e)}/2I_{xx}^{(e)})][(P_x+iP_y)^2/(I_{xx}^{(e)})^2]$$
$$+\tfrac{1}{4}\sum_{k=2,4}(\hbar^4/\lambda_k^2)^{\frac{1}{2}}r_k^2 e^{-2i\chi_k}[(3\gamma_k^2/4)(1-I_{zz}^{(e)}/2I_{xx}^{(e)})][(P_x-iP_y)^2/(I_{xx}^{(e)})^2]+V_2+\cdots, \quad (5c)$$

In the foregoing relations the constants α_1 and β_1 take the values α and β, respectively, defined by Eqs. (10) in reference (3), while α_3 and β_3 take the values β and $-\alpha$, respectively. Similarly, δ_2 and γ_2 assume the values δ and γ in Shaffer's notation and δ_4 and γ_4 take the values $-\gamma$ and δ, respectively. The subscripts k and k' take the values 2 and 4, but $k \neq k'$. The quantities a_i, b_i, etc., are constants which we shall not state explicitly since they do not enter the final result.

It is readily verified that $H^{(1)}$ will have non-vanishing matrix components of the kind

$$(v_i, v_k, l_k, v_{k'}, l_{k'}, K | v_i \pm 1, v_k \pm 1, l_k \pm 1, v_{k'}, l_{k'}, K \pm 1),$$
$$(v_i, v_k, l_k, v_{k'}, l_{k'}, K | v_i, v_k \pm 1, l_k \pm 1, v_{k'} \pm 1, l_k \pm 1, K \mp 1),$$
$$(v_i, v_k, l_k, v_{k'}, l_{k'}, K | v_i, v_k \pm 1, l_k \pm 1, v_{k'}, l_{k'}, K \mp 2),$$

and

$$(v_i, v_k, l_k, v_{k'}, l_{k'}, K | v_i', v_{k'}', l_{k'}', v_{k'}', l_{k'}', K)$$

where l_k is a quantum number characterizing the angular momentum associated with the degenerate vibration ω_k and has the values $v_k, v_k-2, \cdots 1$ or 0. The last type of matrix component stated above originates with the potential energy terms V_1 which is given by Shaffer, but is not stated explicitly here. Except for the first two terms, which are diagonal in K and therefore of no interest here, the

[9] The last two terms in Eq. (5b) may be neglected from here on. They have matrix components of the same kind as the first term in (5b) but are of the order $(B_e/\omega_k)^{\frac{1}{2}}$ times these. The factor $(B_e/\omega_k)^{\frac{1}{2}}$ is, of course, small.

non-vanishing matrix components of H_2 are the following:

$$(v_i, v_k, l_k, v_{k'}, l_{k'}, K|v_i, v_k\pm 2, l_k\pm 2, v_{k'}, l_{k'}, K\pm 2),$$
$$(v_i, v_k, l_k, v_{k'}, l_{k'}, K|v_i, v_k, l_k\pm 2, v_{k'}, l_{k'}, K\pm 2)$$

and $(v_i, v_k, l_k, v_{k'}, l_{k'}, K|v_i', v_k', l_k, v_{k'}', l_{k'}, K)$, the last of these originating with the quartic terms of the potential-energy function.

We are interested in making the computations indicated here only for the normal-vibration state, i.e., where the vibration quantum numbers v_i, v_k, l_k are all equal to zero. To make the calculation for states beyond the normal state would be so laborious as to be hardly practicable and it is doubtful, moreover, that the analysis presented here would be valid in higher states. If the relation (3) is specialized for the case where $n=3$ (i.e., third approximation) it is readily seen that only the first term may yield matrix elements of the kind $(v_i, v_k, l_k, v_{k'}, l_{k'}, K=\pm 3|H^{(3)}|v_i', v_k', l_k', v_{k'}', l_{k'}', K=\mp 3)$ and these must originate with the third type of matrix components of $H^{(1)}$, i.e., the elements $(v_i, v_k, l_k, v_{k'}, l_{k'}, K|H^{(1)}|v_i, v_k\pm 1, l_k\pm 1, v_{k'}, l_{k'}, K\mp 2)$. It is clear, however, that with $v_i=v_k=l_k=0$ the quantum numbers v_i', v_k', l_k' cannot all be equal to zero. There are, therefore, no $(K=\pm 3|H^{(3)}|K=\mp 3)$ elements of third order of magnitude.

Turning now to fourth order we specialize the relation (3) for the case $n=4$. In this case elements of the type $(v_i, v_k, l_k, v_{k'}, l_{k'}, K=\pm 3|H^{(4)}|v_i', v_k', l_k', v_{k'}', l_{k'}', K=\mp 3)$ can originate from all the terms in the expansion. It is quickly verified, however, that none but the first terms are significant here. The latter terms are "cross product" terms between $H^{(1)}$ and $H^{(2)}$ which to give elements $(\cdots K=\pm 3|H^{(4)}|\cdots K=\mp 3)$ must arise with the matrix elements $(\cdots K|H^{(1)}|\cdots K\pm 2)$ and $(\cdots K|H^{(2)}|\cdots K\pm 2)$. It will be seen from the character of these, however, that if $v_i=v_k=l_k=0$ the quantum numbers v_i', v_k' and l_k' cannot all be equal to zero. They do not, therefore, contribute to the energy in fourth order.

There are essentially only two different kinds of contributions of the first type which are caused by "cross product" terms of $H^{(1)}$. There may be $(v_i, v_k, l_k, v_{k'}, l_{k'}, K=\pm 3|H^{(4)}|v_i', v_k', l_k', v_{k'}', l_{k'}', K=\mp 3)$ elements from $(\cdots K|H^{(1)}|\cdots K\pm 2)$ occurring three times and $(\cdots K|H^{(1)}|\cdots K)$ occurring one time. Inspection reveals that if v_i, v_k, l_k, etc., are equal to zero, then, as before, the values of v_i', v_k', l_k', etc. cannot all be equal to zero. Such contributions may therefore be neglected for the normal state. The only remaining types of contributions originate from $(v_i, v_k, l_k, v_{k'}, l_{k'}, K|H^{(1)}|v_i, v_k', l_k\mp 1, v_{k'}, l_{k'}, K\pm 2)$ elements occurring twice with $(v_i, v_k, l_k, v_{k'}, l_{k'}, K|H^{(1)}|v_i\pm 1, v_k'', l_k\pm 1, v_{k'}, l_{k'}K\pm 1)$ elements also occurring twice and from $(v_i, v_k, l_k, v_{k'}, l_{k'}K|H^{(1)}|v_i, v_k', l_k\mp 1, v_{k'}, l_{k'}, K\pm 2)$ elements and $(v_i, v_k, l_k, v_{k'}, l_{k'}K|H^{(1)}|v_i, v_k, l_k, v_{k'}', l_{k'}\mp 1, K\pm 2)$ elements each occurring once with the elements $(v_i, v_k, l_k, v_{k'}, l_{k'}, K|H^{(1)}|v_i\pm 1, v_k', l_k\pm 1, v_{k'}, l_{k'}, K\pm 1)$ and $(v_i, v_k, l_k, v_{k'}, l_k, K|H^{(1)}|v_i\pm 1, v_k, l_k, v_{k'}', l_{k'}\pm 1, K\pm 1)$ each occurring once. These present a possibility since in the one type of element l_k and K vary in the same sense while in the other type they vary in the opposite sense. Thus the original and final K values may be $K=\pm 3$ and $K=\mp 3$, respectively, while v_i, v_k, l_k, etc., and v_i', v_k', l_k', etc., are all equal to zero. Typical examples of such products which go to make up the sum of terms constituting (3) are these $(0, 0, 0, 0, 0, K=3|H^{(1)}|0, 1, 1, 0, 0, K=1)$ $(0, 1, 1, 0, 0, K=1|H^{(1)}|0, 2, 2, 0, 0, K=-1)(0, 2, 2, 0, 0, K=-1|H^{(1)}|1, 1, 1, 0, 0, K=-2)$ $(1, 1, 1, 0, 0, K=-2|H^{(1)}|0, 0, 0, 0, 0, K=-3)$ and $(0, 0, 0, 0, 0, K=3|H^{(1)}|0, 1, 1, 0, 0, K=1)$ $(0, 1, 1, 0, 0, K=1|H^{(1)}|0, 1, 1, 1, 1, K=-1)(0, 1, 1, 1, 1, K=-1|H^{(1)}|1, 1, 1, 0, 0, K=-3)$ $(1, 1, 1, 0, 0, K=-2|H^{(1)}|0, 0, 0, 0, 0, K=-3)$. We have thus the rather surprising result that to this approximation the splitting is independent of the anharmonic constants in the potential energy.

The actual evaluation of the matrix elements $(0, 0, 0, 0, 0, K=\pm 3|H^{(1)}|0, 0, 0, 0, 0, K=\mp 3)$ is a very tedious and laborious task. This is particularly true since, while the matrix elements of e^{+ix_r} have been given by Shaffer,[10] the corresponding elements of $e^{\pm ix}(p_r\pm ip_x/r)$ have not been investigated. The matrix elements required in this calculation have all been evaluated here in the usual

[10] W. H. Shaffer, Rev. Mod. Phys. 16, 245 (1944).

quantum-mechanical manner, i.e.,

$$(v_k, l_k | v_k', l_k') = \int \bar{\Psi}_{v_k, l_k} f(r_k, p_{rk}, \chi_k, p_{\chi k}) \Psi_{v_k', l_k'} d\tau$$

where the functions $\Psi_{v_k l_k}$ used are the ones given by Dennison.[11] These have already been normalized.

No attempt will be made here to set down the details of this calculation. We shall point out only that in the sum of terms which comprise (3) there are twenty components where $(v_i, v_k, l_k, v_{k'}, l_{k'}, K|H^{(1)}|v_i, v_k', l_k \mp 1, v_{k'}, l_{k'}, K \pm 2)$ occur together with the elements $(v_i, v_k, l_k, v_{k'}, l_{k'}, K|H^{(1)}|v_i \pm 1, v_k', l_k \pm 1, v_k', l_k', K \pm 1)$, ten components for each value of K, and of the components where the elements $(v_i, v_k, l_k, v_{k'}, l_{k'}, K|H^{(1)}|v_i, v_k', l_k \mp 1, v_{k'}, l_{k'}, K \pm 2)$ and $(v_i, v_k, l_k, v_{k'}, l_{k'}, K|H^{(1)}|v_i, v_k, l_k, v_{k'}', l_{k'} \mp 1, K \pm 2)$ occur together with the elements $(v_i, v_k, l_k, v_{k'}, l_{k'}, K|H^{(1)}|v_i \pm 1, v_k', l_k \pm 1, v_{k'}, l_{k'}, K \pm 1)$ and $(v_i, v_k, l_k, v_{k'}, l_{k'} K|H^{(1)}|v_i \pm 1, v_k, l_k, v_{k'}', l_{k'} \pm 1, K \pm 1)$, each occurring once, there are twenty-four. When a common denominator for all these components is found and they are all added together the following surprisingly simple relation for the elements which lie off of the principal diagonal of the energy matrix is obtained:[12]

$$(0,0,0,0,0,K=\pm 3|H^{(4)}|0,0,0,0,0,K=\mp 3) = \sum_{i=1,3} (I_{zz}^{(e)}/I_{xx}^{(e)})(h^2/8\pi^2 I_{xx}^{(e)}) \times [(B_e/\omega_2)^2 \delta \xi_{i2} + (B_e/\omega_4)^2 \gamma \xi_{i4}]^2 [J(J+1)][J(J+1)-2][J(J+1)-6]. \quad (6)$$

For the purpose of computation (6) is more conveniently written in the form:

$$(0,0,0,0,0,K=\pm 3|H^{(4)}|0,0,0,0,0,K=\mp 3) = (I_{zz}^{(e)}/2I_{xx}^{(e)})(1+I_{zz}^{(e)}/2I_{xx}^{(e)})(h^2/8\pi^2 I_{xx}^{(e)}) \times [(B_e/\omega_2)^2+(B_e/\omega_4)^2]^2 \{(n_2^2/\mu_2 m)/[(4n_2^2/\mu_2 m)+(n_1/\mu_2 - n_3/m)^2]\} \times \{[J(J+1)][J(J+1)-2][J(J+1)-6]\}. \quad (6')$$

The actual energy values of the molecule will, therefore, be the same as those given by Shaffer[3] for all states except those where $|K| = 3$. In all cases save these the energies are given by the elements along the principal diagonal and for the cases where $|K| = 3$ the elements may be so arranged as to form a little box with two rows and two columns each. These sub-matrices may then be diagonalized independently and the energies will be found to be:

$$E(|K| = 3) = E(s) \pm \epsilon \quad (7)$$

$E(s)$ being the values for the energy states where $K = 3$ given by Shaffer[3] and ϵ has the values (6'). The actual separation in cm^{-1} between the component levels will evidently be:

$$\Delta\nu = (2\epsilon/hc) = (I_{zz}^{(e)}/I_{xx}^{(e)})(1+I_{zz}^{(e)}/2I_{xx}^{(e)}) B_e [(B_e/\omega_2)^2+(B_e/\omega_4)^2]^2 \{(n_2^2/\mu_2 m)/[(4n_2^2/\mu_2 m) + (n_1/\mu_2 - n_3/m)^2]\} \{[J(J+1)][J(J+1)-2][J(J+1)-6]. \quad (8)$$

It has been shown in the introduction that (8) is actually the amount by which the measured lines will be displaced.

4. NUMERICAL RESULTS

The quantities which occur in the relation (8) may all be arrived at from the experimental data on the ammonia and deutero-ammonia spectra and we shall make the calculations for these two molecules where the nitrogen atom is taken to be the more abundant N^{14}. The frequencies ω_2 and

[11] D. M. Dennison, Rev. Mod. Phys. **3**, 380 (1931).

[12] This is a special case of the $(K|K \pm 6)$ matrix elements which may be shown to be

$$[J(J+1)-K(K\pm 1)]^{\frac{1}{2}}[J(J+1)-(K\pm 1)(K\pm 2)]^{\frac{1}{2}} \cdots [J(J+1)-(K\pm 5)(K\pm 6)]^{\frac{1}{2}}.$$

TABLE I. Numerical values for rotational constants for NH_3 and ND_3.

	$I_{zz}^{(e)}\times10^{40}$ g-cm²	$I_{xx}^{(e)}\times10^{40}$ g-cm²	B_e
NH_3	2.816	4.437	9.941
ND_3	5.448	8.868	5.138

ω_4 for these molecules have been determined with considerable precision by Dennison[13] who has made corrections to the observed frequencies for the anharmonicity of the oscillational motion. His values are $\omega_2=3622$ cm^{-1} and $\omega_4=1685$ cm^{-1} for NH_3 and $\omega_2=2670$ cm^{-1} and $\omega_4=1221$ cm^{-1} for ND_3. From these he has evaluated the constants

$$k_1,\ k_2,\ k_3,\ (I_{zz}^{(e)}/2I_{xx}^{(e)})^2n_1,\ (I_{zz}^{(e)}/2I_{xx}^{(e)})n_2,\ n_3$$

retaining Shaffer's notation. We need only the last three of these constants and for these he obtains

$$(I_{zz}^{(e)}/2I_{xx}^{(e)})^2n_1=10.494,$$
$$(I_{zz}^{(e)}/2I_{xx}^{(e)})n_2=4.168$$

and $n_3=4.098\times10^5$ dyne/cm.

The values for the moments of inertia and of $B_e=h/8\pi^2I_{xx}^{(e)}c$ are known with considerable accuracy for the NH_3 and ND_3 molecules from their spectra. The values for these are set down in Table I and are those given by Herzberg.[14]

When these constants are substituted into relation (8) one obtains the values for the K-type splitting given in Table II. Here also are given, for various J values, the shifts of the lines originating in the levels where $K=3$ as measured by Good and Coles[1] as well as the shifts predicted by this theory. In Table II are also given the predicted shifts for the $K=3$ lines in ND_3.

[13] D. M. Dennison, Rev. Mod. Phys. 12, 175 (1940).
[14] G. Herzberg, *Infrared and Raman Spectra* (D. Van Nostrand Company, Inc., New York, 1945), p. 437.

TABLE II. Numerical values of the K-type splitting and line shifts.

J value	NH_3 $\Delta\nu$ (Mc)	NH_3 Calculated shifts (Mc)	NH_3 Measured shifts	ND_3 $\Delta\nu$ (Mc)	ND_3 Calculated shifts (Mc)
3	0.26	−0.26	−0.30	0.03	0.03
4	1.80	1.80	1.76	0.24	0.24
5	7.21	−7.21	−7.17	0.95	0.95
6	21.63	21.63	22.3	2.85	2.85
7	54.27	−54.27	—	7.14	7.14

The values of the constants required in (8) to make the same calculations for the $N^{15}H_3$ and $N^{15}D_3$ molecules have not been evaluated from the experimental data. The values of ω_2 and ω_4 for these molecules can, however, be calculated from a knowledge of the constants k_1, k_2, k_3, etc. which have been evaluated. Similarly, the rotational constants for the $N^{15}H_3$ and $N^{15}D_3$ molecules have not been determined from experiment. They can, nevertheless, be calculated from geometrical considerations.[15] It may be shown, however, that the constants for the ammonia molecules with the isotope N^{15} are the same within a fraction of a percent as those for the molecules with the ordinary nitrogen atom. We shall, therefore, not here give the shifts of the lines for these molecules since within the limits to which these calculations may be regarded as accurate they will be the same as those given in Table II. This is particularly true since $(4n_2^2/\mu_2m)\gg(n_1/\mu_2-n_3/m)^2$ for all these molecules so that the constant $(4n_2^2/\mu_2m)/[(4n_2^2/\mu_2m)-(n_1/\mu_2-n_3/m)^2]$ approaches unity.

[15] It may be shown that $I_{zz}^{(e)}=I_{yy}^{(e)}=\mu h_0^2+\frac{1}{2}I_{xx}^{(e)}$, where h_0 is the height of the pyramid and μ is the reduced mass $3mM/(3m+M)$. The moment of inertia $I_{xx}^{(e)}$ depends only upon the masses of the hydrogen atoms and their distances from the center of gravity of the H_3 triangle. It remains the same for the $N^{14}H_3$ and the $N^{15}H_3$ molecules and for the $N^{14}D_3$ and $N^{15}D_3$ molecules. Also the pyramidal height, h_0, remains the same throughout.

Theory of the Propagation of Shock Waves from Infinite Cylinders of Explosive*

STUART R. BRINKLEY, JR.** AND JOHN G. KIRKWOOD***
Department of Chemistry, Cornell University, Ithaca, New York

(Received August 15, 1947)

The assumption of energy dissipation at a single shock, formulated in an earlier paper, is employed in the formulation of a pair of ordinary differential equations for peak pressure and shock-wave energy as functions of radial distance from the source for the shock wave produced by an infinite cylinder of explosive along which a stationary detonation wave is traveling with finite velocity. The profile of the wave may be determined by means of an auxiliary integration. The theory takes proper account of the finite entropy increment of the fluid produced by the passage of the shock, and permits the use of the exact Hugoniot curve of the fluid in the numerical integration of the basic equations.

1. INTRODUCTION

IN a recently published paper,[1] hereafter designated [*I*], a theory of propagation of one-dimensional, that is, plane, cylindrical, and spherical, shock waves is described. The partial differential equations of hydrodynamics and the Hugoniot relation between pressure and particle velocity are used to provide three relations between the four partial derivatives of pressure and particle velocity, with respect to time and distance from the source, at the shock front. An approximate fourth relation is set up by imposing a similarity restraint on the shape of the energy-time curve and by utilizing the second law of thermodynamics to determine, at an arbitrary distance, the distribution of the initial energy input between dissipated energy residual in the fluid already traversed by the shock front and energy available for further propagation. The four relations are used to formulate a pair of ordinary differential equations for peak pressure and shock-wave energy as functions of distance from the source. The theory takes proper account of the finite entropy increment of the fluid produced by the passage of the shock and permits the use of the exact Hugoniot curve of the fluid in the numerical integration of the basic equations.

In the present communication, we apply the methods of [*I*] to a description of the shock wave produced by an infinite cylinder of explosive along which a detonation wave is traveling with finite velocity. The results of the theory should be applicable to the shock wave produced by changes of finite length up to distances from the charge which are of the order of magnitude of its length.

2. THE PROPAGATION EQUATIONS

For the present purpose, it is convenient to write the equations of hydrodynamics in the Eulerian form,

$$\frac{1}{\rho c^2}\frac{Dp}{Dt}+\frac{1}{r}\frac{\partial}{\partial r}ru_r+\frac{\partial u_z}{\partial z}=0,$$

$$Du_r/Dt=-\partial p/\rho\partial r,\quad Du_z/Dt=-\partial p/\rho\partial z,\quad (1)$$

where r and z are the Euler radial and axial cylindrical coordinates, relative to an origin fixed in the detonation wave with z-axis coincident with the axis of the cylinder, u_r and u_z the radial and axial components of particle velocity, measured relative to the moving coordinate system, p the pressure in excess of the pressure p_0 of the undisturbed fluid, ρ the density, D the detonation velocity in the negative z-direction, and D/Dt is the Euler total-time derivative which follows the fluid. The Euler sound velocity c is equal to $[(\partial p/\partial\rho)s]^{\frac{1}{2}}$. Equations (1) are supplemented by the equation of state of the fluid and the entropy transport equation, $DS/Dt=0$, the latter of which we shall not use explicitly. They are to be solved subject to initial conditions specified on a curve in the r, z, t-space and to the

* This paper is based upon work done at Cornell University under Contract OEMsr-121 with the Office of Scientific Research and Development.

** Present address: Central Experiment Station, U. S. Bureau of Mines, Pittsburgh 13, Pennsylvania.
*** Present address: Department of Chemistry, California Institute of Technology, Pasadena, California.

[1] S. R. Brinkley, Jr. and J. G. Kirkwood, Phys. Rev. 71, 606 (1947).

Rankine-Hugoniot[2] conditions at the shock front,

$$\begin{aligned} p &= \rho_0 u_n U, \\ \rho(U-u_n) &= \rho_0 U, \\ \Delta H &= (p/2)(1/\rho_0 + 1/\rho), \end{aligned} \tag{2}$$

where ΔH is the specific enthalpy increment experienced by the fluid in traversing the shock front, U is the velocity of the shock front, and u_n is the component of particle velocity normal to the shock front. Equations (2) constitute supernumerary boundary conditions which are compatible with Eq. (1) and the specified boundary conditions only if the shock front follows an implicitly prescribed curve $r(t)$, $z(t)$ in the r, z, t-space.

Taylor[3] has shown that the Rankine-Hugoniot and Chapman-Jouget[4] conditions can be satisfied at the front of a stationary detonation wave by solutions of the equations of hydrodynamics which depend only on $\mathbf{r}/t$, where $\mathbf{r}$ is the Euler position vector of a point relative to an origin traveling with the detonation front. For solutions of the Taylor type,

$$D/Dt = (u_r - r/t)\partial/\partial r + (u_z - z/t)\partial/\partial t, \tag{3}$$

and Eqs. (1) become

$$\begin{aligned} &\left(u_r - \frac{r}{t}\right)\frac{\partial p}{\partial r} + \left(u_z - \frac{z}{t}\right)\frac{\partial p}{\partial z} \\ &\qquad = -\frac{\rho c^2}{r}\frac{\partial}{\partial r} r u_r - \rho c^2 \frac{\partial u_z}{\partial z}, \\ &\left(u_r - \frac{r}{t}\right)\frac{\partial u_r}{\partial r} + \left(u_z - \frac{z}{t}\right)\frac{\partial u_r}{\partial z} = -\frac{1}{\rho}\frac{\partial p}{\partial r}, \\ &\left(u_r - \frac{r}{t}\right)\frac{\partial u_z}{\partial r} + \left(u_z - \frac{z}{t}\right)\frac{\partial u_z}{\partial z} = -\frac{1}{\rho}\frac{\partial p}{\partial z}. \end{aligned} \tag{4}$$

The solutions of Eqs. (4) are compatible with the boundary conditions of continuity of pressure and normal component of particle velocity at the boundary between the explosion products and the exterior medium if solutions of the Taylor type, dependent only on r/t and z/t, are valid in the explosion products behind the detonation wave.

The shock front in the exterior medium will be a surface of revolution with a profile

$$z = \zeta(r) \tag{5}$$

in any r, z-plane. The profile of the shock front has the differential equation

$$d\zeta/dr = \tan\vartheta, \tag{6}$$

where ϑ is the angle between the tangent to the profile and the r-axis. Since the distance traveled by the shock front in the direction of its normal in time dt is Udt and the origin of the coordinate system travels a distance Ddt in the negative z-direction in time dt, we have

$$\cos\vartheta = U/D. \tag{7}$$

The normal component of the particle velocity is given by

$$u_n = u_r \sin\vartheta + (D - u_z)\cos\vartheta. \tag{8}$$

For continuity of the tangential component of the particle velocity,

$$u_r \cos\vartheta = (D - u_z)\sin\vartheta. \tag{9}$$

If the second of Eqs. (2) is combined with Eqs. (7), (8), and (9), there result the relations,

$$\begin{aligned} u_r &= (p/\rho_0 D)\tan\vartheta, \\ D - u_z &= p/\rho_0 D. \end{aligned} \tag{10}$$

A derivative along the shock front, for which we use the notation d/dR, is

$$d/dR = (\partial/\partial r)_\sigma + (\partial/\partial z)_\sigma \tan\vartheta, \tag{11}$$

where the subscript σ implies that the partial derivatives are to be evaluated at the shock front $r = R$. When this derivative is applied to Eqs. (10), two new relations are obtained,

$$\begin{aligned} &\beta\left(\frac{\partial p}{\partial r}\right)_\sigma \cot\vartheta + \beta\left(\frac{\partial p}{\partial z}\right)_\sigma \\ &\qquad = -\rho_0 D\left[\left(\frac{\partial u_r}{\partial r}\right)_\sigma + \left(\frac{\partial u_r}{\partial z}\right)_\sigma \tan\vartheta\right], \\ &\left(\frac{\partial p}{\partial r}\right)_\sigma + \left(\frac{\partial p}{\partial z}\right)_\sigma \tan\vartheta \\ &\qquad = -\rho_0 D\left[\left(\frac{\partial u_z}{\partial r}\right)_\sigma + \left(\frac{\partial u_z}{\partial z}\right)_\sigma \tan\vartheta\right], \end{aligned} \tag{12}$$

where $\beta = 1 - g\sec^2\vartheta$, $g = 1 - d(\log U)/d(\log p)$.

[2] W. J. M. Rankine, Phil. Trans. **A160**, 277 (1870). H. Hugoniot, J. de l'ecole polyt. **57**, 3 (1887); **58**, 1 (1888).

[3] G. I. Taylor (Reference is to informal memorandum; more complete citation is not possible (1941).)

[4] D. L. Chapman, Phil. Mag. [5] **47**, 90 (1889); E. Jouget, Comptes rendus **132**, 573 (1901). See also H. L. Dryden, F. D. Murnaghan, and H. Bateman, Bull. Nat. Res. Council, No. 84, 551 (1932).

As in [I], we proceed to set up a supplementary relation involving the reduced energy-time integral, a slowly varying function of distance from the charge which can be estimated without integration of the partial differential equations of hydrodynamics. If $K(R)/a_0$ is the energy transmitted per unit area of the initial generating surface along the z-axis by the excess pressure of the shock wave to the fluid initially exterior to a cylinder of radius a_0, the assumption of dissipation at a single shock formulated in [I] yields

$$K(R)=\int_R^\infty \rho_0 r_0 h[p(r_0)]dr_0, \tag{13}$$

where a_0 is the initial radius of the cylinder and where $h(p)$ is the specific enthalpy increment imparted to an element of fluid traversed by a shock wave of peak pressure p after the excess pressure has returned to the value zero. The energy of explosion released by unit length of the explosive is, of course, $2\pi K(a_0)$. Equating $K(R)$ to the work due to excess pressure per unit area of initial generating surface performed by the fluid initially contained in the cylinder of radius R on the fluid exterior to the cylinder, we obtain

$$2\pi K(R)dz_0=\int_{t_0(R)}^\infty p'\mathbf{u}'\cdot d\mathbf{A}'dt, \tag{14}$$

where $d\mathbf{A}$ is the Euler area element into which the Lagrange area element $2\pi r_0 dz_0 \mathbf{1}_r$ is transformed by the passage of the shock wave, and where $\mathbf{u}$ is the vector particle velocity and $\mathbf{1}_r$ the unit radial vector. The primed symbols denote quantities behind the shock front, unprimed symbols being reserved henceforth for quantities on the shock front. The integral is taken along a path of constant Lagrange coordinates r_0, z_0. Now $d\mathbf{A}=2\pi r ds\mathbf{n}$, where $\mathbf{n}$ is the normal to the vector $d\mathbf{s}$ into which $dz_0\mathbf{1}_z$ is transformed by the passage of the shock wave and $\mathbf{1}_z$ is the unit axial vector. Since

$$\mathbf{n}=\frac{\partial z}{\partial z_0}\frac{dz_0}{ds}\mathbf{1}_r-\frac{\partial r}{\partial z_0}\frac{dz_0}{ds}\mathbf{1}_z,$$

Eq. (14) can be written in the form,

$$K(R)=\int_{t_0(R)}^\infty [u_r'\partial z/\partial z_0 + (D-u_z')\partial r/\partial z_0]r'p'dt. \tag{15}$$

The energy-time integral can be expressed in reduced form

$$K(R)=F\rho\nu,$$

$$F=[u_r\partial z/\partial z_0+(D-u_z)\partial r/\partial z_0]r\rho,$$

$$\frac{1}{\mu}=-(D\log F/Dt)_e,$$

$$\nu=\int_0^\infty f(R,\tau)d\tau,\quad \tau=[t-t_0(R)]/\mu,$$

$$f(R,\tau)=F'/F. \tag{16}$$

The function $f(R,\tau)$ is the energy-time integrand, normalized by its peak value at the shock front, expressed as a function of R and a reduced time τ which normalizes its initial slope to -1 if μ does not vanish. Elimination of μ from Eq. (16) yields an additional relation, supplementing Eqs. (4) and (12) between the partial derivatives at the shock front. This set of equations is exact, involving integrals of Eqs. (4) for a knowledge of the reduced energy-time function $f(R,\tau)$. As in [I], we impose a similarity restraint on the energy-time curve by the assignment of a value independent of R to ν. The peak approximation, appropriate for an initial estimate of $f(\tau)$, leads to the value $\nu=1$. For the asymptotic quadratic energy-time curve, $\nu=2/3$. As a convenient empirical interpolation formula between the two extreme values, we have employed the relation

$$\nu=1-\tfrac{1}{3}\exp(-p/p_0). \tag{17}$$

Reference is made to [I] for a more detailed discussion of the similarity restraint on the energy-time curve.

In order to express $1/\mu$ in terms of partial derivatives at the shock front, use is made of Eq. (3) and of the identities,

$$\frac{D}{Dt}\left(\frac{\partial z}{\partial z_0}\right)=\frac{\partial u_z}{\partial z_0}=\frac{\partial u_z}{\partial z}\frac{\partial z}{\partial z_0}+\frac{\partial u_z}{\partial r}\frac{\partial r}{\partial z_0},$$

$$\frac{D}{Dt}\left(\frac{\partial r}{\partial z_0}\right)=\frac{\partial u_r}{\partial z_0}=\frac{\partial u_r}{\partial z}\frac{\partial z}{\partial z_0}+\frac{\partial u_r}{\partial r}\frac{\partial r}{\partial z_0}. \tag{18}$$

The components of the deformation-rotation tensor at the shock front are determined by the fact that an element of fluid experiences a pure strain of magnitude $\rho_0/\rho-1$ in a direction normal

to the shock front as the result of the passage of the shock wave. Then

$$(\partial r/\partial r_0)_s = 1+(\rho_0/\rho-1)\sin^2\vartheta,$$
$$(\partial z/\partial z_0)_s = 1+(\rho_0/\rho-1)\cos^2\vartheta,$$
$$(\partial r/\partial z_0)_s = (\partial z/\partial r_0)_s = (1-\rho_0/\rho)\sin\vartheta\cos\vartheta. \quad (19)$$

Equations (3), (16), (18), and (19), together with the Hugoniot equations, finally yield

$$\left(\frac{\partial p}{\partial r}\right)_s + \frac{1-\lambda}{\lambda}\left(\frac{\partial p}{\partial z}\right)_s \cot\vartheta + \rho_0 D\left(\frac{\partial u_r}{\partial r}\right)_s \cot\vartheta + \frac{1-\lambda}{\lambda}\rho_0 D\left(\frac{\partial u_r}{\partial z}\right)_s \cot^2\vartheta = -\frac{p}{R}-\frac{\nu R p^2}{K(R)}, \quad (20)$$

where $\lambda = p/\rho_0 D^2$, for the case $r/t = z/t = 0$. (r/t and z/t vanish at any finite distance from an infinite cylinder of explosive.)

Equations (4), specialized to the shock front and to the infinite cylinder, and Eqs. (12) and (20) constitute six relations between six partial derivatives, evaluated at the shock front. They may be solved for the partial derivatives, and an ordinary differential equation for the peak pressure p as a function of the radial distance R may be formulated with the aid of Eq. (11). A second ordinary differential equation relating K to R may be obtained by differentiation of Eq. (13). The resulting expressions may be written in the form,

$$dK/dR = -RL(p),$$
$$dp/dR = -\nu(Rp^3/K)M(p)\Phi(p, D) - (p/2R)N(p)\Phi(p, D), \quad (21)$$

where the functions $L(p)$, $M(p)$, $N(p)$ are identical with the expressions given in [*I*],

$$L(p) = \rho_0 h(p),$$
$$M(p) = \frac{1}{\rho_0 U^2}\frac{G}{2(1+g)-G},$$
$$N(p) = \frac{4(\rho_0/\rho)+2(1-\rho_0/\rho)G}{2(1+g)-G},$$
$$G = 1-(\rho_0 U/\rho c)^2, \quad g = 1-p\,dU/U\,dp,$$

and where

$$\Phi(p, D) = \left[1-\frac{\rho_0}{\rho}\frac{2(1-g)+G}{2(1-g)-G}\frac{U^2}{D^2-U^2}\right]^{-1}.$$

The functions $L(p)$, $M(p)$, and $N(p)$ can be evaluated as functions of the pressure and $\Phi(p, D)$ can be evaluated as a function of pressure and detonation velocity by means of an equation of state of the fluid and the Hugoniot relations, Eqs. (2). We remark that Eqs. (21) are independent of any assumption regarding the equation of state of the fluid, that they take proper account of the finite entropy increment of the fluid produced by the passage of the shock, and that they permit the use of the exact Hugoniot curves of the fluid in their numerical integration.

It is evident from a consideration of the Hugoniot equations as applied to the detonation wave that the assumption of adiabatic isometric conversion of the explosive to its products corresponds to infinite detonation velocity. With instantaneous conversion, the dependence of the properties of the fluid on the axial coordinate vanishes and the shock wave becomes one-dimensional. We note that

$$\lim(D\to\infty)\Phi(p, D) = 1,$$

and in this limit Eqs. (21) become identical with the one-dimensional equations of [*I*] when the latter are written for the cylindrical case. Furthermore,

$$\lim(p\to 0)\Phi(p, D) = 1,$$

and the asymptotic solutions of Eqs. (21) are identical with those for the one-dimensional cylindrical wave, given in [*I*].

When $p(R)$ is known from the integration of Eqs. (21), the profile $\zeta(R)$ of the shock wave may be obtained by an auxiliary integration,

$$\zeta(R) = \int_{a_0}^{R}\left\{\frac{U[p(r_0)]^2}{D^2}-1\right\}^{\frac{1}{2}} dr_0. \quad (22)$$

3. THE IMPULSE

The impulse I delivered by the shock wave at a point of fixed Euler coordinate r is

$$I = \int_{t_0(R)}^{\infty} p'\,dt, \quad (23)$$

along a path of constant r and constant $z-Dt$. If the excess pressure p' has a negative phase, the positive impulse is obtained if the time integral is extended not to infinity, but to the time at which the excess pressure vanishes. The pressure-time integral can be expressed in reduced form in a manner analogous to the reduction of Eq. (15).

$$I=\nu^* p\theta,$$

$$1/\theta=-(\partial \log p'/\partial t)_{r,\, z-Dt,\, t=t_0(R)},$$

$$\nu^*=\int_0^\infty (p'/p)d\tau^*,$$

with

$$\tau^*=(t-t_0(R))/\theta. \tag{24}$$

The partial derivatives at the shock front were obtained as functions of the peak pressure by the solutions of Eqs. (4), (12), and (20). When these results are employed with the definition of θ, one obtains

$$-1/\theta=\left(\frac{D^2-U^2}{D^2}\right)\frac{U}{G}\times\left\{\frac{1}{R}+\left[\frac{\rho}{\rho_0}(1+g)+\left(1-\frac{\rho_0}{\rho}\right)G-(1-g)\left(\frac{U^2}{D^2-U^2}\right)\right]dp/pdR\right\}. \tag{25}$$

We note that in the limit of infinite detonation velocity, Eq. (25) reduces to the expression for the one-dimensional cylindrical wave, given in [*I*]. For an exponential pressure-time curve, the reduced pressure-time integral ν^* is equal to unity, and for the asymptotic linear pressure-time curve, consistent with the asymptotic quadratic energy-time curve, $\nu^*=\frac{1}{2}$ for the positive phase of the wave. As in [*I*], we employ

$$\nu^*=1-\tfrac{1}{2}\exp(-p/p_0)^{\frac{1}{2}} \tag{26}$$

as an empirical interpolation formula between the two values.

4. INITIAL CONDITIONS

The two constants of integration may be determined from the considerations given in [*I*]. The initial pressure p_1, on the generating surface, is determined by the fact that the Riemann r-function, computed normal to the generating surface, initially vanishes in the receding rarefaction wave. In the development of the theory, the rate of energy delivery has been approximated by an exponential function of time. For shock waves from explosive sources in air, it is assumed that the integral of this expression is equal to the total energy of explosion, since experimental evidence suggests that there is little energy available for second shocks. For shock waves in water, experimental evidence suggests that approximately one-half the energy of explosion is delivered to the first shock. The initial value of K is readily calculated from these considerations, and the disadvantages of the approximate nature of this procedure are minimized by the circumstance that except in the immediate vicinity of the explosive charge, the shock wave parameters are not very sensitive to the initial energy.

PHYSICAL REVIEW VOLUME 72, NUMBER 11 DECEMBER 1, 1947

Nuclear Reactions at High Energies

R. SERBER
Radiation Laboratory, Department of Physics, University of California, Berkeley, California
(Received October 13, 1947)

THE general features of the high energy nuclear reactions which have been observed at the Radiation Laboratory can be understood in terms of a picture which is in its main outlines quite simple, though quite different from the description appropriate at lower energies. In trying to understand what happens when a nucleus is bombarded by a high energy neutron or proton, the first consideration that comes to mind is that the collision time between the incident particle and a particle in the nucleus is short compared to the time between collisions of the particles in the nucleus. This suggests that the first step in the process can be regarded in terms of collisions between the incident particle and the individual nuclear particles. We are thus led to ask the properties of the high energy scattering between free nucleons. There are two salient points. First, the total cross section for scattering of one nucleon by another is inversely proportional to the energy of the incident particle. The mean free path of a nucleon traversing nuclear matter increases with its energy; at sufficiently high energies the nucleus begins to be transparent to the bombarding particles. Secondly, the incident particle loses only a small fraction of its energy to the struck one. The momentum transfer, which is nearly perpendicular to the direction of the incident particle, is of the order $\hbar/a$, where a is the range of nuclear forces, and does not increase with increasing energy. In case of an exchange collision, we continue to call the high energy emergent particle the incident one, even though it has changed its charge.

Since the momentum transfer, $\hbar/a$, is not large compared to the characteristic momentum, $\hbar/d$, of particles in the nucleus (with d the mean separation of nuclear particles), it is not true that the collisions made by the incident particle can be considered as collisions between free particles; interference between particles in the nucleus can be important. Such an interference effect can be expected because of the degeneracy of nuclear matter. If nuclear matter is represented as a degenerate Fermi gas, it is clear that collisions with small momentum transfers will be discouraged, since these tend to lead from an occupied state to another already occupied. An estimate of this effect indicates that as a result the mean free path of a high energy particle ($\sim$100 Mev) traversing nuclear matter will be increased over what would be expected for collisions between free particles by a factor of about 5/3. The mean kinetic energy transfer to the struck particle per collision is increased in the same ratio.

We estimate that the mean free path for a 100-Mev nucleon is about 4×10^{-13} cm, and the kinetic energy transfer to the struck particle is about 25 Mev. Since the mean free path is comparable to nuclear radii, one cannot describe what goes on in terms of formation of a compound nucleus. In fact, what happens will depend on the particular trajectory of the incident particle. If it happens to pass through the nucleus near its edge, it may make a single collision and emerge having lost only 25 Mev of its energy, possibly having changed from neutron to proton (or vice versa) as a result of an exchange collision. Or, if it strikes the center of the nucleus and has to pass through the full diameter, it may make several collisions, lose all its energy, and end its range still inside the nucleus. There are thus a variety of possibilities, ranging from the bombarding particle emerging with most of its energy intact to the loss of the entire incident energy to the nucleus.

Since the struck particles have much lower energy and shorter mean free path than the incident one, they can escape from the nucleus without further collisions only if the collision occurs near the edge of the nucleus with the struck particle heading outwards. In this case it may emerge with 15- or 20-Mev energy. Otherwise it will collide with other nuclear particles, the energy will be distributed over the nucleus, and the subsequent events can be described in terms of the usual evaporation model, the nuclear excitation

energy being dissipated by successive boiling off of particles each with a few million volts of kinetic energy.

When the nucleus is bombarded with 200-Mev deuterons, or 400-Mev α-particles, the binding of the incident nucleons is important chiefly in causing a spatial correlation between them, and what goes on can be thought of in terms of a simultaneous bombardment by several individual nucleons.

The description we have given provides an explanation of several features of high energy reactions which have been observed at the Radiation Laboratory. Because of the wide distribution of excitation energies of the struck nucleus, one would expect a wide distribution of residual nuclei after the evaporation processes are complete; loss of a small number of particles should occur, as well as knocking out of many. This feature of high energy reactions has been reported by Seaborg, Perlman, and their collaborators.[1] Then we may ask about the excitation function of a particular reaction leading to a given residual nucleus. At low energies the reaction proceeds through formation of a compound nucleus. If we confine ourselves to this mechanism, the excitation function will go through a maximum when the excitation energy is most appropriate for evaporating the requisite number of particles, then will drop very rapidly as the energy gets higher because at higher excitation energy it is much more likely that more particles will evaporate. However, at high energies the mechanism of the reaction is different, because of the transparency of the nucleus; the reaction can occur through the incident particle carrying off a good fraction of its energy and giving the nucleus approximately the right excitation energy for the reaction in question. Since the probability of leaving a given excitation energy will be determined only by the mean free path, which varies slowly with the energy of the incident particle, we would expect the excitation function at high energies also to vary quite slowly. This has been confirmed in a number of cases.[2]

Finally, we should expect the transparency of nuclear matter to show up in measurements of the total cross section for absorption or scattering of the incident particle. It should be mentioned that the attenuation of the wave representing the incident particle in passing through the nucleus will give rise to diffraction scattering at small angles ($\theta \sim \hbar/Rp$, where R is the nuclear radius, p the momentum of the bombarding particle). The cross section for diffraction scattering is equal to the inelastic and absorption cross section; for good geometry attenuation measurements it just doubles the cross section. For 100-Mev neutrons, with a mean free path of 4×10^{-13} cm, one sees that for the heaviest elements one would expect a total cross section still close to $2\pi R^2$, but for light elements the cross section should drop considerably below this value. This is, in fact, true, as has been shown by experiments by Cork, McMillan, Peterson, and Sewell.

A number of more detailed calculations, based on the considerations given above, have been carried out by members of the theoretical group at this laboratory. Reasonably good agreement has been obtained with experimental results on the excitation curves and absolute cross sections of a few light element reactions, and on curves of star size *versus* frequency which have been measured by E. Gardner.[3] More detailed reports on this work will be published in the near future.

This paper is based on work performed under Contract W-7405-Eng-48 with the Atomic Energy Commission in connection with the Radiation Laboratory, University of California, Berkeley, California.

[1] B. B. Cunningham, H. H. Hopkins, M. Lindner, D. R. Miller, P. R. O'Connor, I. Perlman, G. T. Seaborg, and R. C. Thompson, Phys. Rev. **72**, 739 (1947).

[2] W. Chupp and E. M. McMillan; R. Thornton and R. W. Senseman, to be published.

[3] Eugene Gardner, Phys. Rev. **72**, 743 (1947).

Letters to the Editor

PUBLICATION of brief reports of important discoveries in physics may be secured by addressing them to this department. The closing date for this department is five weeks prior to the date of issue. No proof will be sent to the authors. The Board of Editors does not hold itself responsible for the opinions expressed by the correspondents. Communications should not exceed 600 words in length.

On the Nuclear Electric Quadrupole Interaction in Molecular Spectra*

BERNARD T. FELD
Research Laboratory of Electronics, Massachusetts Institute of Technology, Cambridge, Massachusetts
October 21, 1947

IN recent observations of the absorption spectra of polyatomic molecules at microwave frequencies, many of the lines show fine structure. Fine structure has been reported in lines corresponding to transitions between rotational levels of the molecule in the ground vibrational state,[1-4] as well as in the "inversion lines" of NH_3.[5-8] The observed fine structure patterns have been interpreted as resulting from a splitting of the molecular levels caused by an interaction between nuclear electric quadrapole moments and the gradient of the molecular electric field at the position of the nucleus. This interaction depends on the orientation of the nucleus with respect to the rest of the molecule, and, therefore, causes a given level to split into a series of levels corresponding to the different possible values of the total (nuclear plus rotational) angular momentum. From the spacing and intensities of the lines observed, it is possible to obtain the nuclear spin, I, as well as the "quadrupole coupling" $eQ(\partial^2V/\partial z^2)$, where Q is the nuclear electric quadrupole moment, V is the electrostatic potential at the position of the nucleus, and z is along the symmetry axis of the molecule. Since different investigators have adopted different definitions of these quantities, while still retaining the above symbols, the formulae used to evaluate the data may differ from investigator to investigator, and the values of $eQ(\partial^2V/\partial z^2)$ given are consequently not comparable from experiment to experiment.

The nuclear electric quadrupole moment is usually defined as follows:[9-11]

$$Q=\int\int\int \rho r^2(3\cos^2\theta-1)d\tau, \qquad (1)$$

where the integral is taken over the volume of the nucleus for the state $m_I=I$. The coordinate system is such that the origin is at the center of mass of the nucleus and the z axis (θ is the angle between r and this axis) is taken along the spin axis of the nucleus. $e\rho$ is the nuclear charge density.

Using the above definition of the "quadrupole coupling," the term in the energy of molecules no more complicated than the symmetrical top type caused by the "quadrupole coupling", is

$$E(Q)=-eQ(\partial^2V/\partial z^2)\left[1-\frac{3K^2}{J(J+1)}\right]\times\frac{[\frac{3}{4}C(C+1)-\frac{1}{2}I(I+1)J(J+1)]}{I(2I-1)(2J-1)(2J+3)}, \qquad (2)$$

where

I = nuclear spin,
J = molecular rotational spin,
K = projection of J along the symmetry axis ($J\geqslant K\geqslant -J$, in unit steps),
$C=F(F+1)-I(I+1)-J(J+1)$,
F = total spin $=I+J,\ I+J-1,\ \cdots/I-J/$.

The difference between the form of the dependence on I and the dependence on J arises from the fact that the nuclear electric quadrupole moment is evaluated about the nuclear spin axis while $(\partial^2V/\partial z^2)$ is taken along the molecular axis of symmetry, which is not in the direction of J.[12,10] For diatomic and linear polyatomic molecules ($K=0$), the axis of symmetry is essentially perpendicular to the J axis. For symmetrical top molecules, the J axis may take on different orientations (K values) with respect to the symmetry axis, giving rise to the dependence on K.

Adopting formula (2), with the various quantities as defined above, the "quadrupole couplings" as given by various investigators bear the following relationships to $eQ(\partial^2V/\partial z^2)$:

(1) Nierenberg, Ramsey, and Brody[13] use the quantity e^2qQ as defined by Casimir.[9,10,12] Furthermore, they deal with diatomic molecules and large J.

$$(e^2qQ)_{N,R,B}=-\tfrac{1}{2}eQ(\partial^2V/\partial z^2). \qquad (3)$$

(2) Van Vleck, *et al.*,[7] use a different convention in deriving their formulae.

$$eQ(\partial^2V/\partial z^2)_{VV}=4eQ(\partial^2V/\partial z^2). \qquad (4)$$

When using formula (2) to evaluate the data of the above investigators on the NH_3 inversion lines, one obtains a value of 4.10 megacycles per second for the "quadrupole coupling" of the nitrogen nucleus ($I=1$).

Watts and Williams,[8] from their data on NH_3 inversion lines, obtain a "quadrupole coupling" of 4.26 megacycles per second.

(3) Coles and Good,[6] owing to a difference in the definition of nuclear quadrupole moment, give a different expression for $E(Q)$. The connection between their expression and ours is:

$$(e^2qQ)_{C,G}=\frac{2I+3}{2I}eQ(\partial^2V/\partial z^2). \qquad (5)$$

Applying this correction to their value for e^2qQ of nitrogen in NH_3,

$$eQ(\partial^2V/\partial z^2)=4.08 \text{ megacycles/second}.$$

Averaging the results of the three above-mentioned measurements of the "quadrupole coupling" of N in NH_3, we obtain

$$eQ(\partial^2V/\partial z^2)=4.18\pm0.10 \text{ mc/sec}.$$

The sign of the interaction cannot be determined from the above measurements.

(4) Gordy, *et al.*,[3] use a modified form of the formula given by Coles and Good. The relationship between their

quadrupole interaction and that defined by Eq. (2) is

$$[eQ(\partial^2 V/\partial z^2)]_{a,s,s}=\frac{2I+3}{4I}eQ(\partial^2 V/\partial z^2). \quad (6)$$

Thus, the published values of the "quadrupole coupling" of iodine ($I=5/2$) in CH_3I[2] and ICN[3] should be multiplied by the factor $4I/2I+3=5/4$, giving values of $eQ(\partial^2 V/\partial z^2)$ of -1900 mc/sec. and -2588 mc/sec., respectively.

The factor $4I/2I+3$ for chlorine and bromine ($I=3/2$) turns out to be equal to 1. Thus, the "quadrupole couplings" given by the above authors for these nuclei in BrCN,[3] CH_3Cl, and CH_3Br[4] are identical with those which would have been obtained by the use of Eq. (2).

Although Townes, Holden, Bardeen, and Merritt[1] have not published the formula which they used to determine "quadrupole couplings", their definition of $eQ(\partial^2 V/\partial z^2)$ appears to be identical with ours.

* This work has been supported in part by the Signal Corps, the Air Materiel Command, and the O.N.R.

[1] C. H. Townes, A. N. Holden, J. Bardeen, and E. R. Merritt, Phys. Rev. 71, 644 (1947).
[2] W. Gordy, A. G. Smith, and J. W. Simmons, Phys. Rev. 72, 249 (1947).
[3] W. Gordy, W. V. Smith, A. G. Smith, and H. Ring, Phys. Rev. 72, 259 (1947).
[4] W. Gordy, J. W. Simmons, and A. G. Smith, Phys. Rev. 72, 344 (1947).
[5] W. E. Good, Phys. Rev. 70, 213 (1946).
[6] D. K. Coles and W. E. Good, Phys. Rev. 70, 979 (1946).
[7] B. P. Dailey, R. L. Kyhl, M. W. P. Strandberg, J. H. Van Vleck, and E. B. Wilson, Jr., Phys. Rev. 70, 984 (1946).
[8] R. J. Watts and D. Williams, Phys. Rev. 72, 263 (1947).
[9] H. B. G. Casimir, Archives du Musée Teyler (III) 8, 201 (1936).
[10] B. T. Feld and W. E. Lamb, Jr., Phys. Rev. 67, 15 (1945).
[11] E. H. Rhoderick, Nature 160, 255 (1947).
[12] A. Nordsieck, Phys. Rev. 58, 310 (1940).
[13] W. A. Nierenberg, N. F. Ramsey, and S. B. Brody, Phys. Rev. 70, 773 (1946).

Alpha-2 Neutrons Nuclear Reactions

K. Lark-Horovitz, J. R. Risser,* and R. N. Smith**
Purdue University, Lafayette, Indiana
October 23, 1947

DURING a series of investigations with 15-Mev alpha-particles, we also started a systematic search for the $(\alpha, 2n)$ reaction to test the predictions of the statistical theory[1] of nuclei. The following elements have been investigated:

V, Co, Cu, Ga, As, Rb, Y, Rh, Ag, In, and I.

We found the following reactions:

$Ga^{69}(\alpha, n)As^{72}(26^h)$, $Ga^{71}(\alpha, n)As^{74}(16^d)$,
$Rb^{87}(\alpha, n)Y^{90}(60^h)$, $I^{127}(\alpha, n)Cs^{130}(30\text{ min.})$.

In no case was there any indication of an $(\alpha, 2n)$ reaction.

At the end of 1942~18-Mev alpha-particles became available, and preliminary experiments were carried out with cobalt and rhodium. In bombarding cobalt, both the Cu^{62} activity of 10 min., as well as the Cu^{61} activity of 3.4 hr. were found, indicating the existence of both (α, n) and $(\alpha, 2n)$ reactions. Bombarding rhodium, the 8.2-day activity of Ag^{106} resulting from the (α, n) reaction and, in addition, a ~40-day activity were found, indicating the existence of the $(\alpha, 2n)$ reaction. We assign this period to the Ag^{105} isotope.[2]

The investigation was interrupted because of the authors' assignments to war research activities and was continued only recently.

* Now at Rice Institute, Houston, Texas.
** From Part I, unpublished Ph.D. thesis, Purdue, 1941; now at Boeing Aircraft Company, Seattle, Washington.
[1] See V. F. Weisskopf, Phys. Rev. 52, 295 (1937); D. H. Ewing and V. F. Weisskopf, Phys. Rev. 57, 472 (1940).
[2] T. Enns, Phys. Rev. 56, 872 (1939).

The Relative Yields of (α, n) and $(\alpha, 2n)$ Reactions for Ag and Rh with 15–20-Mev Alpha-Particles*,[1]

H. L. Bradt and D. J. Tendam
Purdue University, Lafayette, Indiana
October 23, 1947

THE statistical theory of nuclear reactions, as developed by Weisskopf and Ewing,[2] predicts a Maxwell-like distribution for the energy spectrum of the neutrons evaporated from a heavy, highly excited compound nucleus formed by α-particle bombardment. If the energy of the emitted neutron is sufficiently small so as to leave the residual nucleus in an excited state above the dissociation energy, the emission of a second neutron will be by far the most probable event.

From the energy distribution of the neutrons given by the statistical theory, the cross section for the $(\alpha, 2n)$ reaction is calculated to be

$$\sigma_{\alpha,2n}=\sigma_\alpha[1-(1+\Delta E/kT)e^{-\Delta E/kT}], \quad (1)$$

where $\Delta E=E_\alpha-T_{\alpha,2n}$ is the excess of the α-particle energy over the threshold $T_{\alpha,2n}$ of the $(\alpha, 2n)$ reaction, T is the temperature of the residual nucleus for an excitation energy

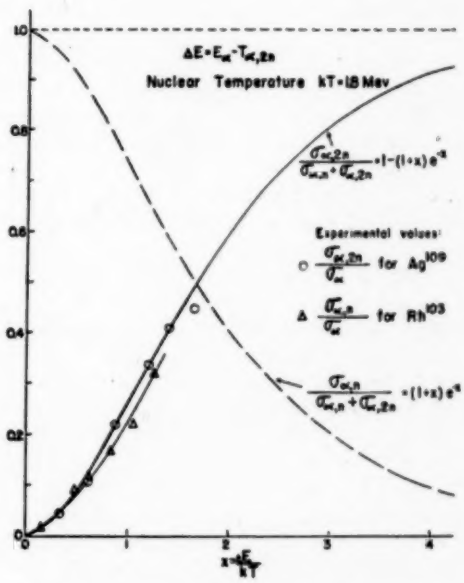

FIG. 1. Excitation curves for the (α, n) and $(\alpha, 2n)$ reactions with Rh.

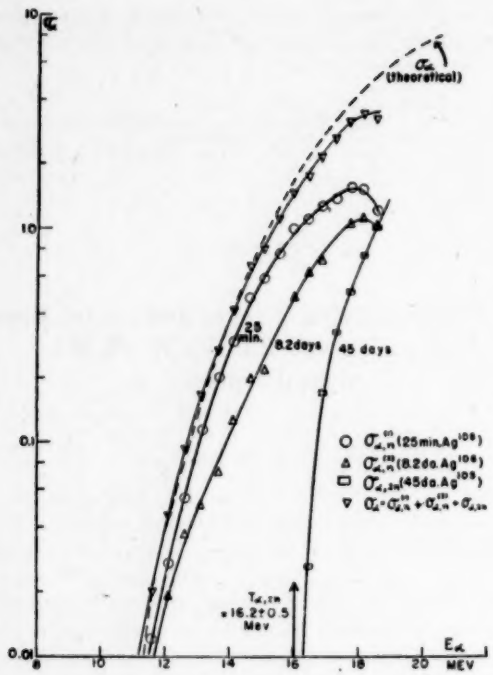

FIG. 2. Relative probabilities of the $Ag^{109}(\alpha, 2n)In^{111}$ and $Rh^{103}(\alpha, 2n)Ag^{105}$ reactions.

equal to the upper limit of the neutron spectrum, and $\sigma_\alpha \approx \sigma_{\alpha,n} + \sigma_{\alpha,2n}$ is the cross section for the formation of the compound nucleus. In order to test the validity of (1), we have, in continuation of experiments started in 1940 by K. Lark-Horovitz in collaboration with J. R. Risser and R. N. Smith,[3] measured excitation curves for the radioactive products of the (α, n) and $(\alpha, 2n)$ reactions, induced by bombardment of stacked Ag and Rh foils with α-particles from the Purdue Cyclotron.

The $Rh^{103}(\alpha, n)Ag^{106}$ reaction leads to the well-known isotope Ag^{106} either in its ground state or in its isomeric metastable state, which decays by β^+ emission with a half-life of 25 minutes, or by K-capture with a half-life of 8.2 days, respectively. The $Rh^{103}(\alpha, 2n)$ reaction leads to the silver isotope Ag^{105}, to which heretofore a period of 45 days has been assigned only tentatively.[4] Bombardment of Rh with α-particles produced these three activities of 25 min., 8.2 days, and 45 days, and the excitation curves for them are reproduced in Fig. 1. It is clear that the 45-day period is the product of the $Rh^{103}(\alpha, 2n)Ag^{105}$ reaction, the threshold being 16.2±0.5 Mev; hence this period must be assigned definitely to the mass number 105.

The ratio of the cross sections for the excitation of the two isomeric states of Ag^{106} was determined by comparing the saturation gamma-activities of the 25-min. (annihilation radiation) and the 8.2-day (nuclear cascade γ-rays[4]) periods. Then the ratio of the $(\alpha, 2n)$ to the (α, n) cross section was determined by comparing the saturation x-ray intensities of the 45-day Ag^{105} and the 8.2-day Ag^{106}. The rapid rise of the $(\alpha, 2n)$ cross section above 16 Mev at the expense of the (α, n) cross section is clearly seen from Fig. 1.

The analogous excitation curves for the $Ag^{109}(\alpha, n)In^{112}$ and $Ag^{109}(\alpha, 2n)In^{111}$ reactions are shown in Fig. 1 of the letter following. For Rh^{103} as for Ag^{109} the sum of the (α, n) and $(\alpha', 2n)$ cross sections in Fig. 1 follows rather closely the theoretical curve for σ_α, given by the figures in Weisskopf's lecture in the Los Alamos (24) report,[5] for both the $Rh^{103}(\alpha, 2n)Ag^{105}$ and the $Ag^{109}(\alpha, 2n)In^{111}$ reactions.

Figure 2 shows the experimental values for $\sigma_{\alpha,2n}/(\sigma_{\alpha,n}+\sigma_{\alpha,2n})$ plotted against $x=\Delta E/kT$. As is seen, good agreement with formula (1) can be obtained by assuming for the nuclear temperature the reasonable value $kT=1.8$ Mev.

* Assisted by the Office of Naval Research under Contract N6ori-222 Task Order I.

[1] D. J. Tendam and H. L. Bradt, Phys. Rev. **72**, 527 (1947).
[2] V. F. Weisskopf and D. H. Ewing, Phys. Rev. **57**, 472 (1940).
[3] Unpublished thesis (1941).
[4] T. Enns, Phys. Rev. **56**, 872 (1939).
[5] $R=1.3\cdot10^{-13}A^{\frac{1}{3}}$ cm has been assumed. In order to obtain an experimental value for the effective nuclear radius, a determination of the absolute cross sections will be made.

The Radioactive Indium Isotopes of Mass Numbers 111 and 112*,[1]

D. J. TENDAM AND H. L. BRADT
Purdue University, Lafayette, Indiana
October 23, 1947

THE irradiation of silver with 15–20-Mev alpha-particles produces the following four periods, all of which have been chemically identified as belonging to indium isotopes: 23 min., 66 min. 6.5 hr., and 2.7 days. Since

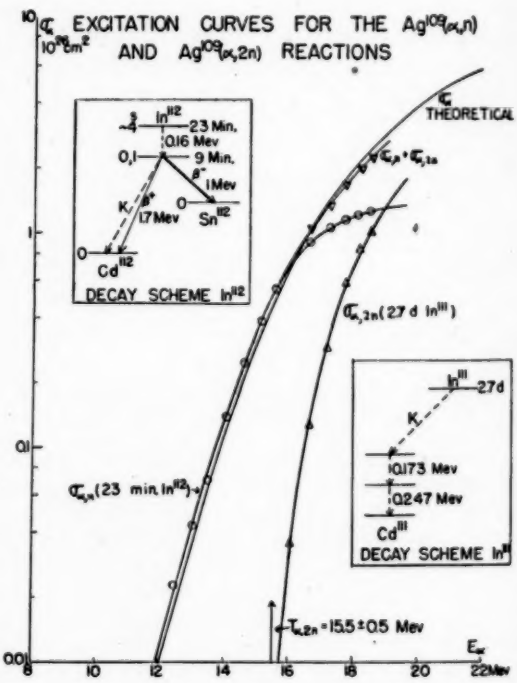

FIG. 1. Excitation curves for the $Ag^{109}(\alpha, n)$ and $Ag^{109}(\alpha, 2n)$ reactions.

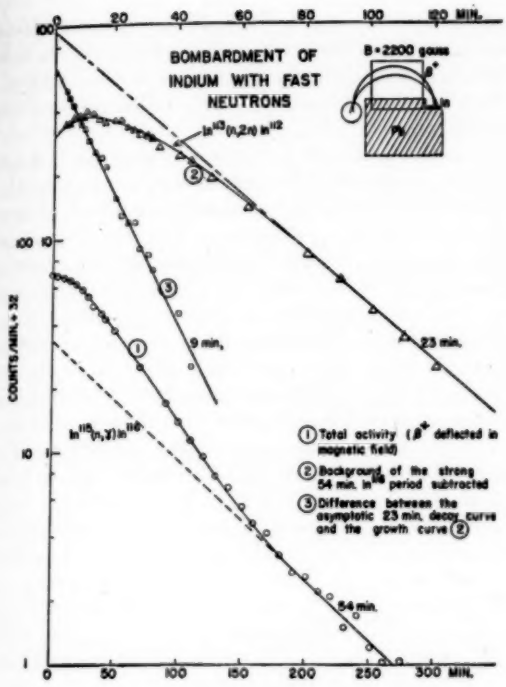
BOMBARDMENT OF INDIUM WITH FAST NEUTRONS
B=2200 gauss
Pb
In
In113(n,2n)In112
23 min.
9 min.
54 min.
In115(n,γ)In116
COUNTS/MIN.+32
① Total activity (β+ deflected in magnetic field)
② Background of the strong 54 min. In116 period subtracted
③ Difference between the asymptotic 23 min. decay curve and the growth curve ②
0 20 40 60 80 100 120 MIN.
0 50 100 150 200 250 300 MIN.

FIG. 2. Bombardment of indium with fast neutrons.

its excitation curve is almost identical with that of the 66-min. In^{110}, produced by the $Ag^{107}(\alpha, n)In^{110}$ reaction, the 23-min. period must be assigned to mass number 112 as the product of the $Ag^{109}(\alpha, n)In^{112}$ reaction. Further proof of this assignment is the fact that the 23-min. isotope decays chiefly by negative electron emission to a Sn isotope; the stable Sn isotope of lowest mass number is Sn^{112}.

It is seen from its excitation curve (Fig. 1) that the 2.7-day period is the product of an $(\alpha, 2n)$ reaction with a threshold of 15.5±0.5 Mev and must be assigned to In^{111}. Lawson and Cork[2] produced a weak 2.7-day activity with fast (Li+d) neutrons and assigned this period of In^{112} as the product of an $(n, 2n)$ reaction. From our result we must conclude that this activity was the product of the $In^{113}(n, 3n)$ reaction. The 2.7-day In^{111} decays by electron capture to an excited state of Cd^{111}, which goes into the ground state by successive emission of two gamma-quanta.[2,3]

The 23-min. period of In^{112} is followed by negative and positive electrons, both In and Cd x-rays, and the conversion electrons of a highly converted 0.16-Mev γ-radiation. While the Cd K-radiation accompanies the K-capture of In^{112}, the emission of In K-radiation can only be due to internal K-conversion of the 0.16-Mev γ-ray. This converted γ-ray hence is emitted in the transition between two isomeric states of In^{112}. Since both the conversion electrons and the In K-x-rays follow the 23-min. period from the beginning, this period is the half-life of the upper, metastable level of In^{112}. The decay curve for the negative and positive electrons follows the 23-min. period only after a certain time; this curve, first recognized by R. N. Smith,[4] as such, is a growth curve, showing that a 9-min. activity grows from the 23-min. activity.[5] Figure 2 shows the decay curve of the positrons from a sample produced by the $In^{113}(n, 2n)In^{112}$ reaction with (Li+10 Mev D_1[6]) neutrons.

The deviation of the growth curve from the asymptotic 23-min. period during the time immediately following bombardment depends on the relative probabilities of excitation of the isomeric states by the nuclear reaction involved. It is largest for samples produced by (γ, n)[6] and $(n, 2n)$ reactions, smaller for those from the $Ag^{109}(\alpha, n)$ reaction, and not noticeable for those from the $Cd^{111}(d, n)In^{112}$ reaction.

The In^{112} isomeric transition belongs in the $l=4$ group. Both the β^- and the β^+ transitions from the ground state to the even, even-nuclei Sn^{112} and Cd^{112} are allowed; the spin quantum number of the lower level is hence 0 or 1.

* Assisted by the Office of Naval Research, Contract N6ori-222 Task Order I.

[1] D. J. Tendam and H. L. Bradt, Phys. Rev. **72**, 527 (1947).
[2] J. L. Lawson and J. M. Cork, Phys. Rev. **57**, 982 (1940).
[3] H. L. Bradt, P. C. Gugelot, O. Huber, H. Medicus, P. Preiswerk, and P. Scherrer, Helv. Phys. Acta **19**, 77 (1945).
[4] R. N. Smith, Phys. Rev. **61**, 389 (1942).
[5] Analysis of the growth curve into exponentials led Smith to assume periods of 16.5±2 min. and 17.5±2 min. for the In^{112} isomers in order to obtain the best fit. The growth curve can be reproduced, over a considerable interval, in this way; the decay curve for the conversion electrons and x-rays, however, shows that the half-life of the upper level is 23 min.
[6] We are indebted to Dr. John McElhinney for irradiating an In foil with the x-rays of the 20-Mev betatron of the University of Illinois and measuring its activity.

Phase Change in Barium Titanate Crystals Induced by Infra-Red Radiation Absorption

NORMAN J. FIELD AND A. P. DEBRETTEVILLE, JR., *Signal Corps Engineering Laboratories, Fort Monmouth, New Jersey*

AND

H. D. WILLIAMS, *Harshaw Chemical Company, Cleveland, Ohio*

October 22, 1947

BARIUM titanate is a ferro-electric material[1-3] or dielectric with a non-linear constant. The microcrystalline material has been reported to have a phase transition[4] from the tetragonal form ($a=3.986$ kX, $c=4.026$ kX for 20°C to the cubic form ($a=4.004$ for 200°C) at 120°C[5] by the x-ray heating camera. A discontinuity in the electrical properties of the material has also been noted at this temperature.[1-3]

These characteristics have now been confirmed by direct microscopic observation of synthetic crystals in polarized light.

Plate-like macrocrystals of barium titanate, grown by the method of Matthias,[6] are optically anisotropic when examined between crossed Nichols with moderate illumination by a tungsten lamp source. Increase in intensity of illumination causes a striking change in the crystal to the isotropic phase. This change is readily observed as the interference colors and patterns give way to a homogeneously grey color which does not vary with rotation of the crystal in the polarized light. The transformation is rapid and reversible, originating at the point of most concentrated illumination, and rapidly spreading towards the periphery of the crystal.

Apparently the crystal: (a) absorbs infra-red radiation from the tungsten lamp and converts this to heat energy; (b) this heat is sufficient to raise the temperature of the crystal from approximately 20°C to above 120°C, the "Curie" point.

Evidence for (a) is the observation that after the crystal has become isotropic, a breath of cool air will cause it to revert to anisotropism momentarily. Also, the insertion of a light blue (daylight) filter in the optical system brings about a similar reversal to the anisotropic state. Observed under carbon arc illumination, the effect does not occur.

Evidence for (b) is that heating the crystal externally with the use of a Kofler micro hot stage, and examining it with the daylight filter in a low intensity light, shows a transition from anisotropic to the isotropic state at 122.0°C–123.0°C. This checks the oscillograph[2,3] and x-ray diffraction heating camera measurements[5] very closely.

An attempt was made to determine whether a selective absorption band existed for the crystal in the infra-red region. Tentative infra-red spectrometer measurements appear to show that the band is exceedingly broad.

The crystals appear in both bluish and yellowish colors. The latter do not seem to exhibit the infra-red absorption effect, although they show the same phase transformation at approximately 121°C in the micro hot stage. Both crystals appear to have the same lattice constants as those published earlier[4] for the microcrystals and the single twinned crystals grown from a $BaTiO_3$ melt, as shown by a Weissenberg moving film camera diffraction pattern.[7]

[1] Titania Ceramics II, Nat. Defense Research Comm. Report XI, Div. 14, No. 540 (October 1945).
[2] A. P. deBretteville, Jr., Phys. Rev. **69**, 687 (1946).
[3] A. P. deBretteville, Jr., J. Am. Ceramic Society **29** (11) 303 (1946).
[4] H. D. Megaw, Proc. Phys. Soc. London **58**, 133 (1946).
[5] Frank G. Chesley, private communication.
[6] B. T. Matthias, Phys. Rev. **72**, 532 (1947).
[7] A. P. deBretteville, Jr. and S. Benedict Levin, Crystallographic Society, Annapolis Meeting, March 20, 1947.

Thallium Halide Crystal Counter

ROBERT HOFSTADTER
Palmer Physical Laboratory, Princeton University, Princeton, New Jersey
October 16, 1947

THE photo-conductivity of thallium chloride, thallium bromide, silver chloride, and silver bromide has been studied by W. Lehfeldt.[1] He found that the thallium salts showed many similarities, in photo-conducting properties, to the silver salts. Van Heerden[2] has shown that silver chloride, when cooled to low temperatures, may be used to detect γ-rays, β- and α-particles. Therefore, it seems likely that the thallium salts may also act as particle detectors or counters. Van Heerden has already suggested this possibility.

It seemed worth while, therefore, to see whether a thallium halide would behave as a counter. Thallium crystals are rather rare in this country, but the author was fortunate in obtaining a sample of a mixed halide crystal through the kindness of Dr. H. C. Kremers of the Harshaw Chemical Company. This crystalline sample is a mixture of approximately 40 percent thallium bromide and 60 percent thallium iodide. The sample is a disk, one inch in diameter and two millimeters thick, orange in color, and seems to be a polycrystal, judging by its appearance in reflected light. The component crystals seem to be a millimeter or a few millimeters on a side.

This crystalline sample was sputtered with one-half inch diameter platinum electrodes, placed in a vacuum chamber, and cooled to liquid nitrogen temperature, at which temperature the crystal is an insulator. The crystal is a conductor at room temperature and is similar to silver chloride in this respect. When connected to an amplifier and voltage supply, the crystal showed no oscilloscope pulses in response to radium γ-irradiation. However the crystal did show photo-conductivity under these conditions.

The crystal was removed and placed in a furnace where it was brought to a temperature of 350°C. It was then slowly cooled to room temperature. During the annealing process the crystal was observed through crossed Nicol prisms so that its strain pattern could be observed. After annealing, the crystal showed very little strain and was transferred to the crystal holder and cooled, over a period of an hour or so, to the temperature of liquid nitrogen (77°K). When exposed to the γ-radiation of radium, pulses were observed on an oscilloscope screen. Thus, this mixed crystal will detect ionizing radiations when properly prepared. It seems very probable, therefore, that the pure materials, thallium bromide and thallium iodide, will also act as counters.

The largest pulses observed (0.2 millivolt), with 500 volts across the crystal, were only about five times the noise level of the Model 501 amplifier which was used in these tests. However, it is felt that much larger signals can be obtained from single crystals of the material. Moreover, the arrangement in which the crystal was mounted introduced a rather large stray capacitance to ground ($\sim$45 micro-microfarads). Nevertheless, the high dielectric constants of the thallium salts ($\sim$30) will tend to make pulses smaller than in silver chloride (dielectric constant $\sim$12) samples of the same dimensions.

A test was made at -115°C. The crystal counted at this temperature also. The rise time of the largest pulses was less than or equal to 0.4 microsecond at this temperature. From Lehfeldt's work it is probable that with pure compounds the thallium salts may insulate well enough to count at temperatures of -70°C. This crystal, however, was a conductor at -70°C. It has been noticed in this work that at -196°C and at higher voltages (>800 volts), direct current flow begins rather abruptly in or over the surface of the crystal. The fluctuations in this current form a background which increases the noise level considerably, until at higher voltages the pulses cannot be observed above the noise. The direct current component is observed even without a radioactive source present, and seems to depend in a non-linear way on voltage. Similar results have been observed in some silver chloride crystals which the author has used as counters. At higher temperatures (-115°C), the crystal showed "fatigue" in the sense that it became conducting after having voltage (500 volts) across it for ten minutes or so.

If some of the above difficulties can be overcome, the use of thallium compounds as γ-ray counters seems quite promising since such crystals are quite dense (TlBr 7.56, TlI 7.09). They are also interestingly complementary to diamond counters[3,4] since pair production and the photoelectric process have a high probability in the thallium salts, while at γ-energies below about eight million electron volts the Compton process is the only one of moment in diamond.

It is also interesting that an "impurity" of bromine in the iodine compound (or *vice versa*) still permits the crystal to count.

This work has been supported in part by U. S. Navy contract N6ori-105 Task I. I wish to thank Dr. H. C. Kremers for the crystal and Messrs. J. C. D. Milton and Chester Grove for their kind help with these experiments.

[1] W. Lehfeldt, Nach. Ges. Wiss. Göttingen, N. F. Fach 2, 171 (1935).
[2] P. J. Van Heerden, "The crystal counter," Dissertation, Utrecht (1945).
[3] D. E. Wooldridge, A. J. Ahearn, and J. A. Burton, Phys. Rev. 71, 913 (1947).
[4] L. F. Curtiss and B. W. Brown, Phys. Rev. 72, 643 (1947).

A Calibration for Eastman Proton Plates

R. A. Peck, Jr.
*Sloane Physics Laboratory, Yale University, New Haven, Connecticut**
September 26, 1947

A BATCH of Eastman nuclear research plates (NTB emulsion No. 347,126) has been calibrated by determination of the emulsion stopping power as a function of proton energy. Until there is some assurance of the reproducibility of Eastman NTB plates, it seems necessary to repeat the calibration procedure for every new batch received.

A thin boron target was bombarded with 3.7-Mev deuterons from the cyclotron, and Eastman plates were used to record the long-range protons from $B^{10}(d, p)B^{11}$. Several exposures were taken with different thicknesses of aluminum foil interposed in the path of the protons. Thus the same group was measured in each plate, with a different effective proton energy in every case. The extrapolated range of the group was determined from each exposure and identified with the extrapolated air range, suitably reduced according to the absorbers used. In this way the emulsion stopping power was determined at each of several proton energy values. The form of the curve so obtained is independent of the deuteron beam energy and the Q-value of the reaction. The absolute values of stopping power will, however, depend on these parameters.

The calibration function obtained is presented in Fig. 1. The errors shown are those which are effective in determining the form of the curve. To them must be added an uncertainty in the level of the curve as a whole, amounting to ± 1.4 percent at 9 Mev. The stopping power function here obtained is constant down to about 5 Mev, below which it rises with decrease of energy. At 3 Mev the slope is -356 per Mev. Similar data obtained for Eastman Experimental Proton emulsion No. 340,506 (same composition as NTB plates) show a stopping power which is constant over roughly the same region, but which increases somewhat more rapidly at low energy.

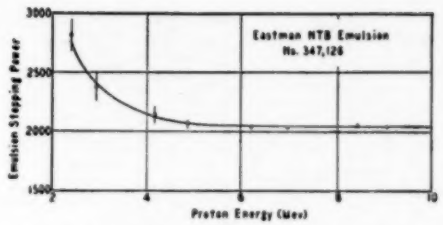

FIG. 1. Stopping power *vs.* energy (Mev) for protons in Eastman NTB emulsion No. 347,126.

For Ilford Nuclear Research emulsions ($B1$ and $C1$) Lattes, Fowler, and Cuer[1] have published a curve which is constant down to 5 Mev, below which it drops with energy decrease. Its slope at 3 Mev is $+70$ per Mev, roughly $\frac{1}{5}$ the corresponding slope for the Eastman emulsion. For Ilford halftone plates Richards[2] found stopping power slightly rising with decreasing energy, and a slope of -19 per Mev at 3 Mev, while Guggenheimer, Heitler, and Powell[3] have observed no energy variation of S for plates of the same type (Ilford halftone) between 2 and 6.5 Mev.

In attempting to account for the difference in direction of the stopping power variation at low energy as found for Ilford and Eastman plates, any slight differences in emulsion composition are of considerable importance. Thus the hydrogen and carbon in the gelatin exhibit a stopping power energy curve with negative slope, while for silver and bromine that slope is positive.[4] Since moisture content influences the amount of hydrogen present, relative humidity also has a considerable effect in determining the effective stopping power of an emulsion. From the different stopping power gradients reported for Ilford emulsions, and the two here found for the Eastman product, it appears that the quanties which vary from batch to batch of plates of a single type are able to evoke some variation in the energy dependence of the stopping power of such plates.

Sincere thanks are due Professor R. F. Humphreys for valuable discussions and suggestions.

* Assisted by the Office of Naval Research, under Contract N6ori-44.
[1] C. M. G. Lattes, P. H. Fowler, and P. Cuer, Nature 159, 301 (1947).
[2] H. T. Richards, Phys. Rev. 59, 796 (1941).
[3] K. M. Guggenheimer, H. Heitler, and C. F. Powell, Proc. Roy. Soc. 190, 196 (1947).
[4] H. Bethe, Rev. Mod. Phys. 9, 272 (1937).

Saturation Effect in Microwave Spectrum of Ammonia

T. Alexander Pond and Walter F. Cannon
Palmer Physical Laboratory, Princeton University, Princeton, New Jersey
October 22, 1947

IN his investigation of absorption line shape in the inversion spectrum of ammonia, Townes[1] has found that at low pressures and powers of the order of 1 μw a saturation effect occurs, causing the absorption to decrease and the width to increase with increase in power. Gordy and

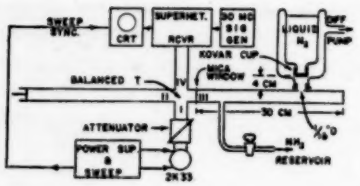

FIG. 1.

Kessler,[2] and Smith and Carter[3] working at approximately the same power levels, have failed to observe any such broadening, although the latter confirmed the saturation of the absorption. We have made an investigation of the 3,3 line at low pressures and powers of the order of 1 μw and find both effects are present.

The equipment is shown schematically in Fig. 1. The output of a frequency-modulated 2K33 reflex klystron is fed through attenuators into arm I of the balanced T. The construction of the T[4] is such that the r-f power divides equally between arms II and III, and none enters IV. Further, if II and III are electrically identical, their fields, after reflection from the ends, will cancel in IV. However, when the absorption in III is changed by introducing a gas, a signal proportional to the change in absorption enters IV and is detected by a superheterodyne receiver with a balanced mixer and band width of 8 Mc, giving an oscilloscope plot of frequency *vs.* absorption. Frequency differences on the oscilloscope are measured by introducing a signal of approximately the intermediate frequency (30 Mc) into the second detector. Each time the i-f sweeps across this signal it produces a video pip around the zero beat which can be positioned on the frequency axis by changing the frequency of the injected signal, allowing calibration of the trace. The ammonia is introduced into the wave guide at atmospheric pressure, then pumped out through a hole $\frac{1}{16}$ inch in diameter. The final pressure is determined by a deposit of solid ammonia at liquid nitrogen temperature on the Kovar cup. From the known variation of absorption with pressure we conclude that this pressure is not greater than 8×10^{-4} mm Hg and may be much less.

Our data on line width at half-intensity ($\Delta\nu$), and attenuation at the center of the line (α_0) as a function of incident power (P) are shown in Fig. 2. Absolute power measurements are accurate to within approximately a factor of 2; relative power measurements, 10 percent; line widths, 20 percent; attenuation, 30 percent.

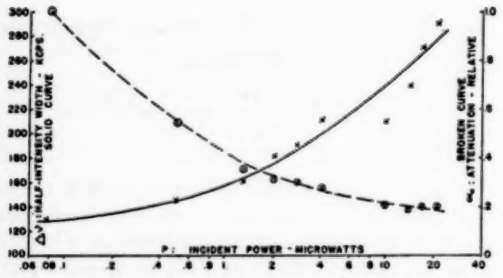

FIG. 2.

According to Townes,[1] saturation sets in when the rate of transition per molecule is approximately equal to the rate of collision. In view of his equation for this condition, which contains the assumption that the distribution of molecules is not affected by the incident power, saturation effects should be evident in our apparatus at powers less than about 100μ watt. Thus our data appear to be in agreement with Townes.

We wish to acknowledge the invaluable assistance of Professor R. H. Dicke in this work.

[1] C. H. Townes, Phys. Rev. **70**, 665 (1946).
[2] W. Gordy and M. Kessler, Phys. Rev. **71**, 640 (1947).
[3] W. V. Smith and R. L. Carter, Phys. Rev. **72**, 638 (1947).
[4] S. E. Miller, Proc. I.R.E. **35**, 345 (1947).

A Double Modulation Detection Method for Microwave Spectra*

RICHARD J. WATTS AND DUDLEY WILLIAMS
The Ohio State University, Columbus, Ohio
October 16, 1947

THE recent publication of a note on the above subject by Gordy and Kessler[1] has suggested to us the desirability of reporting some results of other experiments with a similar arrangement. The arrangement consists of applying a radiofrequency modulation voltage to the reflector of a Klystron in addition to the usual low frequency saw-tooth modulation voltage. The modulated microwave output power is allowed to pass through a wave guide section containing the absorbing gas and is then fed to a communications receiver tuned to the radiofrequency used for modulation. The receiver output is then displayed on an oscilloscope, the horizontal plates of which are synchronized with the low frequency saw-tooth voltage. This scheme has apparently occurred to numerous workers in different laboratories and was apparently first tested by Wilson and his colleagues,[2] who applied a 50-kc square wave to the reflector. They reported that the scheme reduced the crystal noise but did not show marked advantages over the usual low frequency system. The voltages used were apparently high enough to start and stop the Klystron at 50 kc per second. Hershberger[3] was the first to give a public report on this method of detection. In his first work Hershberger used a low voltage modulation frequency of 100 kc and has since worked at 50 kc with most satisfactory results.

In our own experiments we have, in general, used low modulating voltages and have used 20 kc and 600 kc for the modulation frequency. Although low modulating frequencies are to be desired from some points of view,** the results we obtained at 20 kc were disappointing. However, the lack of a good receiver for this extremely low frequency was a contributing factor to our lack of success. Our work at 600 kc has been more successful. In our experiments we found that the gains in signal-to-noise ratio over that obtainable by low frequency methods depend upon how much distortion of signal can be tolerated. Measurements made on one of the weaker ammonia lines indicate that a gain of 30 in signal-to-noise ratio could be

attained without introducing seriously objectionable distortion. Signals resulting from $N^{15}H_3$ lines can readily be observed without introducing serious distortion. If signal size for the 66 line of $N^{15}H_3$ was maximized, the signal-to-noise ratio could be made as large as sixty, but under these conditions the observed signal showed little resemblance to true line shape.

One serious objection to the use of the present double modulation method is that all irregularities in power received by the crystal are amplified in the same manner as the spectral lines. Hence, the beginning and end of the "mode" will always give large signals. Any sharp reflection peaks existing in the transmission line will also give rise to unwanted signals. For short wave guides the reflections are usually much broader than spectral lines observed at low pressure, and hence may be distinguished from lines visually or by means of low frequency rejection filters.[4] However, as the absorption sections are made longer the observed reflection peaks become sharper and hence more difficult to distinguish from spectral lines. Hence, there are definite limitations in the length of "absorption cell" which can be used in this method of detection; these limitations are the same as those for any method involving "sharpness" as a criterion of the recognizability of absorption lines.

We wish to thank Professor E. B. Wilson and Dr. C. H. Townes for helpful discussions last spring during the early stages of our experiments, to thank Professor Walter Gordy for telling us of his work prior to publication of his recent note, and to express our appreciation to Dr. W. D. Hershberger for sending us information concerning his more recent work on the subject.

* This work was done in connection with Contract No. W28-099ac-179 between Watson Laboratories of the Air Materiel Command, Red Bank, New Jersey, and the Ohio State University Research Foundation.
[1] W. Gordy and M. Kessler, Phys. Rev. **72**, 644 (1947).
[2] E. B. Wilson, unpublished report: Progress Report 3, N5ori-76 Harvard.
[3] W. D. Hershberger, paper before Symposium on Molecular Spectra and Molecular Structure, Ohio State University, June 1947.
** Note: For low modulation frequencies, the modulation products are proportional to the "sharpness" of the absorption lines.
[4] The use of low frequency rejection filters obviously introduces distortion of line shapes, since the rejected frequencies make a definite contribution to true line shapes. However, it is possible that properly designed filters can be used without introducing *objectionable* distortion. Gordy and Kessler report that the use of filters can actually result in an apparent gain in resolution. (Phys. Rev. **71**, 640 (1947).) Hershberger, who has used filters in his work for some time, reports definite distortion of line shape but has used filters quite successfully.

On the Pressure-Volume and Pressure-Compressibility Relation of Metals

P. Gombás
Physical Institute of the University for Technical and Economic Sciences, Budapest, Hungary
October 1, 1947

IT has been shown in a previous work[1] of the author that, by further development of the statistical theory of the atom, it is possible to develop a statistical metal theory[2] which enables us to give a full account of the metallic bond of the alkali and alkaline earth metals and, further, to compute the constants of these metals as well as several relations between them without the help of empiric or semi-empiric parameters. The lattice energy U per metal atom—from which all further conclusions can be derived in a simple way—can be expressed as follows:

$$U=A_0+\frac{A_1}{R}+\frac{A_2}{R^2}+\frac{A_3}{R^3}+\frac{A_4}{R^4}, \qquad (1)$$

where R denotes the radius of the elementary sphere containing one metal atom and the coefficients A_i are constants, their value being determined only by the distribution of the electrons and the potential within the ions, and the number of the metal electrons per atom. The constants A_i can be easily calculated.

With the help of (1) the pressure P at the absolute zero point of temperature can be expressed as follows:

$$P=-\frac{dU}{d\Omega}=-\frac{1}{4\pi R^2}\frac{dU}{dR}=\frac{1}{4\pi R^7}\times(A_1R^3+2A_2R^2+3A_3R+4A_4), \qquad (2)$$

where $\Omega=4\gamma R^3/3$ denotes the volume of the elementary sphere. Substituting the expression $(3\Omega/4\pi)^{\frac{1}{3}}$ for R, the equation yields the pressure-volume relation of the metal.

In the above mentioned work I calculated this relation for the metals Na, K, Rb, and Cs up to pressures of about 4.10^4 kg/cm², and I compared the results with those of Bridgman corrected for the absolute zero point of temperature. Recently, the measurements of Bridgman were extended[3] to the alkali metals Na, K, Rb, and to several other elements up to pressures of 10^5 kg/cm² at the temperature $T=296°$K and this induced me to extend theoretical investigations to high pressures of the same order and compare my results with those of Bridgman.

It appears—supposing a constant density distribution of the metal electrons throughout—that the theory is applicable even to these high pressures without change. As long as we apply to the metal ions the statistical model corrected by the electron exchange, the so-called Thomas-Fermi-Dirac model, even at these high pressures there is no overlapping of the electron clouds of neighboring ions. And even calculating the electron distribution of the metal

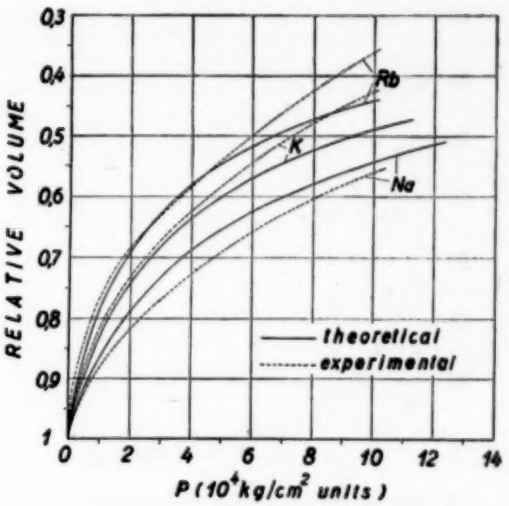

FIG. 1. Comparisons of theoretical and experimental values of pressure-volume relations.

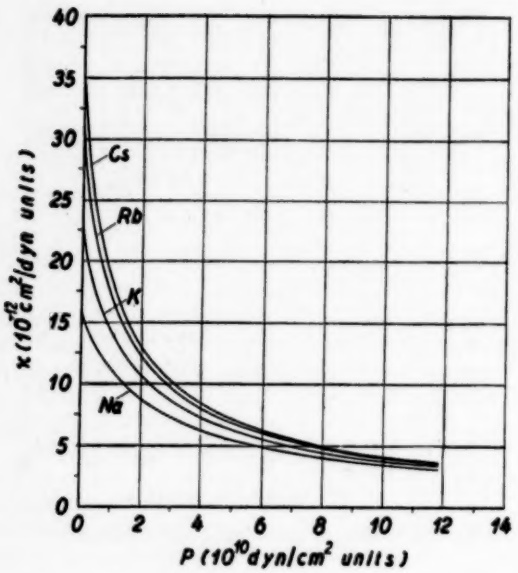

FIG. 2. Pressure-compressibility relations for Cs, Rb, and K.

ions from the more accurate self-consistent field, in the case of alkali and alkaline earth metals, the overlapping of the electron clouds of neighboring ions is negligibly small. It follows, therefore, that the formulae (1) and (2) are applicable even to these high pressures.

For the sake of comparison with the recent experimental results of Bridgman, I calculated the pressure-volume relation for the alkali metals Na, K, and Rb. Since the theory refers to the absolute zero point of temperature, for the purpose of comparison, the theoretical results had to be corrected for the temperature $T=296°$K with Bardeen's formula.[4] Theoretical results as well as those obtained experimentally by Bridgman are graphically recorded in Fig. 1.

The agreement between the theoretical and experimental curves is quite satisfactory, especially if we consider that neither empirical nor semi-empirical parameters were applied in the theory.

With the help of the theoretical explanations given above, the pressure-compressibility relation at the absolute zero point of temperature can be calculated too. The definition of the compressibility κ is as follows:

$$\frac{1}{\kappa}=\frac{1}{12\pi R}\frac{d^2U}{dR^2}.$$

By inserting expression (1) of the lattice energy in this formula, κ appears as the function of R. Connecting that with the expression (2) which gives the relation between R and P, we get the pressure-compressibility relation. That has been calculated for the alkali metals Na, K, Rb, and Cs as well as for the alkaline earths Mg, Ca, Sr, and Ba. The results are graphically recorded in Figs. 2 and 3.

I wish to thank Dr. A. Kónya for performing the calculations.

[1] P. Gombás, Nature 157, 668 (1946).
[2] A detailed presentation of this theory is given in the author's monography, "Die statistische Theorie des Atoms und ihre Anwendungen," Hungarica Acta Physica 1, No. 2 (in print); also in book form (Julius Springer Verlag, Vienna, in press).
[3] P. W. Bridgman, Phys. Rev. 60, 351 (1941). These results of Bridgman are somewhat divergent from his earlier ones and—because of war conditions—became known here only a year ago.
[4] J. Bardeen, J. Chem. Phys. 6, 372 (1938).

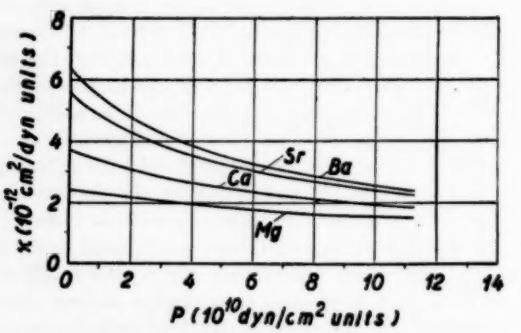

FIG. 3. Pressure-compressibility relations for Ba, Sr, Ca, and Mg.

The β-Radiations of Antimony[124], Tantalum[182], Tungsten[185], and Iridium[192]

SWAMI JNANANANDA
The Harrison M. Randall Laboratory of Physics, University of Michigan, Ann Arbor, Michigan
October 22, 1947

AN investigation of the distribution with momentum of the β-rays of $_{51}$Sb^{124}, $_{73}$Ta^{182}, $_{74}$W^{185}, and $_{77}$Ir^{192} has been made by analyzing them with a magnetic-lens spectrometer. The results were obtained by an electrical counter with automatic registration in the range between $B\rho=560$ and $B\rho=3750$ gauss-centimeters, the lower value being limited by the window of the detecting device.

The spectrometer used in these experiments is based on the selective focusing action of a magnetic lens on β-rays of heterogeneous velocity. The design admits a transmission factor which corresponds to 0.7 percent of 4π in solid angle of β-particles from the source into the field of selective focusing action. From the size of the solid angle used, the chosen focal length, and the magnitude of the linear spread of the focus along the axis, it can be seen that the resolving power $R=\Delta B\rho/B\rho=\pm 0.37$ percent. This resolution value, however, is influenced by the form, size, thickness, and the percental inactive isotopic content of the source.

An electrical counter of the self-quenching type, with Neher-Pickering circuit, is used to detect the β-spectra. The detecting device is further provided with an amplifier, a scale of 64, and an electronic operated mechanical recorder for registration of the impulse frequency.

The spectrometer lens being air-core type, the relation between magnetizing current and $B\rho$ gauss-centimeters is linear. Because of this unique linear relation, the magnetizing current is calibrated once for all in terms of the $B\rho$-value of the well-known and accurately measured F-line of thorium B. ($B\rho=1385.8$ gauss-centimeters[1].)

TABLE I.

Z	Isotope	A	$B\rho$	Energy (Mev)
51	Antimony	124	3494	0.654
73	Tantalum	182	2905	0.499
74	Tungsten	185	3572	0.675
77	Iridium	192	3354	0.617

TABLE II.

Isotope	Reported half-life	Reported energy (Mev)	Method	Present value energy (Mev)
Antimony	60 days	0.74, 2.45	Cl. Ch.[2]	0.654
Tantalum	97 days	0.53	Spec. m.[3]	0.499
Tungsten	77 days	0.67	Abs. mes.[4]	0.675
Iridium	60 days	0.67	Spec. m.[5]	0.617

For each of the isotopes, plots were made of N against $B\rho$, and N/B against $B\rho$. These two different plots represent the natural and the normalized energy spectra. They indicate the end points of the distribution curves from which the maximum disintegration energies of the radioactive isotopes may be readily obtained. These distribution curves, however, need certain corrections. The corrected curves with an analysis will be presented later. The maximum $B\rho$ of the end points and the corresponding energy values in Mev are given in Table I. The present measured energy values of the end points are given along with values previously reported in Table II for easy reference and comparison.

The results of experiments with $_{51}Sb^{124}$ indicate two spectra, the end point of the low energy component being 0.654 Mev, the end point of the high energy component being beyond the upper limit of the spectrograph. It can be seen from Table II that the energy of the upper end point of Tungsten[185] agrees with the value previously reported. It may be pointed out that the sample of $_{77}Ir^{192}$ was not pure, and was mixed with $_{76}Os^{188}$, so that the spectrum of $_{77}Ir^{192}$ overlaps that of $_{77}Os^{193}$.

The radioactive isotopes were obtained by neutron bombardment in the Oak Ridge pile. This investigation was supported by the Office of Naval Research. The author takes this opportunity to express his thanks to Professor James M. Cork for the kind interest and many helpful suggestions made during the work.

[1] C. D. Ellis, Proc. Roy. Soc. **A138**, 318 (1932).
[2] Isotopic Committee, Science **103**, 697 (1946).
[3] Waldo Rall and R. G. Wilkinson, Phys. Rev. **71**, 321 (1947).
[4] K. Fajans and W. H. Sullivan, Phys. Rev. **58**, 276 (1940).
[5] Paul W. Levy, Phys. Rev. **72**, 4 (1947).

Recurrence Formulas for Coulomb Wave Function

I. INFELD
University of Toronto, Toronto, Canada
October 16, 1947

IN a short note[1] under the same title, L. Powell derives the recurrence formulas for the Coulomb wave functions. These formulas, derived by me[2] as particular cases of the factorization method some seven years ago, have been used since in the discrete and continuous spectrum.[3] For their derivation the explicit form of the solution is entirely unnecessary, and the recurrence formulas follow at once from the structure of the differential equation itself.

Indeed the differential equation,

$$\frac{d^2F^L}{d\rho^2}+\left\{1-\frac{2\eta}{\rho}-\frac{L(L+1)}{\rho^2}\right\}F^L=0, \tag{1}$$

can be written in *either* of these two forms:

$$\mathfrak{K}^{(L+1)+}\mathfrak{K}^{(L+1)-}F^L=F^L, \tag{2a}$$

or

$$\mathfrak{K}^{L-}\mathfrak{K}^{L+}F^L=F^L, \tag{2b}$$

where

$$\mathfrak{K}^{L\pm}=\left(1+\frac{\eta^2}{L}\right)^{-\frac{1}{2}}\left(\frac{L}{\rho}+\frac{\eta}{L}\pm\frac{d}{d\rho}\right). \tag{2c}$$

From (2) we have the recurrence formulas

$$\mathfrak{K}^{(L+1)-}F^L=F^{L+1}, \quad \text{and} \quad \mathfrak{K}^{L+}F^L=F^{L-1}. \tag{3}$$

The meaning of (2a) is: go one step up the ladder, then one step down the ladder, and you will arrive at the original function. Similarly, (2b) leads you to the original function by going one step down and one step up. This is only a particular application of the general theory of factorization.[4]

[1] L. Powell, Phys. Rev. **72**, 626 (1947).
[2] L. Infeld, Phys. Rev. **59**, 737 (1941); compare p. 743 and 744; also theorem II on p. 738.
[3] E.g., A. Preson, Phys. Rev. **71**, 865 (1947).
[4] A paper on new types of differential equations on which this factorization method can be used is in preparation.

Relative Nuclear Moments of H^1 and H^2

F. BLOCH, E. C. LEVINTHAL, AND M. E. PACKARD
*Stanford University, Stanford, California**
October 11, 1947

IT was pointed out that nuclear induction is highly suited as a method for comparing, with high precision, the magnetic moments of the neutron, the proton, and the deuteron, and progress of these measurements at Stanford has been announced.[1]

We have just concluded a satisfactory series of experiments on the relative moments of proton and deuteron. In view of their separate interest, particularly in connection with the ratio of the hyperfine structure of H^1 and H^2,[2] we want to report these data while those on the neutron moment are still under careful re-examination.

The method[3] was essentially the same as that used for the relative moments of H^1 and H^3. Both isotopes were contained in about equal amounts in the sample, with the frequencies ν_1 for the proton and ν_2 for the deuteron superimposed in the transmitter and the receiver tuned to simultaneous response for both frequencies by two coupled resonant circuits. Using an r-f amplification stage for ν_2, comparable signals were obtained for the two isotopes, and proper choice of ν_1 and ν_2 resulted in their superposition on the screen at a common value H_0 of the resonance field.

In contrast to H^3 with a moment so close to that of H^1 that their respective signals have practically identical shapes, the considerably smaller moment of H^2 causes the

relaxation time of the deuterons to be much longer than that of the protons in the same sample. The shape of their signals in a common modulated field is therefore rather different, and they cannot be brought to complete superposition (or cancellation). By adjusting the observation to the proper phase, components of the signals (denoted in reverence 1 by the symbol "ν") both can, however, be made to be symmetrical on both sides of the resonance. Proper setting of ν_1 and ν_2, which corresponds to a common value of the resonance field for both isotopes, is then ascertained with high accuracy by the fact that the resultant signal from both isotopes appears again with a common point of symmetry on the screen.

The measurements were carried out with 1.5 cc of a 0.1 molar solution of $MnSO_4$ in water, consisting of about as much H_2O as D_2O. This concentration of the paramagnetic salt was chosen in order to avoid an excessive broadening of the proton signal, caused by too short relaxation times, and yet at the same time to keep the relaxation time for the deuterons well below the modulation period of 1/60 second. Sharp resonance lines were observed in the center of a well shimmed magnet of 8-in. pole diameter with fields in the neighborhood of 10,000 gausses. A relative departure of 1/100,000 from the proper frequency setting caused a noticeable asymmetry of the resultant signal; this determined the accuracy of setting ν_1 and ν_2 to common resonance field.

Taking into account the spin ratio $\frac{1}{2}$:1 for H^1 and H^2, and denoting by $\gamma_{1,2}$ and $\mu_{1,2}$ their respective gyromagnetic ratios and magnetic moments, one has then

$$\mu_1/\mu_2=\gamma_1/2\gamma_2=\nu_1/2\nu_2. \tag{1}$$

The proton transmitter was operating on the 6th harmonic of a master oscillator whose beat frequency,

$$\Delta=\nu_1/6-\nu_2, \tag{2}$$

with the deuteron transmitter was measured together with the frequency ν_2 of the latter. One obtains then from (1) and (2),

$$\mu_1/\mu_2=3(1+\Delta/\nu_2). \tag{3}$$

The following data give the results of many runs obtained for three different values of the resonance field.

ν_2	Δ	μ_1/μ_2
6.35000 Mc	0.544392±0.00006	3.257193±0.00003
6.74000 Mc	0.577807±0.00007	3.257184±0.00003
7.22000 Mc	0.619010±0.00007	3.257206±0.00003

While earlier determinations gave[4] 3.2571+0.001, we can thus state with considerably higher accuracy that the ratio of the moments of proton and deuteron is given by

$$\mu_1/\mu_2=3.257195\pm0.00002.$$

* Work supported by grants from the Office of Naval Research and the Research Corporation.

[1] F. Bloch, Phys. Rev. 70, 473 (1946).
[2] T. E. Nafe, E. B. Nelson, and I. I. Rabi, Phys. Rev. 71, 914 (1947).
[3] F. Bloch, A. C. Graves, M. Packard, and R. W. Spence, Phys. Rev. 71, 551 (1947).
[4] J. M. B. Kellogg, I. I. Rabi, N. F. Ramsey, and J. R. Zacharias, Phys. Rev. 56, 728 (1939); W. R. Arnold and A. Roberts, Phys. Rev. 70, 320 (1946).

On the Symmetrical Vector Meson Pair Theory of Nuclear Interaction

O. Brulin and S. Hjalmars
Institute of Mathematical Physics, University of Stockholm, Stockholm, Sweden
October 21, 1947

SOME features in recent experimental investigations of cosmic-ray mesons[1] may indicate that at least an important part of the nuclear forces is due to interaction between pairs of mesons and the nucleons.[2] As the experiments give rather strong evidence for neutral mesons, it might, therefore, be of interest to extend the previous meson pair theories,[3] where only charged mesons were used, to the case of both charged and neutral mesons, a possibility which was recently suggested for the scalar meson pair theory by Rosenfeld at a discussion in Copenhagen. The authors have now made the corresponding generalization of the charged vector meson pair theory, previously investigated by Klein and the authors.[3] If we denote by U^c and U^n the field vectors of the charged and neutral mesons and by σ_A and τ_A the spin and isotopic spin vectors of the nucleon A, we find that the generalization means that, as an example, the interaction term of the charged pair theory,

$$i\gamma\frac{e^2}{\mu c^2}\Sigma_A(U_A{}^{c*}\times U_A{}^c)\sigma_A,$$

will be replaced by

$$i\frac{e^2}{\mu c^2}\Sigma_A\sigma_A\Big[\Big(\gamma_1\frac{1+\tau_A{}^{(3)}}{2}+\gamma_2\frac{1-\tau_A{}^{(3)}}{2}\Big)(U_A{}^{c*}\times U_A{}^c)$$
$$+\gamma_3\frac{\tau_A{}^{(1)}-i\tau_A{}^{(2)}}{2}(U_A{}^{c*}\times U_A{}^n)+\gamma_3\frac{\tau_A{}^{(1)}+i\tau_A{}^{(2)}}{2}(U_A{}^{n*}\times U_A{}^c)$$
$$+\Big(\gamma_4\frac{1+\tau_A{}^{(3)}}{2}+\gamma_5\frac{1-\tau_A{}^{(3)}}{2}\Big)(U_A{}^{n*}\times U_A{}^n)\Big],$$

and corresponding expressions for the other possible Lorentz-invariant terms. With a suitable choice of the γ:s, it is possible to make these interactions symmetrical with respect to charged and neutral mesons, such as to give a charge-independent interaction between nucleons. The result of the perturbation calculation in the weak coupling case is that the interaction between two nucleons will be the same as in the charged meson pair theory, only that it is multiplied by a factor $(a^2+b^2\tau_1\tau_2)$, where a and b are arbitrary constants, a statement which holds also in the scalar meson pair theory. The investigation shows that it is possible to combine the different interaction terms in such a way that the force between two nucleons will get the general features necessary to account for the scattering experiments and the ground state and quadrupole moment of the deuteron. The forces are in this symmetrical pair theory, of course, of the exchange type in contrast to the force deduced from the charged meson pair theories.

[1] M. Conversi, E. Pancini, and O. Piccioni, Phys. Rev. 71, 209 (1947); C. M. G. Lattes, G. P. S. Occhialini, and C. F. Powell, Nature 160, 453 (1947).
[2] V. F. Weisskopf, Phys. Rev. 72, 155 (1947).
[3] G. Wentzel, Helv. Phys. Acta 15, 111 (1942). J. M. Jauch and J. Leite Lopes, Anais da Acad. Brasil. de Ciencias 16, 281 (1944). R. E. Marshak, Phys. Rev. 57, 1101 (1940). O. Klein, Arkiv f. Matematik, Astronomi och Fysik 30A, No. 3 (1943). O. Brulin and S. Hjalmars, Arkiv f. Matematik, Astronomi och Fysik 33B, No. 4 (1946).

Least Squares Fit of the Fundamental Mass Doublets

E. RICHARD COHEN AND WILLIAM F. HORNYAK
Department of Physics, California Institute of Technology, Pasadena, California
October 21, 1947

ALL calculations of nuclear masses are dependent on three or four "anchor" values which are usually determined by mass spectroscopic comparisons with the ultimate standard $^{16}O=16.000000$. Commonly, the three fundamental mass doublets $^1H_2-^2D$; $^2D_3-^{12}C^{++}$; $^{12}C^1H_4-^{16}O$, which form a closed ring, are used to obtain the secondary standards ^1H, ^2D, ^{12}C. These three values are then considered as established anchor points for computing mass values from other doublets and from reaction energies. Unfortunately, this procedure permits of no external check on the consistency of the anchor values. By extending the ring to include the doublets $^{12}C^1H_2-^{14}N$; $^{12}C^1H_3-^{14}N^1H$; $^{12}C^1H_4-^{14}N^1H_2$; $^{14}N^1H_2-^{16}O$; $^{14}N^1H_3-^{16}O^1H$; $^{14}N_2-^{12}C^{16}O$, we obtain an overdetermined system which does permit an external consistency check, and which provides us with an additional reference point.

From these doublets we obtain an overdetermined system of six equations in four unknowns which can be solved by the usual methods of least squares. The six equations are the condensation of the nine actual doublets quoted. Least squares methods have been previously used to varying extents, Bönisch and Mattauch,[6] Bainbridge and Jordan,[10] and others. The input values of the doublets used in the present determination are, in units of 10^{-4} MU:

$$^1H_2-^2D=15.39\pm0.021,^{2-4,6,9}$$
$$^2D_3-^{12}C^{++}=422.30\pm0.19,^{2-4,6,9}$$
$$^{12}C^1H_4-^{16}O=363.69\pm0.21,^{1,2,4-6,8,9}$$
$$^{12}C^1H_{2+n}-^{14}N^1H_n=125.63\pm0.07,^{1,2,4-7,9}$$
$$^{14}N^1H_{2+m}-^{16}O^1H_m=237.80\pm0.32,^{1,4}$$
$$^{14}N_2-^{12}C^{16}O=112.22\pm0.40.^{1,4}$$

The numerical values used in these equations are the weighted means of all reliable data. The weights were based on the reported errors listed by each experimenter.

The above system yields for the output values of the masses

$$^1H=1.0081284\pm0.0000027,$$
$$^2D=2.014718\pm0.000005,$$
$$^{12}C=12.003847\pm0.000016,$$
$$^{14}N=14.007539\pm0.000015.$$

Furthermore, as a result of the least squares adjustment these mass values can no longer be considered as observationally independent quantities, but are interrelated through the "correlation coefficients": $r_{HD}=0.92$, $r_{HC}=-0.30$, $r_{HN}=0.004$, $r_{DN}=0.05$, $r_{DC}=-0.24$, $r_{NC}=0.86$. The "correlation coefficient" used here is defined in such a manner that the probable error of a linear function $ax+by$ is given by:

$$[a^2\delta_x^2+2abr_{xy}\delta_x\delta_y+b^2\delta_y^2]^{\frac{1}{2}},$$

where δ_x is the probable error in x, δ_y the probable error in y, and r_{xy} the "correlation coefficient" between x and y.

In this manner we then obtain the least squares best values for the doublets:

$$^1H_2-^2D=15.390\pm0.021,$$
$$^2D_3-^{12}C^{++}=422.30\pm0.19,$$
$$^{12}C^1H_4-^{16}O=363.60\pm0.18,$$
$$^{12}C^1H_2-^{14}N=125.64\pm0.08,$$
$$^{14}N^1H_2-^{16}O=237.96\pm0.14,$$
$$^{14}N_2-^{12}C^{16}O=112.32\pm0.19.$$

The comparison of external to internal consistency, following Birge and using his notation, gives $R_e/R_i=0.35$. Apparently this indicates either that the errors ascribed by the experimenters to the individual data were too pessimistic or that our selection of the data has been somewhat too critical. The discrepancy can in part be ascribed to the quotation of "limits of error" by some authors in place of "probable errors".

Work is now in progress which is intended to extend the mass table from ^1n to ^{20}Ne inclusively, based on these secondary standards and the best experimental information available at the present time.

We are grateful to Dr. William R. Smythe for the helpful interest he has shown in this work.

[1] E. Jordan and K. Bainbridge, Phys. Rev. **49**, 883 (1936).
[2] F. Aston, Proc. Roy. Soc. **A163**, 391 (1937).
[3] K. Bainbridge and E. Jordan, Phys. Rev. **51**, 384 (1937).
[4] J. Mattauch, Physik. Zeits. **39**, 892 (1938).
[5] Asada, Okuda, Ogata, and Yoshimoto, Nature **143**, 797 (1939); Proc. Phys. Math. Soc. Japan **22**, 41 (1940).
[6] J. Mattauch, Phys. Rev. **57**, 1155 (1940).
[7] E. Jordan, Phys. Rev. **58**, 1009 (1940).
[8] E. Jordan, Phys. Rev. **60**, 710 (1941).
[9] Flügge and Mattauch, Physik. Zeits. **44**, 181 (1943).
[10] Private communication.

Effects of Space Charge on the Detection of High Energy Particles by Means of Silver Chloride Crystal Counters*

LOUIS F. WOUTERS AND RICHARD S. CHRISTIAN
Radiation Laboratory, Department of Physics, University of California, Berkeley, California
October 14, 1947

SILVER chloride crystals operating at liquid N_2 temperatures are being used for detection of high energy protons produced by recoil and exchange reactions in the neutron beam emitted by the 184-in. cyclotron. Crystals of dimension $\frac{1}{8}''\times1''\times1''$ are annealed and coated by the usual processes;[1] mountings, amplifiers, scalers, and power supplies are more or less conventional. With this apparatus, γ-rays from radium give pulses of about four times the input-stage noise level of 50 microvolts; in the neutron beam, pulses up to 20 times this noise level are observed.

The chief difficulty encountered at any useful counting rate, with either form of radiation, is the gradual decrease in observed pulse height as counting proceeds, because of neutralization of the electric field by the space charge accumulating in the crystal. After perhaps 10,000 pulses, all pulses have noticeably decreased in height and frequency (as observed on a synchroscope); beyond 50,000, the rate and size are but a few percent of initial. This space charge is found to persist for long periods of time, up to 48 hours in one case.

As observed by Woolridge, Ahearn, and Burton[2] in diamond, upon subsequently grounding the high voltage electrode, pulses of reverse polarity and of height equal to those originally observed are now seen; the pulse rate is also fully as great as that originally measured. As the space-charge field is depleted by the ionizing radiation, these "reverse" pulses correspondingly decrease in amplitude and frequency, until they likewise have vanished. The original potential may then by reimpressed, and another complete counting cycle is possible. This process has been repeated several hundred times with various crystals; to insure consistent results, the applied voltage is actually completely reversed after, say, one thousand counts. Over such a small interval the change in pulse height is entirely negligible.

In line with results of Street[3] and Hofstader,[4] pulse rise times were found to be masked by amplifier rise time; in our best tests this was about 0.2 microsecond, with a decay time of the same order.

The silver chloride crystal counter is thus a fast, high density counter of convenient dimension, well suited for detection and discrimination of particles of range upwards of the crystal thickness. In the coincidence equipment now under construction, the crystal voltage will be synchronously reversed between successive cyclotron beam pulses, to preclude missing counts caused by interference of amplifier blanking with beam pulses, as would otherwise be the case; the pulse spectrum will also be more clearly displayed by locking in the synchroscope sweep.

We wish to express our appreciation of the interest and encouragement of Professor Ernest O. Lawrence and the cooperation of the Laboratory staff.

* This letter is based on work performed at the Radiation Laboratory under Contract No. W-7405-Eng-48 with the Atomic Energy Commission.

[1] P. J. Van Heerden, *The Crystal Counter* (Utrecht, 1945).
[2] Woolridge, Ahearn, and Burton, Phys. Rev. **71**, 913 (1947).
[3] C. Street, private communication to Wilson Powell.
[4] R. Hofstader, Phys. Rev. **72**, 747 (1947).

Geophysics and the Radioactivity of Potassium

FRANCIS BIRCH
Harvard University, Cambridge, Massachusetts
October 13, 1947

THE recent publications of Gleditsch and Gráf[1] and of Bleuler and Gabriel[2] lead to a reduction of the effective half-period of K^{40} from 15.7×10^{9} year to 2.4×10^{9} year, and an increase of the present rate of energy production from about 5×10^{-6} cal. per year to 38×10^{-6} cal. per year per g of (ordinary) potassium. As Gleditsch and Gráf make clear, the importance of this revision for geophysics can hardly be overestimated. A few of the major problems which must be re-examined, if these changes are accepted, are the following:

1. The thermal history of the Pre-Cambrian periods.
2. The origin of the moon and of lunar topography.
3. The chemical and mineralogical differentiation of the silicate shell, and the segregation of the radioactive elements.
4. The formation of continents and ocean basins.
5. The origin of folded mountain ranges.

It seems possible, at first glance, that the new constants for K^{40} may aid in resolving some of the difficulties now encountered with all of these studies. On the other hand, certain new problems arise. For example, the most reliable radioactive age determinations[3] agree in giving ages over 1×10^{9} and up to 2×10^{9} year for a number of rocks and minerals. With the new values for heat production from potassium, however, it seems doubtful whether a permanent crust could have existed for more than 10^{9} or at most perhaps 1.5×10^{9} year. Prior to this time, repeated remelting or flooding of the crust must have occurred. Neither the data nor our understanding of the processes are sufficiently exact so that a flat contradiction may be said to exist; but there is at least a suggestion here that the new half-life may be too short. The purpose of this letter is thus to reiterate the importance for geophysical theory of a redetermination of the constants for K^{40} and, in particular, of the period of β-decay upon which the other results depend.

[1] E. Gleditsch and T. Gráf, Phys. Rev. **72**, 640, 641 (1947).
[2] E. Bleuler and M. Gabriel, Helv. Phys. Acta **20**, 67 (1947).
[3] A. O. Nier, Phys. Rev. **55**, 153 (1939). C. Goodman and R. D. Evans, Bull. Geol. Soc. Am. **52**, 491 (1941).

The Role of Exchange Interaction in Paramagnetic Absorption

C. J. GORTER, *Kammerlingh Onnes Laboratory, Leyden, Holland*
AND
J. H. VAN VLECK, *Harvard University, Cambridge, Massachusetts*
October 23, 1947

ACCORDING to theory,[1-3] the paramagnetic absorption per ion in a system of ionic spins should be inversely proportional to the magnetic interaction between the ions, characterized by the so-called internal field H_i.[4] This theory has in general been confirmed by Volger[2,5] for a number of hydrated chromic, manganous, ferric, and gadolinium salts. However, the paramagnetic absorption in a number of anhydrous compounds of the same ions and in a few hydrated cupric salts (notably in $CuCl_2\cdot2_2HO$) is considerably higher than expected.

The absorption in the first-mentioned group of hydrated salts vanishes in accordance with the theoretical expectation[2] when a constant perpendicular field of the order of H_i is applied. In the anhydrous compounds and in the copper salts, on the other hand, the absorption already disappears in much smaller perpendicular fields.

Recently Zavoisky[6] and Cummerow and Halliday[7] have succeeded in observing an absorption band corresponding to the Larmor frequency in large perpendicular fields. In contrast with theoretical expectation, however, the width of this band in anhydrous compounds and copper salts appears to be considerably smaller than the internal field H_i.

From all this it appears that, in the anhydrous and copper salts, the effects of magnetic interaction (characterized by H_i) have been reduced as a consequence of exchange interaction[8,9] between the ions.

The existence of the phenomenon of "exchange narrowing" may be proved mathematically by calculating the mean square and mean fourth power of the absorption frequency of an ensemble of paramagnetic atoms coupled together simultaneously by magnetic (dipolar) and exchange forces. The mean square or second moment is not influenced by the exchange terms since the exchange potential is isotropic and commutes with any Cartesian component of the total spin of the crystal. On the other hand, it may be demonstrated that the fourth moment contains cross terms involving products of the exchange integrals and the dipolar constants. As a result, the addition of exchange coupling enhances the mean fourth power of the absorption frequency. Since the mean square is unaffected, this enhancement is possible only if more of the line strength is located in the tail of the absorption line than otherwise, and if, at the same time, it is peaked more sharply at the center. Hence, the paramagnetic absorption at the resonance maximum is increased. Because of the sharpened peak, the spread in frequency required to reduce the intensity to half its maximum value is diminished and, hence, also the apparent line breadth or effective dipolar field. When exchange effects are important, the shape of the line is so distorted that the usual Gaussian assumption concerning its structure is a bad approximation.

The underlying theory will be considered more thoroughly by one of us (J. H. V. V.), but it may already be worth while to mention an analogy which exists with the narrowing of nuclear Larmor frequency bands of hydrogen in liquids and in compressed hydrogen gas. According to the views developed by Bloembergen, Purcell, and Pound,[10] the effects of magnetic interaction between the nuclear dipoles and of the coupling between these dipoles and the rotation of the molecule are reduced as a consequence of the small but very frequent perturbations caused by temperature motion and collisions between molecules. Correspondingly, in the case of the electronic spin considered in the present note, the exchange effects lead to a rapid interchange of the spins between different lattice points and diminish the coherence and efficacy of the magnetic interaction.

There are indications that the effects of internal electric fields in paramagnetic salts may also be reduced by exchange interaction.

[1] I. Waller, Zeits. f. Physik. **79**, 370 (1932).
[2] L. J. F. Broer, Physics **10**, 801 (1932); Thesis, Amsterdam 1945.
[3] C. J. Gorter, *Paramagnetic Relaxation* (Elsevier Publishing Company, Inc., New York, 1947).
[4] J. H. Van Vleck, J. Chem. Phys. **5**, 320 (1937).
[5] J. Volger, Thesis, Leyden, 1946.
[6] E. Zavoisky, J. Phys. Sowjetunion. **10**, 170 (1945).
[7] R. L. Cummerow and D. H. Halliday, Phys. Rev. **70**, 433 (1946).
[8] B. H. Schultz, Thesis, Leyden, 1940.
[9] D. De Klerk, Physica **12**, 513 (1946).
[10] N. Bloembergen, R. V. Pound, and E. M. Purcell, Phys. Rev. **71**, 466 (1947); N. Bloembergen, R. V. Pound, and E. M. Purcell, Nature (in press) 1947; N. Bloembergen, Thesis, Leyden, 1948.

Erratum: Second Sound in Liquid Helium II

[Phys. Rev. **71**, 600 (1947)]

C. T. LANE, HENRY A. FAIRBANK, AND WILLIAM M. FAIRBANK
Sloane Physics Laboratory, Yale University, New Haven, Connecticut

OUR attention has been called to a regrettable error in our paper entitled "Second sound in liquid helium II." We ascribed to Tisza the formula

$$C=\left[-\frac{\rho_s}{\rho_n}\frac{\partial}{\partial T}\left(\frac{1}{S}\right)^{-1}\right],$$

whereas it was first derived by Landau. We regret our failure to acknowledge Landau's priority and assure him that this failure was unintentional.